



# **Experimental Validation of the Shakedown Concept for Pavement Analysis and Design**

by

Sumyaty Juspi, BEng (Hons)

*Thesis submitted to The University of Nottingham  
for the degree of Doctor of Philosophy*

April 2007

## **ABSTRACT**

The shakedown concept has been widely applied in structural and mechanical engineering numerical models. The concept is related to the response of a structure to load repetitions in a resilient manner without further permanent deformation. More than 40 wheel tracking tests were conducted with various wheel load levels for each test to check the validity of the shakedown concept in the pavement foundation. Six different types of soils with different characteristics were used in the wheel tracking tests. These were a silt (from gravel pit washings), a silty-clay (Mercia Mudstone, referred to here by its earlier name of Keuper Marl), two sands (Portaway and Langford Fill), and two crushed rocks (Carboniferous Limestone and Granite). Three different sized wheel-tracking facilities were used; a small wheel tracker (SW), a larger Slab Testing Facility (STF) and the half-scale Nottingham Pavement Testing Facility (PTF). These allowed various wheel specifications and test specimen sizes to be investigated. The test programme embraced one, two and three layered systems. The permanent vertical deformation of each system was measured after a certain number of passes. The soil is said to be under shakedown if after a certain number of passes, there is no further permanent deformation. The experimental result was compared with the theoretical shakedown prediction. A series of static triaxial tests for each soil, with the test conditions close to the wheel tracking tests, was carried out to identify the shear strength to be used as input parameters for the theoretical shakedown prediction. The theoretical shakedown limits of the various soil combinations show a good agreement with the wheel tracking test results.

# ACKNOWLEDGEMENTS

I would like to thank Professor Hai-Sui Yu and Professor Stephen Brown who gave me the opportunity to work on this project with an excellent guidance and a continuous encouragement and support during this study.

I would also like to express my gratitude to the following people for their help and advice:

Professor Alan Ponter and Dr Mustafa Boulbibane of the University of Leicester and Dr Huaxiang Li of the University of Nottingham for their assistance in theoretical modelling;

Pratapha Ravindra for useful discussion on our common research interest;

Barry Brodrick and Christopher Fox for the laboratory support, discussion and providing an excellent guidance during experiments;

All the technicians in the Nottingham Centre for Pavement Engineering (NCPE) and Nottingham Centre for Geomechanics (NCG) in preparing the specimens;

Barry Brodrick and Dr Cuong Doan Khong for their valuable time spent proof reading this thesis;

The Engineering and Physical Sciences Research Council (EPSRC) for sponsoring the research project;

All colleagues in the School of Civil Engineering for their help and friendship,

Finally, my greatest gratitude goes to my parents, sisters, brother, nieces, and nephews for their love, belief, support, and encouragement throughout the period of my studies.

# Table of Contents

<b>ABSTRACT .....</b>	<b>1</b>
<b>ACKNOWLEDGEMENTS.....</b>	<b>2</b>
<b>Table of Contents.....</b>	<b>i</b>
<b>APPENDICES .....</b>	<b>v</b>
<b>List of Figures.....</b>	<b>vi</b>
<b>List of Tables .....</b>	<b>xi</b>
<b>1 INTRODUCTION .....</b>	<b>1</b>
1.1 BACKGROUND .....	1
1.2 OBJECTIVES.....	4
1.3 RESEARCH OVERVIEW .....	5
<b>2 LITERATURE REVIEW .....</b>	<b>8</b>
2.1 PAVEMENT ENGINEERING .....	8
2.1.1 Introduction.....	8
2.1.2 Pavement Distress Modes.....	8
2.1.3 Pavement Designs.....	10
2.1.4 Experimental Observation of Shakedown Behaviour in the Pavement.....	14

2.1.5	Wheel Load on a Pavement Surface .....	22
2.1.6	Response of a Pavement Structure .....	29
2.2	NUMERICAL MODELLING USING THE SHAKEDOWN CONCEPT .....	38
2.2.1	Introduction.....	38
2.2.2	Lower Bound Theorem.....	39
2.2.3	Upper Bound Theorem .....	43
2.2.4	Factors Affecting the Shakedown Limit.....	48
2.3	SUMMARY .....	50
3	MATERIAL CHARACTERISATION .....	53
3.1	INTRODUCTION .....	53
3.2	THE MATERIALS.....	54
3.2.1	Keuper Marl.....	54
3.2.2	Portaway Sand .....	55
3.2.3	Silt.....	55
3.2.4	Langford Fill Sand.....	55
3.2.5	Crushed Carboniferous Limestone .....	56
3.2.6	Crushed Granite .....	56
3.3	PARTICLE SIZE ANALYSIS .....	57
3.4	COMPACTION-RELATED TEST.....	59
3.5	THE MONOTONIC LOAD TRIAXIAL TEST.....	62
3.5.1	The Equipment.....	63

3.5.2	The Specimen Preparation .....	66
3.5.3	Test Procedure .....	71
3.5.4	Test Result .....	72
3.6	DISCUSSION .....	75
3.7	SUMMARY .....	78
4	WHEEL TRACKING TESTS .....	79
4.1	INTRODUCTION .....	79
4.2	WHEEL TRACKING FACILITIES .....	80
4.2.1	Small Wheel Tracker (SW) .....	81
4.2.2	Slab Test Facility (STF).....	83
4.2.3	Pavement Test Facility (PTF).....	86
4.3	THE SPECIMEN PREPARATION .....	89
4.4	TEST CONDITIONS .....	93
4.5	DATA COLLECTION PROCEDURES .....	94
4.5.1	The Procedures for the Contact Pressure Measurement .....	94
4.5.2	The Procedures for the Transverse Profile and Vertical Permanent Deformation Measurement .....	96
4.6	SUMMARY .....	97
5	RESULTS OF WHEEL TRACKING TESTS .....	99
5.1	INTRODUCTION .....	99
5.2	TEST PROGRAMME .....	99

5.3	CONTACT PRESSURE.....	101
5.3.1	The Solid Wheel .....	102
5.3.2	The Pneumatic Wheel.....	102
5.4	TRANSVERSE PROFILE .....	107
5.5	VERTICAL PERMANENT DEFORMATION .....	111
5.6	DISCUSSION.....	124
5.7	SUMMARY .....	126
6	THE APPLIED SURFACE STRESSES RATIO ASSR.....	129
6.1	INTRODUCTION .....	129
6.2	THE METHOD TO MEASURE THE VERTICAL AND HORIZONTAL FORCES .....	130
6.3	THE RESULTS .....	134
6.4	SUMMARY .....	136
7	APPLICATION OF THE SHAKEDOWN CONCEPT IN PAVEMENT ENGINEERING .....	137
7.1	INTRODUCTION .....	137
7.2	PHILOSOPHY OF THE SHAKEDOWN LIMIT COMPUTATION... ..	138
7.2.1	For a Single Layered Pavement.....	138
7.2.2	For Multi-Layered Cases .....	141

7.3	COMPARISON OF THE EXPERIMENTAL RESULTS AND THEORETICAL PREDICTIONS .....	144
7.4	SUMMARY .....	152
8	SUMMARY, CONCLUSIONS AND RECOMMENDATIONS FOR FUTURE WORK.....	153
8.1	SUMMARY .....	153
8.2	CONCLUSIONS .....	154
8.3	RECOMMENDATIONS FOR FUTURE WORK .....	158
	References.....	160

## APPENDICES

Appendix A.	Monotonic Load Triaxial Test Results .....	169
Appendix B.	Wheel Load Calibrations.....	178
Appendix C	The Contact Patches of Various Wheel Loads Using the Wheel Tracking Facilities .....	182
Appendix D.	Properties of the Wheel Tracking Test Specimens .....	196
Appendix E	The vertical permanent deformation data.....	202
Appendix F	The Charts of the Deformation Rates against the Number of Passes of Various Soil Combinations .....	228



## List of Figures

Figure 1. 1 Deformation Schemes under Various Wheel Loads .....	3
Figure 2. 1 Typical pavement cross sections (after Highways Agency, 2003) ..	9
Figure 2. 2 Types of distress in pavements .....	10
Figure 2. 3 Variation of Permanent Vertical Deformation with Number of Load Applications for the Rutting Tests carried out in the Slab Test Facility (after Chan, 1990).....	17
Figure 2. 4 Variation of Permanent Vertical Deformation with Number of Passes of Wheel Load for the Rutting Tests carried out in Pavement Test Facility (after Chan, 1990).....	18
Figure 2. 5 Cumulative permanent strain versus strain rate of Granodiorite, with $\sigma_3 = 70\text{kPa}$ (after Werkmeister et al., 2001).....	19
Figure 2. 6 Horizontal stress distribution from full scale experiment (after Radovsky and Murashina, 1996) .....	21
Figure 2. 7 Definition of vertical, longitudinal and transverse/lateral direction .....	25
Figure 2. 8 Typical contact stress distributions measured with VRSPTA system (after de Beer et al., 1997) .....	26
Figure 2. 9 Relationship between maximum horizontal longitudinal force and amount of acceleration/deceleration (after Bonse and Kuhn, 1959) .....	28
Figure 2. 10 Stresses beneath rolling wheel load (after Lekarp and Dawson, 1997).....	29
Figure 2. 11 Stress pulses induced by a moving wheel (after Chan, 1990).....	30
Figure 2. 12 Strains as results of stress pulses during one cycle of load application.....	31

Figure 2. 13 Elastic and plastic ranges of repeated loadings (after Wilson and Greenwood, 1974) .....	35
Figure 2. 14 Representation of elastoplastic half-space under a rolling cylinder .....	40
Figure 2. 15 Typical load distributions for shakedown analysis .....	41
Figure 2. 16 The failure Mode for frictional material under 3D moving hertz load .....	46
Figure 2. 17 Rut failure mechanisms for half space (after Collins and Boulbibane, 2000).....	48
Figure 2. 18 Effect of $E_b/E_s$ and $C_b/C_s$ on dimensionless shakedown limits (after Shiau and Yu, 2000).....	50
Figure 3. 1 Particle size distribution of the test materials.....	58
Figure 3. 2 Schematic diagram showing the layout of the triaxial system (GDS Instruments Ltd., 2002).....	64
Figure 3. 3 University of Nottingham repeated load triaxial (RLT) apparatus (after Arnold, 2004) .....	65
Figure 3. 4 Schematic of University of Nottingham's RLT apparatus (after Pappin, 1979).....	66
Figure 3. 5 The compaction tools for fine grained soils .....	68
Figure 3. 6 Stress-strain relationship of Keuper Marl .....	73
Figure 3. 7 Mohr-Coulomb circles and failure line of.....	73
Figure 4. 1 Diagram of small wheel tracker .....	82
Figure 4. 2 A small wheel tracker.....	82
Figure 4. 3 Diagram of the Nottingham Slab Test Facility (after Chan, 1990) .....	84

Figure 4. 4 Side view of the Nottingham Slab Test Facility and the control equipment .....	85
Figure 4. 5 Side view of the Nottingham Slab Testing Facility .....	85
Figure 4. 6 The Nottingham Slat Testing Facility's control equipment .....	85
Figure 4. 7 Diagram of the Nottingham Pavement Test Facility (after Brown and Brodrick, 1999) .....	87
Figure 4. 8 The Nottingham Pavement Test Facility .....	88
Figure 4. 9 Vibrating hammer used on soils for the SW .....	91
Figure 4. 10 Vibrating plate used on soils for the STF .....	91
Figure 4. 11 Vibrating plate used on Keuper Marl and sand for the PTF .....	91
Figure 4. 12 Single drum vibrating roller used on Limestone for the PTF .....	91
Figure 4. 13 Typical specimen profiles for the STF test .....	92
Figure 4. 14 Two specimen profiles for the PTF test .....	92
Figure 4. 15 Definition of the vertical permanent deformation .....	96
Figure 5. 1 The contact pressures of the SW's rigid wheel on three different types of materials .....	103
Figure 5. 2 Typical prints of the contact pressure distributions using the PTF .....	104
Figure 5. 3 The surface pressures at different wheel loads and for different materials (STF) .....	105
Figure 5. 4 The cell pressures and contact pressures for different PTF wheel loads .....	106

Figure 5. 5 Portaway Sand after 8000 passes with contact pressure of 100kPa using the SW .....	108
Figure 5. 6 Keuper Marl after 650 passes with contact pressure of 301kPa using the SW .....	108
Figure 5. 7 Silt after 16000 passes with the contact pressure of 229kPa using the SW .....	108
Figure 5. 8 Crushed Granite after 10000 passes with contact pressure of 355kPa using the STF .....	108
Figure 5. 9 Section transverse profiles measured manually before and after the two layers tests of PTF for all three test sections .....	109
Figure 5. 10 Section transverse profiles measured manually before and after the three layered tests for all four test sections (PTF) .....	110
Figure 5. 11 Variation of the vertical permanent deformation and the deformation rate of PS1 with number of passes for various wheel pressures	113
Figure 5. 12 Variation of the vertical permanent deformation of PS2 with number of passes for various wheel pressures.....	115
Figure 5. 13 Variation of the vertical permanent deformation of KM with number of passes for various wheel pressures.....	116
Figure 5. 14 Variation of the vertical permanent deformation of Silt with number of passes for various wheel pressures.....	117
Figure 5. 15 Variation of the vertical permanent deformation of Gr with number of passes for various wheel pressures.....	118
Figure 5. 16 Variation of the vertical permanent deformation of Gr-PS with number of passes for various wheel pressures.....	119
Figure 5. 17 Variation of the vertical permanent deformation of Gr-Silt with number of passes for various wheel pressures.....	120

Figure 5. 18 Variation of the vertical permanent deformation of CI-KM1 with number of passes for various wheel pressures.....	121
Figure 5. 19 Variation of the vertical permanent deformation of CI-KM2 with number of passes for various wheel pressures.....	122
Figure 5. 20 Variation of the vertical permanent deformation with number of passes for various wheel pressures of CI-LFS-KM .....	123
Figure 5. 21 Variation of the vertical permanent deformation for different soil combinations.....	125
Figure 6. 1 A load cell and the digital read-out at the SW .....	131
Figure 6. 2 The arrangement to measure the horizontal force of the SW.....	132
Figure 6. 3 The arrangement to measure the horizontal force for the STF ....	133
Figure 7. 1 The coordinates and notation for stresses .....	140
Figure 7. 2 Finite element model for three layered pavement.....	142
Figure 7. 3 The finite element mesh .....	143
Figure 7. 4 Theoretical shakedown limits against the wheel pressures.....	148
Figure 7. 5 Theoretical shakedown limits against the angle of frictions .....	149
Figure 7. 6 Theoretical shakedown limits against the cohesions.....	150
Figure C. 1 The cell pressures and contact pressures for different PTF wheel loads on the crushed Carboniferous Limestone placed above the Langford Fill Sand and Keuper Marl .....	195
Figure D. 1 DCP Test Results in the PTF.....	201

Figure F. 1 Variation of the deformation rate of PS2 with number of passes for various wheel pressures .....	229
Figure F. 2 Variation of the deformation rate of KM with number of passes for various wheel pressures .....	229
Figure F. 3 Variation of the deformation rate of Silt with number of passes for various wheel pressures .....	230
Figure F. 4 Variation of the deformation rate of Gr with number of passes for various wheel pressures .....	231
Figure F. 5 Variation of the deformation rate of Gr-PS with number of passes for various wheel pressures .....	231
Figure F. 6 Variation of the deformation rate of Gr-Silt with number of passes for various wheel pressures .....	232
Figure F. 7 Variation of the deformation rate Cl-KM1 with number of passes for various wheel pressures .....	232
Figure F. 8 Variation of the deformation rate of Cl-KM2 with number of passes for various wheel pressures .....	233
Figure F. 9 Variation of the deformation rate of Cl-LFS-KM with number of passes for various wheel pressures .....	233

## List of Tables

Table 2. 1 Summary of experiments using repeated load triaxial apparatus associated with shakedown concept .....	15
Table 2. 2 Sensors or methods to measure tyre and road interaction .....	24
Table 3. 1 Description of the test materials .....	57
Table 3. 2 Summary of the compaction-related Tests .....	61

Table 3. 3 Summary of the static triaxial tests of various materials.....	77
Table 4. 1 Specification of the Wheel-tracking Facilities .....	80
Table 4. 2 Summary of the wheel tracking specimen test conditions .....	93
Table 5. 1 Summary of the wheel tracking test specimens .....	100
Table 6. 1 Summary of the specimen properties for the ASSR measurement	130
Table 6. 2 Summary of the rolling resistances of various materials.....	135
Table 7. 1 Comparison of the experimental and computed shakedown limit for a homogeneous pavement.....	145
Table 7. 2 Comparison of the experimental and computed shakedown limit of layered pavement.....	146
Table 7. 4 Relative densities of various materials .....	151
Table C. 1 The wheel contact patches on the Keuper Marl.....	183
Table C. 2 The wheel contact patches on the Silt.....	184
Table C. 3 The wheel contact patches on the Portaway sand.....	185
Table C. 4 Summary of the contact areas using the SW .....	186
Table C. 5 The STF wheel contact patches on the Granite .....	187
Table C. 6 The STF wheel contact patches on the crushed Carboniferous Limestone .....	188
Table C. 7 The STF wheel contact patches on the crushed Granite placed above the Portaway Sand.....	189
Table C. 8 The STF wheel contact patches on the crushed Granite placed above the Silt .....	190

Table C. 9 Summary of the contact areas using the STF.....	191
Table C. 10 The PTF wheel contact patches on the crushed Granite placed above the Keuper Marl .....	192
Table C. 11 Summary of the contact areas using the PTF .....	193
Table C. 12 The PTF wheel contact patches on the crushed Granite placed above the Langford Fill Sand and Keuper Marl .....	194
Table D. 1 The soil properties for single layered tests using the SW .....	197
Table D. 2 The soil properties for single layered tests using the STF.....	197
Table D. 3 The soil properties for two layered tests using the STF .....	198
Table D. 4 The soil properties for two layered test using the PTF .....	198
Table D. 5 The soil properties for three layered test using the PTF .....	199



# **1 INTRODUCTION**

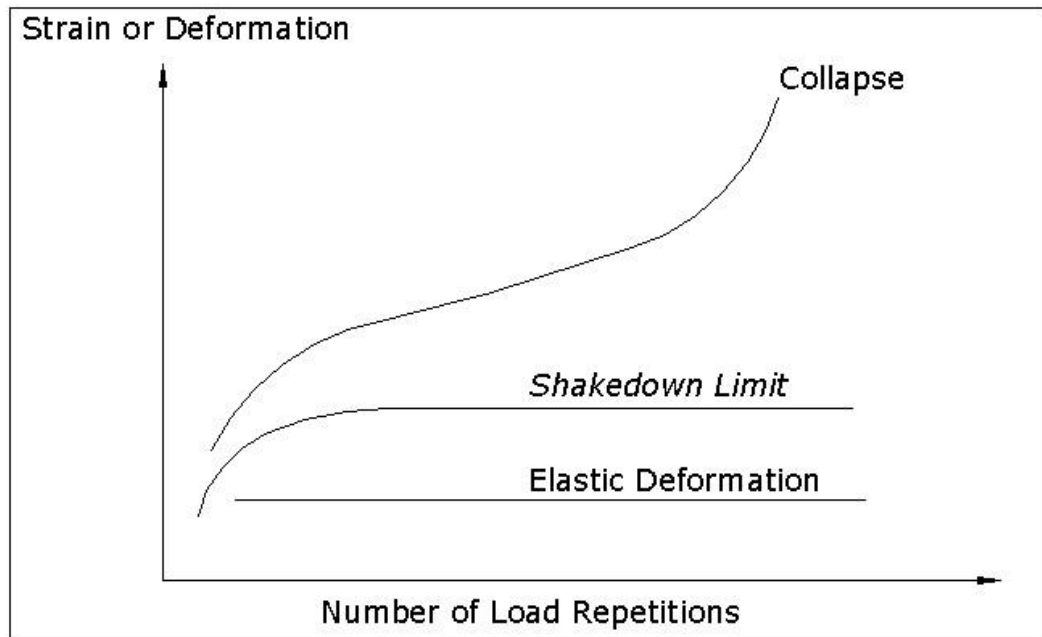
A pavement, a combination of layer thicknesses and material types, is designed to carry the traffic loads safely and economically during the service life or longer. It deteriorates in a variety of distress modes such as cracking, surface deformation or rutting, patching and potholes, surface defects, bleeding. The current empirical pavement design curves which are related to subgrade strength and traffic load cannot imply a specific pavement distress mode. In recent years, a shakedown concept has been widely applied for pavement analysis and design. A design method based on the shakedown concept has been developed. A series of triaxial tests and wheel tracking tests for the investigation are the basis of these studies to validate the shakedown concept.

## **1.1 BACKGROUND**

Rutting, one of the pavement distress modes, is due to the accumulation of vertical permanent strains in the wheel track, which includes contributions from all layers in the pavement and is mostly caused by heavy vehicles. It has become a big issue in most countries as the cost to rehabilitate the pavement structure and the effect on the road users, such as delay and congestion, is more expensive than top/surface layer renewal. From the safety issue, rutting may develop hazards for road users due to the unevenness on the road surface.

Therefore, the rutting problem is the top priority for highway engineers to be examined and solved.

Based on the literature review, research on pavement rutting has been conducted since the 1950s. From the observations, using repeated load triaxial tests, most of the research has concentrated on predicting the amount of permanent deformation (rutting) under repeated loading or has studied the effects of repeated stresses. This research has similar results in that an infinite number of stress repetitions can be applied without causing failure of the specimen if the applied stresses are sufficiently low. For this level of stress, Wood and Goetz (1956), Goetz et al. (1957), and Larew and Leonards (1962) referred to an 'endurance limit', Sangrey et al. (1969) defined it as 'critical level of repeated stress', Trollope et al. (1962) and Werkmeister et al. (2001) used the 'shakedown limit' term, and Heath et al. (1972) and Loach (1987) defined that level of stress as a 'threshold level'. For future reference, the maximum limit of repeated stresses without causing further permanent deformation of the soil specimen will be defined as the 'shakedown limit', the most common term that was found and used in the literature review. Figure 1.1 illustrates the definition of the shakedown limit by using the deformation schemes under various wheel loads.



**Figure 1. 1 Deformation Schemes under Various Wheel Loads**

In numerical modelling, the shakedown concept has been widely applied in structural and mechanical engineering [see Johnson (1962 and 1985), Maier (1969), Kapoor and Williams (1996), Wong et al (1997a and b)]. The shakedown concept was first introduced by Melan (1938 cited in Sharp, 1983). Sharp (1983) [see also Sharp and Booker (1984) and Sharp (1985)] was among the first to introduce the application of the shakedown concept for determining the long-term behaviour of a pavement structure subjected to variable and repeated moving loads. By comparing the one dimensional computed results based on the shakedown concept with the life of a number of local pavements under normal traffic conditions, Sharp (1985) found that the shakedown approach could provide a convenient design tool in pavement design.

Sharp's work in 1980s has inspired other researches to develop the shakedown theory from various points of view and approaches including full-scale

experiment and laboratory tests. Due to the cost of purchasing and running this type of equipment, most of work has focussed only on numerical model analysis for pavement design. Although some research has included some laboratory tests and full-scale experiments, they were limited to a single layer or simply to check the applicability of the shakedown theory without further application in pavement design [see Radovsky and Murashina (1996)]. Therefore, it would seem appropriate to conduct a series of wheel load tests on a pavement structure to validate the shakedown concept for pavement design and analysis. In the light of such a need or to improve the current pavement foundation design method, the Engineering and Physical Sciences Research Council (EPSRC) initiated a research programme to validate the shakedown concept. The work presented in this thesis was part of this programme and was sponsored by EPSRC.

## **1.2 OBJECTIVES**

The overall objective of the research is to check the application of the shakedown concept, as another simple design criterion, for pavement analysis particularly for the sub-base and sub-grade layer.

The following specific objectives are required to achieve the aim of the research:

1. Report on the type and the physical properties of soils that were used in the experiments.

2. Carry out a series of laboratory tests to identify the strength and stiffness properties of the specimens.
3. Identify the applied surface stresses ratio ASSR between the specimen surface and the wheel tracking apparatus.
4. Use the applied surface stresses ratio ASSR, the strength and stiffness properties of the specimen to compute the shakedown limit.
5. Develop the existing wheel tracking facilities in order to achieve the general objective.
6. Perform a series of wheel tracking tests on homogeneous and layered pavements under various wheel loads which are below and above the theoretical shakedown limit.
7. Check the computed shakedown limit against the experimental results obtained from the wheel tracking tests.

### **1.3 RESEARCH OVERVIEW**

This thesis consists of eight chapters. A brief outline of this thesis is given below.

Following the introductory chapter, Chapter 2 contains a literature review, consisting of two sections: pavement engineering and numerical modelling. The pavement engineering section covers the current pavement design methods and the limitations, type of pavement distresses, experimental investigation in connection with the shakedown response, what sort of load runs on a real

pavement surface, and the typical response of the pavement structure under load repetitions.

The principle of the shakedown concept and the application of the concept in the lower and upper bound theorems by various researchers are reviewed in the numerical modelling section together with the assumptions that were used to simplify the pavement models for both the upper and lower bound approaches. The factors that may affect the shakedown limit of the pavement from the theoretical viewpoint are examined. The required soil parameters to compute the shakedown limit of a pavement structure are summarised in this section.

Before the soils were tested with any load tests, some basic laboratory tests were carried out to reveal the characteristic of the soils. The type of basic tests that were performed and the type of soils including the origin of the soils that were used in the experiments are reported in Chapter 3.

The wheel tracking facilities are designed and used to check and compare the performance of new or improved pavement materials or to design with existing materials before introducing into an in-service pavement or modifying the existing design code. If the pavement test under controlled conditions using the wheel tracking facilities fails, it is very unlikely to be successful in practice. To validate the shakedown concept for soil and pavement analysis and design, various types of soils were tested using the wheel tracking facilities, which involve the study of the permanent surface deformation of soil subjected to traffic load repetitions ranging from below to above the theoretical shakedown

limits under drained conditions. Details of the different wheel tracking equipment that was used and the procedures to prepare the specimen and perform the wheel load tests are presented in Chapter 4. The wheel tracking test results are reported and discussed in Chapter 5. The procedures to measure the applied surface stresses ratio (ASSR) as one of the parameters to compute the shakedown limit, involved the direct measurement on the wheel tracking equipment. These are presented in Chapter 6 together with the presentation of the test results.

How to obtain the theoretical shakedown limit for the homogeneous and layered pavements is described in Chapter 7, including the implication of this research for engineering practice. The computed shakedown limits are then compared to the experimental results and reported in this chapter. Finally, Chapter 8 presents the conclusions of this research and gives suggestions for future work.

## **2 LITERATURE REVIEW**

### **2.1 PAVEMENT ENGINEERING**

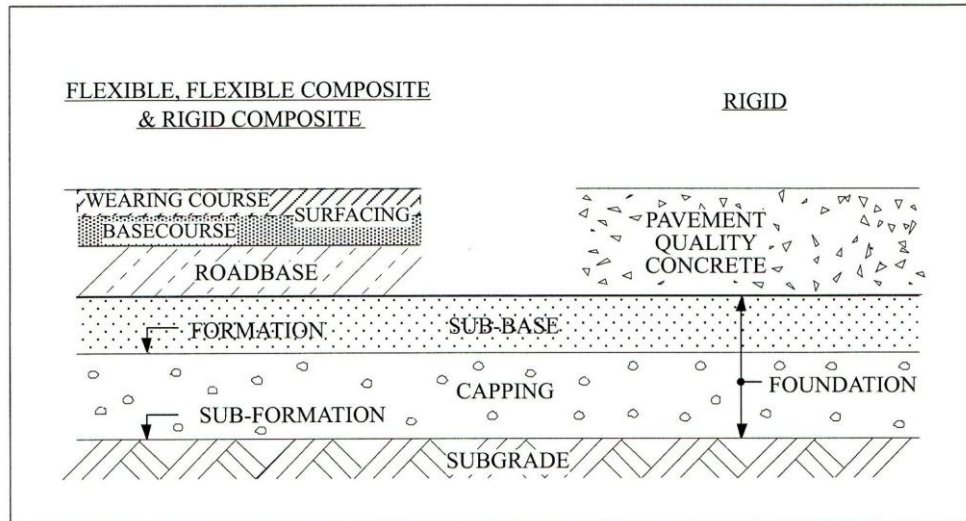
#### **2.1.1 Introduction**

This chapter presents a literature review of the typical pavement distress modes that are identified in practice, current pavement design methods and the limitations, the experimental investigations proving the existence of the shakedown behaviour, and the understanding of the soil and granular material response under repeated wheel load based on experiments. Due to the wide scope of pavement engineering and limited time, the research and review will only be focused on the sub-grade and foundation layers of a pavement.

#### **2.1.2 Pavement Distress Modes**

Pavements are designed and built to support wheel loads of widely different magnitudes, speeds and intervals between their applications at any given point on the pavement surface. Two types of pavements that are generally found in service are flexible and rigid (see Figure 2.1).

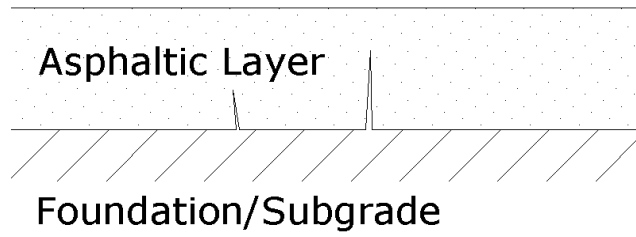




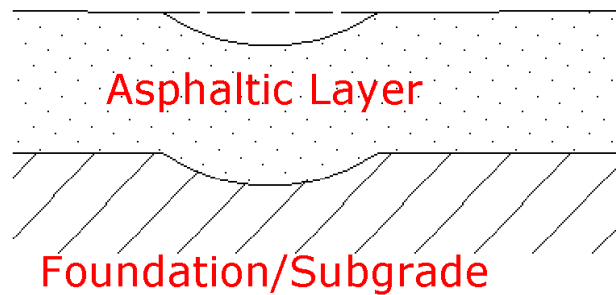
**Figure 2. 1 Typical pavement cross sections (after Highways Agency, 2003)**

There are several types of pavement distresses. Miller and Bellinger (2003) categorised the modes of pavement distress normally encountered in asphalt flexible pavements into five groups, which are as follows: (a) fatigue cracking; (b) surface deformation or rutting; (c) patching and potholes; (d) surface defects such as bleeding, polished aggregate and ravelling; and (e) miscellaneous distress such as bleeding and lane to shoulder drop off.

An adequate resurfacing or removing the excess bituminous binder will cope with the problems from (c) to (e). Fatigue cracking and surface deformation (see Figures 2.2a and b respectively) are of most concern to highway engineers. In practice, these two are frequently used as design criteria. More about the adoption of these two as design criteria can be found in the analytical pavement design method section (2.1.3).



**(a) Fatigue cracking**



**(b) Surface deformation**

**Figure 2. 2 Types of distress in pavements**

### **2.1.3 Pavement Designs**

The two basic pavement design methods for flexible pavements are empirical and analytical. The empirical method is derived from observations of the performance of experimental pavements laid either on public roads subjected to normal road traffic, or on test tracks where the loading is controlled. The analytical method is based on the structural analysis of pavements and the prediction of their performance from the computed parameters.

### ***The Empirical Pavement Design Method***

The development of the empirically based pavement design method from various organisations has been comprehensively reviewed by Monismith and Brown (1999). It was noted that one of the oldest empirical methods and still widely used around the world including the United Kingdom is based upon the California Bearing Ratio (CBR) test. The CBR test procedure is described in the British Standard 1377:4 (1990). The principle is to determine the relationship between force and penetration when the plunger is penetrated into the soil sample at a given rate. The loads at a penetration of 2.5mm and 5mm are compared with the result of a standard sample and the ratio, expressed as a percentage, is the CBR value of the soil. The soil CBR value is used to identify the thickness of the foundation layers that is required to improve and protect the subgrade. A step by step account of the current British pavement design procedure is described in HD24, 25 and 26 Volume 7 of the Design Manual for Roads and Bridges (Highways Agency, 2003). The thicknesses of the foundation layers (see Figure 2.1) for new roads in Britain are calculated using empirical derivation design charts based on the sub-grade CBR (Highway Agency, 2003).

According to Croney and Lister (1965), the CBR method which only considers the sub-grade strength may be applicable for a thin layer of surfacing. For the thick surfacing, the deformation of the surfacing under the application of heavy axle loads becomes crucial and needs to be taken into account in pavement

design for longer pavement serviceability. The application of the CBR method in the latter case becomes inappropriate.

Brown (1996) in the 36<sup>th</sup> Rankine Lecture to the British Geotechnical Society has highlighted the important roles of soil mechanics in pavement engineering. The background of the CBR method as an essential tool for pavement design and the shortcomings of the method in connection with soil mechanics principles has been reviewed and presented by Brown (1996 and 1997). He highlighted the problems of the CBR test, which does not comply with soil mechanics principles, for example having no control over the effective stress in the mould and the drainage conditions, and no correlation between the CBR tests and resilient modulus.

### ***The Analytical Pavement Design Method***

The point of the analytical design method is to find an appropriate combination of thickness and material types for a pavement that either precludes or minimises the various forms of distress induced in a specific pavement from traffic and environmentally related factors for the selected design periods (Monismith and Brown, 1999). The majority of the current analytical design methods assume a simplified multi-layer linear elastic model for the pavement structure. Each layer is characterised by the stiffness or resilient modulus of that layer to represent the stress versus strain relationship of the pavement material. The stiffness or resilient modulus becomes an input to the theoretical models to calculate stresses, strains and deflections (the ‘response’ of the

pavement) for given loadings in a pavement structure. These computed values are used to estimate the pavement performance associated with the distress modes: fatigue cracking and rutting. The process is repeated with different layer thicknesses and/or materials until the performance criteria are attained.

Fatigue cracking is normally considered by limiting the horizontal tensile stress or strain at the bottom of a bituminous or cement bound road base due to traffic loading. There are two approaches to consider rutting which are by limiting the vertical compressive strain on the sub-grade and by estimating the surface rutting from each of the pavement components. The estimation criteria for rutting and fatigue cracking are empirically derived from observed performance of in-service or test roads or laboratory tests.

The limitation of the limiting strain is that the empirically derived limiting strains are valid for certain materials, environmental, and loading conditions. The application to other materials becomes inappropriate. Barksdale (1972) compared the plastic stress-strain response for different densities, water contents, and road base materials after 100,000 load repetitions and found a different rutting characteristic from each material. Brown and Brunton (1987) performed repeated load triaxial tests on various road base materials and found a different permanent deformation characteristic for each material. There is clearly a need for a more unified procedure which considers both the elastic and plastic properties in terms of stiffness and shear strength respectively of each proposed material.

### **2.1.4 Experimental Observation of Shakedown Behaviour in the Pavement**

The test results from experimental observations by various investigators which involved a series of direct repeated wheel load or repeated load tests have shown the existence of the shakedown behaviour in pavement materials. When the applied load on the pavement surface was above the shakedown limit, the vertical surface deformation increased rapidly and caused rutting or failure on the pavement surface after a lower number of load repetitions. However, when the applied load was below the shakedown load, the vertical surface deformed initially and remained constant for a large number of load repetitions. For design purposes, this implies that the maximum shakedown limit must be known and then not exceeded, thus uncontrolled permanent deformations can be prevented.

A list of observations that involved repeated load triaxial tests and are related to the shakedown response of various types of pavement materials is shown in Table 2.1. A comparison of the deformation data under repeated stresses and the maximum compressive stresses of the test materials ( $\sigma_{s \max}$ ) shows that the shakedown limit may be significantly lower than  $\sigma_{s \max}$  (see Table 2.1).

These experimental observations relate the test results with the soil compressive strength only. Therefore, the objective of the research is to compute the shakedown based numerical model that uses the soil shear

strength as an input parameter and compare the computational results with the experimental results which involves a series of direct wheel tracking tests.

**Table 2. 1 Summary of experiments using repeated load triaxial apparatus associated with shakedown concept**

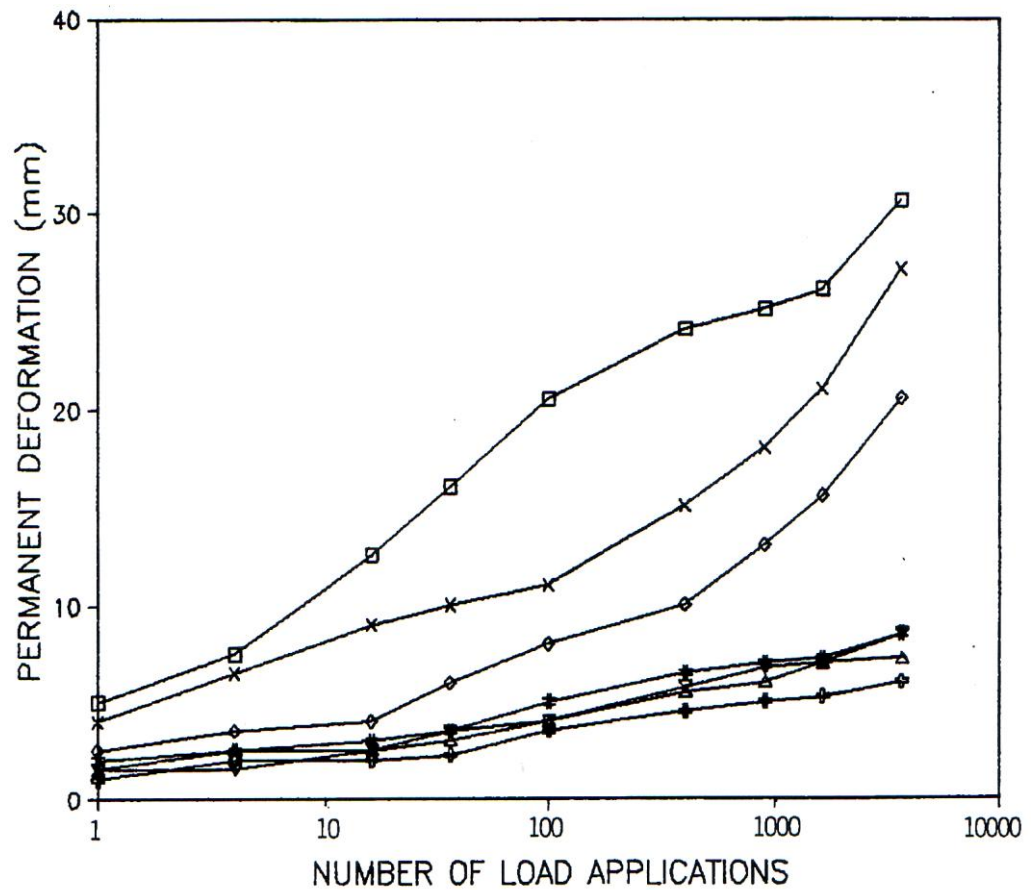
<b>Researches</b>	<b>Types Observation using Repeated Load Triaxial</b>	<b>Type of Specimen</b>	<b>Shakedown Limit</b>
Larew and Leonards (1962)	Varying the deviator stress under undrained repeated load triaxial tests with a constant confining pressure for all the tests.	• Compacted limestone residual clay with 80% of degree of saturation	Between 0.84 and 0.91 of $\sigma_{smax}$
Sangrey et al. (1969)	Varying the deviator stress under undrained cyclic compression loading with axial strain rate of 0.0002%/min.	• Isotropically normally consolidated undisturbed saturated clay	Two-third of $\sigma_{smax}$
Lashine (1971)	Varying the deviator stress under undrained cyclic compression loading with the fixed frequency of load application of 5Hz, and constant confining pressure of 20psi.	• Anisotropically normally consolidated Keuper Marl	Between 0.75 and 0.85 of $\sigma_{smax}$
Wilson and Greenwood (1974)	Observing the relationship between pore water pressure and axial strains under undrained repeated load tests.	• Isotropically normally consolidated lacustrine silty clay	0.37 of $\sigma_{smax}$
France and Sangrey (1977)	Each specimen has different deviator stress levels ranging from 40-88% under semidraind cyclic compression loading	• Isotropically over-consolidated clay with OCR=8	0.65-0.7 of $\sigma_{smax}$

Larew and Leonards (1962) did a series of undrained repeated load tests on Piedmont Micaceous silt and coastal plain sandy clay in which the deviator stress for each test was varied and the confining pressure was constant. They only reported there was a critical value for sandy clay but no further information regarding the exact critical limit or the range for the critical limit. However, from the plot of the deformation against number of load repetition curves for sandy clay, it seemed that the critical limit for sandy clay is ranging from 0.98 to 1.11 of  $\sigma_{\text{smax}}$ .

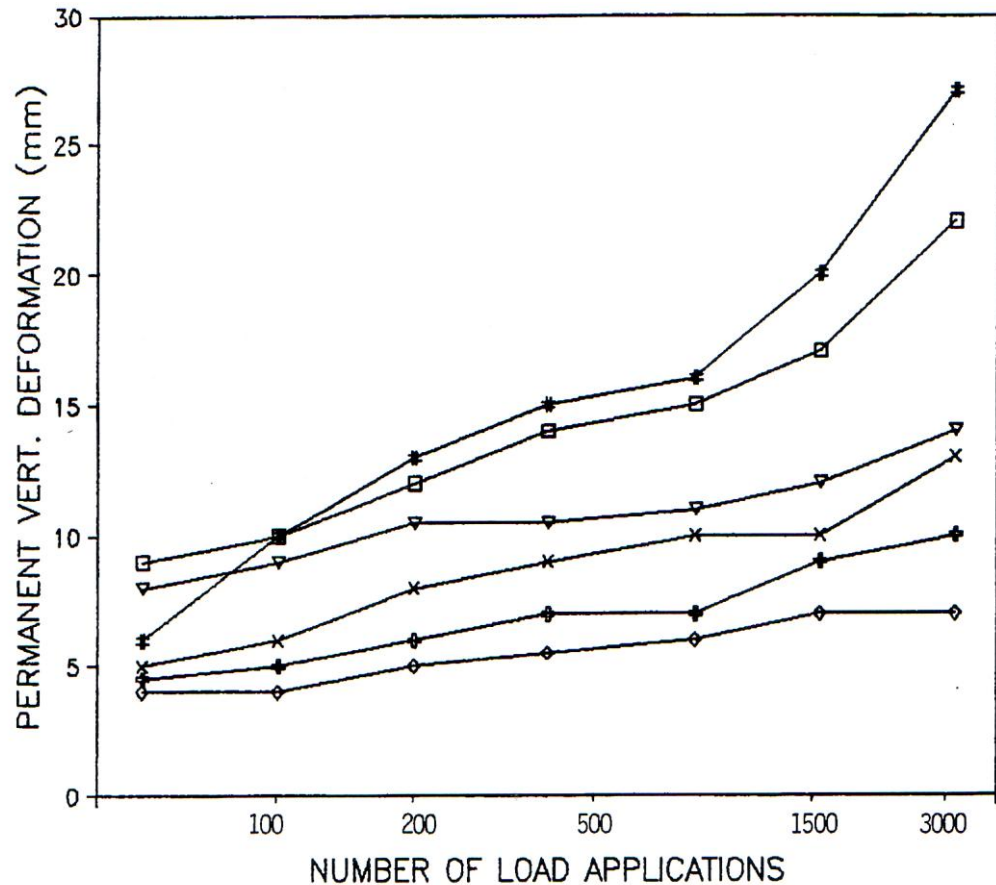
Sangrey et al. (1969) found, for various consolidation histories of saturated clay such as overconsolidated, isotropic and anisotropic normally consolidated, that the shakedown behaviour existed and varied for any consolidation history.

An extensive work on prediction of permanent deformation in soils and granular materials has been carried out in Nottingham University. Typical forms of the permanent deformation curves versus logarithmic scale of number of load applications are presented in Figures 2.3 and 2.4.





**Figure 2. 3 Variation of Permanent Vertical Deformation with Number of Load Applications for the Rutting Tests carried out in the Slab Test Facility (after Chan, 1990)**

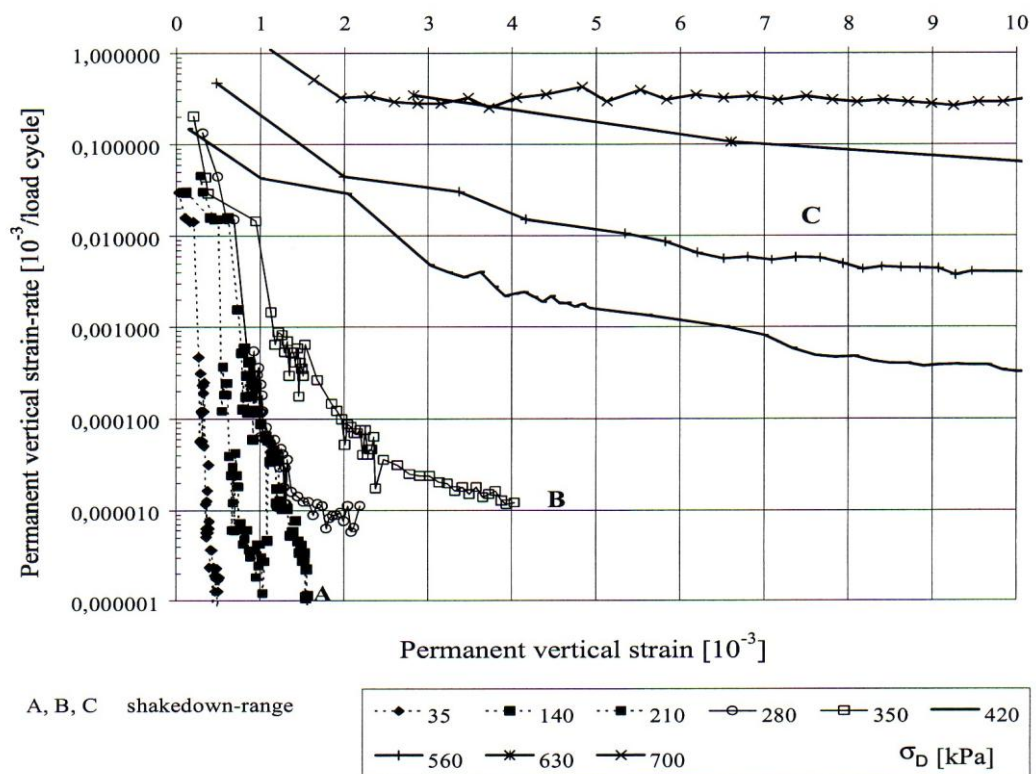


Symbol	Type of Granular Base	Grading of Granular Base	Type of Loading
⊕	Dolomitic Limestone	Type I	Uni-directional
▽	Dolomitic Limestone	Type I	Bi-directional
◇	Dolomitic Limestone	Optimum	Uni-directional
×	Dolomitic Limestone	Optimum	Bi-directional
#	Carboniferous Limestone	Open	Uni-directional
□	Carboniferous Limestone	Open	Bi-directional

**Figure 2. 4 Variation of Permanent Vertical Deformation with Number of Passes of Wheel Load for the Rutting Tests carried out in Pavement Test Facility (after Chan, 1990)**

Werkmeister et al. (2001) working on repeated load tests on granular materials reported the results by plotting the permanent vertical strain rate against permanent vertical strain accumulations. Based on the plot (see Figure 2.5), they categorised the response of the granular materials to three regions which

are region A, B and C. The granular materials with the shakedown response are categorised as in region A or the plastic shakedown range. Meanwhile, the regions B and C represent the intermediate response or plastic creep and incremental collapse respectively. Region A is for all the responses that are related to the elastic response which is initially plastic indicating the compaction period. After the post-compaction period the response becomes purely resilient. When the load increases to a certain level, the response in region B is initially plastic, then elastic for a certain number of cycles and then continues with plastic behaviour. At the region C, the response is always plastic and further load repetitions increase the permanent strain and lead to failure.



**Figure 2. 5 Cumulative permanent strain versus strain rate of Granodiorite, with  $\sigma_3 = 70\text{kPa}$  (after Werkmeister et al., 2001)**

Werkmeister et al. (2005) proposed a model to define the boundary of each region as follows:

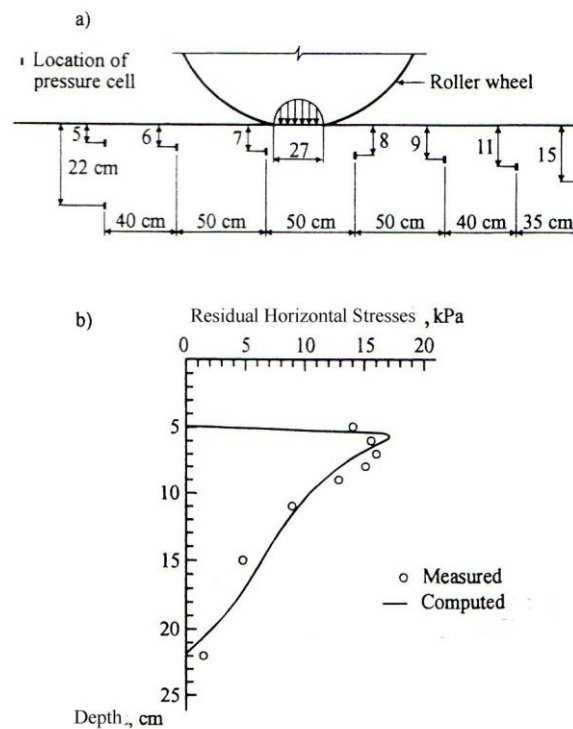
$$\sigma_{1\max} = \alpha \cdot \left( \frac{\sigma_{1\max}}{\sigma_3} \right)^\beta \quad (2.1)$$

where	$\sigma_{1\max}$	[kPa]	peak axial stress,
	$\sigma_3$	[kPa]	confining pressure (minor principal stress),
	$\alpha$	[kPa]	material parameter,
	$\beta$	[-]	material parameter.

According to Werkmeister et al. (2005), the material parameters,  $\alpha$  and  $\beta$ , were likely to depend on the grading, particle shape, degree of compaction, and the moisture content of the materials.

Instead of performing the repeated load triaxial tests and measuring the permanent vertical strain, Radovsky and Murashina (1996) conducted a full-scale experiment to prove the applicability of the shakedown concept in soil under repetitive loads. The full-scale experiment was conducted on the road between Kiev and Kharkov in the Ukraine. The residual horizontal stresses were measured using pressure cells which were installed below the subgrade surface at various depths as illustrated in Figure 2.6a. Silty loam as a sub-grade layer with an initial dry density and moisture content of 1.52Mg/m<sup>3</sup> and 15% respectively was compacted, using a semitrailer roller with five tyres and a wheel weight of 14.8kN, to a final dry density of 1.72 Mg/m<sup>3</sup>. From the measurement results (see Figure 2.6b), they found that the residual stress

increased with the number of repetitions and reached a constant value after a few dozen repetitions. The maximum residual horizontal stress did not occur immediately below the loaded area. A comparison of the residual horizontal stresses within the soil sub-grade from the full-scale experiment measurements and a theoretical analysis model shows that the shakedown theory may apply to describe the behaviour of sub-grade soils. The theoretical analysis developed by Radovsky and Murashina (1996) will be reviewed in section 2.2.2.



**Figure 2. 6 Horizontal stress distribution from full scale experiment (after Radovsky and Murashina, 1996)**

### **2.1.5 Wheel Load on a Pavement Surface**

The wheel load is transmitted to the pavement surface through the tyre. The pavement structure then reduces the intensity of the load stresses with depth. The pavement performance depends on the intensity and distribution of these load stresses. From the experimental measurements by various investigators using different sensor devices and methods (see Table 2.2), it shows that the moving wheel load transmitted to the pavement surface through the tyre is not constant, and is influenced by irregularities in the road surface, inflation pressure, speed and running conditions, e.g. acceleration, braking, and deceleration.

The limitations of the observations using the wheel tracking apparatuses in this research are the inability to vary the speed of the wheel, performing the acceleration, and deceleration to demonstrate the loading condition on a real pavement which may affect the pavement performance. Therefore, factors that may affect the direct wheel tracking test results are reviewed and discussed in this section.

#### ***Typical Design Traffic Load***

The design of new roads in UK over the design life requires knowledge of the total flow of commercial vehicles in one direction per day at the road's opening, and the proportion of these vehicles with more than four axles, either rigid or articulated, which are categorised as the Others Goods Vehicle (OGV) 2 (Highway Agencies, 2003). Generally, the commercial vehicles are defined as

those over 15kN unladen vehicle weight and wear from private cars is deemed negligible. According to HD24/96 (Highways Agency, 2003), the total flow of commercial vehicles is calculated using the commercial vehicles, traffic growth and wear factors. The Asphalt Institute and Shell pavement design manual develop equivalence factors to convert each load group into repetitions of an equivalent 80kN single axle load. This approach has been widely adopted in many countries.

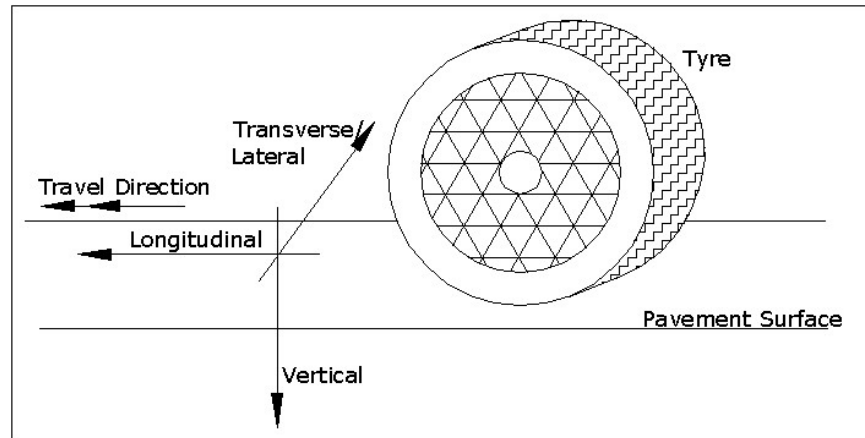
**Table 2. 2 Sensors or methods to measure tyre and road interaction**

<b>Researchers</b>	<b>Sensor Types/Methods</b>	<b>Usage</b>
Marwick and Starks (1941)	The mechanical stress was converted into an electrical quantity using carbon resistor element ( $\frac{1}{8}$ inch in diameter and $\frac{3}{8}$ or $\frac{5}{8}$ inch long and a resistance of approximately 50,000 ohms) in road to record the stress distribution under the tyre.	To measure normal and shear stresses on a road surface under stationary and moving wheels.
Bonse and Kuhn (1959)	The stress recorder box was installed under the road surface in a special manhole on the centre line of the road, with electronic and photographic gear housed in a mobile laboratory on the roadside.	To measure vertical, longitudinal, and transverse forces through the photographic traces.
Himeno et al. (1997)	Piezo electric ceramics sensors, 14mm wide and 18mm long.	To detect loading weight and vehicle speed applied on the sensor while a tyre passes by.
De Beer et al. (1997)	The Vehicle-Road Surface Pressure Transducer Array (VRSPTA) consists of an array of triaxial strain gauged steel pins fixed to a steel base plate, together with additional non-instrumented supporting pins, fixed flush with the road surface.	To measure contact stresses under moving loads.

### ***Types of Stresses between Tyre and Road***

From the experimental investigations, the researches identified three different directions of basic stresses/forces under a moving wheel load, namely: vertical, longitudinal, and transverse/lateral. Definition of each stress is illustrated in Figure 2.7. The effect of each stress direction as a result of the contact between the tyre and the road surface was investigated.





**Figure 2. 7 Definition of vertical, longitudinal and transverse/lateral direction**

Typical contact stress distributions for a slow moving (1.2km/h) free rolling smooth single truck tyre, Goodyear 11.00x20.14 ply rating measured with the VRSPTA systems by de Beer et al. (1997) is shown in Figure 2.8. The inflation pressure of the wheel was kept constant at 620kPa but the wheel load was varied between 20kN and 80kN. It shows that the maximum vertical stress is not centred, and the transverse stress is zero at the tyre centre, and also the instability of the longitudinal stress distribution due to the moving wheel load depending on load and inflation pressure. Marwick and Starks (1941) found that the horizontal stresses under a moving tyre in dry conditions experienced a rapid alternation as the tyre left the road whereas under wet conditions these alternations did not occur.

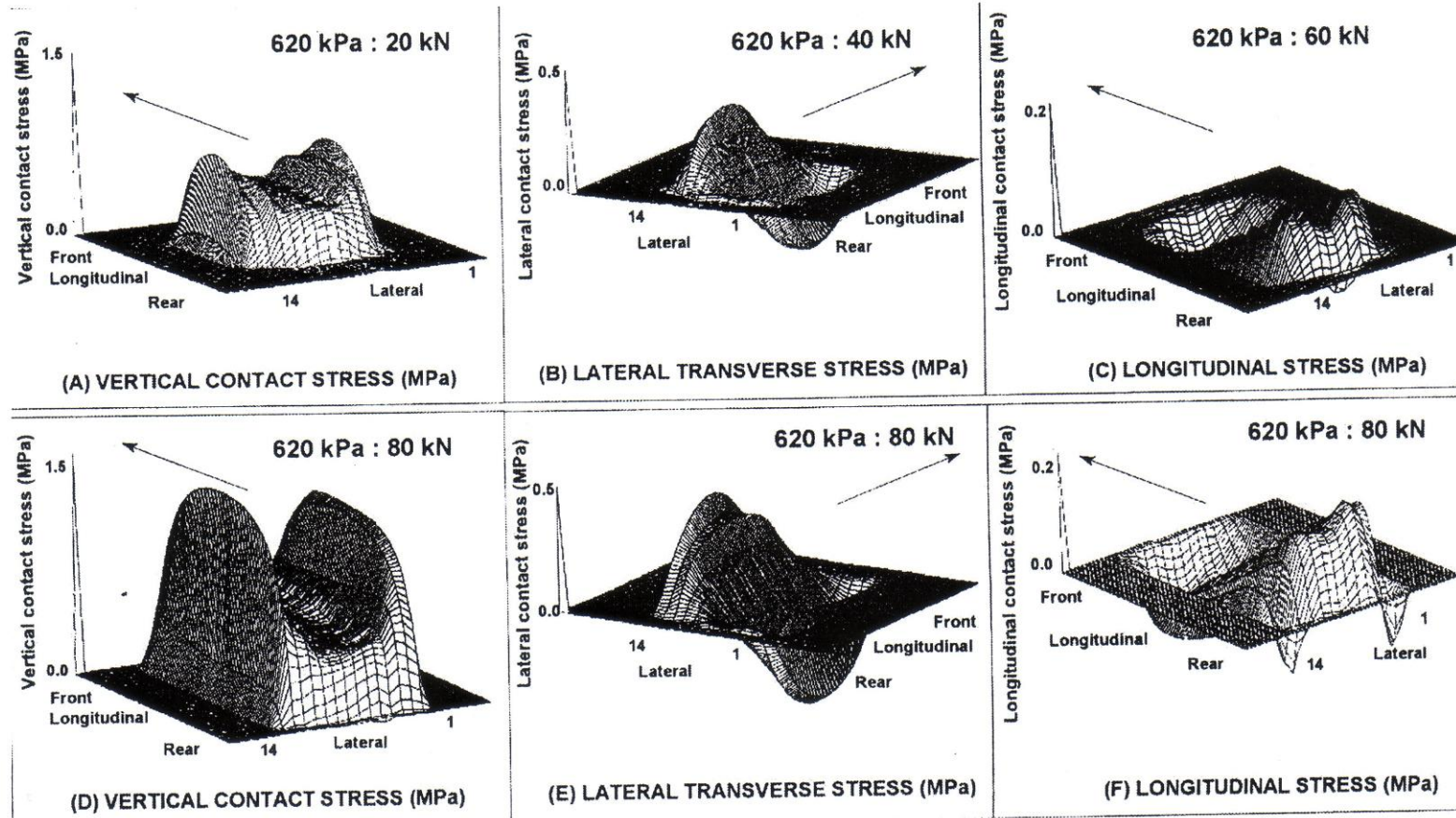


Figure 2. 8 Typical contact stress distributions measured with VRSPTA system (after de Beer et al., 1997)

### ***Effect of the axle configuration***

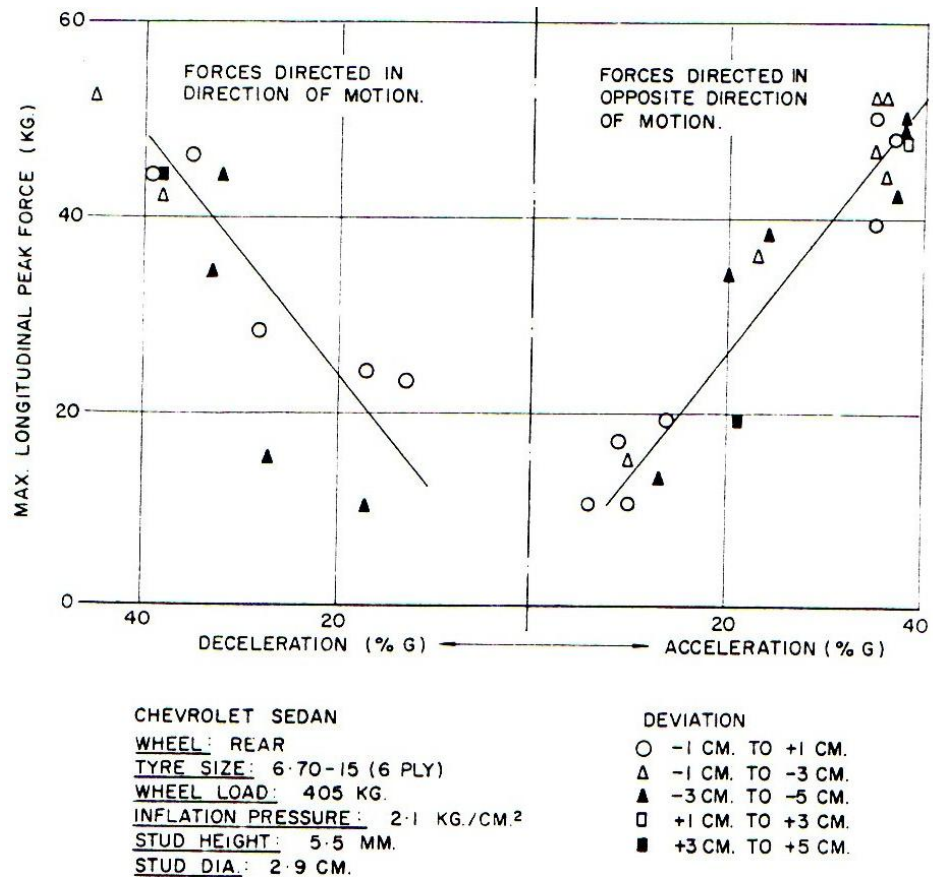
The wheel tracking tests involve a single wheel load test. In service, the road is normally subjected to at least dual wheels and various axle configurations. Fernando et al. (1987) found that the axle configuration (single-, tandem, and triple-axle assemblies) did not significantly affect the pavement response, provided that the load per tyre remained the same. According to Huang (1993), the pavement structure is overdesigned if each axle is treated independently and considered as one repetition, and underdesigned if the tandem and tridem axles are treated as a group and considered as one repetition.

### ***Effect of wheel load when it is stationary and moving on the contact stresses***

In-service pavements always experience stationary, deceleration and acceleration effects at various wheel loads. Bonse and Kuhn (1959) varying the acceleration rate between 10%g and 30%g and deceleration rate between 20%g and 40%g found a significant impact on the stress distribution in the longitudinal or travel direction. The 'g' represents the gravitational acceleration. Figure 2.9 shows that the acceleration or deceleration of the Chevrolet Sedan with wheel load of 405kg increases the maximum longitudinal stresses.

Bonse and Kuhn found an insignificant difference between the vertical stresses under moving and stationary wheels and that vertical stresses are independent of speed. This later finding confirmed the earlier result that was obtained by Marwick and Starks (1941) who compared the results from a stationary wheel

and a wheel with a speed of 40mph. Although Himeno et al. (1997) changed the speed by  $\pm 30$ km/h from an original speed of 30km/h, the vertical stress distribution was unaffected.



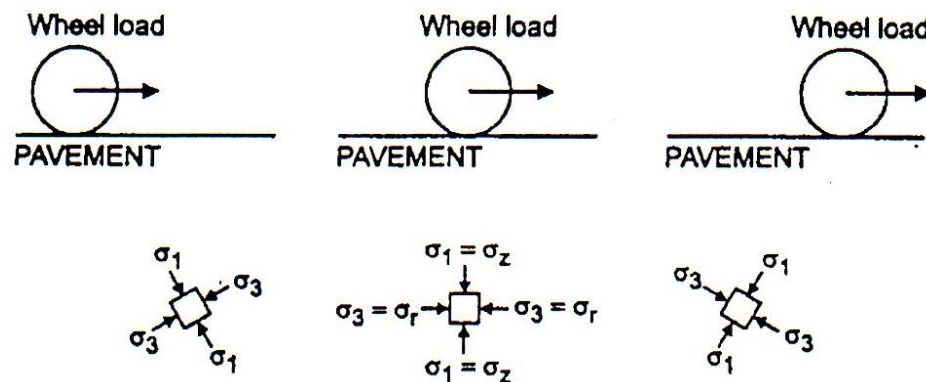
**Figure 2. 9 Relationship between maximum horizontal longitudinal force and amount of acceleration/deceleration (after Bonse and Kuhn, 1959)**

The significant difference in the longitudinal stress between the moving and stationary wheel will affect the shakedown limit of the structure. A review of the shakedown based analysis is provided in Section 2.2. The ratio between the horizontal and vertical stresses is expressed as the applied surface stresses ratio (ASSR). Beside the acceleration and deceleration of the wheel, the applied surface stresses ratio of the vehicle depends on the surface roughness and the

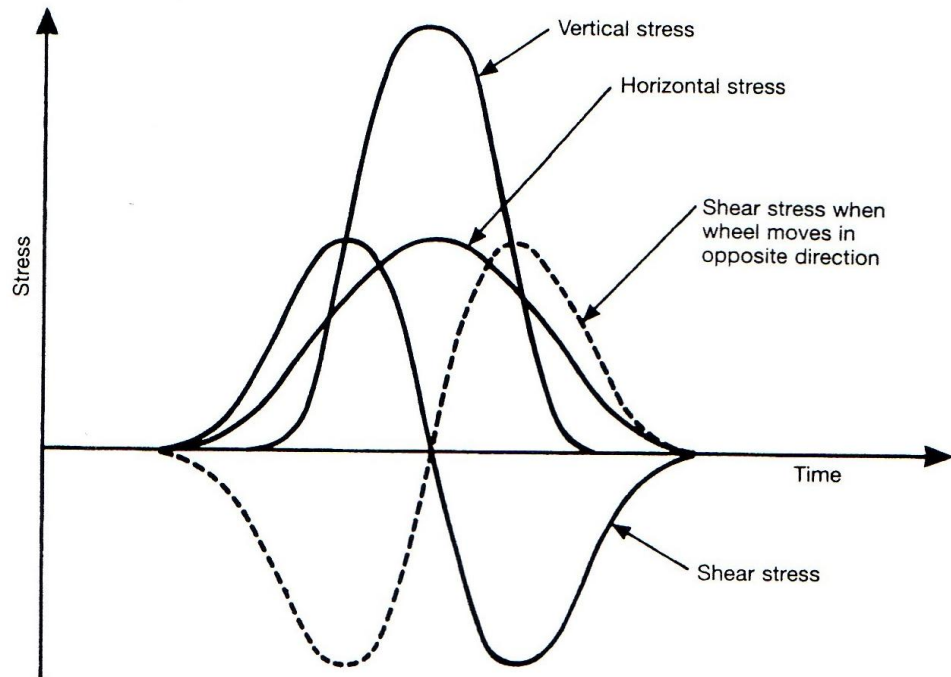
friction in the wheel bearings. Further discussion regarding the variety of the applied surface stresses ratio is given in Chapter 7.

### 2.1.6 Response of a Pavement Structure

When a wheel travels on a pavement surface, the response of the soil element beneath the wheel, as illustrated in Figure 2.10, depends on the stress strain characteristic from each layer of the pavement structure. A stress pulse induced in the subgrade/granular layer as result of the moving wheel is shown in Figure 2.11. When the wheel travels in the opposite direction, the shear stress direction will reverse (see the dash line in Figure 2.11). The shear reversal may contribute to the development of permanent deformation (Chan, 1990).

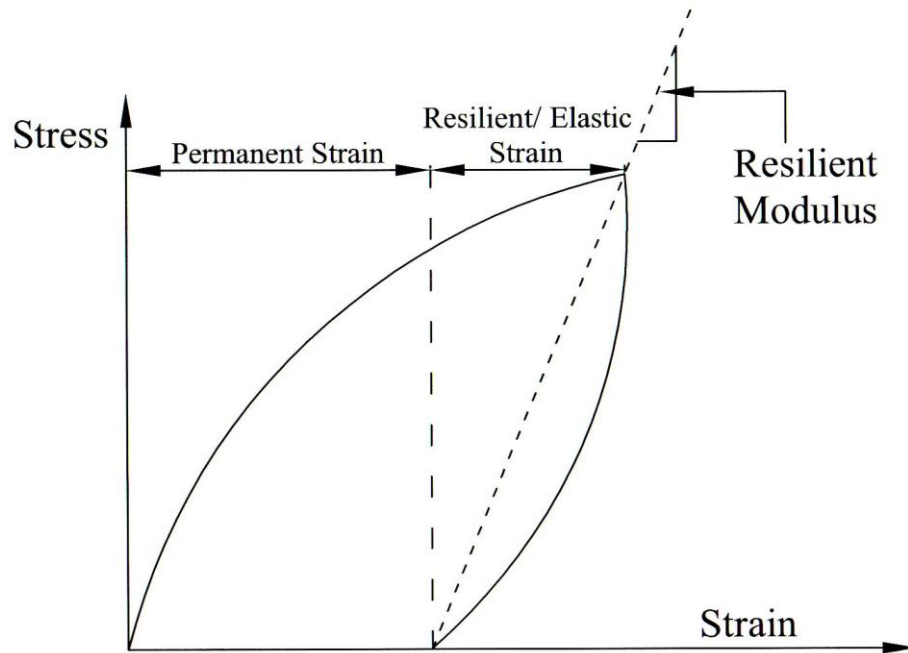


**Figure 2. 10 Stresses beneath rolling wheel load (after Lekarp and Dawson, 1997)**



**Figure 2. 11 Stress pulses induced by a moving wheel (after Chan, 1990)**

Two types of pavement response that are widely observed and analysed by researchers are elastic (recoverable/resilient) and plastic (permanent). These responses are identified from the two different strains that were measured during the unloading and reloading process: recoverable (resilient) strain and permanent strain (see Figure 2.12). The resilient modulus of the sub-grade soil or the granular material under repeated load is defined as the ratio of the repeated deviator stress to the recoverable (resilient) axial strain (see Figure 2.12).



**Figure 2. 12 Strains as results of stress pulses during one cycle of load application**

### ***Granular Materials***

Lekarp et al. (2000a and 2000b) carried out an extensive review on the resilient and permanent strain response of unbound aggregates and pointed to the applied stress level as the most significant factor affecting those responses.

The number of load applications to reach the equilibrium state in which the permanent strain ceases to increase depends on the applied stress. Brown (1974) investigated the behaviour of crushed granite and found that an equilibrium state was reached after approximately 1000 cycles. Werkmeister et al. (2004 and 2005) conducting a series of repeated load triaxial tests on sandy gravel noted a small increment of plastic strain after more than 700,000 load repetitions.

### *Clayey Soil*

The factors affecting the response of clay are the stress level, stress history, the material strength and probably the plasticity, moisture content and degree of saturation.

Seed and Chan (1958) applied higher repeated loads to two specimens after trying the same lower repeated load with a different loading period. They found that the specimen with a longer loading period at the lower load has a better resistance to deformation and at least 1000 repetitions were required to produce any appreciable deformation.

Cheung (1994) proved that the permanent deformation resistance of soils was a function of material strength by examining the permanent deformation characteristics of three different types of clayey soils after 1000 passes of wheel loading. He postulated the plasticity of the soil has a relation with the permanent deformation resistance and stiffness. For soils with the same strength, he found that the soils with the higher plasticity performed better in resisting permanent deformation.

Seed et al. (1958) studying the effect of repeated loading on the strength of a partially saturated clay found that the clay subjected to a certain number of load repetitions had a better resistance to permanent deformation than the one without any load repetitions. France and Sangrey (1977) working on a laboratory sedimented and aged illite clay confirmed the effect of stress history



on the clay and reported that the strength of the material was approximately 30% and 15% higher than its original undisturbed undrained strength test for isotropically and anisotropically consolidated soils respectively.

Seed and Chan (1958) varying the degree of saturation of a silty clay and with a loading frequency range of 3 to 20 applications per minute reported that the frequency of stress application is more significant for the higher degree of saturation of a silty clay than the lower one.

### ***The Mechanism of the Elastic Response of a Pavement Structure***

Elastic response normally occurs when the repeated stress level is either lower or higher than the applied stress during the preloading period but below the maximum compressive strengths of the paving materials. The maximum stress level in which the paving materials behave elastically is known as the shakedown limit. When the applied stress is higher than the preloading, the pavement may respond plastically during the initial loading showing further densification or shear distortion at the loaded area.

Trollope et al. (1962) examined the behaviour of sand and sand bitumen under slow repeated loading and recommended applying a few slow passes of a heavy pneumatic tired roller, rather than a large number of passes of a light roller to eliminate the undesirable plastic response during initial loading.

Densification may cause the insignificant unbound aggregate particles reorientation and breakage in the sub-base layer (Werkmeister et al., 2005), and the reduction of pore pressure in the subgrade layer bringing the particles slightly closer together at the points of contact (Seed and Chan, 1958). The densification may occur in any or all pavement layers. Nevertheless, the densification increases the strength and stiffness of the materials.

According to Sangrey et al. (1969), when the stress level was below the shakedown limit, the pore water pressure and the deformation in the saturated clay, with an axial strain rate of about 0.0002%, increased as the number of repetitions increased until a maximum value was reached. Once the maximum value of the sample was reached, further load repetitions caused no changes in the deformation and pore water pressure and the stress-strain and pore water pressure-strain curves formed closed hysteresis loops. The stress paths for elastic response do not approach the failure envelope. The build up of pore water pressure leads to migration of the stress path towards the stress origin until non-failure equilibrium is reached. Wilson and Greenwood (1974) found that the relationship between pore pressure and strain was linear when the applied load was in the elastic range. The plot of pore pressure and strains measured against the repeated load is shown in Figure 2.13.  $\sigma_s$  represents the compressive strength of the specimen obtained from a standard consolidated undrained strength test with a constant axial strain rate of 0.055%/min.

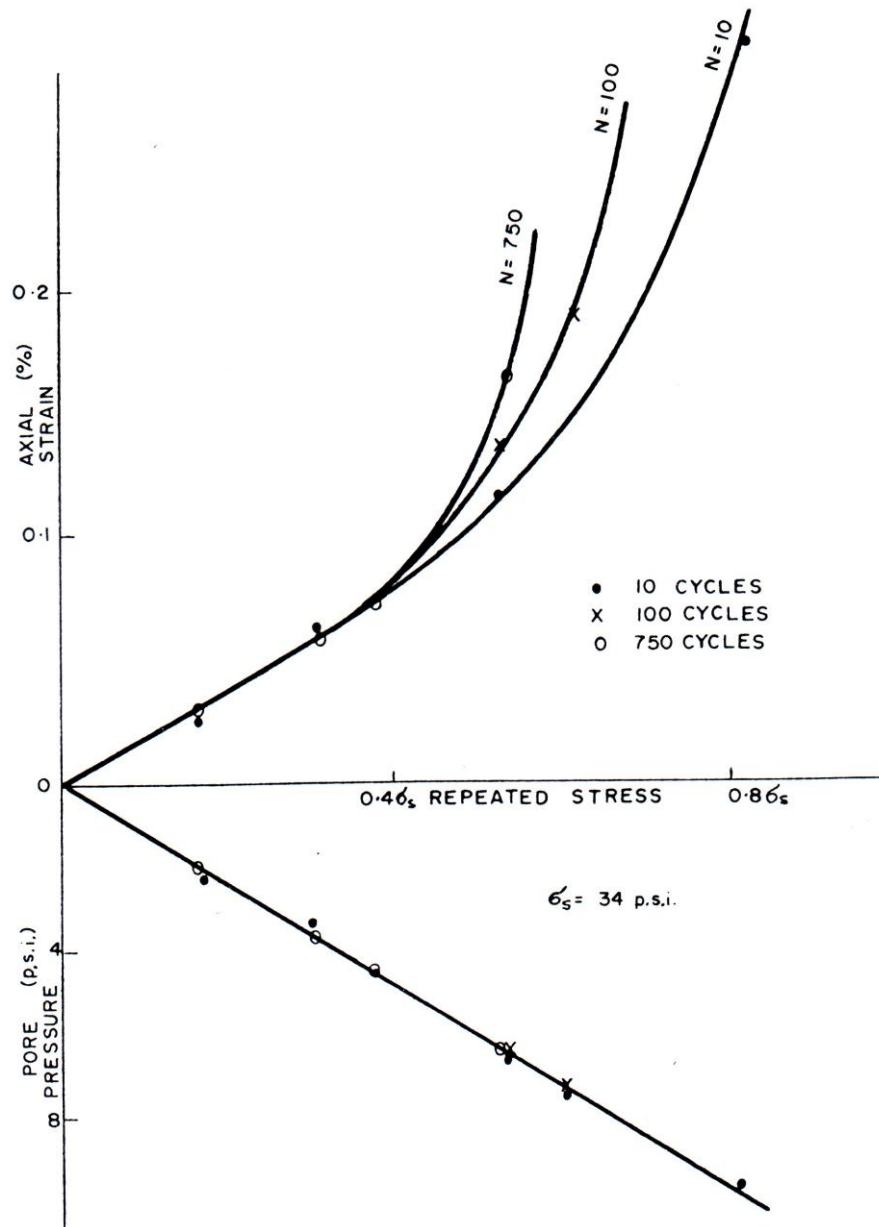


Figure 2. 13 Elastic and plastic ranges of repeated loadings (after Wilson and Greenwood, 1974)

### *The Mechanism of Plastic Response of Pavement Structure*

According to Monismith and Brown (1999), rutting as a form of excessive plastic response may be due to the densification (decrease in volume and hence increase in density) and/or the shear distortion at the pavement surface below

the wheel. It appears as longitudinal depressions in the wheel paths accompanied by small upheavals to each side.

According to Werkmeister et al. (2004 and 2005), specimens consisting of a granular material initially experienced the development of a denser structure and an increment in the number of grain contacts which was associated with a stiffening response. In this period, the breakage of the material occurred as a result of the applied load exceeding the strength of the grains. The breakage of material may be followed by large scale particle reorientation and instability of the aggregate skeleton at the initial loading period or after a further number of load repetitions. Until a certain level, the friction between the grains was insufficient to support the external stress and incremental collapse occurred. No information regarding the pore water pressure condition in a granular material was reported.

Beside the extreme plastic response (referred to region C in Figure 2.5) which may only involve a small number of load repetitions, Werkmeister et al. reported another type of response (referred to region B in Figure 2.5) which was initially elastic but a small increment of plastic strain was observed, yet without stiffening (without strain hardening) after more than 700,000 load repetitions. They considered this response as a slow rate of damage which may be due to the particle contact attrition rather than particle breakage although there was some minor particle breakage. The grain attrition decreases the resistance to the friction between the grains and angle of internal friction.

Sangrey et al. (1969) reported that under higher stress level the pore water pressure in saturated clay was increased markedly during the loading period and increased further on unloading. This pattern was repeated until the effective stress of the sample reached the failure envelope and the permanent deformation increased remarkably.

The plot of the pore pressure and strain against repeated stress in Figure 2.13 above shows a curve away from linearity when the applied load is above the elastic range. According to Wilson and Greenwood (1974), the individual grains started to shear between each other and this was accompanied by the continuing process of grain structure collapse under load.

## **2.2 NUMERICAL MODELLING USING THE SHAKEDOWN CONCEPT**

### **2.2.1 Introduction**

When a material is under repeated load, its response may be irreversible or plastic for a certain number of initial repetitions and eventually either purely elastic in a resilient manner or continue to be plastic which eventually leads to collapse or failure. The shakedown limit is the limit that separates these two types of responses and in which the material under repeated load satisfies the yield condition. For a proper evaluation of the material response under repeated loading, it is insufficient to define alone the elastic or subfailure characteristics which relate to the lower bound limit of the material. It is essential to recognise the upper limit of possible elastic behaviour and it therefore becomes necessary to establish a failure criterion that takes full account of this upper limit. The unknown exact shakedown load must lie between these two limits.

Theoretical work based on the shakedown concept for pavement analysis using either lower or upper bound approaches has been carried out since the 1980s. Sharp (1983) modelled the pavement as an elastoplastic material and used the lower bound approach and the Mohr-Coulomb yield criterion to compute the shakedown limit. His work was followed up by Raad et al. (1988 and 1989),

Radovsky and Murashina (1996), Yu and Hossain (1997 and 1998), Yu and Shiau (1999 and 2000), and Yu (2005).

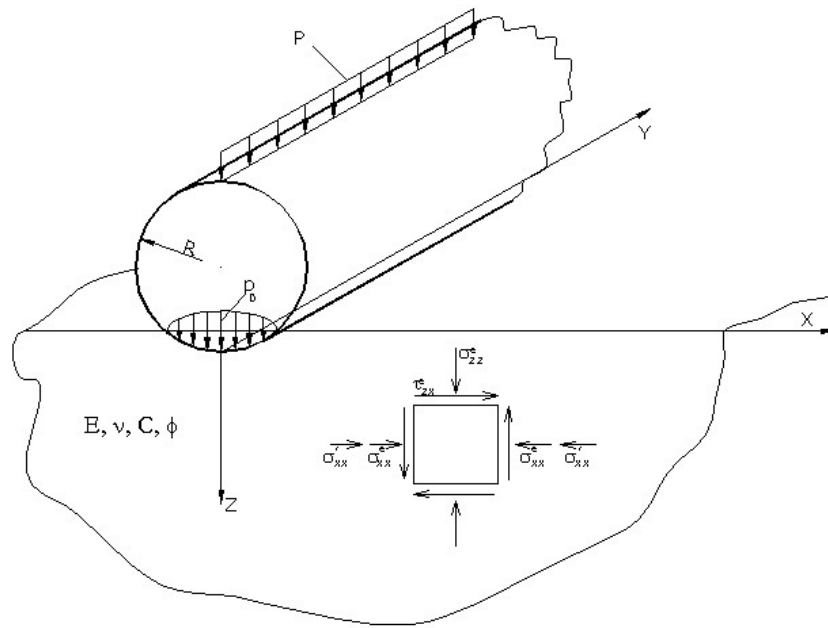
Collins and Cliffe (1987), Collins and Boulbibane (2000) [see also Boulbibane et al. (2005)], Chen and Ponter (2005), and Raad and Minassian (2005) [see also Zhang and Raad (2002)] employed the upper bound or kinematical approach with various proposed failure mechanisms. From their computation results, they concluded that the shakedown limit using the upper bound theorem provides a rational approach to pavement analysis.

Review of the principle of the shakedown concept, the application of the shakedown concept in the lower and upper bound approaches and the assumptions that were used to derive the shakedown based formulation for the application in pavement engineering is presented in this chapter.

### **2.2.2 Lower Bound Theorem**

Basically, the analyses involve finite element programs to compute the elastic stresses and a linear programming procedure to compute the best lower bound for the shakedown load. For ease of analysis, Sharp (1983) [see also Raad et al. (1988 and 1989), Radovsky and Murashina (1996), Yu and Hossain (1997 and 1998), Yu and Shiau (1999 and 2000), and Yu (2005)] simplified the single layered pavement structure as an isotropic homogeneous half space which is then applied for each layer of a multilayered structure. Elasticity modulus,  $E$ ,

and Poisson's ratio,  $\nu$ , of the material are used to represent the elastic constraints. The plastic constraints or strength of the material are represented by the *cohesion*  $c$  and the *angle of friction*  $\phi$ . The typical modelled structure and response of the soil element after a rolling load application for the one dimensional (1D) and two dimensional (2D) plane strain problems is shown in Figure 2.14.

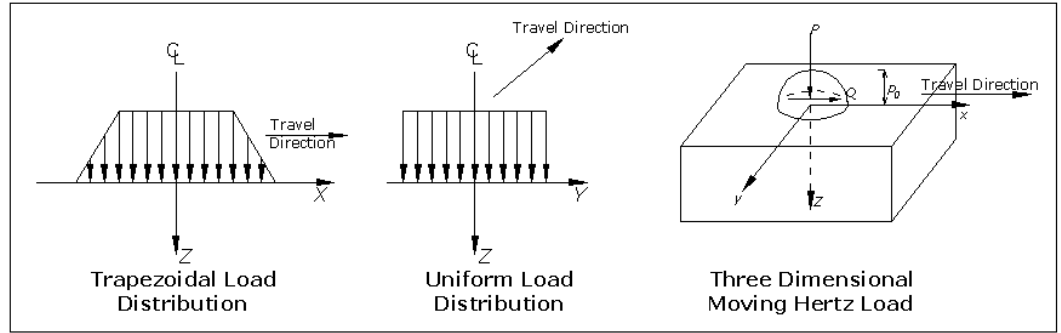


**Figure 2. 14 Representation of elastoplastic half-space under a rolling cylinder**

For 1D plane strain, the moving load was assumed to induce a trapezoidal load distribution along the travel direction and the wheel load was considered to be an infinitely wide roller [Sharp (1984), Sharp and Booker (1984), Sharp (1985), Yu and Hossain (1998), Yu and Shiau (1999 and 2000)]. The 2D plane strain moving load was considered to have uniform wheel load distribution in a vertical plane across the travel direction [Sharp (1983), Raad et al. (1988 and



1989), Radovsky and Murashina (1996), Yu and Hossain (1997 and 1998)]. For both the 1D and 2D plane strain moving loads, the permanent deformation and residual stress distribution will be uniform over any horizontal plane and vary with the depth only. The analysis of the 3D moving Hertz load assumed a circular loaded area with radius and stress distribution as in Yu (2005). The typical load distributions for the 1D, 2D and 3D shakedown analysis are illustrated in Figure 2.15.



**Figure 2. 15 Typical load distributions for shakedown analysis**

Melan's static shakedown theorem, which is known as the lower bound theorem, states that the material will be 'shaken' down if the combination of a time independent, self equilibrated residual stress field  $\sigma_{ij}^r$  and the elastic stresses  $\lambda\sigma_{ij}^e$  can be found which does not violate the yield condition anywhere in the region. Supposing that elastic stresses are proportional to a load factor  $\lambda$ , the total stresses are therefore

$$\sigma_{ij}^t = \lambda\sigma_{ij}^e + \sigma_{ij}^r \quad (2.2)$$

where

$\lambda$  = shakedown load factor

$\sigma_{ij}^e$  = elastic stresses resulting from a unit pressure application

$\sigma_{ij}^r$  = residual stresses remaining after load application as a function of depth.

For the yield criterion, the investigators who did lower bound approach used Mohr-Coulomb. The combination of elastic stresses and residual stresses had to satisfy the Mohr-Coulomb yield criterion which is expressed as follows:

$$(\sigma_1)_t - (\sigma_3)_t - [(\sigma_1)_t + (\sigma_3)_t] \sin \phi - 2C \cos \phi \leq 0 \quad (2.3)$$

where  $(\sigma_1)_t$  and  $(\sigma_3)_t$  are the total major and minor principal stresses respectively. An elastoplastic half space in a numerical model assumes that the residual horizontal normal compressive stress increases the shear resistance at all planes except the horizontal plane. Therefore, shakedown load depends on the maximum reduced shear stress on the horizontal plane in the elastic half-space due to the applied load. The structure is ‘shaken’ down if the following inequality is satisfied:

$$\left\{ \left( \lambda \sigma_{xx}^e + \sigma_{xx}^r - \lambda \sigma_{zz}^e \right)^2 + 4 \left( \lambda \tau_{xz}^e \right)^2 \right\}^{1/2} + \left( \lambda \sigma_{xx}^e + \sigma_{xx}^r + \lambda \sigma_{zz}^e \right) \sin \phi \leq 2C \cos \phi \quad (2.4)$$

The maximum shakedown load must satisfy the following expression:

$$\lambda \leq \frac{C}{|\tau_{xz}^e| + \sigma_{zz}^e \tan \phi} \quad (2.5)$$

All the researchers used the same principle to compute the lower bound shakedown limit. The differences between the models that were proposed by them are in the finite element programs that were used and application of the criteria within the element, for example Raad et al. (1988 and 1989) used a 4-noded rectangular element, Yu and Hossain (1997 and 1998) and Yu and Shiau (1999 and 2000) used a 3-noded triangular element. In Yu and Hossain's model, the total stresses were enforced at many sampling points within an element and the yield criterion was imposed at corner nodes for the residual stresses. Meanwhile, in Yu and Shiau's model, the yield conditions in terms of total stresses were satisfied at any point within an element provided that the yield criterion was enforced at corner nodes. Radovsky and Murashina (1996) and Yu (2005) referred to Johnson (1985) and Hamilton (1983) respectively to analyse the elastic stress fields. However, the difference in the computed shakedown limit between the models is insignificant.

### 2.2.3 Upper Bound Theorem

Koiter's kinematical shakedown theorem or upper bound theorem states that shakedown will not occur if any kinematically admissible plastic strain cycle can be found in which the work done by the external loads exceeds the internal rate of plastic work. Consider  $\varepsilon_{ij}^*$  and  $\sigma_{ij}^*$  as being the plastic strain-rate and

associated stress fields respectively which are obtained from any virtual velocity field,  $v_i^*$ , the shakedown can not occur if

$$\sigma_{ij}^* \varepsilon_{ij}^* = D(e_{ij}^*) \geq (\lambda \sigma_{ij}^e + \sigma_{ij}^r) \varepsilon_{ij}^* \quad (2.6)$$

at all points of a body V and at all times during a cyclic load. D represents the dissipation rate. By integrating this inequality over any points of a body V during a time period and using the principle of virtual work in which  $\sigma_{ij}^r$  vanishes due to self-equilibration with zero-tractions on the surface of V, the inequality can be rewritten as:

$$\lambda \leq \frac{\int_0^T \int_V \sigma_{ij}^* \varepsilon_{ij}^* dv dt}{\int_0^T \int_V \sigma_{ij}^e \varepsilon_{ij}^* dv dt} \quad (2.7)$$

in which the shakedown occurs. The numerator in this expression is the internal plastic dissipation rate,  $D^P$ , as in conventional limit analysis calculations. The denominator is the virtual elastic dissipation rate,  $D^e$ , obtained by multiplying the elastic stresses by the plastic strain rates and can be expressed as follows:

$$D^e = c^e [v_{xz}] \quad (2.8)$$

where

$v_{xz}$  = tangential velocity,

$c^e$  = elastic cohesion, defined by

$$c^e = |\tau_{xz}^e| - \sigma_{zz}^e \tan \phi \quad (2.9)$$

where  $\sigma_{zz}^e$  and  $\tau_{xz}^e$  are the normal and tangential elastic stress components respectively and  $\phi$  is the material friction angle. To facilitate the computation of the upper bound, the investigators proposed various failure mechanisms. Hence, the best upper bound condition is obtained by finding the smallest value of  $\lambda$ .

Collins and Cliffe (1987), and Collins and Wang (1992) considered failure mechanisms which consisted of sliding along channels under a wheel load in the travel direction as shown in Figure 2.16 to analyse the upper bound shakedown limit of the material under 3D moving Hertz load. They evaluated the elastic stress components (the normal and tangential elastic stresses) for each point on ST (see Figure 2.16) and on each x-coordinate from the formula given by Hamilton (1983). The maximum value of *elastic cohesion*  $c_{\max}^e$  and I as a function of the inclination  $\alpha$  of ST and of the depth  $z_0$  of S could be numerically determined along ST such that the best upper bound is the inverse of the maximum value from computing the function of the inclination  $\alpha$  of ST

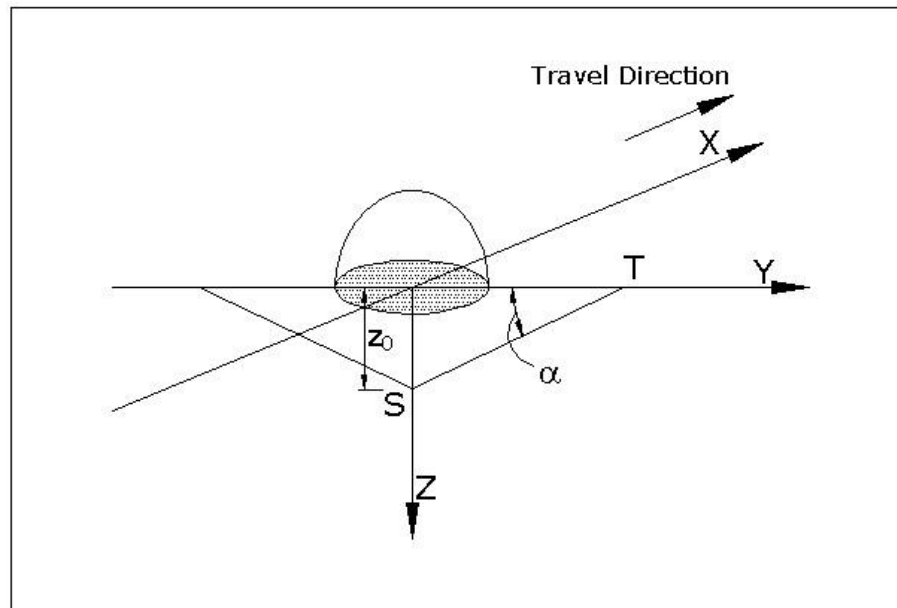
and of the depth  $z_0$  of S,  $\left(I_{\max}\right)^{-1}$ .

$$I = \frac{\int c_{\max}^e dl}{cl} \quad (2.10)$$

$$\lambda \leq \frac{1}{I} \quad (2.11)$$

where

$l$  = length of the channel wall.



**Figure 2. 16 The failure Mode for frictional material under 3D moving hertz load**

Collins and Boulbibane (2000) [see also Boulbibane et al. (2005)] proposed the failure mechanisms that consist of sliding or rotating rigid blocks in which the energy is only dissipated on the interfaces between the moving blocks. They

used Coulomb's failure criterion, characterised by the *cohesion*  $c$  and the *angle of friction*  $\phi$ . The plastic energy dissipation rate per unit length of a discontinuity is

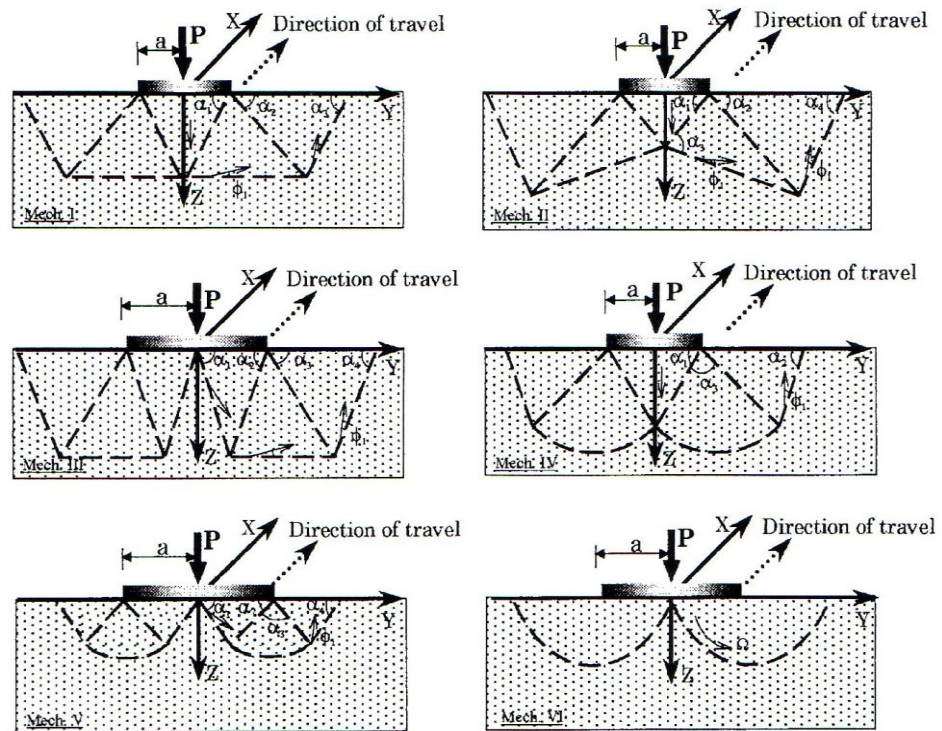
$$D^P = -\sigma^e_{zz} [v_{zz}] + |\tau^e_{xz}| [v_{xz}] \quad (2.12)$$

where  $\sigma^e_{zz}$  and  $\tau^e_{xz}$  are the normal and tangential elastic stress components respectively with compressive stresses being taken as positive; and  $[v_{zz}]$  and  $[v_{xz}]$  denote the jumps in normal and tangential velocity respectively. Taking the normal flow assumption in which the jump in the total velocity across such a discontinuity line must make an angle of  $\phi$  with this line; and using the Coulomb condition, the upper bound shakedown limit can be evaluated from

$$\lambda = \frac{c \sum_i [v_{xz}]_i l_i}{\sum_i \int c_i^e [v_{xz}]_i dl_i} \quad (2.13)$$

where  $l_i$  is the length of the  $i^{\text{th}}$  discontinuity [see Collins and Boulbibane (2000)]. Figure 2.17 illustrates the failure mechanisms for a homogeneous isotropic half space that were investigated by Collins and Boulbibane (2000) in which the Mechanism V with a log-spiral fan failure zone gave the best results for their problem.

The optimal solution of the Mechanism V in which the angle of friction is zero as shown in Figure 2.17 parallels exactly that observed by Kapoor (1997) for the formation of thin wear particles extruded sideways due to sliding processes on metal surfaces.



**Figure 2. 17 Rut failure mechanisms for half space (after Collins and Boulbibane, 2000)**

## 2.2.4 Factors Affecting the Shakedown Limit

The difference of the predicted shakedown load for 2D plane strain and 3D moving load is between 17% and 27% for the lower bound approach (Yu, 2005) or by a factor ranging from 1.5 to 2.5 for the upper bound approach (Collins and Cliffe, 1987). Factors that may affect the shakedown limit



according to the sensitivity analysis in pavement modelling using the shakedown limit are described and summarised below.

#### ***a. Homogeneous Isotropic Half Space***

##### *-Effect of Material Friction Angle $\phi$ , Poisson's Ratio $\nu$ and Loading Conditions*

All the investigators agree that an increase in internal friction angle will increase the shakedown limit value. Sharp and Booker (1984) found that there is a significant difference between the first yield and shakedown loads at higher values of angle of friction which reveals the possibility of a reserve of strength within the continuum. Collins and Wang (1992) found that at larger values of the *angle of internal friction  $\phi$* , an increase of *Poisson's ratio  $\nu$*  would increase the shakedown limit. Under the same angle of friction, a drained loading system will give a higher shakedown limit than undrained loading (Collins and Boulbibane, 2000).

##### *-Effect of the applied surface stresses ratio, ASSR*

The shakedown limit decreases with the increase in the applied surface stresses ratio, ASSR; particularly, at small values of ASSR, the shakedown limit decreases exponentially.

#### ***b. Two Layered Half Space***

##### *-Effect of Relative Stiffness Ratio for Layered Pavements*

Sharp and Booker (1984), Raad et al. (1988 and 1989), Yu and Hossain (1997 and 1998), and Yu and Shiau (1999 and 2000) have a similar pattern of shakedown limit for the effect of relative stiffness ratio between subbase layer and subgrade ( $E_b/E_s$ ) for different values of relative strength ratio between subbase layer and sub-grade ( $C_b/C_s$ ). For a given value of relative strength ratio there exists an optimum relative stiffness ratio (see Figure 2.18) at which the resistance to incremental collapse is maximised. A higher relative stiffness ratio does not contribute to an increase in the shakedown limit.

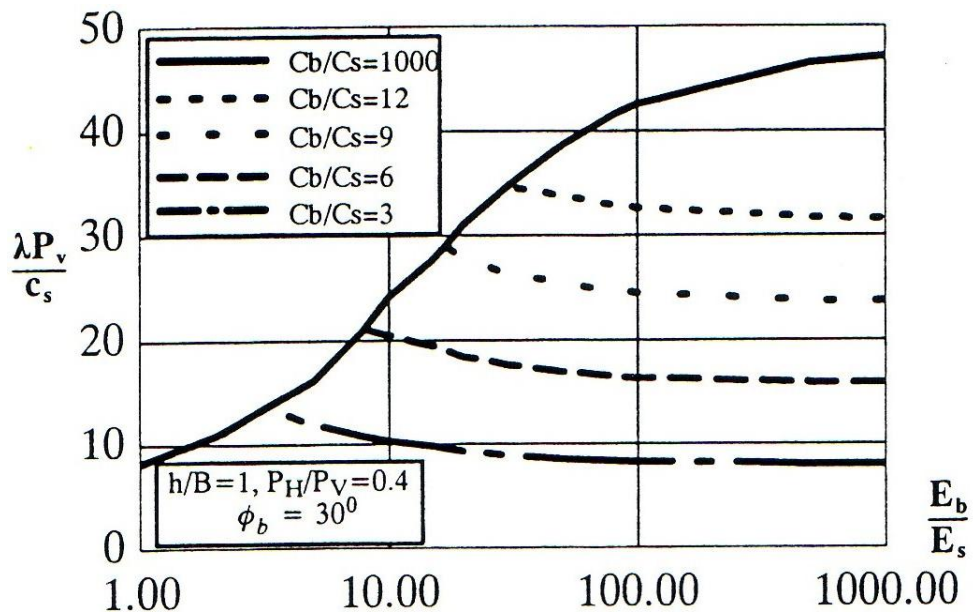


Figure 2. 18 Effect of  $E_b/E_s$  and  $C_b/C_s$  on dimensionless shakedown limits (after Shiau and Yu, 2000)

## 2.3 SUMMARY

A series of experimental observations from various investigators on various pavement materials using either wheel tracking or repeated load triaxial apparatus demonstrated that shakedown behaviour of specimens occurred below a certain stress level after a number of load repetitions. The existence of

the shakedown behaviour in a soil was observed by collecting either the deformation data or the residual horizontal stress after a certain number of repetitions.

The wheel load is transmitted to the pavement surface through the tyre generating three different types of stress distributions on the pavement, depending on the tyre type and pattern, changing speed, the inflation pressure and the stress level. No significant effect of the axle configuration was identified on the pavement response.

The pavement response mainly depends on the applied stress level. There is no fixed number of passes that achieves the soil equilibrium state. When a lower stress level is applied repeatedly, the pavement may deform initially and after a certain number of repetitions it responds elastically. The initial deformation may be due to the reduction of the pore pressure between the particles bringing the particles closer together. The plastic response as a result of repetitions of higher stress may cause the reorientation of the particles and after a certain number of repetitions of the pavement materials may lead to failure.

The principle of the shakedown concept for pavement analysis is described including the application of the concept with the lower and upper bound approaches. The sensitivity analyses on the factors that may affect the shakedown limit are presented above. It is found that the shakedown limit of a layered pavement depends on the five parameters ( $c$ ,  $\phi$ ,  $E$ ,  $\nu$  and  $ASSR$ ). The

shakedown limit of a homogeneous pavement depends on three parameters which are  $c$ ,  $\phi$ , and  $ASSR$ . To compute the shakedown limit, those parameters need to be obtained.

The procedures and the apparatuses that were used to obtain the  $c$ ,  $\phi$ , and  $E$  parameters of the soil are presented in Chapter 3. The technique to measure the  $ASSR$  between the specimen surface and the wheel is presented in Chapter 6 together with the presentation of the results. The  $\nu$  for each soil is assumed. The computed shakedown limit is reported and is compared with the experimental results in Chapter 7.

### **3 MATERIAL CHARACTERISATION**

#### **3.1 INTRODUCTION**

The objective of the research was to check the validation of the shakedown concept for pavement analysis and design. In order to validate the shakedown concept, the computed shakedown limit is checked against the wheel tracking test results. A series of monotonic load triaxial tests was performed to obtain the strength and stiffness properties of the test specimen. Both properties are the input parameters to the pavement model to compute the theoretical shakedown limit. The relations between these two parameters and the shakedown limit have been reviewed in Section 2.2. The type of apparatuses that were used, the preparation methods, the test procedures and the test results are presented in this chapter.

This chapter covers the visual description of each material used in the experiments and the soil classification. To specify the requirements for soils compacted in the experiments, a compaction-related test for each type of soil was performed and reported in this chapter.

## **3.2 THE MATERIALS**

Three different types of soils were observed: silt, silty clay (Keuper Marl), sands (Portaway and Langford Fill) and crushed rocks (Carboniferous Limestone and granite). These soils were chosen due to their variation in soil properties (physical, chemical and the strength properties). The response of each material under repeated loading was observed in the wheel tracking test and compared to verify the shakedown behaviour of each soil.

### **3.2.1 Keuper Marl**

Keuper Marl is one of the clayey soils that are found in the sub-grade layer of a pavement. Keuper Marl is now known as Mercia Mudstone and is a silty clay which has been widely observed and used in laboratory tests by Lashine (1971), Brown and Bell (1979), Loach (1987), Chan (1990) and Cheung (1994). For the thesis purposes, the earlier name of 'Keuper Marl' is used.

The Keuper Marl used in this study was supplied in the form of wet unfired bricks by a brick manufacturer located in Ibstock, Leicestershire. The Keuper Marl has a liquid limit (LL), plastic limit (PL) and plasticity index (PI) of 30%, 16% and 14% respectively.

### **3.2.2 Portaway Sand**

Portaway sand was supplied from Grimsby Quarry (Lincolnshire). It came in bags and was air-dried. The particle shape was sub-angular. Portaway sand is dominated mainly by quartz and a small amount of coarse grain limestone and gravel passing the 6mm sieve size. It is normally used for building purposes to give bulk to concrete, mortars, and plasters. Sand is found naturally combined with clayey soils as a sub-grade in the pavement.

### **3.2.3 Silt**

Silt was taken from Holme Pierrepont Gravel Pit (Nottinghamshire). It was a waste product of the aggregate washing process which was generally dumped into a pond. It is a mixture of clay and quartz but the quartz was more dominant. It was delivered in a wet condition and mixed with some plant roots. Therefore, it was decided to air dry and sieve the material with a sieve opening diameter of 6mm to separate it from the plant roots before using it in testing.

### **3.2.4 Langford Fill Sand**

Langford fill sand was another waste product of aggregate washing from Langford Quarry (Nottinghamshire). As with the silt, it is normally used as fill for the local construction of embankments. It has the same feature as Portaway

sand but it is finer and dominated mainly by quartz. This may be due to both sands coming originally from the same river (River Trent).

### **3.2.5 Crushed Carboniferous Limestone**

The crushed Carboniferous Limestone that was tested was delivered from Dene Quarry (Derbyshire). It has an angular shape and a rough surface texture. Crushed Carboniferous Limestone is generally used in pavement construction as a sub-base layer. This type of limestone has been extensively investigated together with the other granular materials by Thom (1984).

### **3.2.6 Crushed Granite**

Apart from crushed limestones, another type of aggregate that is used as a sub-base in pavement construction is crushed granite. According to Thom (1984), crushed granite has a lower stiffness and less shear strength than crushed carboniferous limestone. The crushed granite that was used in this research had been used previously as a sub-base layer by Brown (1997) in studying the causes of failure of road ironwork installations. It originated from Mountsorrel Quarry, Leicestershire. The surface texture is slightly rough and it has a sub angular shape.

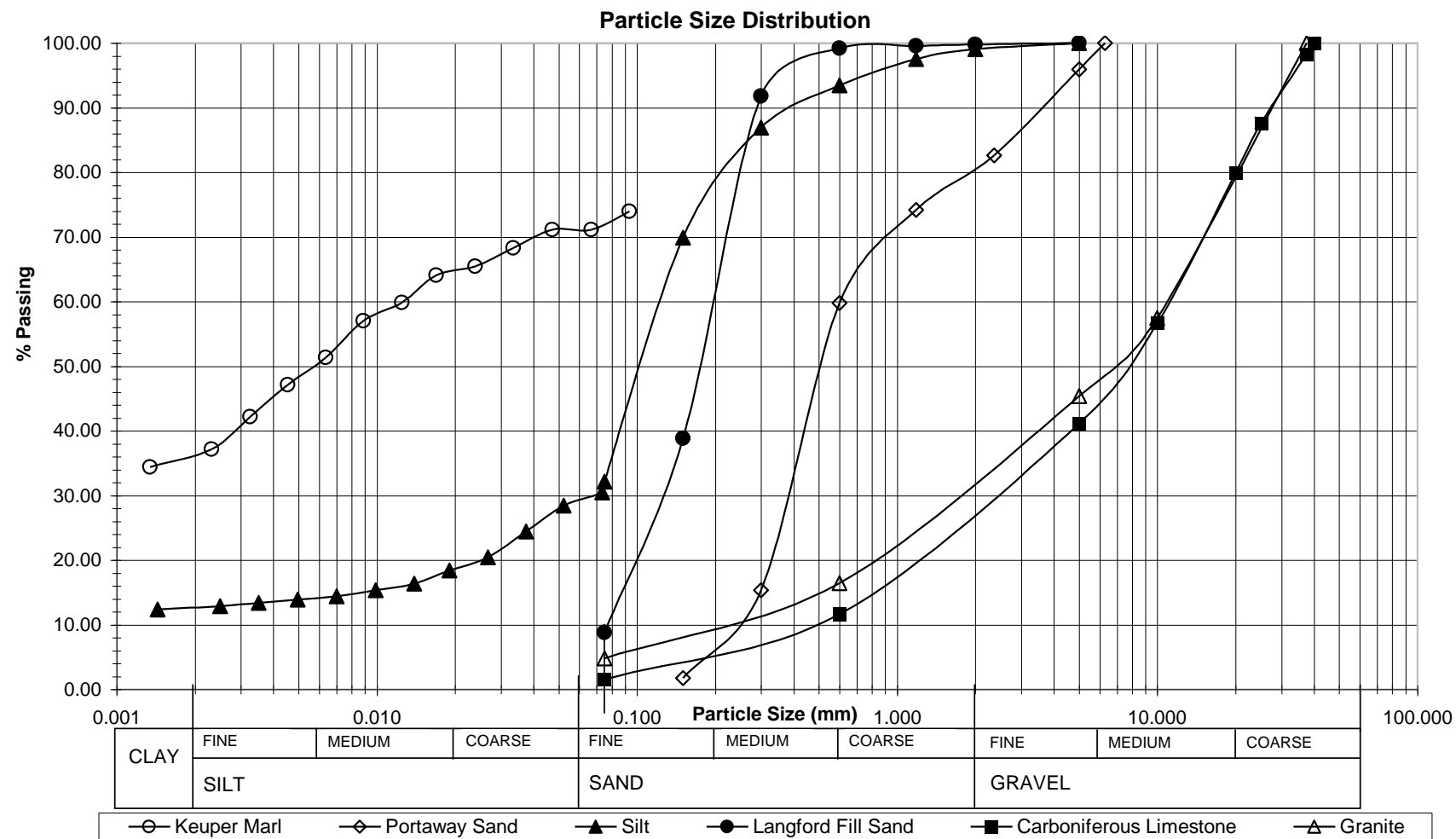


### 3.3 PARTICLE SIZE ANALYSIS

All the samples of each material were dried in the oven. The two methods that were used to determine the particle size distribution in a soil were dry sieving and sedimentation. Dry sieving was conducted for all the materials except Keuper Marl. The particle distribution of the Keuper Marl and the silt passing the no.200 sieve (opening diameter=75 $\mu$ m) involved sedimentation by the hydrometer method. The techniques for particle size analysis were adopted from the British Standard 1377-2(1990). The chart of the particle size distribution and the description of the test materials mentioned above are shown in Table 3.1 and Figure 3.1 respectively.

**Table 3. 1 Description of the test materials**

<b>Test Material</b>	<b>Description of Particle Size Distribution</b>
Keuper Marl (KM)	29% of Sand, 35% of Silt and 36% of Clay
Portaway Sand (PS)	Uniform and poorly graded sand
Silt	71% of Sand, 16% of Silt and 13% of Clay
Langford Fill Sand (LFS)	Silty sand
Crushed Carboniferous Limestone (Cl)	Well graded and it is classified as Type 1 Sub-base range of grading according to Department of Transport (DoT, 1986).
Crushed Granite (Gr)	



**Figure 3. 1 Particle size distribution of the test materials**

### 3.4 COMPACTION-RELATED TEST

The purpose of the compaction test is to determine the relationship between the dry unit weight of a soil and its moisture content, which relates to the state of the material and its characteristic strength and other properties. The dry unit weight depends primarily on three important factors: (i) soil moisture content during compaction, (ii) soil type, and (iii) the amount of compactive effort.

The compaction apparatus and the test method are specified in BS 1377-4 (1990). Table 3.2 shows the compaction test results including the specific gravity of each specimen's particles. The compaction-related tests were split into three different types which are determination of dry density/moisture content relationship, maximum and minimum possible dry densities (the limiting densities). The maximum and minimum possible dry densities (the limiting densities) are to identify the state of compaction of a cohesionless soil or relative density which is expressed as follows:

$$\left( \frac{\rho_d - \rho_{d \min}}{\rho_{d \max} - \rho_{d \min}} \right) \left( \frac{\rho_{d \max}}{\rho_d} \right) \quad (3.1)$$

where

$\rho_d$  the maximum dry density from the dry density and moisture content relationship,

$\rho_{d \max}$  the maximum possible dry density, and

$\rho_{d \min}$  the minimum possible dry density.

### ***Determination of dry density/moisture content relationship***

The air dry soil was mixed thoroughly with a suitable amount of water for the compaction test. For Silt, Portaway Sand and Langford Fill Sand, the soil was used several times after progressively increasing the amount of water. For crushed Carboniferous Limestone and Granite, materials with various water contents were prepared. For Keuper Marl, samples with various amount of water for each sample were prepared and left overnight. A 152mm diameter CBR mould was used and the samples were compacted with a 900W vibrating hammer, except in the case of Keuper Marl. The vibrating hammer gave a static downward force of 184N. Keuper Marl was compacted using a 2.5kg rammer. More details on the compaction procedure are in BS 1377-4 (1990).

### ***The maximum possible dry density***

The specimen was poured into warm water in a bucket, stirred thoroughly to remove the air bubbles and left overnight. The specimen was compacted under water with a 900W vibrating hammer in a 1 litre mould for Portaway Sand and Langford Fill Sand and in a CBR mould for the crushed Carboniferous Limestone and Granite.

### *The minimum possible dry density*

The weighed sample of Portaway Sand or Langford Fill Sand was placed in a 1 litre glass cylinder. A stopper was fitted before shaking the cylinder upside down to loosen the sand and inverting it a few times. The volume reading was recorded. The test was repeated at least 10 times and the greatest value was taken. For the crushed Carboniferous Limestone and Granite, the dry soil was released freely from a height of approximately 0.5m into the CBR mould. Then the mould extension was removed carefully without disturbing the soil. The large particles were picked off by hand, the surface was checked and any cavity as a result of removing the large particle was filled with smaller particles. The mass reading was taken and recorded. The test was repeated at least ten times and the lowest mass was taken.

**Table 3. 2 Summary of the compaction-related Tests**

Type of Materials	Specific Gravity	Maximum Possible Dry Density (kg/m <sup>3</sup> )	Minimum Possible Dry Density (kg/m <sup>3</sup> )	Vibratory Hammer Compaction	
				MDD (kg/m <sup>3</sup> )	OMC (%)
Keuper Marl (KM)	2.70	-	-	1882	15.45
Silt	2.62	-	-	1723	15.10
Langford Fill Sand (LFS)	2.65	1688	1290	1620	11.24
Portaway Sand (PS)	2.66	1865	1449	1813	4.20
Crushed Carboniferous Limestone (Cl)	2.71	2450	1842	2310	3.10
Crushed Granite (Gr)	2.77	2480	1613	2193	4.76

Note: “-“means the test is not applicable for the material.

MDD=the dry density corresponding to the maximum dry density on the moisture content/dry density curve.

OMC=the percentage moisture content corresponding to the maximum dry density on the moisture content/dry density curve.

### **3.5 THE MONOTONIC LOAD TRIAXIAL TEST**

The monotonic load triaxial tests were conducted on all materials to determine the shear strength characteristic. The shear strength characteristic of the specimen is determined using the Mohr-Coulomb failure line. During the test, the cylindrical specimen that was supported by various known confining pressures was axially loaded until failure occurred. The combinations of confining and axial pressures required to induce failure in the specimens were plotted as Mohr stress circles. The shear strength relates to the common tangent to these circles. The specimens for triaxial tests were partially saturated which gave the same test condition as the wheel track specimens.

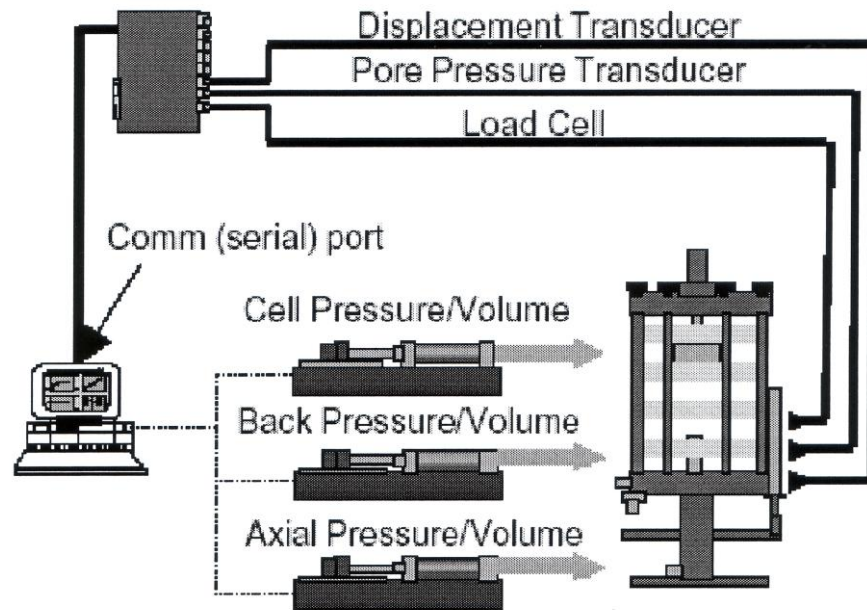
Due to the various sizes of the tested materials, two triaxial apparatuses were used to perform the static triaxial tests. The triaxial test was chosen as being a good compromise between accurate simulation of in-situ stress conditions and experimental practicality. Each apparatus had a different preparation method but the same triaxial test procedure. The apparatus with a 38mm diameter by 76mm high specimen was used to characterise the material passing 6mm such as sand, silt and Keuper Marl. Another apparatus with a 150mm diameter and 300mm high specimen is used to test the material passing 35mm such as crushed Carboniferous Limestone and Granite.

### 3.5.1 The Equipment

#### *The Triaxial Apparatus for 38mm Diameter Specimens*

The GDS advanced triaxial testing system was set up in the University of Nottingham in 2001. A detailed description of the triaxial apparatus can be found in Hau (2003). Basically the triaxial system, as shown in Figure 3.2, consists of a triaxial cell, three 2MPa pressure/volume controllers: two standard pressure/volume controllers to control the cell pressure and lower chamber pressure and one advanced pressure/volume controller for the back pressure source, an eight-channel data acquisition pad, a computer and a multiplexer which allows up to four devices to be connected to a communication port on the computer. The volumetric capacity of these controllers is  $2 \times 10^{-4} \text{ m}^3$ . The resolution of the pressure control is 2kPa and the resolution of pressure measurement is 1kPa.

The triaxial cell has a maximum safe working pressure of 1700kPa. Both 38mm and 50mm diameter specimens can be tested using this cell. Axial force is applied to the test specimen by a piston fixed to the base pedestal. This piston moves vertically upwards and downwards actuated hydraulically from the lower chamber in the base of the cell which contains water. GDS standard pressure/volume controllers are used to control both the lower chamber pressure and the cell pressure. A 2kN internal submersible load cell which has an accuracy of 2N, one external axial displacement transducer with a range of 40mm and an accuracy of 0.1mm, and one 2000kPa range pore pressure transducer with an accuracy of 2kPa are used.



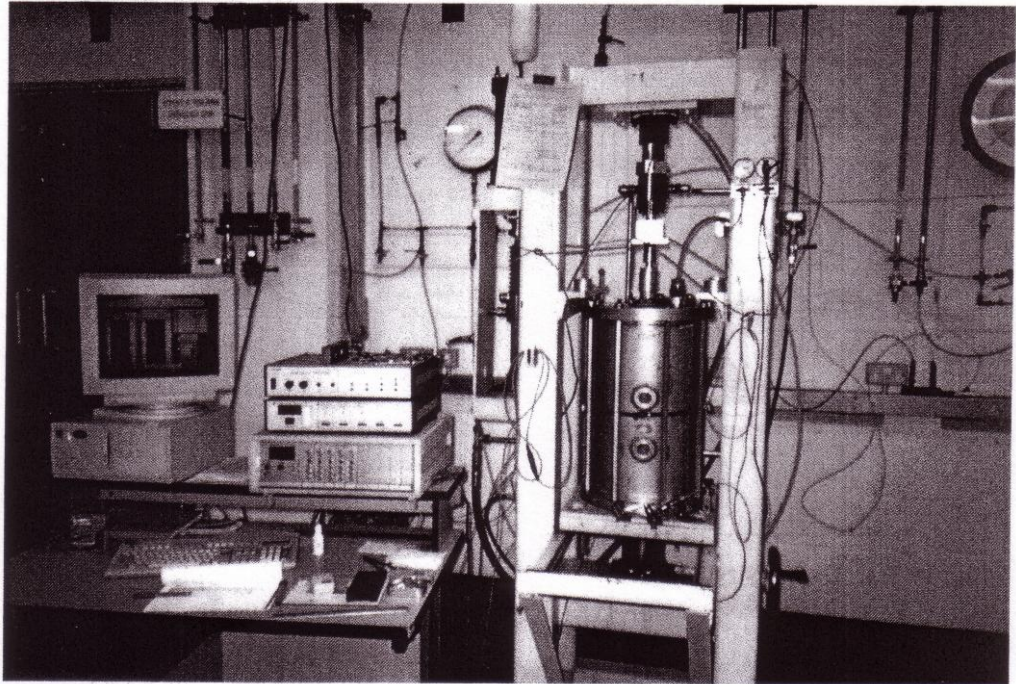
**Figure 3. 2 Schematic diagram showing the layout of the triaxial system (GDS Instruments Ltd., 2002).**

### ***The Triaxial Apparatus for 150mm Diameter Specimens***

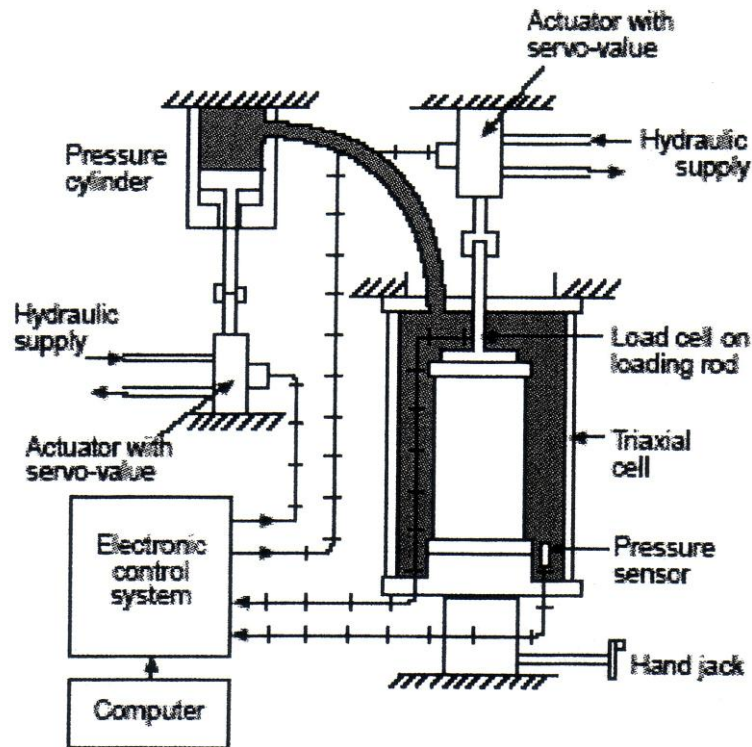
Since the Nottingham triaxial apparatus for 150mm diameter specimen was first developed by Boyce (1976), it has been utilised to study the performance of granular materials under repeated loading by other researchers such as Pappin (1979), Thom (1984), Lekarp et al. (1996), Nunes and Dawson (1997), and Arnold (2004). It was noted that there had been some modifications to the apparatus. Instead of the silicone oil, air pressure could be used as a medium to provide the confining pressure up to 400kPa and can be recorded by a pressure cell in the triaxial cell. The axial load is applied to the specimen through a hydraulic actuator controlled by a servo valve and monitored by a feedback load cell to an accuracy of  $\pm 2\text{kPa}$ , and this forms an integral part of the axial loading arrangement. The maximum working load for the axial actuator is



20kN, which corresponds to axial stresses up to approximately 1150kPa on a 150mm diameter specimen. The axial deformation is measured using an external linear variable differential transformer (LVDT) mounted between the hydraulic ram and the support frame. Figures 3.3 and 3.4 show the picture and schematic of the triaxial apparatus for 150mm diameter specimens respectively.



**Figure 3. 3 University of Nottingham repeated load triaxial (RLT) apparatus (after Arnold, 2004)**



**Figure 3. 4 Schematic of University of Nottingham's RLT apparatus (after Pappin, 1979)**

### **3.5.2 The Specimen Preparation**

#### *Silt and Sands*

The soils were mixed with water to achieve the required moisture content and stored overnight to allow water absorption. In all cases, the water content used was the same as in the wheel tracking tests. For both Silt and Portaway Sand, these were tested at optimum moisture content and for Langford Fill Sand, the as-delivered water content was used because of the quantity of material involved. For moist soils like Silt, Langford Fill sand and Portaway Sand, the specimens were prepared in the triaxial apparatus. A step by step specimen

preparation procedure is given in BS 1377-7(1990). The moist soil was weighed according to the desired density for a 38mm diameter and 76mm high specimen and then subdivided into five layers. Each layer was under compacted into the mould up to the certain height (Ladd, 1978) using a small tamping rod with a 30mm diameter compaction foot and a height controller attached (see Figure 3.5) to obtain the uniform density throughout the specimen. Each layer was compacted to a lower density than the final desired value. The required height for each layer of the specimen was calculated using the formula given by Ladd (1978) which is as follows:

$$h_n = \frac{h_t}{n_t} \left[ (n-1) + \left( 1 + \frac{U_n}{100} \right) \right] \quad (3.1)$$

where  $h_n$  = height of compacted material at the top of the layer being considered,

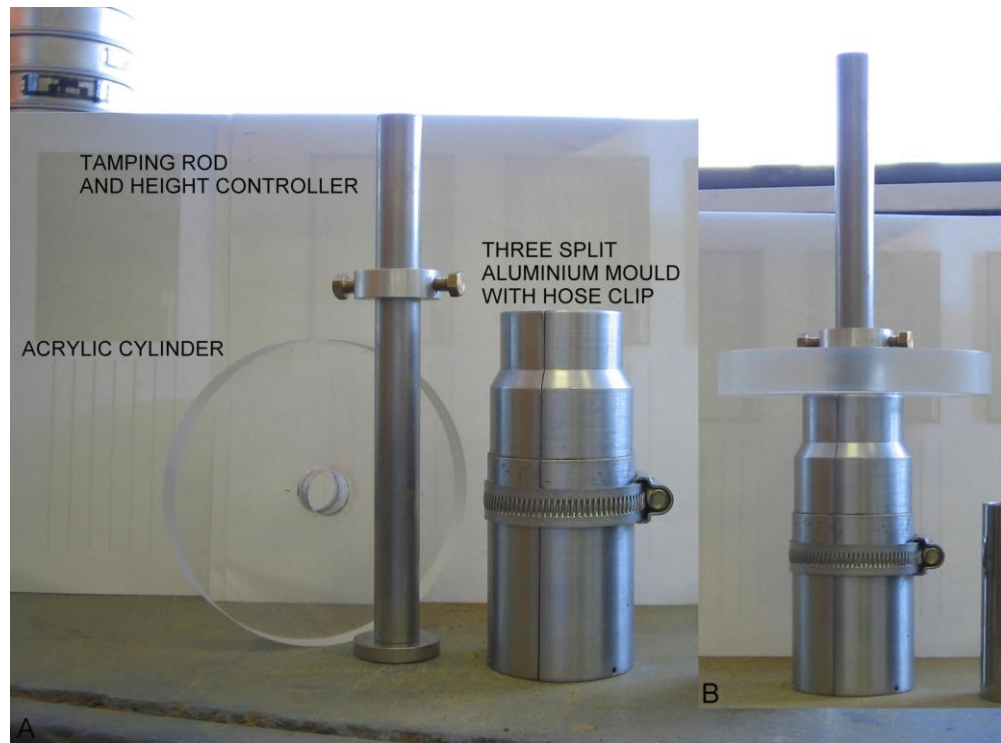
$h_t$  = final (total) height of the specimen,

$n_t$  = total number of layers,

$n$  = number of layer being considered,

$U_n$  = percent under compaction selected for layer being considered.

The surface of the compacted layer was scarified before compacting the next layer to minimise the particle segregation between each layer.



**Figure 3. 5 The compaction tools for fine grained soils**

### ***Keuper Marl***

The setting up procedure was similar to the one for the silt or sand specimens except for the sample preparation method. In order to minimise the segregation between each layer of the Keuper Marl during compaction, the moist Keuper Marl from the supplier was compacted into the test box that was used for the wheel tracking test using a 680W vibrating hammer which gave a static downward force of 100N. The compaction procedure was similar to the material preparation for the wheel tracking test by subdividing the soil into three layers. The moisture content and density were checked to ensure the same state as the one for the wheel tracking test. Then the compacted moist soil was taken out from the test box and trimmed to a 38mm diameter by

76mm high specimen using a wire saw and a trimming apparatus so that it could be slid down the 40mm diameter mould with a rubber membrane on it.

Because the brick manufacturer was unable to supply the Keuper Marl with the same moisture content, the Keuper Marl that was used as the sub-grade layer in the Pavement Test Facility has a different moisture content from the one used for the other wheel tracking facilities. The Keuper Marl specimen was obtained directly by cutting it from the compacted clayey soil from the unloaded area of the test pit by firstly removing the sub-base layer. It was then trimmed to the required size for the triaxial test.

#### ***Crushed Carboniferous Limestone and Granite***

The step by step procedure to prepare and set up the specimen followed the internal safety document procedure for triaxial test except that the on-sample instrumentation was not used. Basically, the specimen material was weighed out according to the desired density and then divided into six layers. The four-part split aluminium mould was assembled, bolted tightly together, and placed on top of the bottom platen on which an inner rubber membrane was attached. Then the inner membrane was stretched over the top of the mould to ensure a snug fit, and a steel ring extension was bolted on top of the mould to hold the membrane and overflow materials when compacting the final layer. A round geotextile filter fabric was placed on top of the bottom platen inside the membrane before the specimen was poured inside the mould for compaction. The specimen was compacted using a 900W vibrating hammer with static

downward force of 184N for 40 seconds on the first layer, and then the compaction duration was increased by 10seconds for the next layer until the final layer was compacted for 90seconds to obtain uniform density within the soil. The surface of each compacted layer except the final layer was scarified before placing the soil for the next layer to reduce the segregation between each compacted layer. The steel ring was removed; another geotextile filter fabric was placed on top of the specimen followed by the top platen. Then the compaction mould with top and bottom platens was lifted onto the triaxial apparatus. The vacuum was introduced to the specimen once the vacuum hoses were connected to the specimen via the top and bottom platens. Then the four-part split aluminium mould was dismantled with extra care. The vacuum hose on the top platen was removed for access in order to fit an outer membrane onto the specimen. Then the vacuum hose on the top platen was reconnected once both membranes were fitted onto the top and bottom platens and sealed with double O-rings at each platen. A load cell was placed on top of the top platen and connected to the computer. Before fitting the pressure chamber, holding rods and lid to provide an airtight cell, a pressure cell that was connected to the computer, was placed inside the chamber to measure the applied confining pressure. The pressure chamber and lid were then locked by nuts and washers. An air pressure hose was connected to the pressure chamber via the attachment on the lid of the pressure chamber. The vacuum hose was removed and the specimen was ready for a drained test.

### 3.5.3 Test Procedure

The quick undrained shear strength was carried out for the Keuper Marl. The other soils were tested drained. It was considered that during the wheel tracking tests, the applied wheel load may be high enough to cause failure of the soil which left insufficient time for the Keuperl Marl to gain additional strength by consolidation. The specimens under the standard drained test were first consolidated under an equal all round pressure and then the axial stress increased under conditions of full drainage until the specimens failed. The deviator stress of the drained test at failure depends on the cell pressure. This is not the case in the quick undrained test.

Considering low moisture contents of the specimens and the problem in measuring the pore water pressure in the triaxial apparatus for the 150mm diameter specimen, the pore water pressures of crushed Carboniferous Limestone and Granite were not measured. The reported cohesion and angle of friction of the latter specimens would therefore be a total cohesion and angle of friction respectively.

At least three static triaxial tests with different confining pressures ranging from 10kPa to 100kPa were carried out for each material [see Table 3.3]. The specimens were axially loaded until they reached failure. The loading rate for all soils except the Keuper Marl was controlled by a strain rate of 10% per hour to avoid internal excess pore pressure in a drained test. Yamamuro and Lade (1993) varying the strain rate of dense uniform Cambria sand between

0.0517%/min (=3.1%/hour) and 0.74%/min (=44.4%/hour) concluded that an increase in the strain rate slightly increased the friction angle and maximum deviator stress. They found that the effects of the strain rate on a granular material like sand or silt during the drained triaxial compression tests were less significant compared to the undrained condition. The strain rate for Keuper Marl was 2%/min as recommended by Head (1982) and Bishop and Henkel (1962). According to Head (1982), varying the rates of strain between 0.3%/min and 10%/min made little difference to the results. During the test, the displacement under working loads and external forces required to cause shear failure of a soil were recorded through the electronic control system.

### 3.5.4 Test Result

The plots of the stress-strain relationship and Mohr-Coulomb circles and failure line of Keuper Marl (22.5% moisture content) are presented in Figures 3.6 and 3.7 respectively. The cohesion of Keuper Marl would be the undrained shear strength. The plots of the stress-strain relationship and Mohr-Coulomb circles and failure lines for other specimens are given in Appendix A. Table 3.3 summarises the soil shear strength properties, *cohesion*  $c$  and *angle of friction*  $\phi$ , of each test material.



### Monotonic Shear Failure Tests for Keuper Marl (KM) with 22.5% Moisture Content

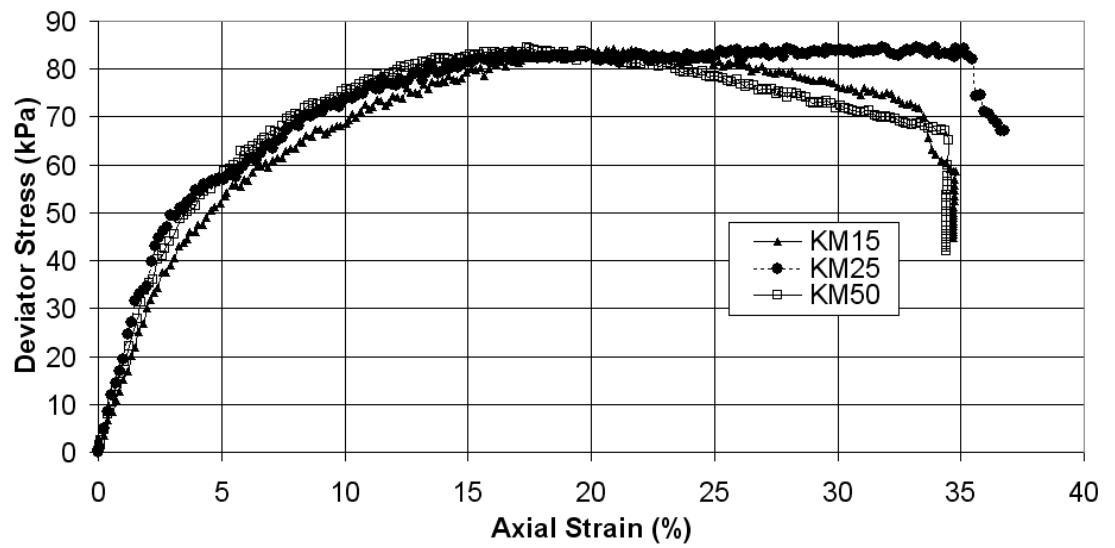


Figure 3. 6 Stress-strain relationship of Keuper Marl  
with 22.5% moisture content

### Mohr Circles for Keuper Marl with 22.5% Moisture Content

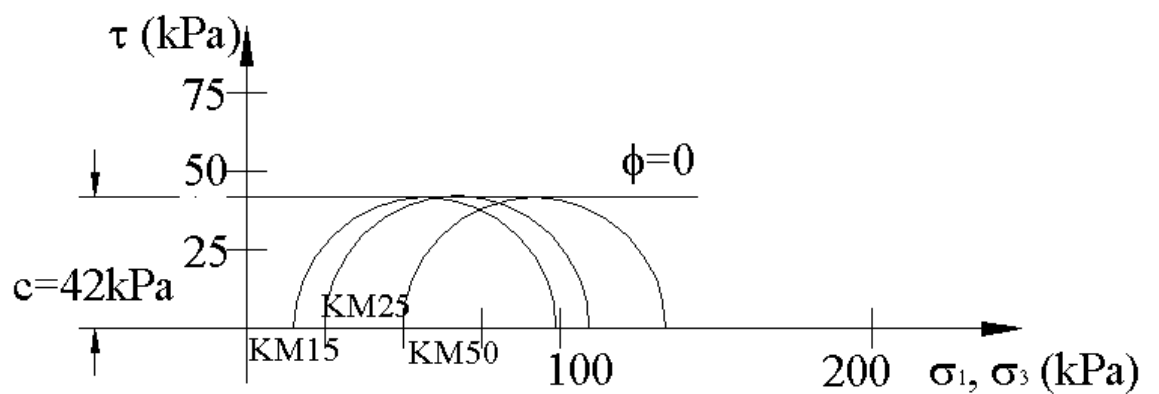


Figure 3. 7 Mohr-Coulomb circles and failure line of  
Keuper Marl with 22.5% moisture content

Shear strength parameters,  $c$  and  $\phi$ , are not a true cohesion and angle of friction respectively. The parameter  $c$  represents that part of the shear strength which is independent of the normal stress and is called apparent cohesion. The angle of friction  $\phi$  which is known as the angle of shearing resistance is the angle of the line representing shear strength in terms of normal stress on the failure line.

The highest *angle of friction*  $\phi$  is exhibited by crushed Carboniferous Limestone (the average bulk density of  $2143\text{kg/m}^3$ ). The frictionless specimen Keuper Marl has the highest cohesion.

According to Berry and Reid (1987) and Scott (1980), the cohesive strength of the clay mineral particles is due to the influence of the electro-chemical activity on the surface of the particles. Unlike the clay particles, the cohesive strength in coarse grained soils like sand and rocks is due to the effect of matrix suction and particle interlock. The latter one is mainly for rocks. Matrix suction is effectively negative pore water pressure that occurs in partially saturated materials. The effect of the suction is to pull particles together and significantly increase the effective stress and apparent cohesion of the coarse grained soils.

The average stiffness of the specimen used as the input parameter was taken from the axial stress-axial strain plot of the monotonic load triaxial tests. Two points are noted from the literature review about soil stiffnesses. Firstly, soils are very stiff under cyclic loading. Secondly, soils exhibit very high stiffnesses at low strain levels; therefore on-sample strain measurement may need to be

considered. However, the influence of the soil stiffnesses on the calculation of shakedown load depends on the relative stiffnesses and shear strengths between the layers. In these experiments, the ratios of the relative strengths between top and bottom layers were approximately 3. According to Figure 2.18 in Chapter 2, with a relative strength ratio of 3 there is insignificant difference in shakedown limit for sub-base to sub-grade stiffness ratios between 1 and 100. The effect of material stiffnesses on the shakedown limit seems insignificant. Sharp (1983), who was amongst the first to introduce the shakedown concept for pavement analysis, determined the stiffness of the specimen by adopting the Modified Texas Triaxial Test Procedure. The stiffness was identified by taking the slope of a straight line joining the point of zero strain to the point of 0.75% strain on the axial stress-axial strain plot ( $E_{0.75\%}$ ). According to Sharp (1983), the assumption of linear elasticity-perfect plasticity is satisfactory for the great majority of material tested, with an 'average modulus' computed from the linear portions of the stress-strain curves. This procedure has therefore been adopted here.

### **3.6 DISCUSSION**

Each type of soil has a different shear strength. Portaway Sand was reported with the lowest shear strength compared with other types of sand. This may be due to the uniform shape and poorly graded nature of the sand particles. Langford Fill Sand with particle sizes in between Silt and Portaway Sand has higher shear strength than the Portaway Sand. Silt which consisted of 13% of

clay mineral was identified as being more cohesive than Langford Fill Sand and Portaway Sand.

The series of monotonic load triaxial tests of Keuper Marl with two different moisture contents showed that Keuper Marl at optimum moisture content (15.2%) has higher undrained shear strength than at higher moisture content (22.5%).

An increase in compaction effort on the crushed Carboniferous Limestone improved the shear strength of the specimen. The crushed Carboniferous Limestone with an average bulk density slightly higher than crushed Granite had slightly higher shear strength than crushed Granite.

Cheung (1994) studying the effect of the cohesion and angle of friction of granular materials found that the aggregates with higher angle of friction or higher apparent cohesion had better resistance to permanent deformation.

The different stiffness values obtained from different types of aggregate are not surprising. This is because each type of aggregate has different shapes, frictional properties, and slightly differing gradation.

$E_{0.75\%}$  has been used for pragmatic reasons. The real resilient modulus under repeated load is higher. The experience suggests a factor of 4 or 5. The purpose of identifying the stiffnesses is to get the right stresses. Therefore, the use of  $E_{0.75\%}$  will not affect the results as long as the stiffness ratios are correct.

**Table 3. 3 Summary of the static triaxial tests of various materials**

Test Material	Average Bulk Density (kg/m <sup>3</sup> )	Moisture Content (%)	Sr (%)	Relative Density (%)	E <sub>average</sub> (MPa)	Mohr-Coulomb	
						c (kPa)	$\phi$ (°)
Keuper Marl*	1933	22.5	85	-	2	43.5	0
	2162	15.2	94	-	7	55	0
Silt**	1694	15.5	52	-	22	14	38
Portaway Sand**	1860	4.2	23	84	26	8.5	36
Langford Fill Sand**	1613	9	30	54	17	9.5	44
Crushed Carboniferous Limestone***	2099	2.8	23	39	10	11.5	51
	2143	2.9	26	47	46	15.5	55
Crushed Granite***	2141	4.0	32	62	22	13	49

*Notes:*

Sr means degree of saturation.

\* The reported c is undrained cohesion ( $c_u$ ) which represents the undrained shear strength.

\*\* The reported c and  $\phi$  are the effective cohesion and angle of friction respectively.

\*\*\* The reported c and  $\phi$  are the total cohesion and angle of friction respectively.

### 3.7 SUMMARY

This chapter was focussed around the physical description and the strength and stiffness properties of the materials that were used in the wheel tracking tests. The description of the apparatuses and the procedure to identify the strength and stiffness properties was reported in this chapter as well. Types of soils that were used in the experiment are generally found in pavement construction. They have different characteristics and particle sizes. The characterisation tests were carried out for each type of soil if applicable. The drainage condition and the loading rate during the monotonic triaxial tests for each type of soil was varied depending on the drainage condition in practice, the in-situ soil condition and the loading period. The results of the monotonic load triaxial tests show that the shear strength of the soil depends on the type of the soil, particle grading and shape, density and moisture content.

The reported  $c$ ,  $\phi$ , and  $E$  values were used where applicable together with the ASSR to compute the theoretical shakedown limit in Chapter 7. The equipments and procedures to obtain the ASSR are presented in Chapter 6 including the test results.

## **4 WHEEL TRACKING TESTS**

### **4.1 INTRODUCTION**

To validate the theoretical pavement model based on the shakedown concept, a series of wheel tracking tests was conducted in the laboratory. In terms of the pavement geometry and material properties, the laboratory wheel tracking tests are cheaper and easier to control than full-scale field tests. Compared to the repeated load triaxial test in terms of loading conditions and pavement geometry, the wheel tracking test is more realistic. However, the limitations of the tests are the inability to alter variables such as climate conditions (sun, rain, snow, and salt) as in the real pavement situation.

This chapter describes the experimental process and gives brief information on each of the wheel tracking facilities used in the experiments, the specimen preparation method, types of data that were collected from the experiments and the test conditions. The results of the experiments are shown and discussed in the next chapter. A summary of the soil properties for each wheel tracking test is given in Chapter 5 Table 5.1.

## 4.2 WHEEL TRACKING FACILITIES

The wheel tracking facilities that were used in this research are small-, medium- and large-scale wheel-tracking devices. The medium- and large scale tracking devices are known as the Slab Test Facility (STF) and the Pavement Test Facility (PTF) respectively. All the facilities vary in wheel size, size of test specimen, and wheel load capacity as shown in Table 4.1.

**Table 4. 1 Specification of the Wheel-tracking Facilities**

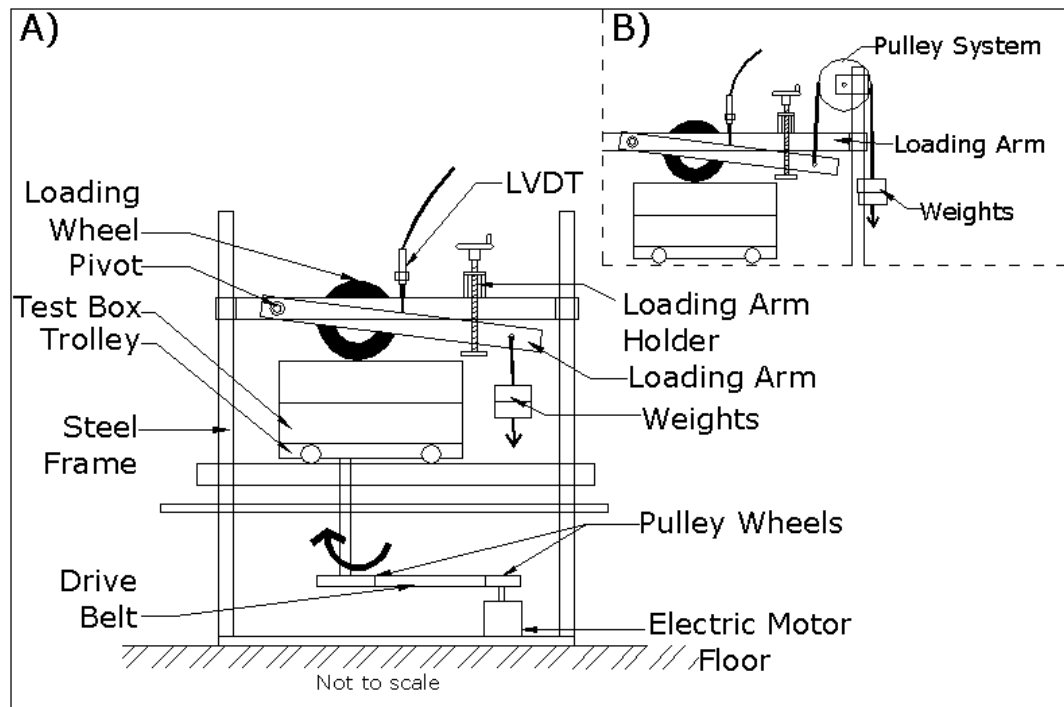
<b>Specification</b>	<b>Small Wheel Tracker (SW)</b>	<b>Slab Testing Facility (STF)</b>	<b>Pavement Testing Facility (PTF)</b>
<b>Range of Contact Wheel Load (kN)</b>	0-0.210	Up to 7	Up to 15
<b>Speed (km/h)</b>	0.58	0-3	0-16
<b>Tyre Width (m)</b>	0.05	0.12	0.15
<b>Tyre Diameter (m)</b>	0.20	0.46	0.56
<b>Tyre Pressure/Hardness</b>	80 on the Dunlop hardness scale	276kPa	646kPa
<b>Loading Directions</b>	Two ways	One or two way	One or two way
<b><i>Specimen Dimension</i></b>			
<b>Length (m)</b>	0.4	1	7
<b>Width (m)</b>	0.28	0.6	2.4
<b>Maximum Depth (m)</b>	0.250	0.36	1.5



#### **4.2.1 Small Wheel Tracker (SW)**

The SW was formerly used to measure the rutting resistance of asphalt wearing course mixtures. It consists of a 200mm diameter and 50mm wide solid rubber tyred wheel mounted between a pair of beams, which act as pivoted lever arms through which a constant load is applied as shown in the SW diagram and picture in Figures 4.1 and 4.2 respectively. An electric motor rotates a drive shaft on which a cam is fitted to convert the rotation of the drive shaft to a linear reciprocating motion. This moves a trolley, to which the specimen is attached, a fixed distance of 230mm. The wheel rotates when it touches the surface of the moving test specimen. The rate of reciprocation is controlled by the speed of the motor and is set at 40 passes per minute.

As noted earlier, the wheel load is controlled by the lever arm. To increase the applied wheel load, weights are added to the lever arm through a loading plate (see Figure 4.1A). Conversely, the weights could be used to pull upwards on the lever arms to reduce the wheel load caused by the weight of the wheel and lever arms, by means of pulley wheel and wire system as illustrated in Figure 4.1B. Before testing, a load cell was used to measure the wheel load. The calibration charts of the wheel load against the applied weight on the loading plate are shown in Appendix B Section 1.



**Figure 4. 1 Diagram of small wheel tracker**

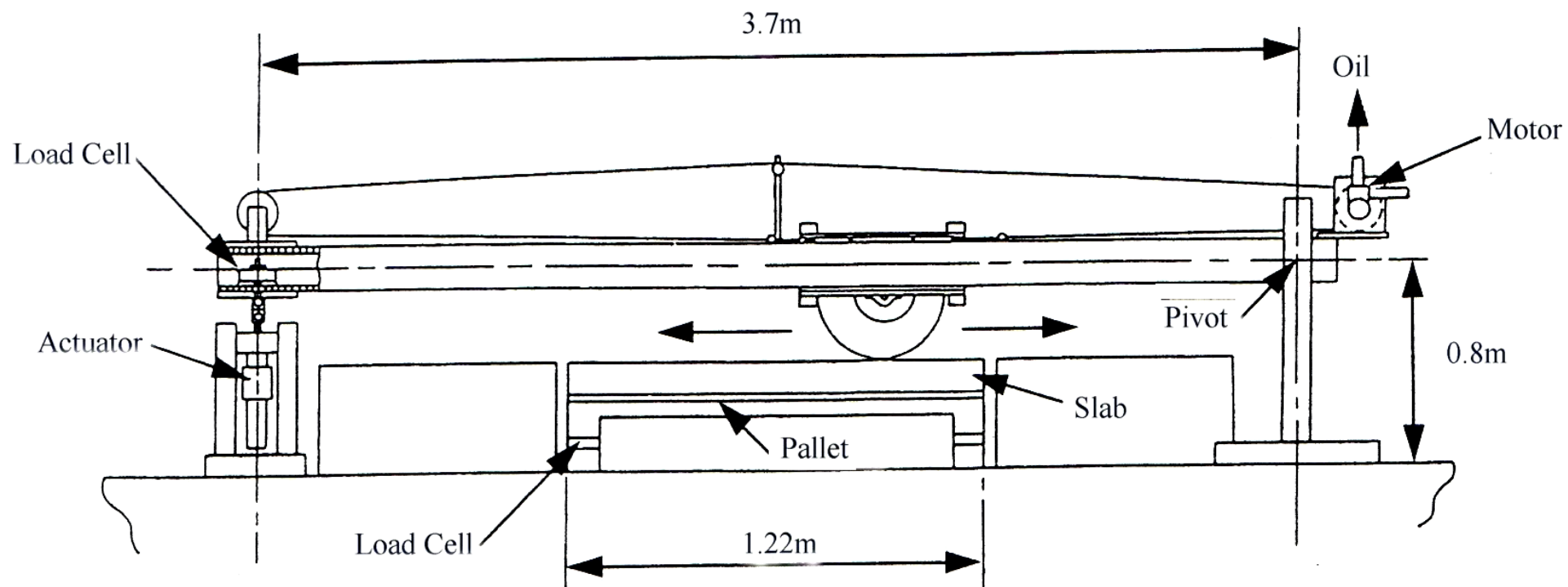


**Figure 4. 2 A small wheel tracker**

### **4.2.2 Slab Test Facility (STF)**

The Nottingham Slab Test Facility (STF) was originally used to investigate cracking and rutting in slabs of bituminous materials Hughes (1986). Brown and Chan (1996) used it to study rutting of compacted granular materials.

The STF comprises a wheel which is fitted to a carriage and guided by a pair of beams. The carriage is connected to a wire rope tensioned around a drum, which is axially coupled to a hydraulic motor. The motor rotation is controlled by a servo valve from an electrical command signal, which effectively reciprocates the carriage at the desired speed. Loading is provided by way of a hydraulic actuator located at one end of the hinged guide beams under which the wheel runs. Load cells are used to measure the slab load and placed under each corner of the pallet. A digital real-time oscilloscope is used to monitor the average of these load cells. Constant wheel load over the slab is maintained by changing the actuator load to compensate for the lever arm effect as the wheel travels over the slab. This process is done automatically through a closed loop servo controlled system. A diagram of the STF and pictures of the test facility and the equipment to control the test facility are shown in Figures 4.3 to 4.6.



**Figure 4. 3 Diagram of the Nottingham Slab Test Facility (after Chan, 1990)**



**Figure 4. 4 Side view of the Nottingham Slab Test Facility and the control equipment**



**Figure 4. 5 Side view of the Nottingham Slab Testing Facility**



**Figure 4. 6 The Nottingham Slab Testing Facility's control equipment**

### **4.2.3 Pavement Test Facility (PTF)**

The Nottingham Pavement Test Facility (PTF) has been in use for a variety of pavement research projects for over 30 years (Brown and Brodrick, 1999). Figures 4.7 and 4.8 show a diagram and photograph of the PTF respectively. Brown and Brodrick (1981) give a detailed description of the PTF including its operation and control systems. It is equipped with a 560mm diameter and 150mm wide pneumatic tyred loading wheel fitted to a carriage, which runs on bearings between two beams spanning the long side of a rectangular laboratory. The beams are in turn mounted on end bogies that run along rails which are set at right angles to the beams to allow the whole assembly to traverse across the pavement. Two transverse portal frames placed across the longitudinal beams resist the upthrust of the carriage when wheel load is introduced to the pavement. For continuous lateral traversing of the wheel under load, small wheels are installed on the beams under the portal frames. A servo-hydraulic system controls the magnitude of the applied load, speed and position. Load is controlled via two ultra low friction rams by lifting and lowering the wheel. A load feedback mechanism is incorporated to maintain constant load. The wheel load was calibrated using a load cell that was placed under the wheel and levelled with the specimen surface. The load cell was connected to a digital voltmeter to identify the voltage output. A table of the wheel load, the control potentiometer reading and the voltage output is provided in Appendix B Section 2. The wheel is driven by a wire rope tensioned around a centrally located drum and axially coupled to a hydraulic motor. The wheel speed is controlled through velocity feedback from a tachogenerator which is axially coupled to the motor shaft.

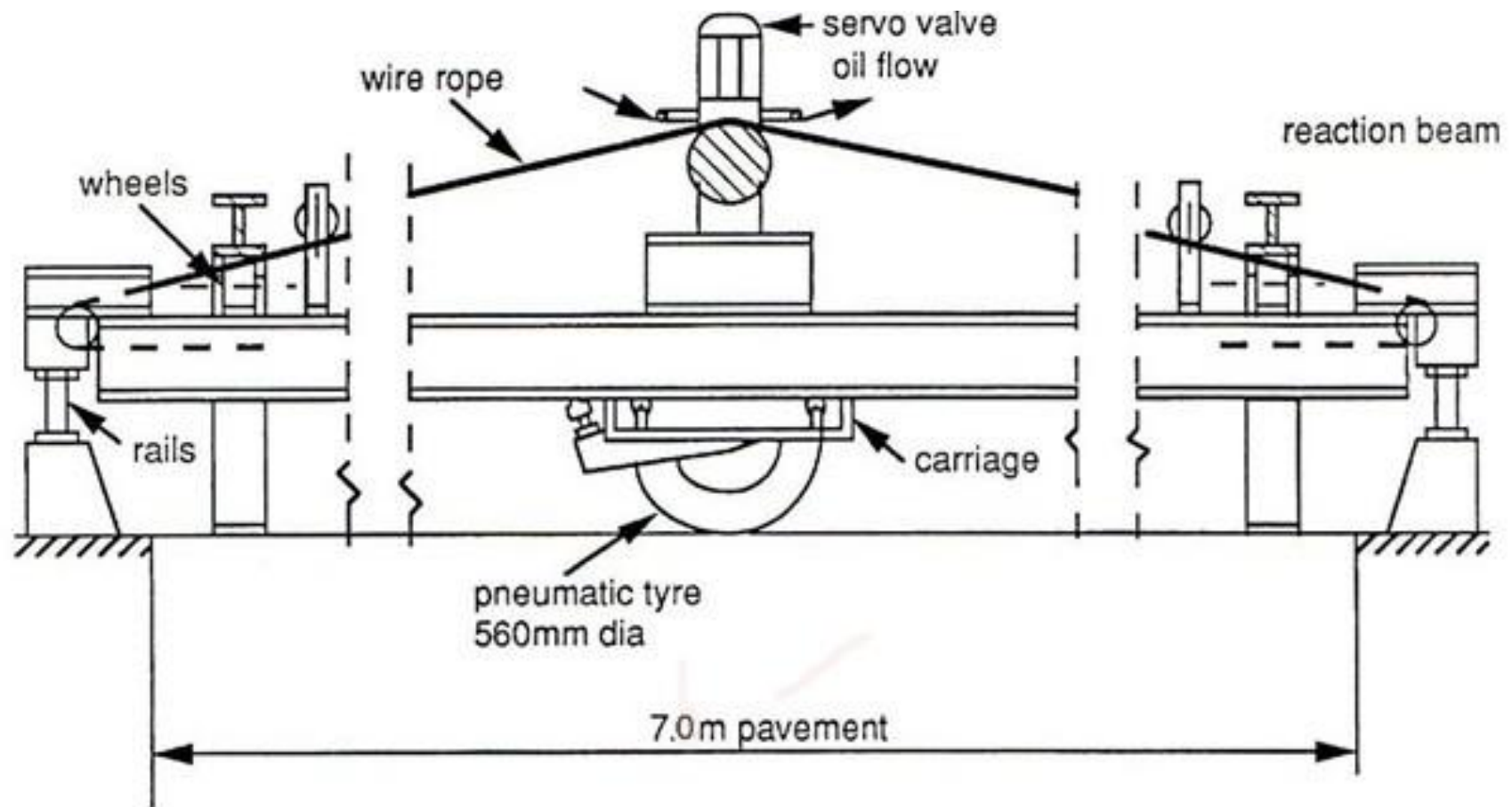


Figure 4. 7 Diagram of the Nottingham Pavement Test Facility (after Brown and Brodrick, 1999)





**Figure 4. 8 The Nottingham Pavement Test Facility**



### **4.3 THE SPECIMEN PREPARATION**

#### ***The SW specimen***

The test section for this equipment was 400mm long by 280mm wide and 125mm deep. Three different types of soils were tested and these were Portaway Sand, Keuper Marl, and Silt. They were wetted to their optimum moisture content and compacted in three layers to a specific height using a 680W vibrating hammer (see Figure 4.9). This had a working diameter of 100mm and static downward force of 100N.

#### ***The STF specimen***

The test specimen prepared for the STF was 600mm wide by 1000mm long. The STF was used to perform single layered and two layered tests. The dry crushed Granite or Carboniferous Limestone or sand was mixed with water to the required moisture content using a concrete mixer. All the material for the STF was weighed to give the target density before being placed into the test box. Three-layer compaction was also used for STF specimens. The specimen was compacted to a fixed height (approximately 60mm thick for each layer) using a vibrating plate with a working area of 150x265mm (see Figure 4.10) and a basic weight of 18kg. Typical test profiles for the single layer and two layers are shown in Figure 4.13.

### ***The PTF specimen***

The two test profiles used for the PTF are shown in Figure 4.14. Initially, the Keuper Marl was split into six layers. Due to the softness of the Keuper Marl and the larger specimen area (=2.4m by 7m), a vibrating plate with a working area of 300x300mm (Figure 4.11) and a basic weight of 19kg was used to compact the specimen. The compacted layer was left overnight before placing the next layer. This sub-grade layer was overlaid with a sub-base layer for other projects prior to the shakedown project which had to be removed from the test pit so that the Keuper Marl could be recompacted using a vibrating plate on the exposed surface. Samples of the subgrade were taken to identify the moisture content and the strength properties. The Langford Fill Sand in the second profile was prepared by dividing the sand into two layers and compacted using the same vibrating plate that was used to compact the Keuper Marl. The crushed Carboniferous Limestone was split into four layers and compacted using a BOMAG BW55E Single Drum vibrating roller (see Figure 4.12) with an operating weight of 136kg. The test pit was split into four test sections approximately 2.5m long by 1.25m wide so that four constructions could be tested. The density of each layer was identified by using the sand replacement method (BS 1377-9, 1990).



**Figure 4. 9 Vibrating hammer used on soils for the SW**



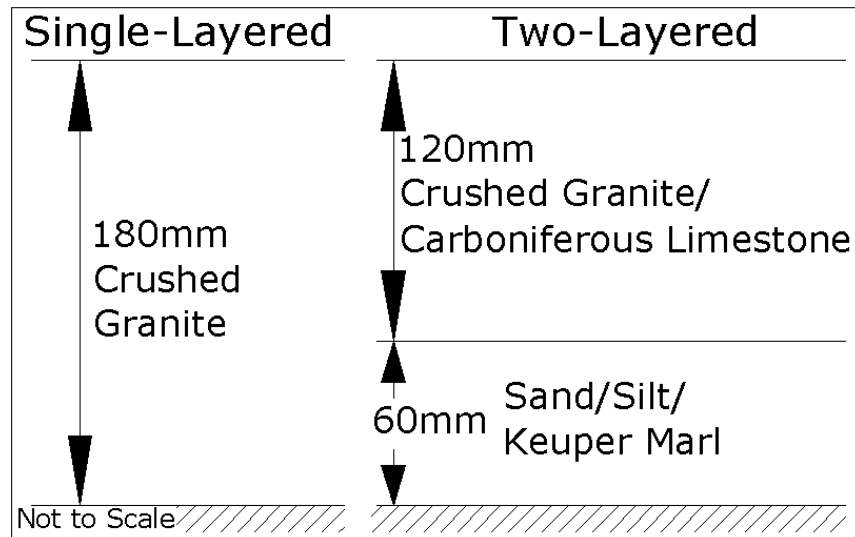
**Figure 4. 10 Vibrating plate used on soils for the STF**



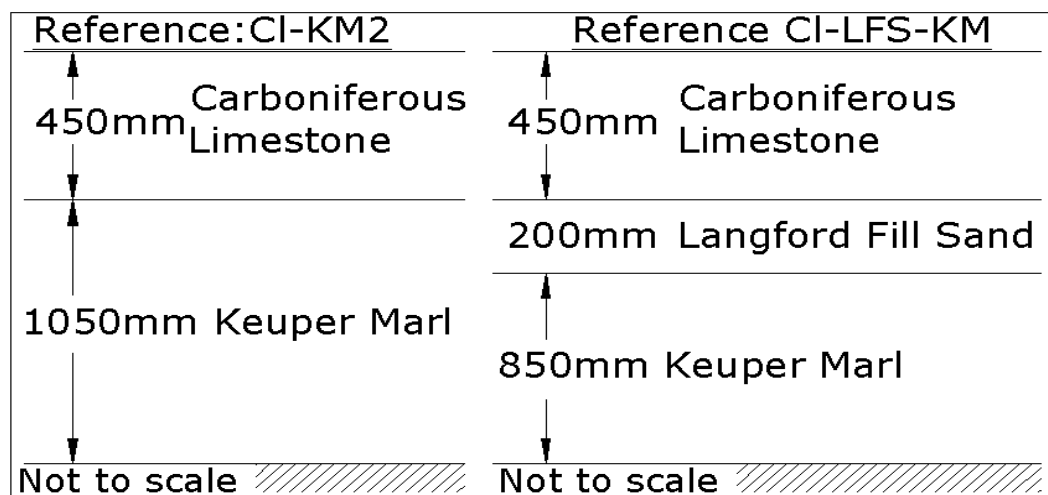
**Figure 4. 11 Vibrating plate used on Keuper Marl and sand for the PTF**



**Figure 4. 12 Single drum vibrating roller used on Limestone for the PTF**



**Figure 4. 13 Typical specimen profiles for the STF test**



**Figure 4. 14 Two specimen profiles for the PTF test**

## 4.4 TEST CONDITIONS

A summary of the wheel tracking specimen test conditions is presented in Table 4.2.

**Table 4. 2 Summary of the wheel tracking specimen test conditions**

Test Condition	Small Wheel Tracker (SW)	Slab Testing Facility (STF)	Pavement Testing Facility (PTF)
<b>Loading Directions</b>	Two ways	Two ways	Two ways
<b>Tyre Inflation Pressure (kPa)</b>	n/a	276	650
<b>Speed (km/hour)</b>	0.55	approx. 1.4	approx 2.5
<b>Temperature</b>	$20 \pm 2^{\circ}\text{C}$	$20 \pm 2^{\circ}\text{C}$	$20 \pm 2^{\circ}\text{C}$

Notes: n/a means not applicable.

Considering the changes in the specimen moisture content and the difficulty in sealing the specimen for the next day test, the moving wheels of all the facilities were programmed to run only in a specified position and were bi-directional although the STF and PTF can operate as one-way. This is not the case in a real pavement, where the vehicle moves in different lateral positions on the road and uni-directionally. However, Brown and Chan (1996) studying the effect of the uni-directional and bi-directional wheel loading found that the bi-directional loading was more damaging than uni-directional loading and the rut depth of the bidirectional loading can be up to 60% higher than under uni-directional loading. The wheel tracking test results in this case will be overestimated.

The tyre inflation pressures used for the STF and the PTF were maintained constant at 276kPa and 650kPa respectively. A constant wheel load was applied at each test. The applied wheel load levels were varied from above to below the predicted shakedown loads corresponding to the test specimen.

Each wheel tracking facility has a different speed. However each specimen that was tested using the same facilities was tested at the same speed.

All the specimens were tested with direct contact with the wheel except for the Portaway Sand. The wetted sand loses the moisture very quickly especially on the surface once it is exposed to the air. It became dry and changed the characteristic of the soil specimen. Therefore, the wheel load test was carried out on top of 1.5mm thick rubber sheet. The temperature of the specimen for all the wheel load tests was kept at  $20 \pm 2^{\circ}\text{C}$  throughout the testing.

## **4.5 DATA COLLECTION PROCEDURES**

### **4.5.1 The Procedures for the Contact Pressure Measurement**

To identify the contact pressure of the applied load, the applied wheel load and contact area need to be measured. The applied wheel loads were measured using a load cell. Each of the wheel tracking facilities has a different method in measuring the wheel loads. More details on the wheel load measurement of

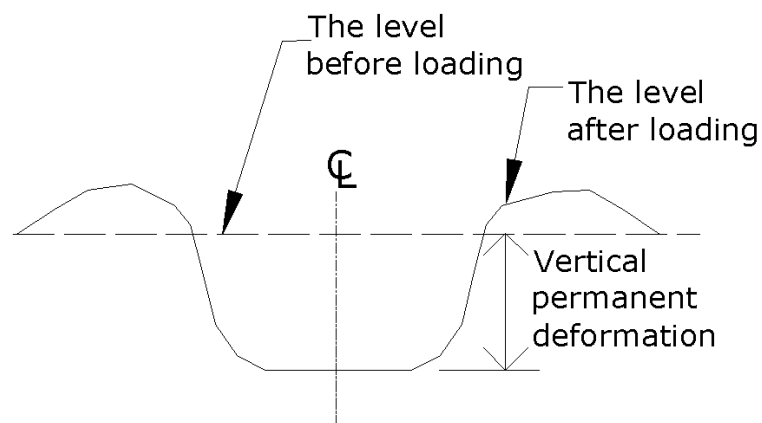
each wheel tracking facility are given in Sections 4.2.1, 4.2.2 and 4.2.3 for the SW, the STF and the PTF respectively.

The contact area of the applied wheel load for all the facilities was obtained using ink on the wheel/tyre tread and loading the wheel onto graph paper which was placed on the surface of the test specimen. However, surface irregularities can cause an unclear tread print and sometimes running ink distorts the tread print. To minimise these problems, more than one tread print for each wheel load of the SW and the STF were taken. The ink prints were scanned and analysed electronically using a computer software package called AutoCAD. The contact patch of the tyre through the tread pattern was assumed uniform. The average values of the contact areas were plotted against the wheel load and are reported in the next chapter. The ink print contact patches on various soils under each wheel loading facility are provided in Appendix C.

For the PTF, the contact pressure that was calculated from the applied wheel load divided by the ink print contact area was checked against pressure cells placed under the wheel path, at about 100mm below the surface. The pressure cells were calibrated using a mechanical bench calibration test in which a known stress was applied directly to the strain gauge diaphragm to give an electrical output from the pressure cell (Brown, 1977). The results of the measured contact pressure and the cell pressure outputs against the wheel load are reported in the next chapter. It is expected that the pressure readings from the cells should be less than the surface pressures generated by the wheel load. This is because the applied wheel load is spread out by the soil over the cell.

#### 4.5.2 The Procedures for the Transverse Profile and Vertical Permanent Deformation Measurement

The permanent vertical deformation is defined as the vertical distance between the undisturbed pavement surface and the bottom of the deformed wheel path on its centre line (see Figure 4.15).



**Figure 4. 15 Definition of the vertical permanent deformation**

#### *SW*

Due to the sensitivity of the specimen and limited access for taking measurements, this facility only involved an indirect vertical permanent deformation measurement system. A linear variable differential transformer (LVDT) or displacement transducer was mounted on the lever arm [see Figure 4.1 above] to measure the development of the surface deformation as the test progresses to an accuracy of 0.01mm. The initial LVDT reading, which could be read through an Analogue-Digital Read Out, was recorded manually as the



zero pass reading. The moving wheel was stopped periodically at the initial position to record the Analogue-Digital Read Out as deformation developed.

#### ***STF and PTF***

For these two facilities, the transverse profile and vertical permanent deformation were measured by using a steel ruler with a straight edge as a reference beam. The reading was to the nearest 0.5mm. The data collection routine for vertical permanent deformation was organised so that trafficking was stopped periodically for intermediate measurements to be taken. The transverse profile of the test specimen was measured at the end of test.

## **4.6 SUMMARY**

A brief description of the wheel tracking facilities that were used in the experiments is given in this chapter including the loading mechanism. The load for the SW's specimen is applied via the loading arm. Both the STF and PTF loading system are provided by a hydraulic actuator.

The specimen preparation procedure for all of the wheel tracking facilities is almost the same. Most of the specimens were wetted to their optimum moisture content and compacted in layers. The difference is the compactor that was used depended on the size of the specimen and the material characteristic.

The wheel tracking test was programmed to run only in a specified position and with bi-directional loading and was conducted at various speeds depending on the type of the wheel tracking facilities that were used. Types of data that were collected from the experiments are the contact area, the wheel load, the transverse profile and the vertical permanent deformation. The results are reported in Chapter 5.

## **5 RESULTS OF WHEEL TRACKING TESTS**

### **5.1 INTRODUCTION**

This chapter reports the experimental results which are split in three categories: the contact pressure, the transverse profile and the permanent vertical deformation. The presentations of the results from the latter two are based on the material type. The contact pressure is presented based on the type of wheel trackers. When more than one point was measured, an average is reported.

### **5.2 TEST PROGRAMME**

A summary of the test material properties are shown in Table 5.1. The average value is reported. More details on the test specimen properties for each test section are given in Appendix D including the details of the applied stresses. For each material or combination, at least three different wheel load levels were tested.

**Table 5. 1 Summary of the wheel tracking test specimens**

	Number of layers	Three	Two				One				
	Reference	CI-LFS-KM	Gr-PS	Gr-Silt	CI-KM1	CI-KM2	PS1	PS2	KM	Silt	Gr
	Type of wheel tracking facilities	PTF	STF	STF	STF	PTF	SW	SW	SW	SW	STF
Layer 1	Type of material	Crushed Carboniferous Limestone	Crushed Granite	Crushed Granite	Crushed Carboniferous Limestone	Crushed Carboniferous Limestone	Portaway Sand	Portaway Sand	Keuper Marl	Silt	Granite
	Thickness (mm)	450	120	120	120	450	250	125	125	125	180
	$\gamma_{ave}$ (kg/m <sup>3</sup> )	2314	2138	2142	2099	2192	1888	1886	2166	1734	2200
	$w_{ave}$ (%)	0.9	4.1	4.2	2.8	2.9	4.1	4.1	15.1	15.2	4
	$RD_{ave}$ (%)	79	61	62	39	55	90	90	n/a	n/a	68
	$Sr_{ave}$ (%)	13	33	33	23	29	24	24	94	54	36
	Type of material	Langford Fill Sand	Portaway Sand	Silt	Keuper Marl	Keuper Marl	<div>Layer 1</div> <div>Layer 2</div> <div>Layer 3</div> <div>Typical Test Section Profile</div>				
Thickness (mm)	200	60	60	60	1050						
$\gamma_{ave}$ (kg/m <sup>3</sup> )	1504	1885	1736	2010	2200						
$w_{ave}$ (%)	7.7	4.1	15.5	22.5	23						
$RD_{ave}$ (%)	27	90	n/a	n/a	n/a						
$Sr_{ave}$ (%)	23	23	55	94	122						
Layer 3	Type of Material	Keuper Marl	<div>Notes:</div> <ul style="list-style-type: none"><li><math>\gamma_{ave}</math> means the average bulk density.</li><li><math>w_{ave}</math> means the average moisture content.</li><li><math>RD_{ave}</math> means the average relative density.</li><li><math>Sr_{ave}</math> means the average degree of saturation.</li></ul>				<ul style="list-style-type: none"><li>Details on how to calculate the RD and Sr are given in Appendix D.</li><li>PTF=Pavement Testing Facility</li><li>STF=Slab Testing Facility</li><li>SW=Small Wheel Tracker</li></ul>				
	Thickness (mm)	850									
	$\gamma_{ave}$ (kg/m <sup>3</sup> )	2200									
	$w_{ave}$ (%)	23									
	$RD_{ave}$ (%)	n/a									
	$Sr_{ave}$ (%)	122									
	Range of the applied stresses (kPa)	310-453	152-269	145-390	141-224	215-333	100-154	100-154	225-301	193-261	289-384

Table 5.1 shows that the average bulk density of the crushed Carboniferous Limestone in the PTF was higher than others. The crushed Carboniferous Limestone layer was compacted using vibrating roller therefore it had higher average bulk density compared to the ones using vibrating plate. An additional layer of the Langford Fill Sand between the Keuper Marl and crushed Carboniferous Limestone improved the density of the crushed Carboniferous Limestone layer which may increase the resistance to permanent deformation.

### **5.3 CONTACT PRESSURE**

The contact pressure is the applied wheel load divided by the contact patch area. The contact patches of various wheel loads using various wheel tracking facilities were taken vertically under a stationary wheel before trafficking. According to Marwick and Starks (1941), the difference in the vertical stress distribution under a moving or a stationary wheel was insignificant. The load was assumed to be distributed uniformly over the imprint area and the effect of the tread gap was ignored. The tread pattern is probably only significant at the surface. As the wheel penetrates the surface, the stress distribution will be more even with depth. Saraf et al. (1987) studying the effect of the tread pattern on the contact pressure distribution found that the tread gap reduced the number of contacts. The calculated contact pressures are likely to be less than the actual maximum contact pressures.

### **5.3.1 The Solid Wheel**

The plots of the contact pressures of various types of materials against the applied solid wheel loads of the SW are presented in Figure 5.1. It was found that each material had a different contact pressure pattern. The effect of the inflation pressure on the contact pressure in this case is not applicable because the wheel is solid. Compared with the other materials under the same wheel load (see Figure 5.1), Portaway Sand has the lowest contact pressure or largest contact area. It seems that there is a correlation between the contact pressure and the material shear strength. Portaway Sand, with the lowest shear strength amongst the others, has the lowest resistance to the applied wheel load.

### **5.3.2 The Pneumatic Wheel**

A comparison of the contact patches with the tyre treads of the 1.7kN and 9kN wheel loads of the PTF is shown in Figure 5.2. Under the same inflation pressure, the contact area of the 1.7kN wheel load is concentrated in the centre of the tyre but the 9kN wheel load is distributed to the tyre edge. Freitag and Green (1962) and de Beer et al. (1997) who varied the inflation pressure and the wheel load found similar behaviour. According to Freitag and Green (1962) and de Beer et al. (1997), the inflation pressure predominantly controlled the contact stress at the tyre centre, and the load controlled the contact stresses at the tyre edges.

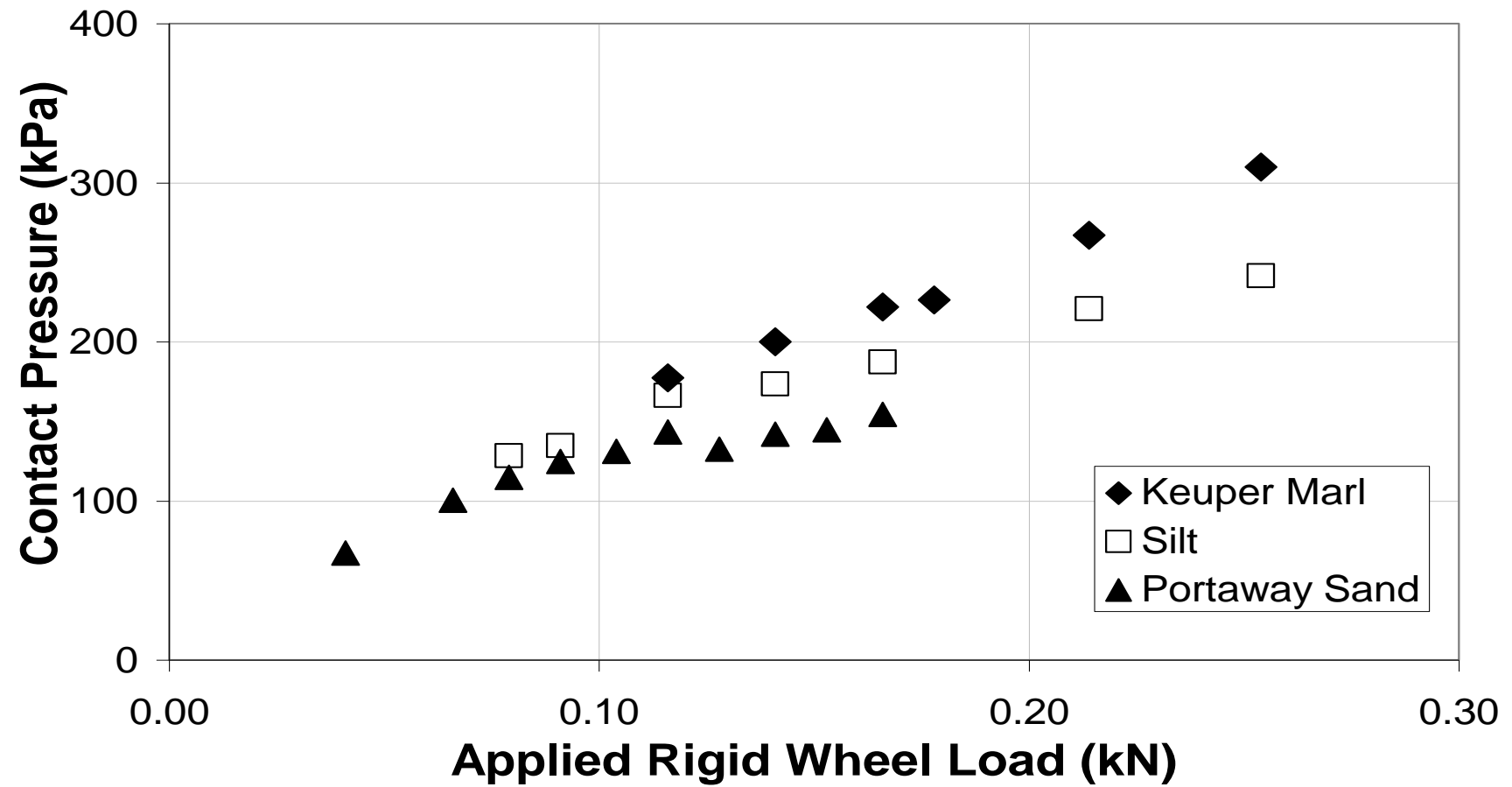
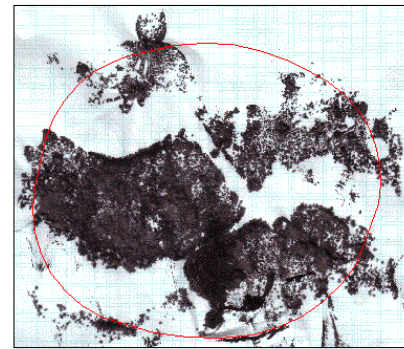
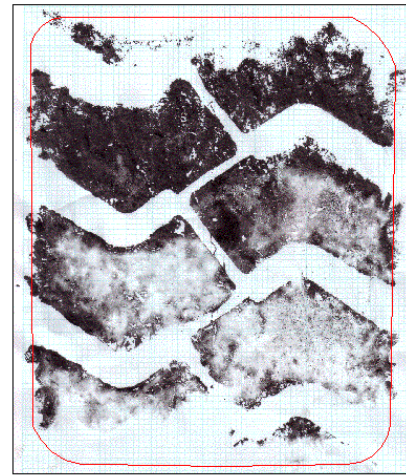


Figure 5. 1 The contact pressures of the SW's rigid wheel on three different types of materials



(a) Wheel load=1.7kN



(b) Wheel load=9kN

Note: Both contact patches are not to scale

**Figure 5. 2 Typical prints of the contact pressure distributions using the PTF**

Figures 5.3 and 5.4 show the plots of the measured pressures against the applied pneumatic wheel load of the STF and PTF respectively of various soil combinations. The plots show that the relationship between the pressure and the applied load is not linear. As the pneumatic wheel load increases, the contact pressure tends to level off.

The pressure readings from the pressure cells which were placed at approximately 100mm below the surface (see Chapter 4 Section 4.5.1) were well below the contact pressure values and are presented in Figure 5.4. The increase of the applied wheel load was followed by the increase of the pressure on the cell.



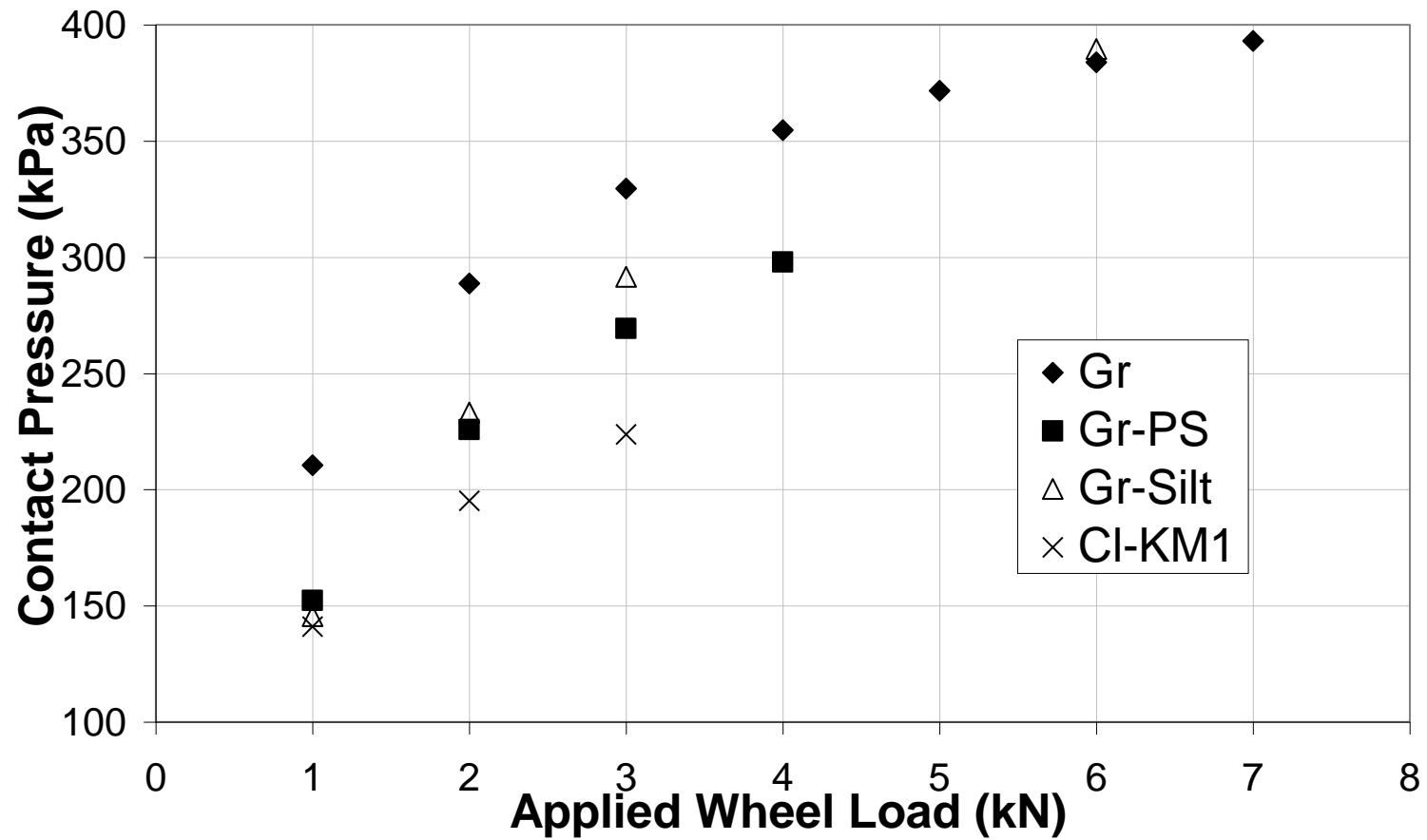
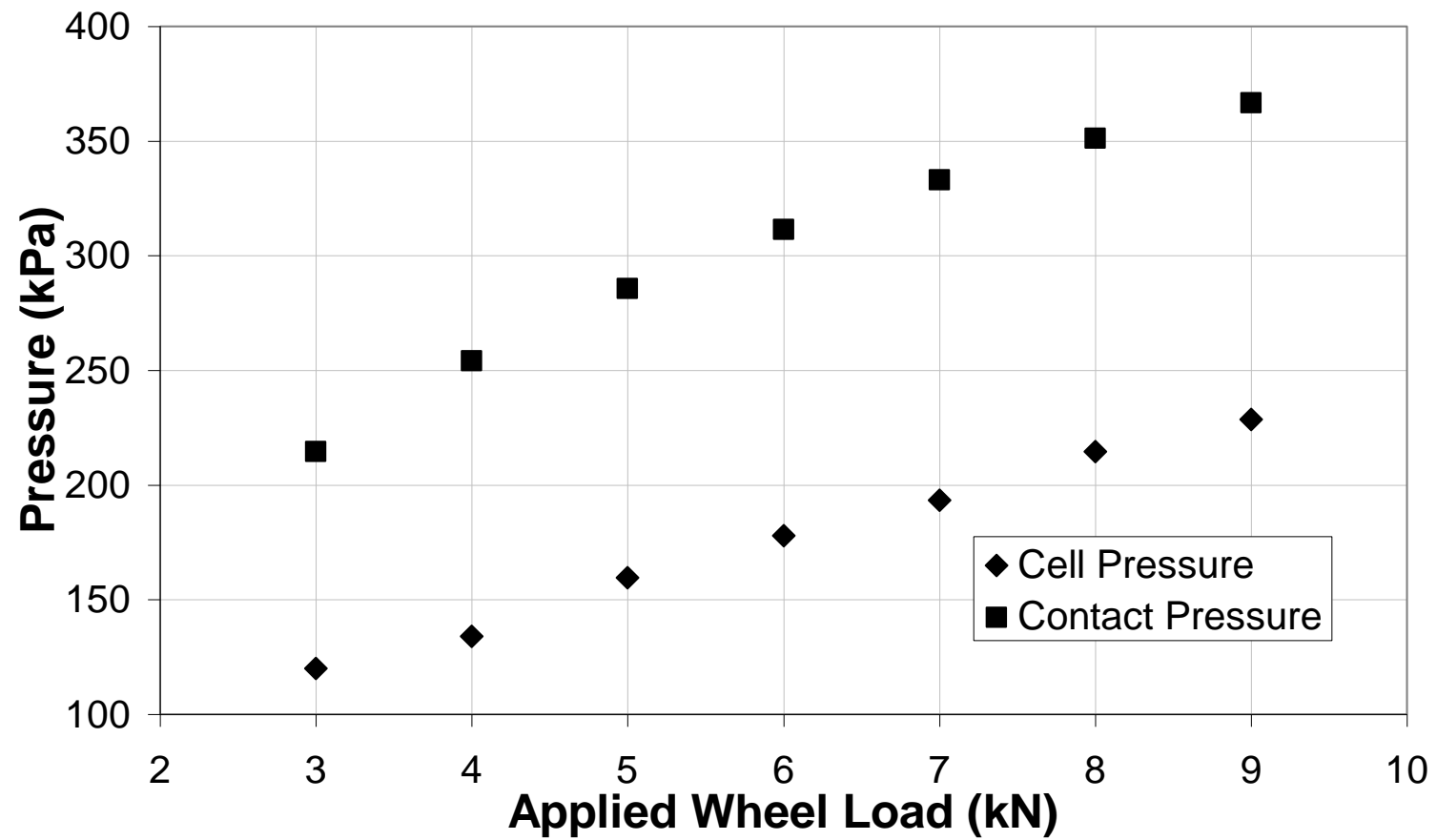


Figure 5. 3 The surface pressures at different wheel loads and for different materials (STF)



**Figure 5. 4 The cell pressures and contact pressures for different PTF wheel loads**

Figure 5.3 shows that the Gr had a better resistance to the applied static wheel load compared with the other specimens. Under the same wheel load, higher contact pressures were obtained for the Gr compared to the other specimens (Gr-Silt and Gr-PS). The differences were between 11% and 30%. The contact area reduced due to less penetration. There was slight difference in the contact pressures between the Gr-Silt and Gr-PS, but it was insignificant compared to the Gr. The relative density of the crushed Granite of the Gr ( $RD_{ave}=65\%$ , see Table 5.1) was slightly higher than the Gr-Silt ( $RD_{ave}=62\%$ , see Table 5.1) and Gr-PS ( $RD_{ave}=61\%$ , see Table 5.1) which means the crushed granite of the Gr has a higher compaction than the Gr-Silt and Gr-PS. It seems the lower layer as the platform for the top layer has an effect on the compaction of the top layer particularly for a thin top layer (120mm thick crushed Granite in this case).

## **5.4 TRANSVERSE PROFILE**

Due to lack of access to measure directly the transverse profile of the SW's specimens and the difficulty in moving the specimen from the SW without disturbing it, the photographs of the test material post-loading were taken and presented in Figures 5.5 to 5.7. The pictures show the deformed surface as a result of further densification and the shear deformation accompanied by upheavals to the side due to the lateral forces moving particles from the loaded area to the nearest unloaded area. The profiles of the two crushed rocks

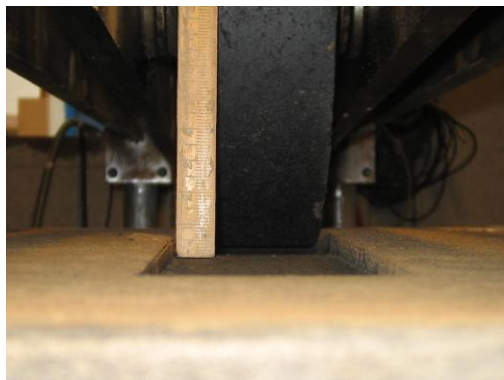
(crushed Granite and Carboniferous Limestone) in Figures 5.8, 5.9 and 5.10 show the deformed surface is accompanied by very small upheavals.



**Figure 5. 5 Portaway Sand after 8000 passes with contact pressure of 100kPa using the SW**



**Figure 5. 6 Keuper Marl after 650 passes with contact pressure of 301kPa using the SW**



**Figure 5. 7 Silt after 16000 passes with the contact pressure of 229kPa using the SW**



**Figure 5. 8 Crushed Granite after 10000 passes with contact pressure of 355kPa using the STF**

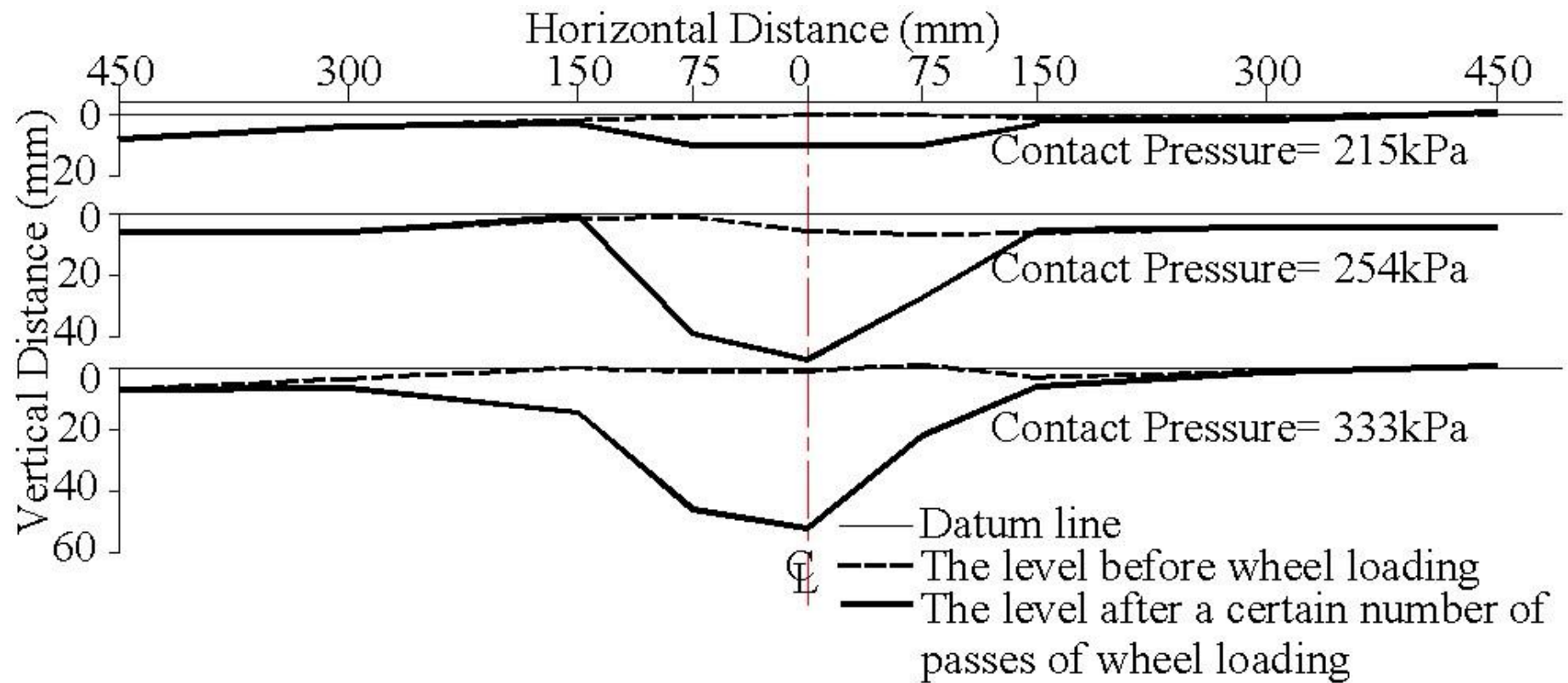


Figure 5. 9 Section transverse profiles measured manually before and after the two layers tests of PTF for all three test sections

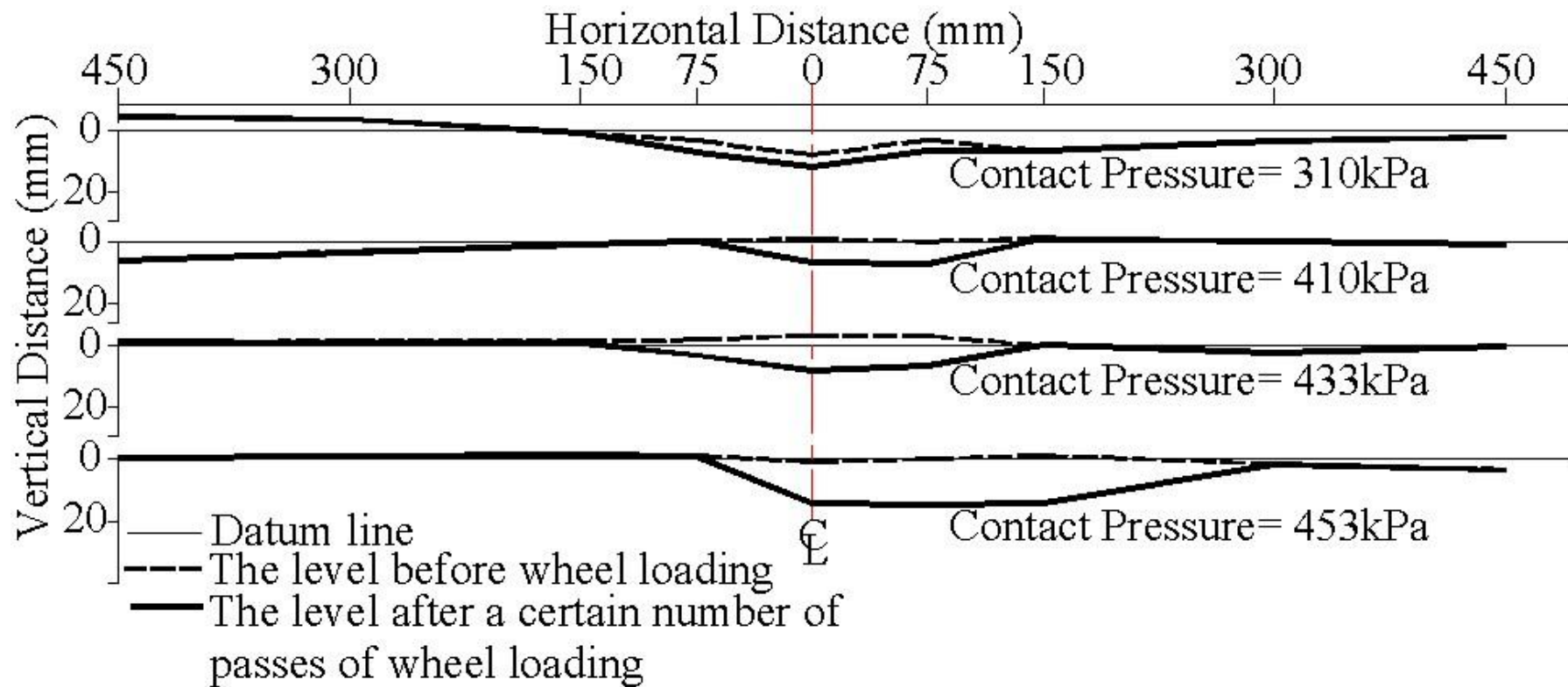


Figure 5. 10 Section transverse profiles measured manually before and after the three layered tests for all four test sections (PTF)

## **5.5 VERTICAL PERMANENT DEFORMATION**

Unless failure intervened, the tests were carried out in one day with up to 16,000 passes using the SW or 10,000 passes using the STF. This was to minimise the loss of moisture during the testing. However, a few tests were carried out up to 100,000 passes and no significant changes were found. For the PTF, the specimens were tested during working days only and up to 50,000 passes which took approximately two weeks. The PTF specimen was sealed either side of the wheel path, and this was also covered when the loading was not taking place.

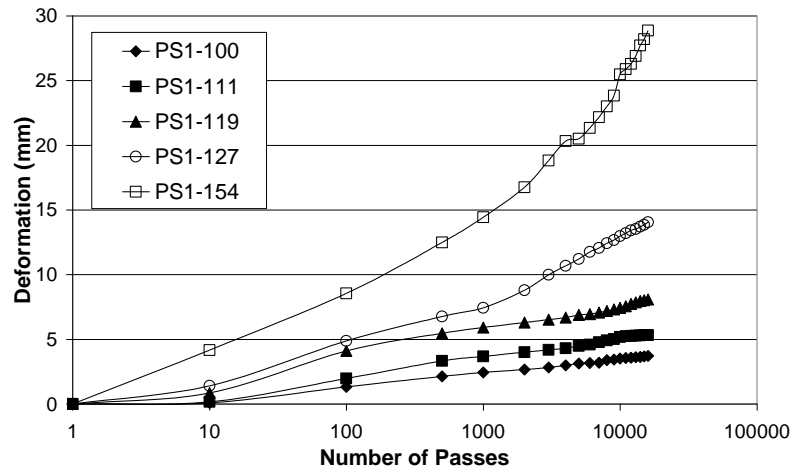
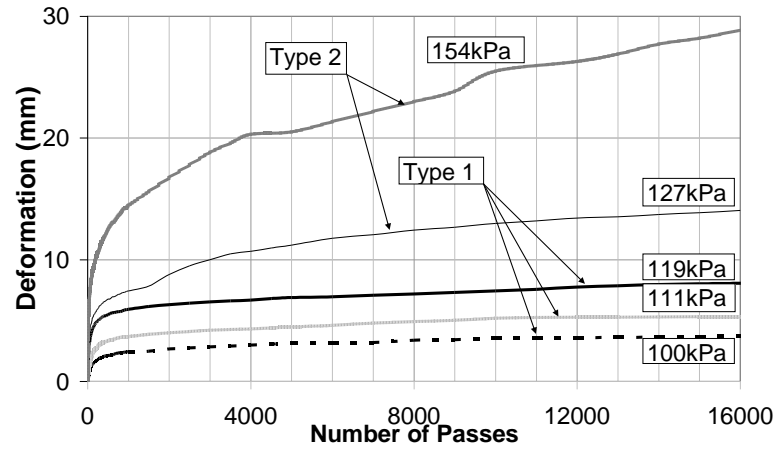
Plots of vertical permanent deformation against the number of passes for the different materials and types of wheel tracking facilities at various wheel loads are presented in Figures 5.11 to 5.20. Increasing the load magnitude resulted in an increase in plastic deformation. The amount of vertical permanent deformation occurring depended on the applied load magnitudes and the soil shear strength which indirectly depends on the density of the specimen, and the compaction effort during the preparation period.

From the plots, two distinct phases of the vertical permanent deformation development were identified: a rapid rate and gradual rate of plastic deformation. Based on the two phases, three types of vertical permanent deformation curves were observed (labelled as Types 1, 2, and 3). If the specimens only experienced a rapid plastic deformation rate and showed no sign of shakedown, the deformation curve is categorised as Type 3. The

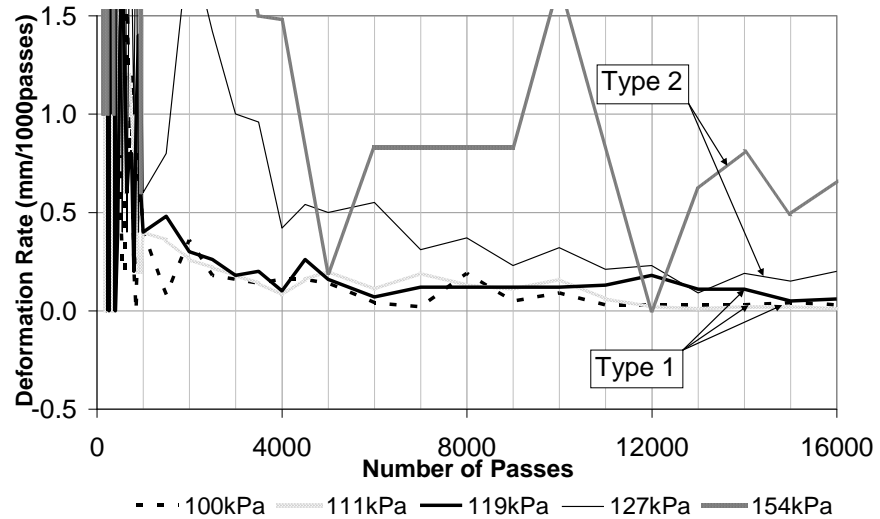
deformation rate for Type 3 is generally above 0.018mm/pass after 500 passes. If the specimen has a rapid plastic deformation at the beginning of the test then followed by a gradual decrease in the plastic deformation rate, two different types of deformation curves were identified. If the deformation rate approaches 0.001mm/pass or zero after 1000 passes, the curve is categorised as Type 1, if not it is Type 2 (see the plot of the deformation rate against number of passes in Figure 5.11b). Plots of the deformation rate against the number of passes to clarify the difference between Types 1 and 2 for various materials are presented in Appendix F. Type 2 can be said to form the boundary between the Types 1 and 3 curves. The deformation rate curve for Type 3 may not be found in the plots because of the large deformation rate per pass. Due to the limitation of the wheel trackers' load and the shear strengths of the specimens, some specimens showed only Type 2 or Type 2 and 3 or Types 1 and 2 curves. The complete curves of Types 1, 2 and 3 can be found in Figures 5.13, 5.17 and 5.19.

From the deformation rate plots, it was found that the gradual rate phase occurred after approximately between 200 and 500 passes. The specimens with Type 1 response had a deformation rate approaching zero at various numbers of passes. The Gr-Silt reached shakedown after approximately 500 passes (see Figure 5.17), but the Cl-KM2 required at least 10000 passes (see Figure 5.19). This shows that the number of passes that is required to reach shakedown depends on the applied stresses and type of materials and it may be followed by a gradual increment of permanent deformation.





(a) Variation of the vertical deformation of PS1 with number of passes for various wheel pressures



Note: SW was used in the tests.

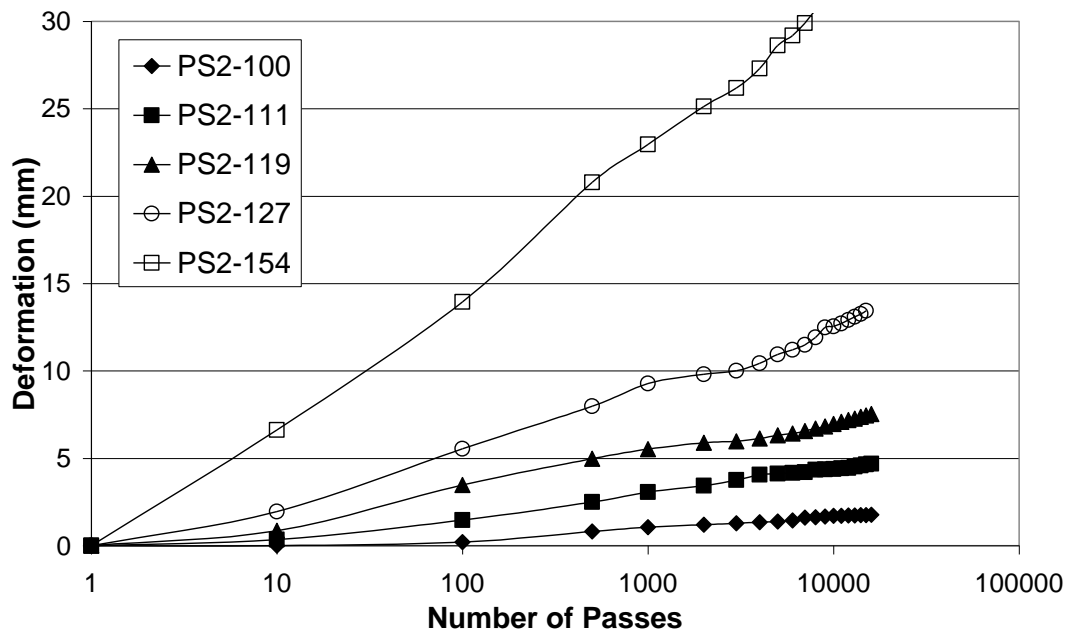
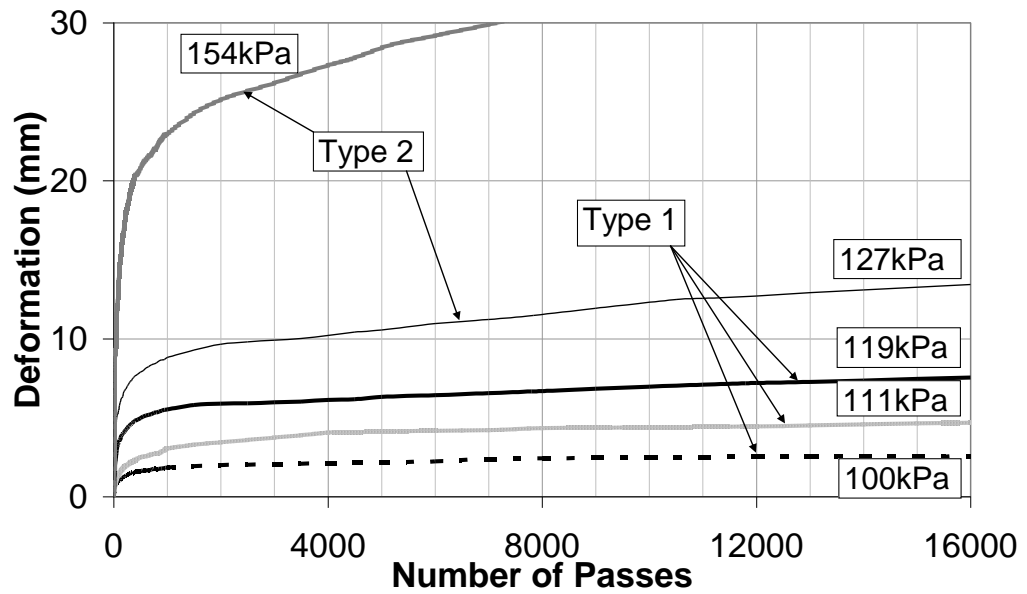
For PS1 refer to Table 5.1. 100kPa means the applied wheel load was 100kPa.

(b) Variation of the vertical deformation rate of PS1 with number of passes for various wheel pressures

**Figure 5. 11 Variation of the vertical permanent deformation and the deformation rate of PS1 with number of passes for various wheel pressures**

The curves of the permanent deformation versus logarithm of number passes have similar patterns to that found by Chan (1990) in Nottingham University.

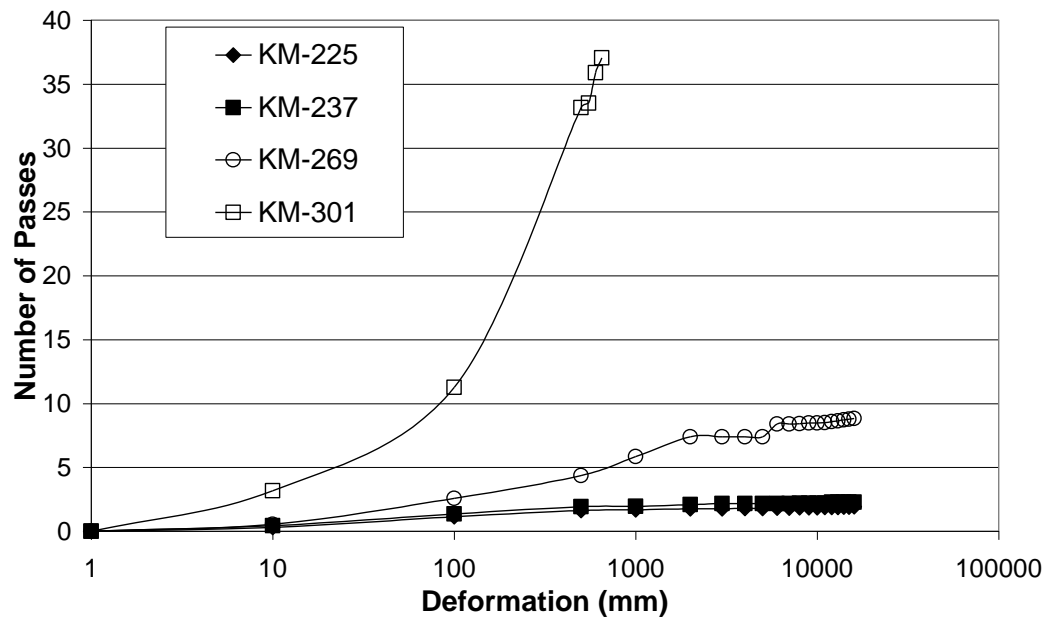
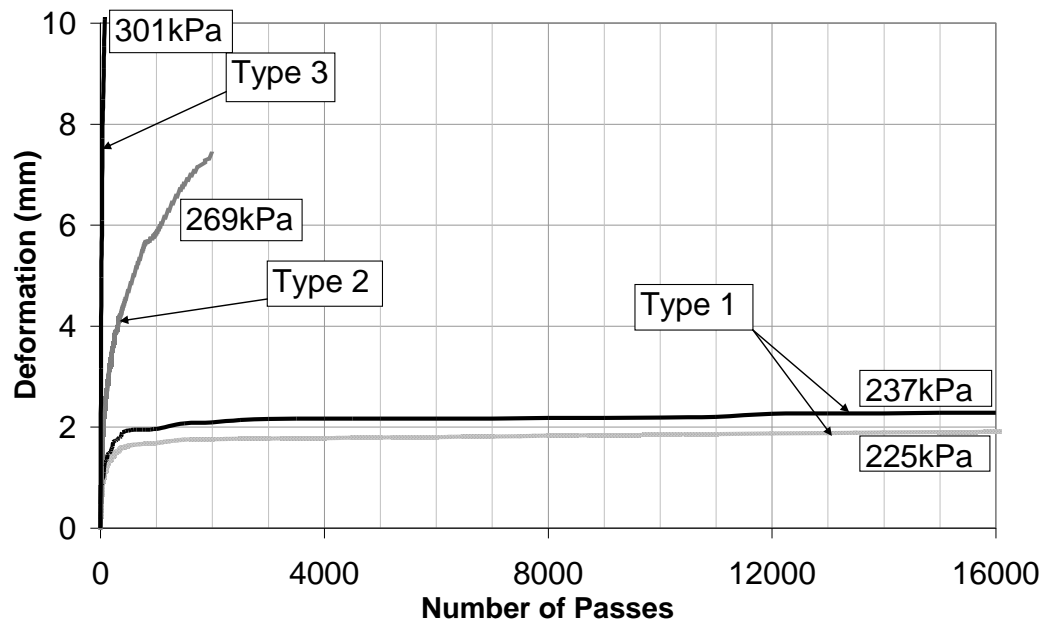
For the test materials used in the one layered test (see the results of the one layer tests from Figures 5.11 to 5.15), Portaway Sand with the lowest shear strength has the least resistance to permanent deformation. Similar results were found for two different thicknesses (125mm and 250mm) of Portaway Sand but with the same density (see Figures 5.11 and 5.12).



Note: SW was used in the tests.

For PS2 refer to Table 5.1. 100kPa means the applied wheel load was 100kPa.

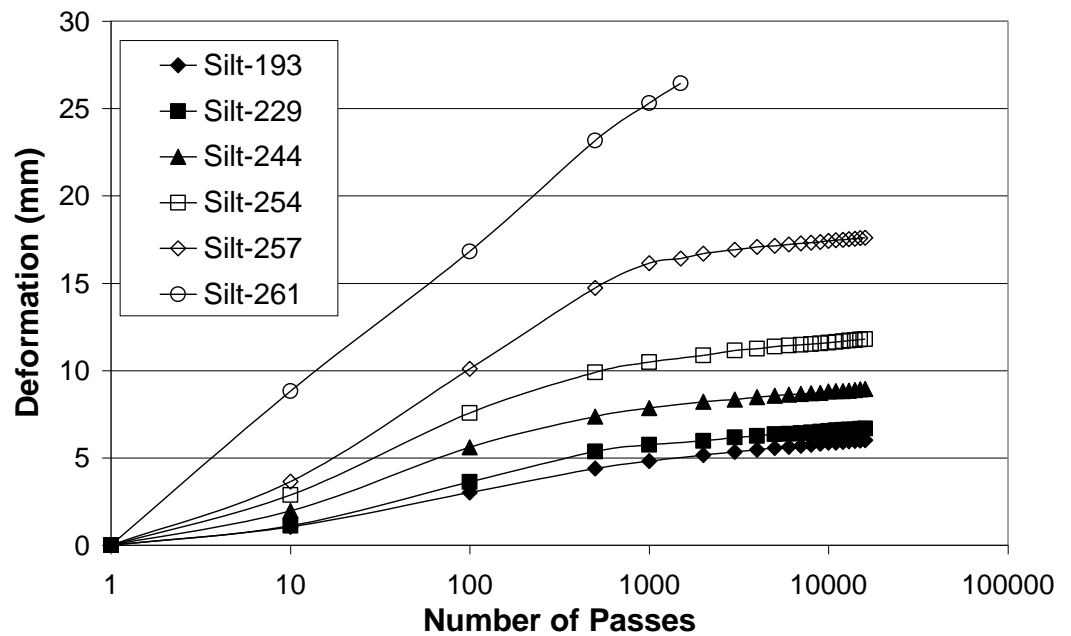
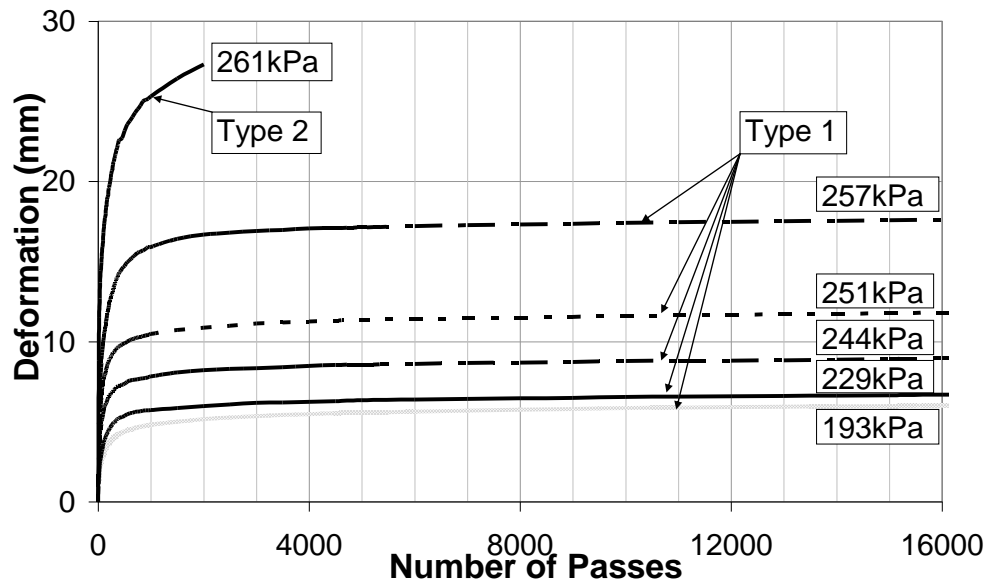
**Figure 5. 12 Variation of the vertical permanent deformation of PS2 with number of passes for various wheel pressures**



Note: SW was used in the tests.

For KM refer to Table 5.1. 225kPa means the applied wheel load was 225kPa.

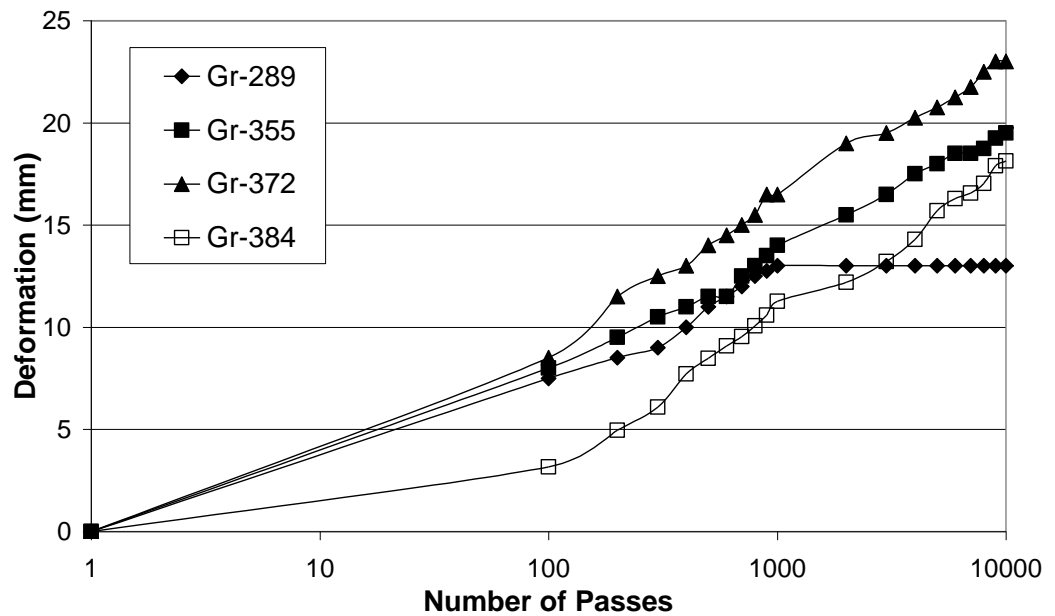
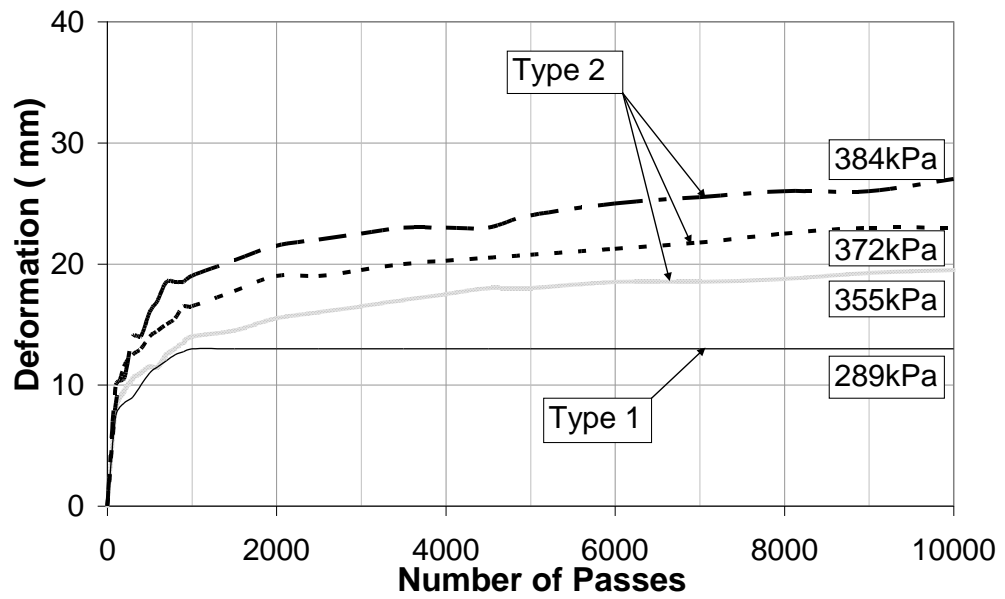
**Figure 5. 13 Variation of the vertical permanent deformation of KM with number of passes for various wheel pressures**



Note: SW was used in the tests.

For Silt refer to Table 5.1. 193kPa means the applied wheel load was 193kPa.

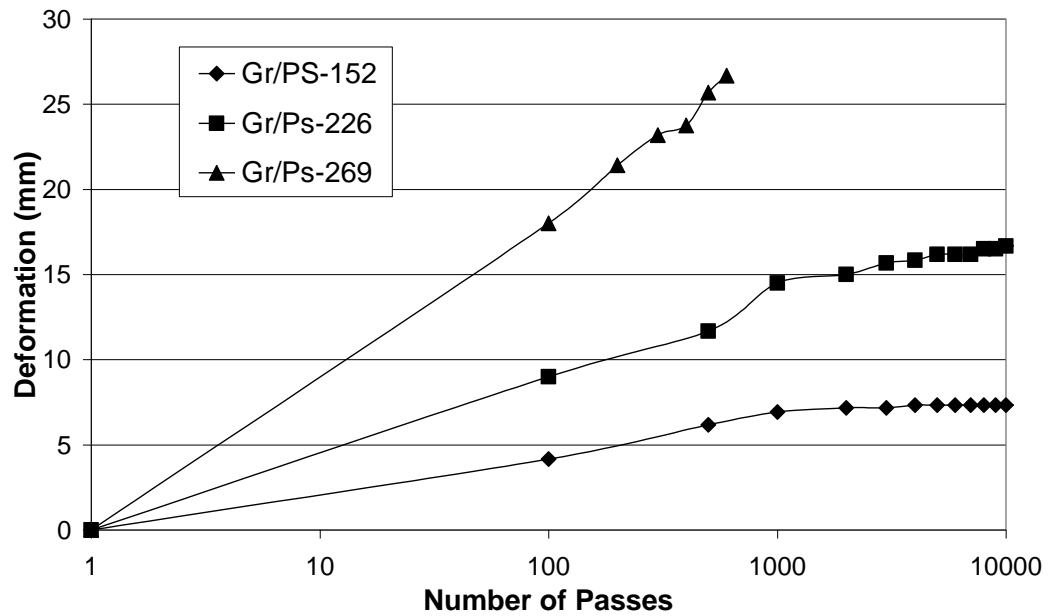
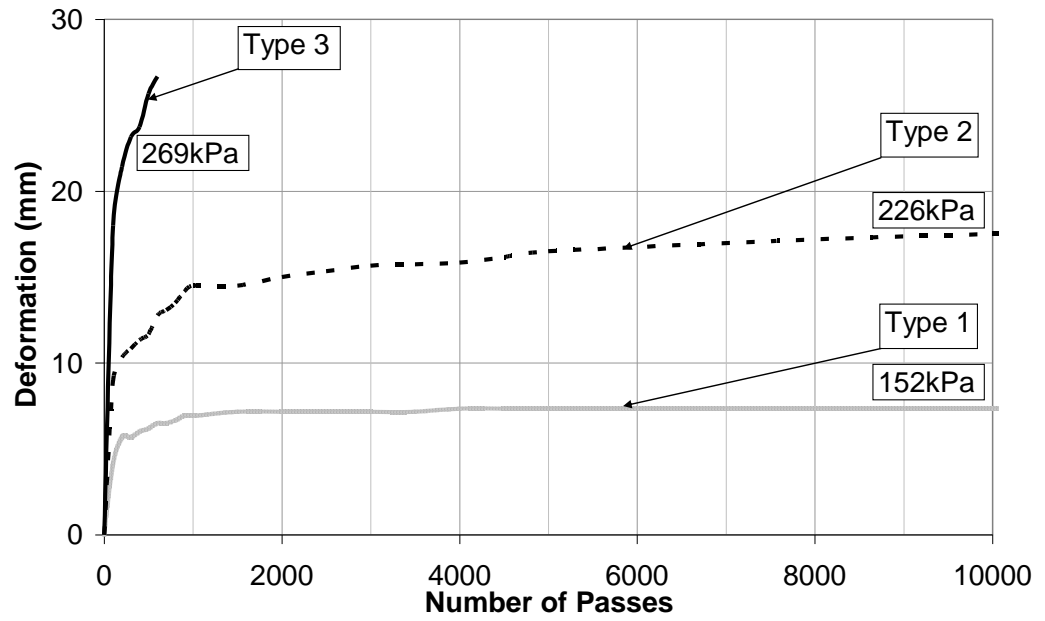
**Figure 5. 14 Variation of the vertical permanent deformation of Silt with number of passes for various wheel pressures**



Note: STF was used in the tests.

For Gr refer to Table 5.1. 289kPa means the applied wheel load was 289kPa.

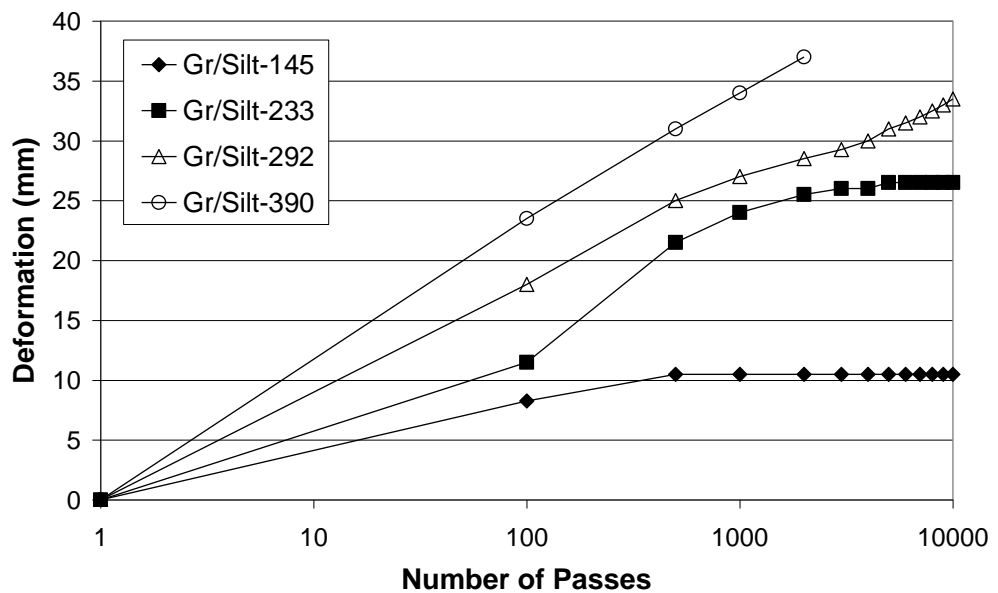
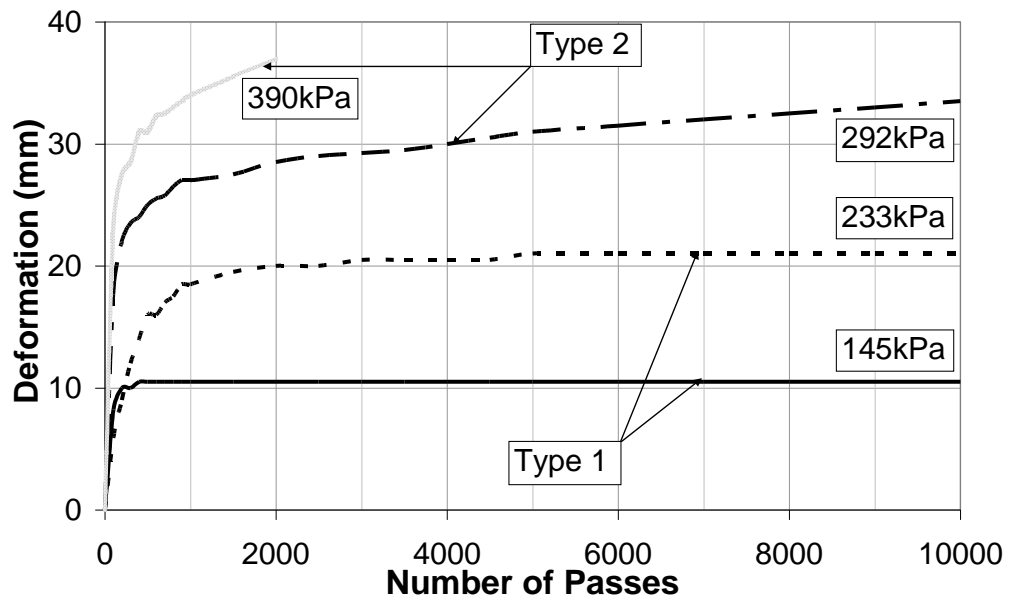
**Figure 5. 15 Variation of the vertical permanent deformation of Gr with number of passes for various wheel pressures**



Note: STF was used in the tests.

For Gr-PS refer to Table 5.1. 152kPa means the applied wheel load was 152kPa.

**Figure 5. 16 Variation of the vertical permanent deformation of Gr-PS with number of passes for various wheel pressures**



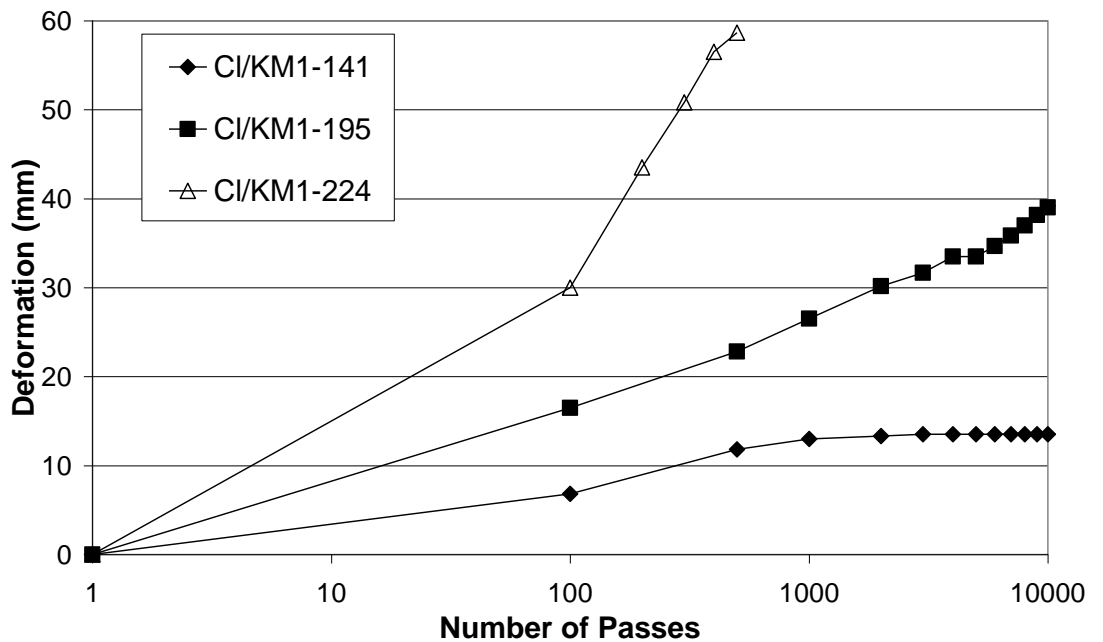
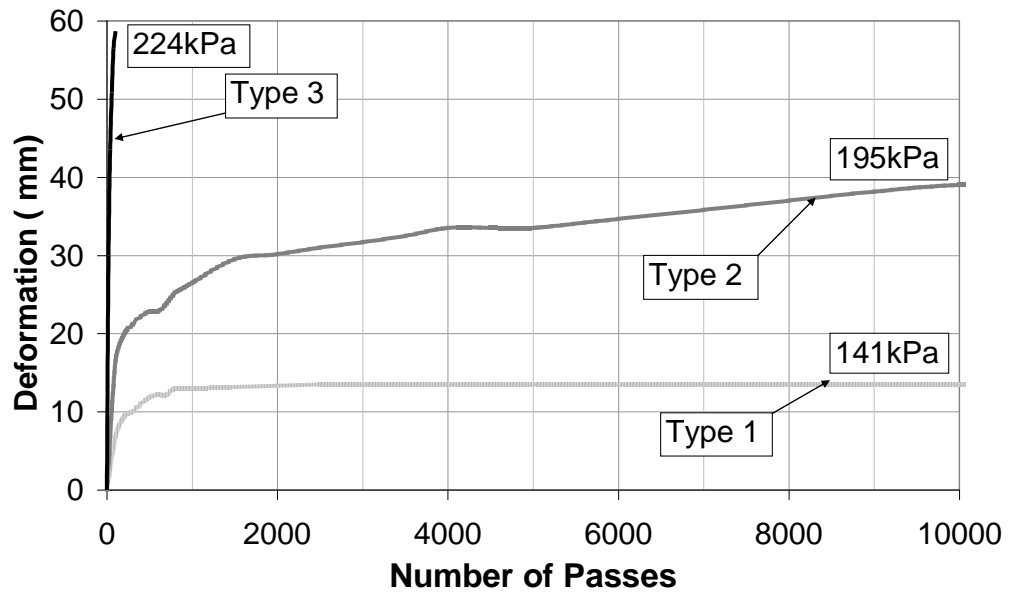
Note: STF was used in the tests.

For Gr-Silt refer to Table 5.1.

145 kPa means the applied wheel load was 145kPa.

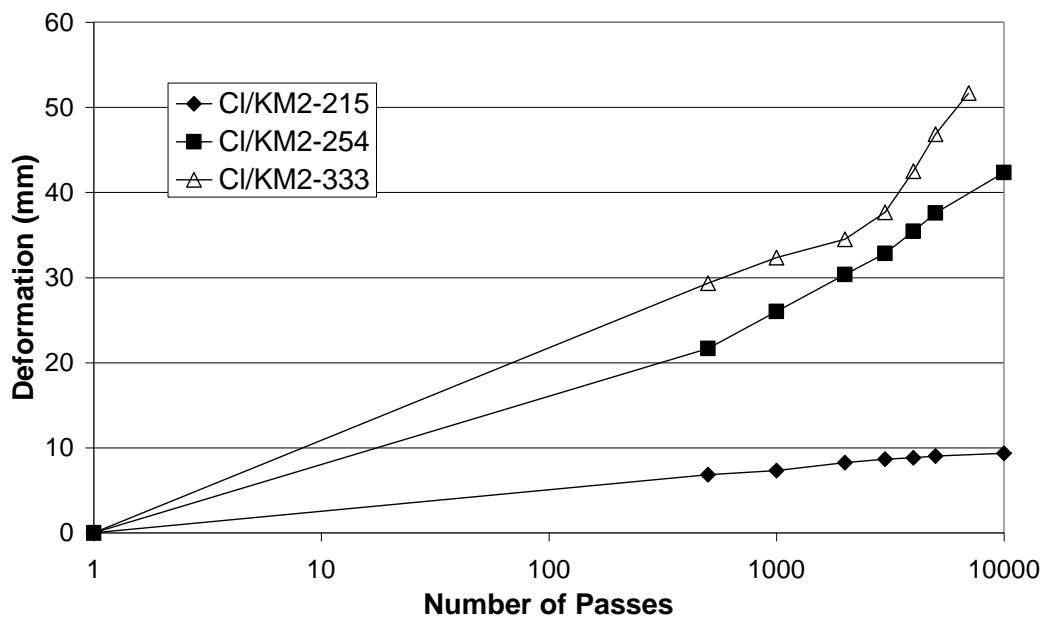
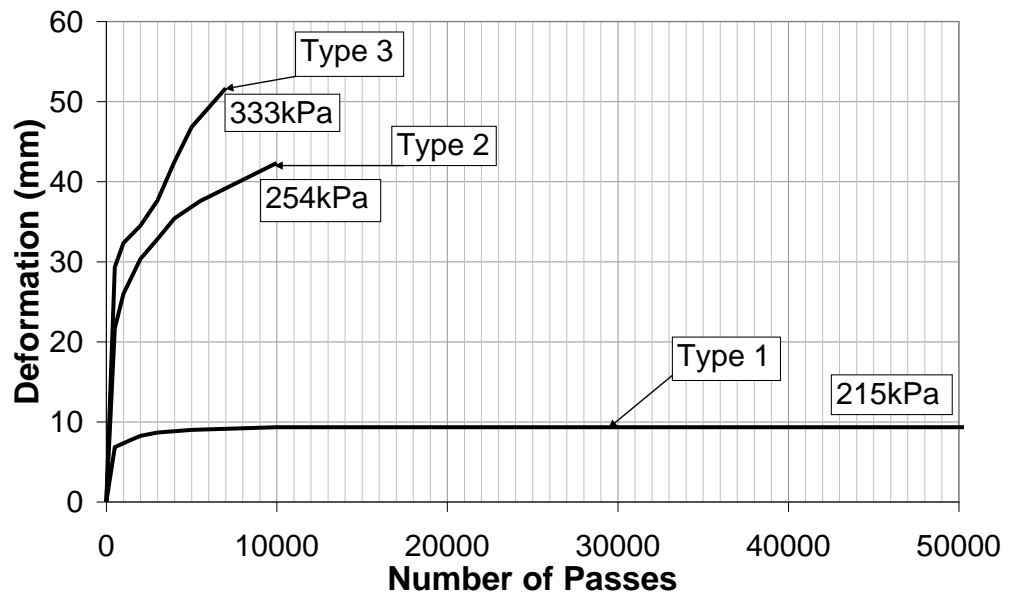
**Figure 5. 17 Variation of the vertical permanent deformation of Gr-Silt with number of passes for various wheel pressures**





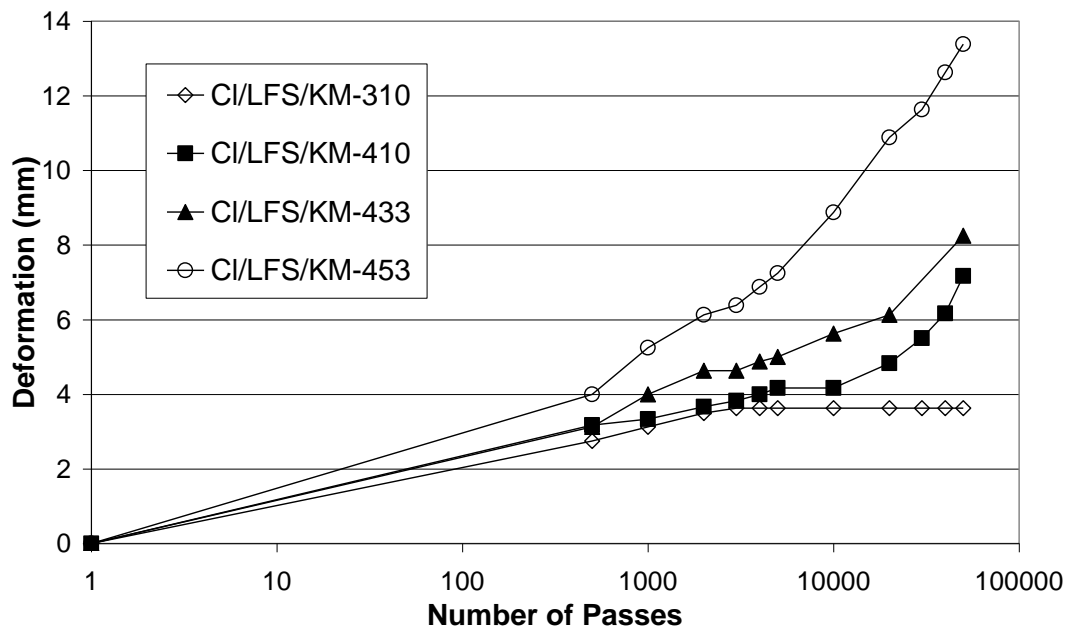
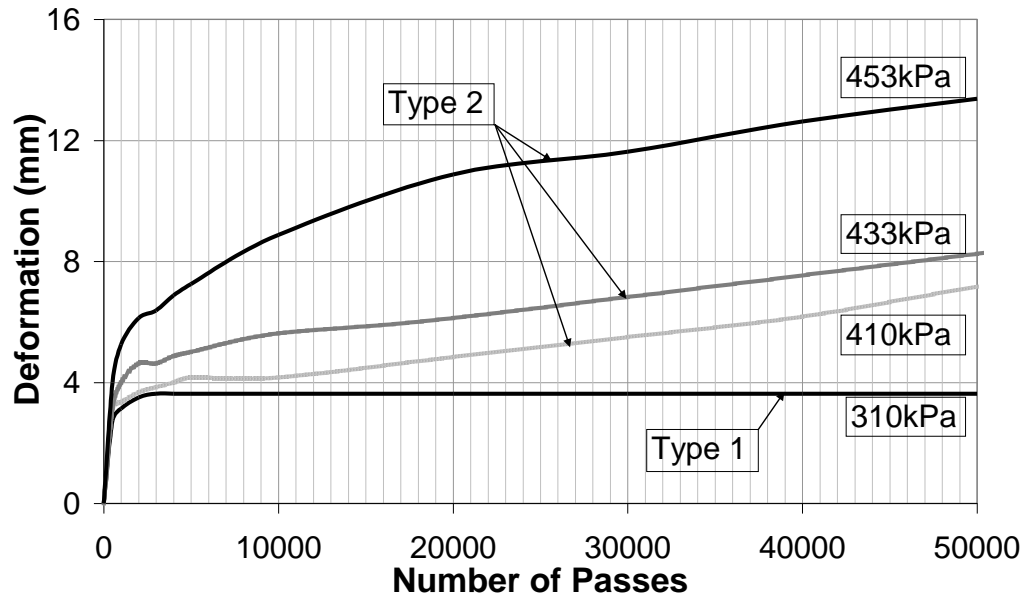
Note: STF was used in the tests.  
 For CI-KM1 refer to Table 5.1.  
 141kPa means the applied wheel load was 141kPa.

**Figure 5. 18 Variation of the vertical permanent deformation of CI-KM1 with number of passes for various wheel pressures**



Note: PTF was used in the tests.  
 For CI-KM2 refer to Table 5.1.  
 215kPa means the applied wheel load was 215kPa.

**Figure 5. 19 Variation of the vertical permanent deformation of CI-KM2 with number of passes for various wheel pressures**



Note: PTF was used in the tests.  
 For CI-LFS-KM refer to Table 5.1.  
 310kPa means the applied wheel load was 310kPa.

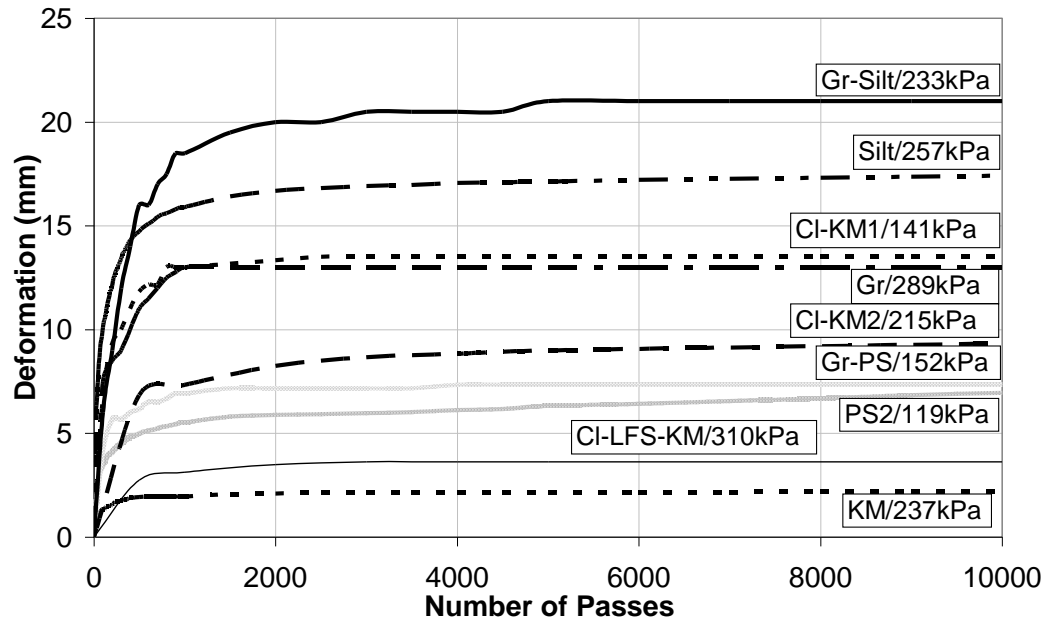
**Figure 5. 20 Variation of the vertical permanent deformation with number of passes for various wheel pressures of CI-LFS-KM**

Placing a 200mm thick layer of Langford Fill Sand between the layer of crushed Carboniferous Limestone and the Keuper Marl improved the

resistance of the structure to the permanent deformation (see Figures 5.19 and 5.20). An additional layer of the Langford Fill Sand made it easier to compact the crushed Carboniferous Limestone in comparison to directly compacting the crushed Carboniferous Limestone over the Keuper Marl. The crushed Carboniferous Limestone achieved higher density and had better resistance to permanent deformation.

## **5.6 DISCUSSION**

From the experimental results, it can be said that the soil specimen with Type 1 response reaches shakedown (no further permanent deformation). The number of passes required to reach shakedown and the accumulation of the vertical permanent deformation during soil stabilisation varied for each type of soil. The plots of the accumulation of the vertical permanent deformation at the maximum wheel contact pressure that related to the Type 1 response are shown in Figure 5.21. Most of the soil specimens reached a shakedown state after 2,000 passes. The accumulation of the vertical permanent deformation varied between 2.2mm and 21mm. However, since this research is only concerned with the onset or otherwise of shakedown, no analysis of deformation magnitude is presented.



Notes:

The references are provided in Table 5.1.

**KM/237kPa** means the Keuper Marl at an applied wheel pressure of 237kPa.

**Gr-PS/152kPa** means the Granite as the top layer and the Portaway Sand as the bottom layer at an applied pressure of 152kPa.

**Figure 5. 21 Variation of the vertical permanent deformation for different soil combinations**

From a series of wheel tracking tests, it can be seen that a well-compacted specimen during the preparation period will exhibit less vertical permanent deformation. The CI-LFS-KM/310, a three layered specimen with a better compaction of the granular layer (RD=79%, see CI-LFS-KM in Table 5.1) has better resistance to the permanent deformation than the CI-KM2/215, a two layered specimen with the relative density of 55% for the granular layer (see CI-KM2 in Table 5.1). Therefore, it is important to ensure the specimen is well-compacted prior to testing during the preparation period.

For the two and three layered tests, the soil of the bottom layer may influence the compaction of the material above it. With the same compaction method, the density of the material that was compacted on the weak soil was less than

the one on the stronger soil. The crushed Granite (see Gr in Table 5.1) compacted on the rigid base had an average relative density ( $RD_{ave}$ ) of 68% and performed better than the 450mm thick crushed Carboniferous Limestone compacted on the soft Keuper Marl (moisture content=23%) which had an average relative density of 55% (see Cl-KM2 in Table 5.1). The crushed Carboniferous Limestone achieved a higher density (with  $RD=79\%$ ) when 200mm of Keuper Marl was replaced by a layer of the Langford Fill Sand (see Cl-LFS-KM in Table 5.1).

## **5.7 SUMMARY**

This chapter reports the test results from three wheel tracking facilities. Each specimen was prepared and compacted so that the specimen had a consistent density and moisture content. Each type of specimen was tested over a range of wheel loads. The wheel load was kept constant for each wheel tracking test.

The contact area under the applied wheel load was measured to identify the applied contact pressure. The plots of the contact pressures for different wheel loads on each soil show that the deformation resistance of the specimen to the wheel load depends on the strength of the specimen. A soil specimen with a higher strength has a better resistance to deformation. The relationship between the applied pneumatic wheel load and the contact pressure may not be linear.

A key output from the wheel tracking test is the vertical permanent deformation relationship with loading, the number of passes and the type of specimen. It was found that the specimen response depends on the shear strength of the specimen and the applied load. Based on this information, three different types of response (Types 1, 2, and 3) were identified. Type 1 response may consist of a rapid rate of deformation depending on the soil strength followed by a gradual rate of deformation and after a certain number of passes the rate of deformation approaches zero. If it experiences a rapid rate of deformation only without any stabilisation, it is classified as a Type 3 response. Type 2 response is in between these two responses.

Based on the definition of the shakedown concept, the specimen with a Type 1 response can be said to have ‘shaken’ down. The maximum shakedown limit of the specimen may be within the maximum wheel contact pressure that gave a Type 1 response and the minimum wheel contact pressure that gave a Type 2 response. A summary of the wheel loads between these limits is presented and compared to the theoretical predictions in Chapter 7.

From the wheel tracking test results, it is noted that some specimens experienced a large vertical permanent deformation before reaching the shakedown state. However, a well compacted specimen reached the shakedown state with less initial vertical permanent deformation. To obtain better resistance to permanent deformation, it is suggested to provide a good compaction to the soil during the preparation period to reduce the vertical permanent deformation that may develop as result of load repetitions before

reaching the shakedown behaviour. Some ground improvement such as replacing the weak soil with a better quality soil, or reducing the moisture content of the weak soil may be needed to provide a good platform for the compaction of the soil placed above it if the support soil is too weak.



## **6 THE APPLIED SURFACE STRESSES RATIO**

### **ASSR**

#### **6.1 INTRODUCTION**

As mentioned before in Chapter 2.3, in addition to the shear strength ( $c$  and  $\phi$ ) and the elastic properties ( $E$  and  $\nu$ ) of the soil specimen, the applied surface stresses ratio ASSR between the wheel and the specimen is also required to compute the theoretical shakedown load of a pavement structure. The ASSR is the ratio of the horizontal and vertical stresses or forces acting on the specimen surface as a result of the wheel load. The vertical force corresponds to the applied load and weight of the wheel which is perpendicular to the contact surface. The horizontal force is related to a force that is required to cause the wheel to rotate on the surface.

The measurements of the vertical and horizontal forces were carried out directly using the wheel tracking facilities. Additional specimens were prepared to identify the ASSR between the wheel and the specimen surface for the SW and the STF. A summary of the specimen properties is given in Table 6.1. The ASSR of the PTF was measured on the unloaded surface of the PTF specimen. The details of the PTF specimen have been presented in Chapter 5 Table 5.1. The method to obtain the ASSR and the results are presented below.

**Table 6. 1 Summary of the specimen properties for the ASSR measurement**

<b>Material Type</b>	<b>Bulk Density (kg/m<sup>3</sup>)</b>	<b>Moiture Content (%)</b>	<b>Relative Density (%)</b>	<b>Sr (%)</b>	<b>Thickness (mm)</b>
<b><i>SW</i></b>					
Portaway Sand	1890	4.2	90	24	125
Keuper Marl	2162	15.0	n/a	93	125
Silt	1732	15.2	n/a	54	125
<b><i>STF</i></b>					
Crushed Granite	2232	4.0	71	38	180
Crushed Carboniferous Limestone-	2099	2.8	39	23	120
Keuper Marl*	2002	23.0	n/a	94	60

Notes:

\* means two layer specimen in which the Carboniferous Limestone was placed over the Keuper Marl.

‘n/a’ means no applicable for this soil.

Sr means degree of saturation.

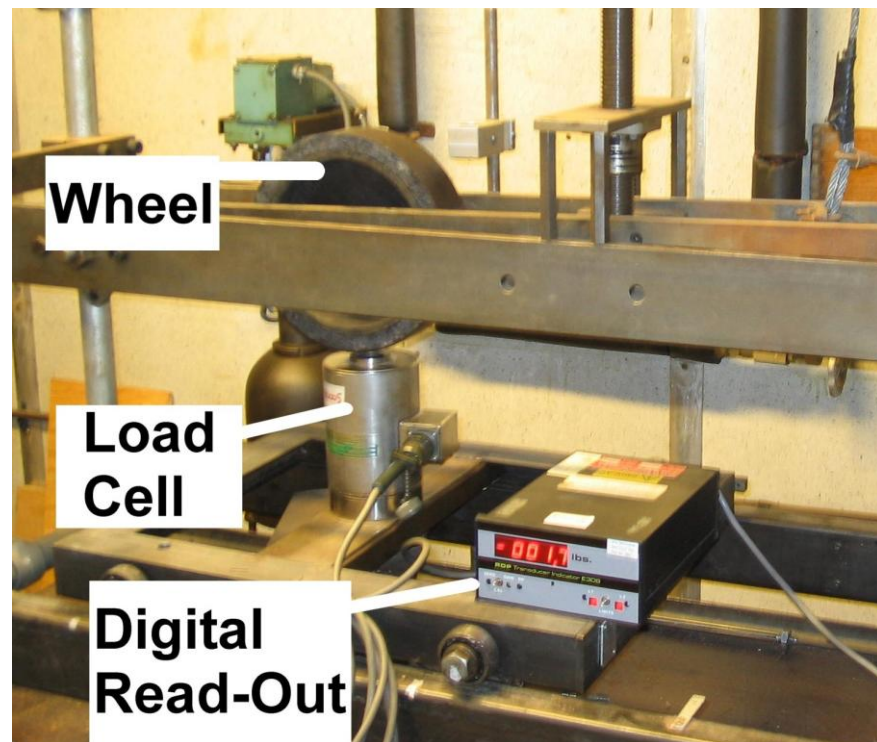
## **6.2 THE METHOD TO MEASURE THE VERTICAL AND HORIZONTAL FORCES**

### ***The Vertical Force***

The vertical force can be measured using a load cell. The load cell was placed just below the wheel and connected to the digital read-out to identify the applied wheel load. Figure 6.1 shows a typical arrangement of the load cell in measuring the vertical force of the SW.

### *The Horizontal Force*

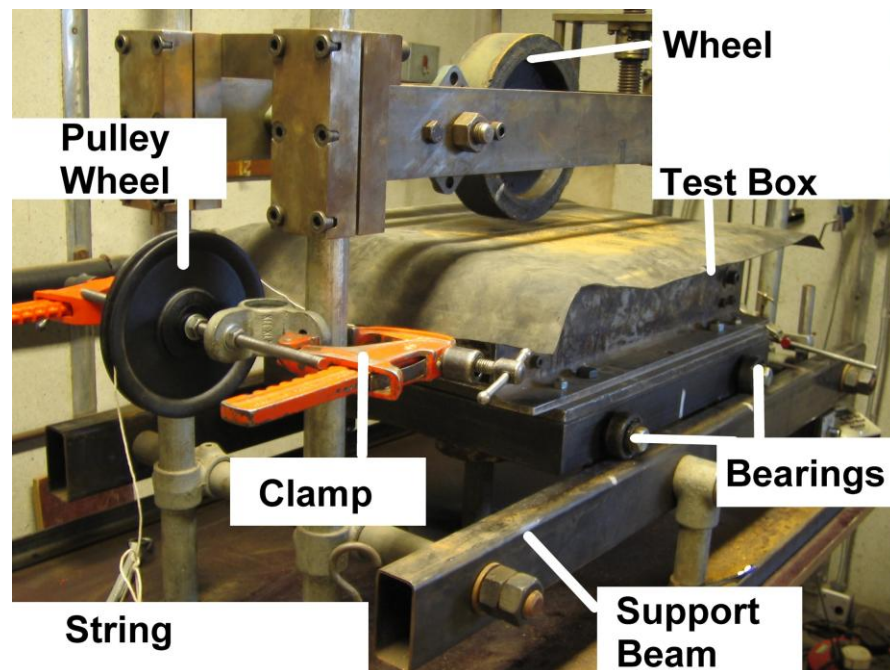
To identify the horizontal force between the wheel and specimen surface, it was necessary to measure the horizontal force to rotate the bearings only and the total horizontal force to rotate the bearings on the support beams with the wheel running on the specimen surface. This is because the wheel carriages of the STF and PTF and the test box of the SW ran on the support beams via the small bearings.



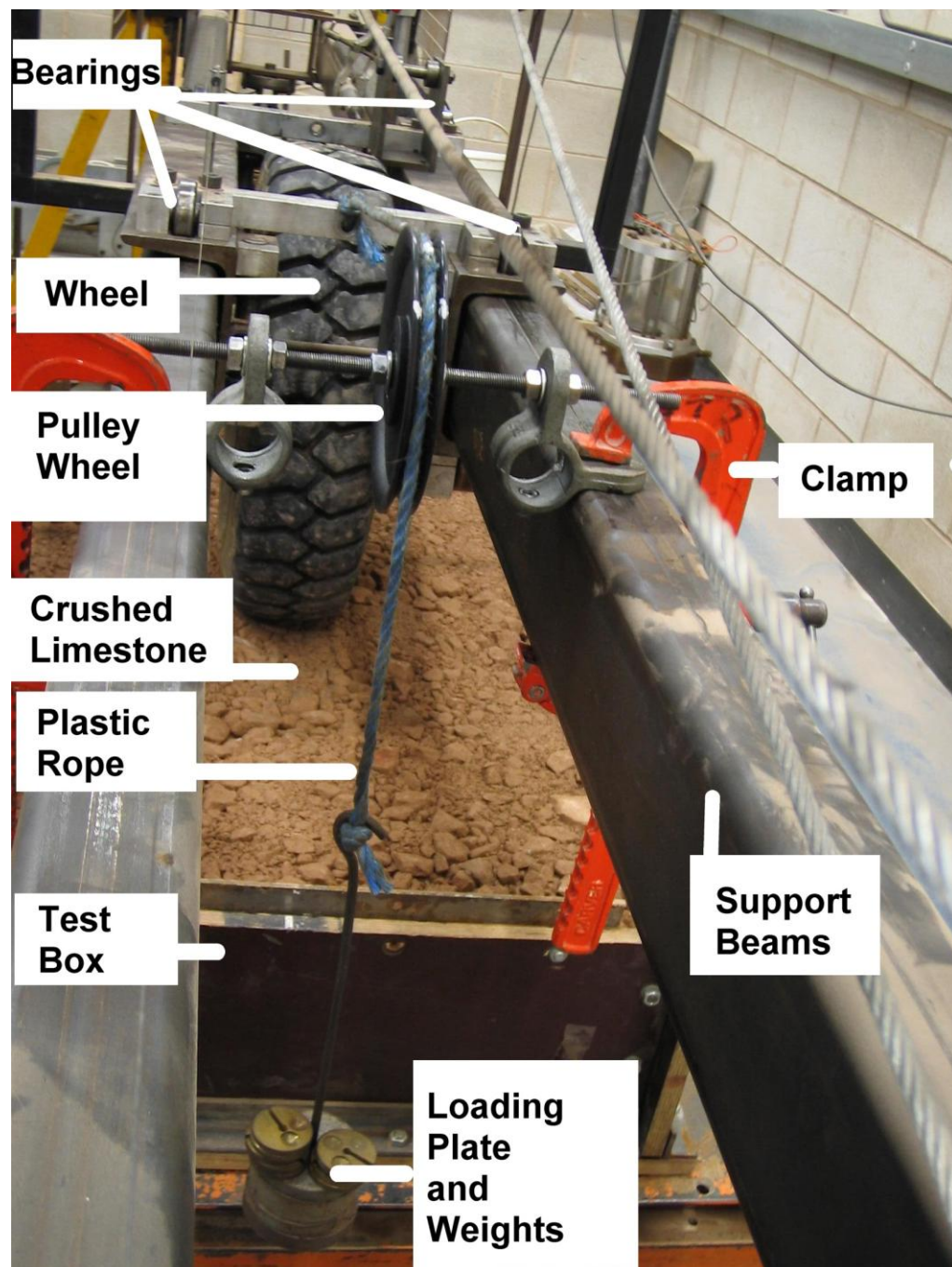
**Figure 6. 1 A load cell and the digital read-out at the SW**

For the SW, the horizontal force was applied to pull the test box instead of the wheel because the wheel was attached to the immobile loading arm (see section 4.2.1). The arrangement for measuring the horizontal force in the SW is

shown in Figure 6.2. A pulley wheel was used to convert the applied weights to a horizontal force. A string was attached to the test box, which went over a pulley wheel and was connected to a loading plate. Small weights were added on to the loading plate until the test box moved. The total weight on this loading plate was the required horizontal force to move the test box. The measurement was repeated three times and an average value was taken. For the STF and the PTF, a similar pulley arrangement was used to pull the wheel (see the arrangement for STF in Figure 6.3). The friction between the pulley wheel and plastic rope and the friction between the pulley's bearing were assumed to be negligible.



**Figure 6. 2 The arrangement to measure the horizontal force of the SW**



**Figure 6. 3 The arrangement to measure the horizontal force for the STF**

The ASSR of the wheel could be identified by the following expression:

$$ASSR = \frac{Q_2 - Q_1}{P} = \frac{Q}{P} \quad (6.1)$$

where

$Q_1$  = the horizontal force to cause the bearings on the support beams to rotate,

$Q_2$  = the horizontal force to cause the bearings and the wheel to rotate, and

$P$  = the vertical force which was measured using the load cell.

### 6.3 THE RESULTS

Because the horizontal forces to cause the bearings to rotate in the SW and the STF were very small and because of the difficulty in avoiding the wheel touching the specimen surface while measuring the horizontal force to pull the bearings only in the PTF, the horizontal force to cause the bearings to rotate in the PTF is assumed to be negligible. The bearings on the support beams' ASSRs of the SW and the STF are 0.0045 and 0.0042 respectively. The ASSRs of each material are listed in Table 6.2 and are assumed to be independent of vertical wheel load. These values were used to compute the shakedown limit of the specimen which is presented in the next chapter.

**Table 6. 2 Summary of the rolling resistances of various materials**

<b>Type of Wheel Tracking Facility</b>	<b>Surface Material</b>	<b>ASSR</b>
SW	1.5mm thick rubber on Portaway Sand	0.08
	Silt	0.08
	Keuper Marl	0.08
STF	Crushed Granite	0.12
	Crushed Carboniferous Limestone	0.15
PTF	Crushed Carboniferous Limestone	0.15

The ASSR between the surface material and the rigid wheel of the SW is lower than the ones obtained using STF and PTF. It may be due to the coarser particles used for both the STF and PTF specimens, and the tread pattern on the pneumatic wheel of the STF and PTF which created an interlock with the surface.

The ASSR of the crushed Carboniferous Limestone was higher than for crushed Granite. This might be due to the coarser particles of the crushed Carboniferous Limestone compared to the crushed Granite or the wider wheel used in the PTF which required more horizontal force to pull it. From the particle size distribution chart, there were 45% of the crushed Granite particles passing 5mm sieve compared to 40% of the crushed Carboniferous Limestone particles. All the specimens tested using the SW had the same ASSR. The size of soil particle such as Keuper Marl and Silt which was less than 2mm and a thin rubber sheet on the Portaway Sand may provide the same surface roughness.

## **6.4 SUMMARY**

This chapter focussed on identifying the ASSR parameter which related to the wheel loading tests' condition to compute the theoretical shakedown limit. All the materials that were in contact with the wheel were measured. The preparation procedure for each specimen was similar to the preparation procedure for the wheel tracking specimens (see Chapter 4). The usage and influence of the ASSR parameter have been reviewed in Chapter 2. The computed shakedown limit is presented in Chapter 7 and compared to the experimental results.

It was found that the ASSR for all the specimens tested using the SW is the same. For the STF, with the same wheel, the ASSR between the wheel and Granite was lower than the ASSR between the wheel and Carboniferous Limestone. Under the same type of specimen surface, which was Carboniferous Limestone, both wheels of STF and PTF gave the same ASSR.



## **7 APPLICATION OF THE SHAKEDOWN CONCEPT IN PAVEMENT ENGINEERING**

### **7.1 INTRODUCTION**

The main objective of the wheel tracking tests is to check the applicability of the shakedown concept for pavement analysis and design. Each specimen was tested with different levels of wheel load to identify the maximum load which relates to the shakedown response. The concept of shakedown relates to the resilient response of the soil in which no further permanent deformation occurs after a certain number of load repetitions. The experimental results will be compared with the theoretical shakedown limits. The theoretical shakedown limits will be calculated using the lower bound theorem's equation (Yu, 2005). A major advantage of using this method is that it only needs the soil strength parameters for a single layered structure and gives more conservative design. For a multi-layered pavement, the soil strength and stiffness parameters are required, which are in general much easier to measure than the deformation properties (which are needed for a load-path finite element analysis). For a one layered system, the experimental result is compared directly with the formulation derived by Yu (2005). For the multi layered system, firstly, it is necessary to analyse the stresses within the multi-layered pavements, e.g. by using a simplified multi-layered linear elastic model of the pavement structure

then using the shakedown limit formulation to calculate the shakedown limit of the pavement structure. The critical stresses in this case are the stresses that give the maximum shakedown limit.

The experimental results of the multi-layered structures presented in this thesis were compared with the computed shakedown limits modelled using finite elements by Li and Yu (2006). The assumptions and input parameters that were used by Li and Yu (2006) to compute the shakedown limit are reviewed in this Chapter. The comparison of the computed shakedown limit and the experimental results is presented in this chapter and followed by a discussion.

## **7.2 PHILOSOPHY OF THE SHAKEDOWN LIMIT COMPUTATION**

### **7.2.1 For a Single Layered Pavement**

A review on how to derive the shakedown based formulation for soil and pavement analyses, including the assumptions that were used, has been presented in Chapter 2 Section 2. The elastic stresses,  $\tau_{xz}^e$  and  $\sigma_{zz}^e$  which gives the maximum value of  $|\tau_{xz}^e| + \sigma_{zz}^e \tan \phi$  need to be identified to obtain the shakedown limit of a single layered pavement. In this case, Hamilton's

equations (1983) which were presented in Yu (2005) are used and defined in equations 7.1 -7.4.

The elastic stresses due to the normal force P are given as follows:

$$\sigma_{zz}^e = \frac{3P}{2\pi a^3} \left[ -N + \frac{azM}{S} \right] \quad (7.1)$$

$$\tau_{xz}^e = \frac{3P}{2\pi a^3} \left[ -z \left\{ \frac{xN}{S} - \frac{xzH}{G^2 + H^2} \right\} \right] \quad (7.2)$$

where

$$A = r^2 + z^2 - a^2; S = \sqrt{A^2 + 4a^2 z^2}; r^2 = x^2 + y^2$$

and

$$M = \left( \frac{S+A}{2} \right)^{1/2}; N = \left( \frac{S-A}{2} \right)^{1/2}; \phi = \tan^{-1} \left( \frac{a}{M} \right)$$

and

$$G = M^2 - N^2 + zM - aN; H = 2MN + aM + zN.$$

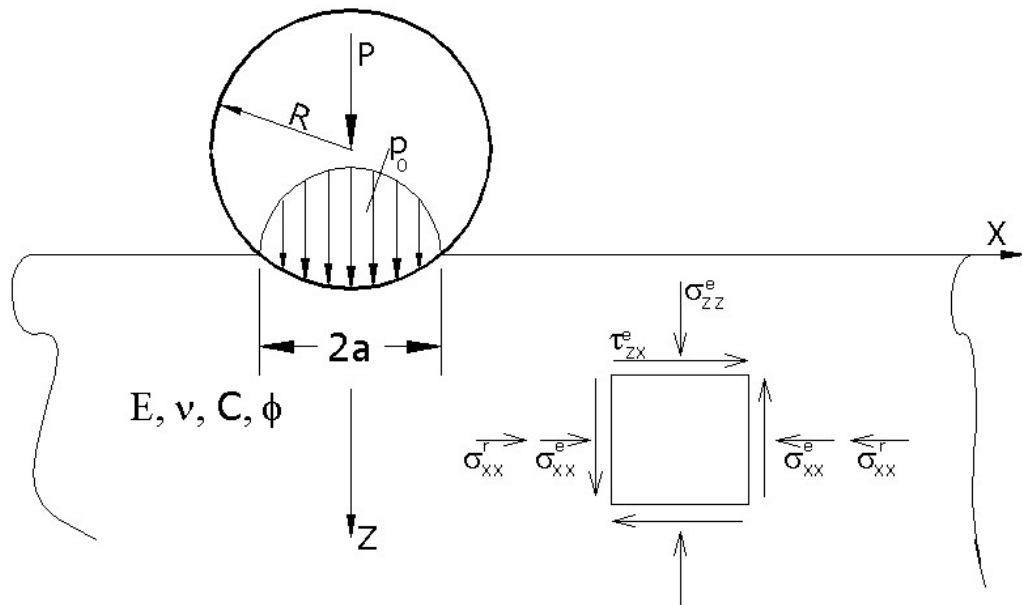
The elastic stresses due to the tangential force Q are given as follows:

$$\sigma_{zz}^e = \frac{3Q}{2\pi a^3} \left[ \frac{zxN}{2r^2} \left\{ 1 - \frac{r^2 + z^2 + a^2}{S} \right\} \right] \quad (7.3)$$

$$\tau_{xz}^e = \frac{3Q}{2\pi a^3} \left[ \frac{3z\phi}{2} + \frac{azM}{r^2} \left\{ 1 + \frac{x^2}{r^2} - \frac{x^2}{S} \right\} \right] + \frac{3Q}{2\pi a^3} \times \frac{N}{r^2} \times$$

$$\times \left[ -\frac{3}{4}(S+2A) + z^2 - \frac{3}{4}a^2 - \frac{1}{4}r^2 + \frac{z^2}{2} \left( \frac{1}{2} - \frac{2x^2}{r^2} \right) \right] \quad (7.4)$$

The relationship between the vertical and horizontal force has been defined as the ASSR (see Chapter 6, Section 1, Equation 6.1). A cohesive-frictional half space is subjected to a circle of radius  $a$ , (i.e.  $x^2 + y^2 \leq a^2$ ) as shown in Figure 7.1.



**Figure 7. 1 The coordinates and notation for stresses**

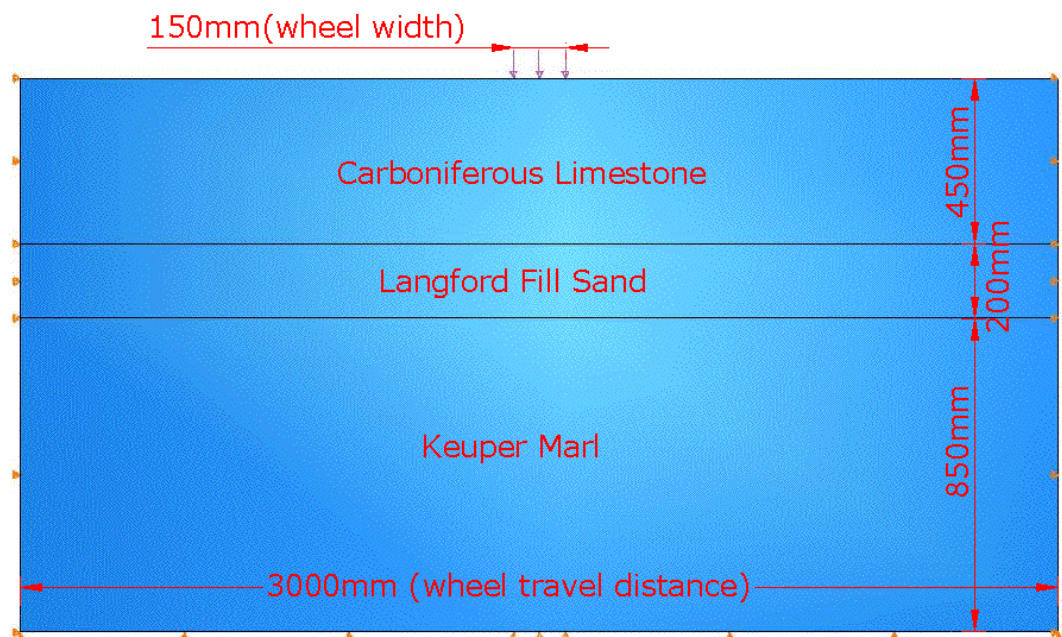
The parameters that are required to calculate the shakedown limit are the ASSR between wheel and specimen surface, the *angle of friction of the soil*  $\phi$ , the *cohesion of the soil*  $c$ .

## 7.2.2 For Multi-Layered Cases

Li and Yu (2006) used a computer program called ABAQUS to build the pavement model. ABAQUS is one of the finite element programs, which enables the user to define user interfaces for creating, submitting, monitoring and evaluating results from the finite element simulations. The steps of the numerical simulations for shakedown analysis that were taken by Li and Yu (2006) are as follows:

1. The geometry of the finite element model of the layered pavement was modelled to have the same soil thicknesses as in the experiment (see Chapter 4 for more details of the specimen geometry) and was defined as symmetrical hence the number of elements and the computational effort were reduced.
2. The soil properties such as elasticity  $E$ , cohesion  $c$  and angle of friction  $\phi$  for each layer of the specimen listed in Tables 7.1 and 7.2 respectively which were taken from Table 3.3 Section 3.5.4. The Poisson's ratio for each specimen was assumed to be 0.3 for the crushed Carboniferous Limestone and crushed Granite and 0.4 for the other materials such as Silt, Keuper Marl, Portaway Sand and Langford Fill Sand.

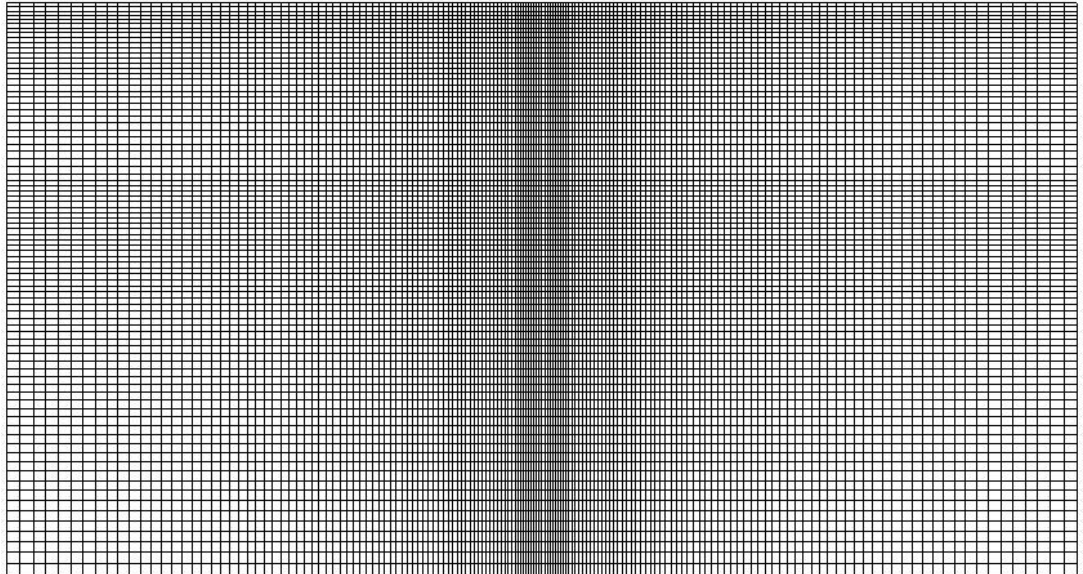
3. Hertz stress distribution was used to formulate the vehicle wheel loading on the pavement. Details of Hertz stress distribution have been reviewed in Chapter 2 Section 2.2.2.
4. The left, right and bottom boundary conditions were set to be fixed. The typical finite element model for three layered pavement including the information that was inserted to the model are illustrated in Figure 7.2. A typical finite element mesh used in the model is shown in Figure 7.3.



**Figure 7. 2 Finite element model for three layered pavement**

5. According to Yu's formulation (Yu, 2005), the importance of identifying a lower-bound shakedown limit is the optimisation of the residual stress field that satisfies the equations of equilibrium and stress boundary conditions (see the lower-bound shakedown theorem in

Chapter 2 Section 2.2) and the residual stress field which is independent of the travel direction.



**Figure 7. 3 The finite element mesh**

6. Once the finite element model for the pavement is set up, the numerical simulation is performed. In order to introduce the shakedown theory into ABAQUS, a user subroutine based on the analytical solution to shakedown analysis, which was defined in equation 3.4, 7.1-7.4, was inserted.

### **7.3 COMPARISON OF THE EXPERIMENTAL RESULTS AND THEORETICAL PREDICTIONS**

A list of the theoretical shakedown limits and the input parameters is presented in Tables 7.1 and 7.2 including the maximum and minimum wheel loads with Types 1 and 2 deformation curves for homogeneous and layered pavements respectively. The measured ASSR of each wheel tracking facility was assumed independent of vertical wheel load. Refer to an earlier chapter where shakedown limits were defined for each type of deformation response. The Type 1 deformation curve is associated with the response of the specimen to load repetitions in a resilient manner such that the deformation rate approaches zero after a certain number of passes. Based on the definition of the shakedown concept, a specimen with a Type 1 curve can be said to be have ‘shaken’ down. The Type 2 deformation curve is associated with the response of the specimen to load repetitions in which the deformation rate increases gradually.

The theoretical shakedown limits for all homogeneous soils are well below the minimum wheel pressure for a Type 2 response and for about 80% of the soil specimens they were above the maximum wheel pressure for a Type 1 response. The shakedown limits, which were calculated using the shakedown based formulation, are in a good agreement for a one layered or homogeneous system where the minimum thickness of the wheel tracking specimen is 2.5 times the width of the wheel.



**Table 7. 1 Comparison of the experimental and computed shakedown limit for a homogeneous pavement**

Test Specimen	Cohesion, $c$ ( $kPa$ )	Angle of Friction, $\phi (^{\circ})$	Applied Surface Stresses Ratio, $ASSR$	Maximum Wheel Pressure with Type 1 Response ( $kPa$ )	Minimum Wheel Pressure with Type 2 Response ( $kPa$ )	Theoretical Shakedown Limit ( $kPa$ )
<b><i>One Layer</i></b>						
Portaway Sand (PS1)	8.5	36	0.08	119	127	122
Portaway Sand (PS2)	8.5	36	0.08	119	127	122
Silt	14	38	0.08	257	261	217
Keuper Marl (KM)	55	0	0.08	237	269	233
Crushed Granite (Gr)	13	49	0.12	289	355	290

**Table 7. 2 Comparison of the experimental and computed shakedown limit of layered pavement**

Test Specimen	Thickness (mm)	Cohesion, $c$ (kPa)	Angle of Friction, $\phi(^{\circ})$	Poisson's Ratio	Stiffness, $E$ (MPa)	Applied Surface Stresses Ratio, ASSR	Maximum Wheel Pressure with Type 1 Response (kPa)	Minimum Wheel Pressure with Type 2 Response (kPa)	Theoretical Shakedown Limit (kPa)
Two Layers									
Granite- Portaway Sand (Gr-PS)	120	13	49	0.30	22	0.12	152	226	193
	60	8.5	36	0.40	26				
Granite- Silt (Gr-Silt)	120	13	49	0.30	22	0.12	233	292	236
	60	14	38	0.40	22				
Carboniferous Limestone- Keuper Marl (Cl-KM1)	60	11.5	51	0.30	10	0.15	141	195	183
	120	43.5	0	0.40	2				
Carboniferous Limestone- Keuper Marl (Cl-KM2)	450	15.5	55	0.30	46	0.15	215	254	248
	1050	43.5	0	0.40	2				
Three Layers									
Carboniferous Limestone- Langford Fill Sand- Keuper Marl (Cl-LFS-KM)	450	15.5	55	0.30	46	0.15	310	410	257
	200	9.5	44	0.40	17				
	850	43.5	0	0.40	2				

For layered pavements, most of the theoretical shakedown limits are around the minimum and maximum wheel pressure for Types 2 and 1 responses respectively, except for the three layered pavement. The computed shakedown limit of the three layered pavement is below the maximum wheel pressure of a Type 1 response.

Figure 7.4 plots the theoretical shakedown limits of homogeneous and layered pavements against the maximum wheel pressure with Type 1 response and minimum wheel pressure with Type 2 response. The theoretical shakedown limit lies between the maximum wheel pressure with Type 1 response and minimum wheel pressure with Type 2 response with a ratio between 0.9958 and 1.2201.

The plots of the theoretical shakedown limits of various types of materials against the angles of friction and cohesions are shown in Figures 7.5 and 7.6 respectively including the minimum wheel pressure with Type 2 response and maximum wheel pressure with Type 1 response. They demonstrate that the shakedown limits depend on the soil shear strength which is represented by *cohesion  $c$*  and *angle of friction  $\phi$* . Increasing the *cohesion  $c$*  and *angle of friction  $\phi$*  were followed by the increase of the shakedown limit.

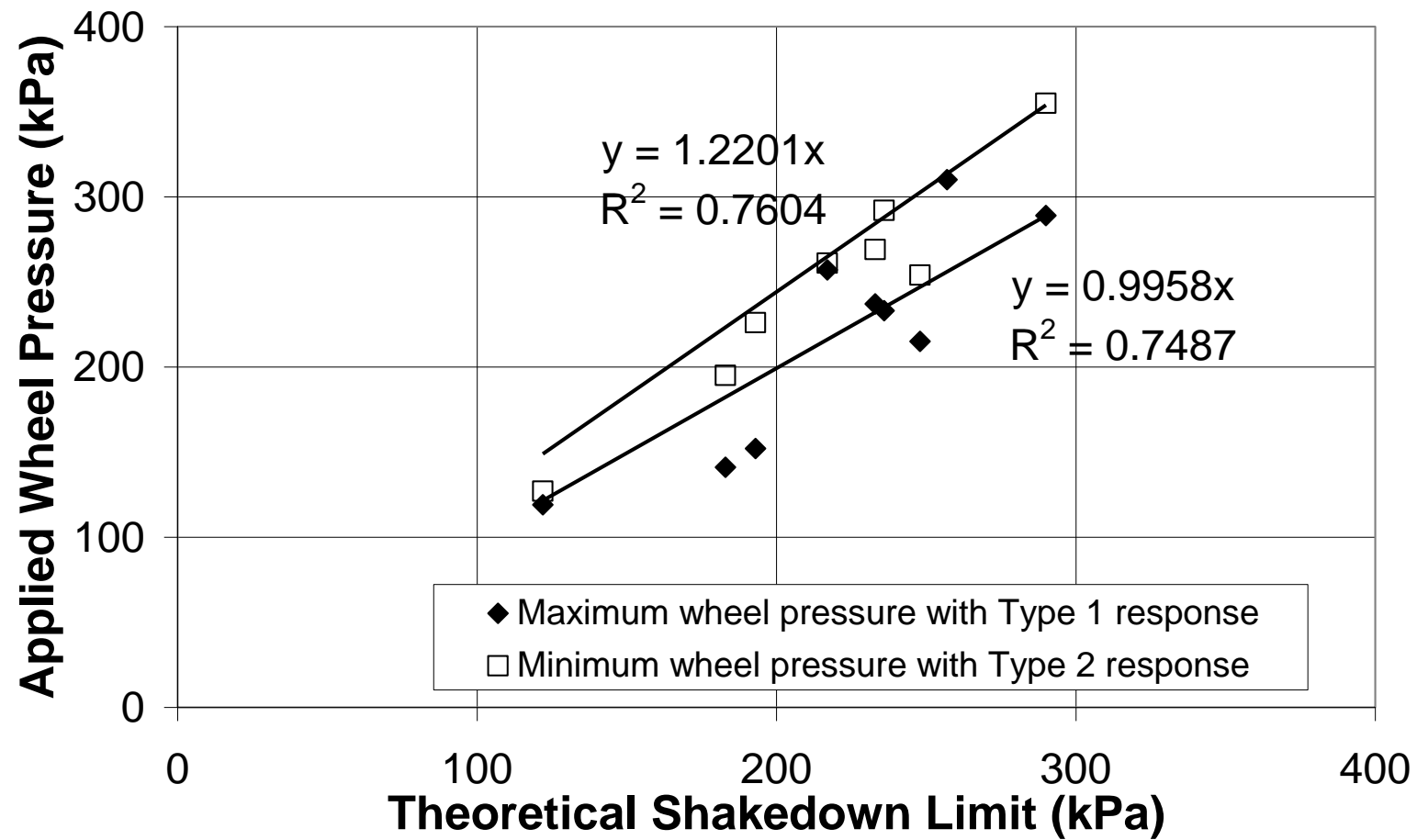


Figure 7. 4 Theoretical shakedown limits against the wheel pressures

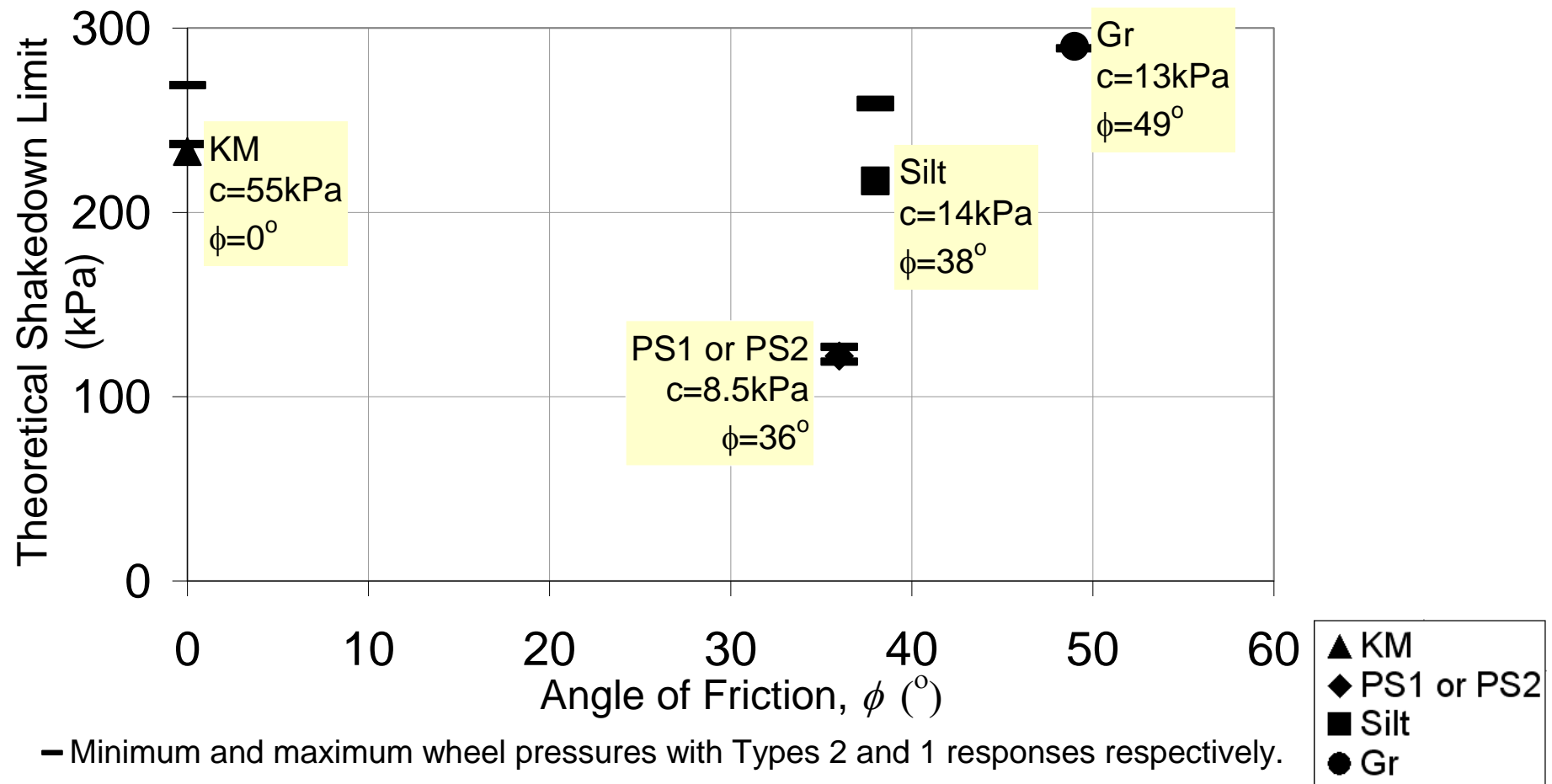


Figure 7. 5 Theoretical shakedown limits against the angle of frictions

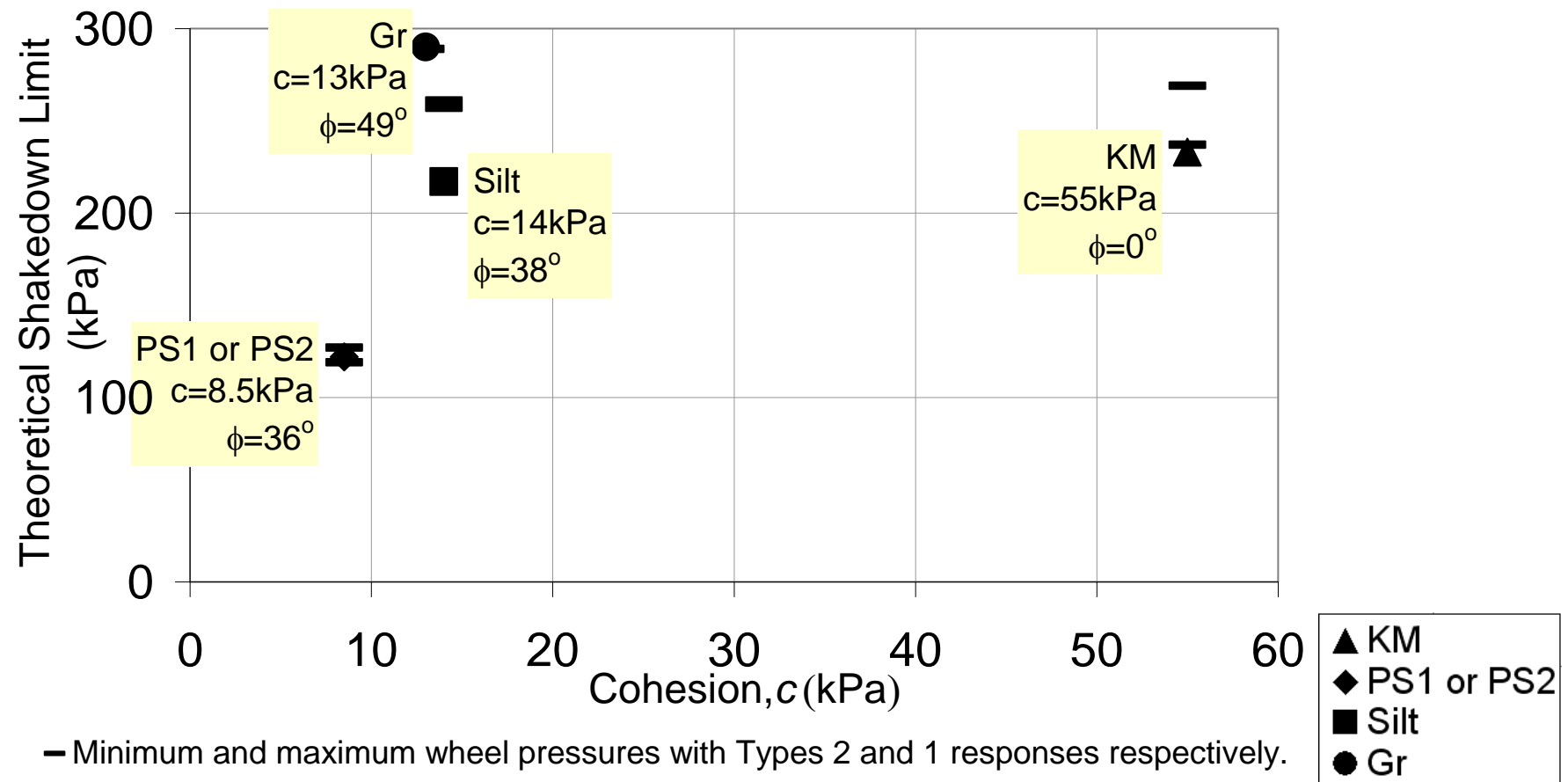


Figure 7. 6 Theoretical shakedown limits against the cohesions

A comparison between the relative densities of the triaxial test specimens and wheel tracking specimens in Table 7.4 shows that the densities of the triaxial test specimens were slightly below those for the wheel tracking specimens. The underlying layer, Keuper Marl, which had a moisture content of 23%, may affect the compaction of Langford Fill Sand. The shear strengths that were obtained from a series of triaxial tests may therefore be less than what they should be.

From the overall comparison for the layered pavements, the computed shakedown limits using the ABAQUS finite element package to model the layered pavements are in good agreement with the experimental results.

**Table 7. 3 Relative densities of various materials**

Type of Material	Relative Density, RD (%)		
	Triaxial Test	Wheel Tracking Test	Type of Wheel Tracker
<b>Portaway Sand</b>	<b>84</b>	<b>90</b>	<b>SW and STF</b>
<b>Langford Fill Sand</b>	<b>54</b>	<b>27</b>	<b>PTF</b>
<b>Crushed Carboniferous Limestone</b>	<b>39</b>	<b>39</b>	<b>STF</b>
<b>Crushed Carboniferous Limestone</b>	<b>47</b>	<b>55 and 79</b>	<b>PTF</b>
<b>Crushed Granite</b>	<b>62</b>	<b>61 and 62</b>	<b>STF</b>

## **7.4 SUMMARY**

A step by step method to compute the shakedown limits is described in this chapter. The shakedown limit of a single layer of soil could be calculated directly by using the equations that are given above (see equations 2.5, 7.1-7.4). The assumptions and the derivation of the equations have been reviewed in Chapter 2. For multilayered layered pavements, the ABAQUS finite element package was used to model the layered pavement and calculate the stresses, and then the shakedown based formulation was inserted into the finite element model to compute the shakedown limit. The computed shakedown limits of single and multilayered pavements are in good agreement with the experimental results.

For the application of the shakedown concept in pavement engineering, preliminary site investigation is required. The possibilities of the changes in moisture content or density or soil characteristics after a certain period of service time may need to be taken into account to identify the critical shear strength of the soil.



## **8 SUMMARY, CONCLUSIONS AND RECOMMENDATIONS FOR FUTURE WORK**

### **8.1 SUMMARY**

This thesis has presented a preliminary validation of the application of the shakedown concept in pavements. As long as the shear strength and elastic properties of each soil layer or the shear strength of a single layered pavement and the rolling resistance between the wheel and surface are known, the maximum shakedown limit of a soil on pavement layered system can be identified.

The experimental results from direct wheel load tests were carried out and were compared with the computed shakedown limits. The wheel tracking tests were conducted on various soil combinations at various stress levels. The vertical surface permanent deformation after a certain number passes was recorded and plotted against the number of passes. The specimen is said to be *shaken* down if, after a certain number of load repetitions, the soil or layered system responds in an elastic manner without further permanent deformation. The experimental results show a good agreement with the computed shakedown limits.

## 8.2 CONCLUSIONS

### *Monotonic Load Triaxial Tests*

- The quick undrained shear strength test was carried out for the Keuper Marl. The other soils like Portaway Sand, Silt, Langford Fill Sand, crushed Granite and Limestone were tested drained. It was considered that during the wheel tracking tests, the applied wheel load may be high enough which would leave insufficient time for the Keuperl Marl to gain additional strength by consolidation.
- The shear strength of the soil is represented by the *cohesion*  $c$  and the *angle of friction*  $\phi$ . However, they are not the true cohesion and angle of friction respectively. The *cohesion*  $c$  is an apparent cohesion which is due to either the influence of the electro-chemical activity on the surface of the clay particles or the effect of matrix suction and particle interlock for the coarse grained soils. The *angle of friction*  $\phi$  is an angle of shearing resistance and represents the slope of the failure line.
- The shear strength of the material depends on type of soil, particle size, moisture content, and density.
- The Portaway sand with the uniform shape and the poorly graded sand particles had the lowest shear strength compared to the other materials.

### ***Wheel tracking Tests***

- It was found that by using the wheel tracking facilities in the experiments it was possible to have control of the specimen moisture content, density and the wheel load. It was a simple procedure to monitor the permanent deformation, and testing time was reduced in comparison to full-scale testing.
- The contact pressure measurements under various wheel loads using both the pneumatic and rigid wheels show that the relationship between the contact pressure and the applied load is approximately linear for the rigid wheel but not for the pneumatic wheels.
- All the wheel tracking specimens were tested directly on the surface except Portaway Sand. A 1.5mm thick rubber sheet was placed on the sand surface to avoid the loss of moisture content during the test which may change the soil shear strength characteristic.
- The wheel load distribution through the contact area for the pneumatic wheel depends on the wheel load magnitude and the inflation pressure. As the wheel load increases under the same inflation pressure, the contact area is distributed and expanded from the centre to the edge of the tyre.
- The test specimen under the repeated wheel load experienced surface deformation, followed by upheavals to the side of the wheel path. The

magnitude of these responses depended on the soil shear strength, type of soil, and the particle size distribution.

- The resistance of the specimen to vertical permanent deformation increased with increasing shear strength of the specimen.
- Three types of vertical permanent deformation curves (labelled as Types 1, 2, and 3) were identified. Types 1 and 3 represent the stabilisation or equilibrium state and the failure of the specimen respectively after a certain number of passes and Type 2 is the border region between Types 1 and 3. These responses are similar to the ones that were found in the repeated load triaxial tests by Werkmeister et al. (2001, 2004 and 2005).
- It is categorised as Type 3 if the deformation rate after 500 passes is still above 0.018mm/pass. If the deformation rate is below 0.018mm/pass after 500 passes and approaches zero or 0.001mm/pass after 1000 passes, it is categorised as Type 1. If the deformation rate after 1000 passes is still above 0.001mm/pass, it is categorised as Type 2.
- The vertical permanent deformation of the soils ceased to increase and the shakedown state was reached (categorised as Type 1 response) at various numbers of passes between approximately 500 and 10,000 passes depending on the applied stresses.

- Each soil specimen reached the shakedown state at a different accumulation of the vertical permanent deformation.
- Well-compacted soil gives less initial deformation and has better resistance to the vertical permanent deformation.

### ***The Theoretical Shakedown and Experimental Shakedown Limit***

- The shakedown limit of a single layered pavement or soil depends on the shear strength parameters of the soil, *cohesion*  $c$  and *angle of friction*  $\phi$ , and the applied surface stresses ratio *ASSR*.
- Increasing the *cohesion*  $c$  and *angle of friction*  $\phi$  resulted in an increase of the shakedown limit.
- The theoretical shakedown limit of the layered pavement depends on the boundary of the pavement model, the shear strength parameters, *cohesion*  $c$  and *angle of friction*  $\phi$ , and elastic properties ( $E$  and  $\nu$ ) of each layer and the applied surface stresses ratio between the wheel and the specimen surface (*ASSR*).
- The parameters needed for the shakedown limit of a multilayered pavement are  $c$ ,  $\phi$ ,  $E$ ,  $\nu$  of each soil layer, and *ASSR*.

- The computed shakedown limits and experimental results are in good agreement for both the single and layered pavements.
- The shakedown based formulation takes account of the shear strength of the soil and could be used as one of the design tools for pavement analysis and design particularly for the subgrade and the foundation layers.

### **8.3 RECOMMENDATIONS FOR FUTURE WORK**

The application of the shakedown based formulations for pavement analysis and design has been validated in this thesis by comparing the computed shakedown limit with the experimental results. The shakedown limit uses the lower bound approach. For a single layered pavement, the shakedown limit can be calculated directly using the shakedown based formulations. For the multilayered pavement, the ABAQUS Finite Element Model was used to calculate the stresses of the multilayered pavement and the shakedown based formulations were inserted to compute the shakedown limit. For future research, it is recommended to:

- Introduce other computer programs to calculate the stresses of the multilayered pavement such as BISAR and compute the theoretical shakedown limit by using the shakedown based formulations then compare with the experimental results. BISAR is a computer program

that is widely used in industry to calculate the stresses, strains and displacements of a multilayered pavement structure.

- Perform the shakedown limit computation by using the upper bound approach and compare with the experimental results and the lower bound shakedown limit.
- Develop a computer program so that the pavement engineer can calculate directly the shakedown limit of single and multi layered pavements with various thickness, various elastic and plastic properties of the soil, and various rolling resistance, by using the philosophy given in Chapter 7 Section 2.
- Extend the application of the shakedown concept for the behaviour of railway foundations by performing a series of rail track settlement tests.

## References

- ARNOLD, G. K. (2004) *Rutting of granular pavements*. Ph.D Thesis. University of Nottingham, Nottingham, United Kingdom.
- BARKSDALE, R. D. (1972) Laboratory evaluation of rutting in base course materials. *Proc. 3rd Int. Conf. on the Structural Design of Asphalt Pavements*. London.
- BERRY, P. L. & REID, D. (1987) *An Introduction to Soil Mechanics*, England, McGraw Hill Book Company (UK) Limited.
- BISHOP, A. W. & HENKEL, D. J. (1964) *The Measurement of Soil Properties in the Triaxial Test*, London, Edward Arnold Ltd.
- BONSE, R. P. H. & KUHN, S. H. (1959) Dynamic forces exerted by moving vehicles on a road surface. *Highway Research Board Bulletin* 233, 9-23.
- BOULBIBANE, M., COLLINS, I. F., PONTER, A. R. S. & WEICHERT, D. (2005) Shakedown of unbound pavements. *Int. Jnl. Road Materials and Pavement Design*, 6, No. 1, 81-96.
- BOYCE, J. R. (1976) *The behaviour of granular material under repeated loading*. Ph.D Thesis. University of Nottingham, Nottingham, United Kingdom.
- BS1377:2 (1990) Methods of test for soils for civil engineering purposes. Classification tests.
- BS 1377:4 (1990) Soils for engineering purposes. Compaction related tests.
- BS 1377-7 (1990) Methods of test for soils for civil engineering purposes. Shear strength tests (total stress)
- BS 1377-9 (1990) Methods of test for soils for civil engineering purposes. In-situ tests.
- BROWN, C. J. (1997a) *The performance of road ironwork installations*. Ph.D Thesis. University of Nottingham, Nottingham, United Kingdom.



- BROWN, C. J. (1997b) *The performance of road ironwork installations*. Ph.D Thesis. University of Nottingham, Nottingham, United Kingdom.
- BROWN, S. (1996) Soil mechanics in pavement engineering. *Geotechnique*, 46, No. 3, 383-426.
- BROWN, S. (1997c) Achievements and Challenges in Pavement Engineering, Keynote Lecture. *Proceedings International Society for Asphalt Pavements*. University of Washington, Seattle, WA.
- BROWN, S. F. (1974) Repeated load testing of a granular material. *Proceedings ASCE*, 100, GT 7, 825-841.
- BROWN, S. F. (1977) State-of- the-art report on field instrumentation for pavement experiments. *Transportation Research Record* 640, 13-27.
- BROWN, S. F. & BELL, C. A. (1979) The prediction of permanent deformation in asphalt pavements. *Proc. AAPT*, 48, 438-474.
- BROWN, S. F. & BRODRICK, B. V. (1981) Nottingham Pavement Test Facility. *Transportation Research Record* 810, 67-72.
- BROWN, S. F. & BRODRICK, B. V. (1999) 25 years' experience with the pilot-scale Nottingham Pavement Test Facility. *International Conference on Accelerated Pavement Testing*. Reno, Nevada.
- BROWN, S. F. & BRUNTON, J. M. (1984) Improvements to pavement subgrade strain criterion. *ASCE Journal*, 110.
- BROWN, S. F. & CHAN, F. K. W. (1996) Reduced rutting in unbound granular pavement layers through improved grading design. *Proc. Instn. Civ. Engrs. Transp*, 117, 40-49.
- CHAN, F. K. W. (1990) *Permanent deformation resistance of granular layers in pavements*. Ph.D Thesis. University of Nottingham, Nottingham, United Kingdom.
- CHAN, F. K. W. & BROWN, S. F. (1993) *Granular bases for heavily loaded pavements*. Final Report, ESL-TR-91-06, University of Nottingham, Nottingham, March 1993.

- CHEN, H. F. & PONTER, A. R. S. (2005) The linear matching method for shakedown and limit analyses applied to rolling and sliding point contact problems *Int. Jnl. Road Materials and Pavement Design*, 6, No.1, 9-30.
- CHEUNG, L. W. (1994) *Laboratory assessment of pavement foundation materials*. Ph.D Thesis. University of Nottingham, Nottingham, United Kingdom.
- COLLINS, I. F. & BOULBIBANE, M. (2000) Geomechanical analysis of unbound pavements based on shakedown theory. *Journal of Geotechnical and Geoenvironmental Engineering*.
- COLLINS, I. F. & CLIFFE, P. F. (1987) Shakedown in frictional materials under moving surface loads. *International Journal for Numerical and Analytical Methods in Geomechanics*, 11, 409-420.
- COLLINS, I. F. & WANG, A. P. (1992) *Shakedown analysis of layered pavements*. Report no. 505, University of Auckland, New Zealand.
- CRONEY, D. & LISTER, N. W. (1965) Research into the design of flexible road pavements. Proceedings of the Sixth International Conference on Soil Mechanics and Foundation Engineering. Canada.
- DE BEER, M., FISHER, C. & JOOSTE, F. (1997) Determination of pneumatic tyre/Pavement interface contact Stresses under moving loads and some effects on pavements with thin asphalt surfacing layers. *Eighth International Conference on Asphalt Pavements*. Seattle, Washington.
- DoT (1986) Specification for Highway Works. Part 3 Series 800. London: HMSO, August 1986.
- EVDORIDES, H. T. & SNAITH, M. S. (1996) A knowledge-based analysis process for road pavement condition assessment. *Proc. Instn Civil. Engrs Transp.*, 117, 202-210.
- FERNANDO, E. G., LUHR, D. R. & SAXENA, H. N. (1987) Analysis of axle loads and axle types for the evaluation of load limits on flexible pavements. *Transportation Research Record* 1136, 7-14.
- FRANCE, J. W. & SANGREY, D. A. (1977) Effects of drainage in repeated loading of clays. *Proceedings ASCE*, 103, 769-785.

- FREITAG, D. R. & GREEN, A. J. (1962) Distribution of stresses on an unyielding surface beneath a pneumatic tyre. *Highway Research Board Bulletin*, 342, 14-23.
- GIBB, J. M. (1996) *Evaluation of resistance to permanent deformation in the design of bituminous paving mixtures*. Ph.D Thesis. University of Nottingham, Nottingham, United Kingdom.
- GOETZ, W. H., MC LAUGHLIN, J. F. & WOOD, L. E. (1957) Load-deformation characteristics of bituminous mixtures under various conditions of loading. *Proceedings of the Association of Asphalt Paving Technologists*. Atlanta, Georgia.
- HAMILTON, G. M. (1983) Explicit equations for the stresses beneath a sliding spherical contact. *Proceeding of Institution of Mechanical Engineers*, 197c, 53-59.
- HAU, K. W. (2003) *Application of a three-surface kinematic hardening model to the repeated loading of thinly surface surfaced pavements*. Ph.D Thesis. University of Nottingham, Nottingham, United Kingdom.
- HD28/04. Skidding Resistance. Design Manual for Roads and Bridges Volume 7 Section 3 Part 1, Highways Agency, 2004.
- HEAD, K. H. (1982) Manual of Soil Laboratory Testing. Volume 2: Permeability, Shear Strength and Compressibility Tests, London, Pentech Press.
- HEAD, K. H. (1986) Manual of Soil Laboratory Testing, Volume 3: Effective Stress Tests, London, Pentech Press.
- HEATH, D. L., SHENTON, M. J. & SPARROW, R. W. (1972) Design of conventional rail track foundations *Proceedings of the Institution of Civil Engineers*, 51.
- HIGHT, D. W. & STEVENS, M. G. H. (1982) An analysis of the California bearing ratio test in saturated clays. *Geotechnique*, 32, 315-322.
- Highways Agency (2003) Design Manual for Roads and Bridges Volume 7. August 2003.

- HIMENO, K., KAMIJIMA, T., IKEDA, T. & ABE, T. (1997) Distribution of tire contact pressure of vehicles and its influence on pavement distress. *Eighth International Conference on Asphalt Pavements*. Seattle, Washington.
- HUANG, Y. H. (1993) *Pavement Analysis and Design*, Englewood Cliffs, N J, Prentice Hall.
- HUGHES, D. A. B. (1986) *Polymer grid reinforcement of asphalt pavements*. Ph.D Thesis. University of Nottingham, Nottingham, United Kingdom.
- JOHNSON, K. L. (1962) A shakedown limit in rolling contact. *Proceedings 4th US National Congress of Applied Mechanics*, 2, 971-975.
- JOHNSON, K. L. (1985) *Contact Mechanics*, Cambridge, Cambridge University Press.
- JONES, E. R. & CHILDERS, R. L. (1993) *Contemporary College Physics*, Addison-Wesley.
- KAPOOR, A. (1997) Wear by plastic ratchetting. *Wear*, 212, 119-130.
- KENNEDY, C. K. (1974) *An experimental investigation of behaviour of wet-mix road base material*. Ph.D Thesis. University of Birmingham, Birmingham, United Kingdom.
- LADD, R. S. (1978) Preparing test specimens using undercompaction. *Geotechnical Testing Journal, GTJODJ*, Vol. 1, No. 1, 16-23.
- LAREW, H. G. & LEONARDS, G. A. (1962) A strength criterion for repeated loads. *Proceedings Highway Research Board*, 41, 529-556.
- LASHINE, A. K. F. (1971) *Some aspects of the behaviour of Keuper Marl under repeated loading*. Ph.D Thesis. University of Nottingham, Nottingham, United Kingdom.
- LEKARP, F., ISACSSON, U. & DAWSON, A. R. (2000a) State of the art. I: resilient response of unbound aggregates. *ASCE Journal of Transportation Engineering* 126, No. 1, 66-75.

- LEKARP, F., ISACSSON, U. & DAWSON, A. R. (2000b) State of the art. II: permanent strain response of unbound aggregates. *ASCE Journal of Transportation Engineering* 126, No. 1, 66-75.
- LEKARP, F., RICHARDSON, I. R. & DAWSON, A. R. (1996) Influences on permanent deformation behavior of unbound granular materials. *Transportation Research Record* 1547, 68-75.
- LI, H. X. & YU, H. S. (2006) Three dimensional solutions for shakedown of layered pavements under moving surface loads. *Int. J. Num. Analy. Meth. Geomech.*
- LOACH, S. C. (1987) *Repeated loading of fine grained soils for pavement designs*. Ph.D Thesis. University of Nottingham, Nottingham, United Kingdom
- MAIER, G. (1969) Shakedown theory in perfect elastoplasticity with associated and nonassociated flow-Laws: a finite element , linear programming approach. *Meccanica*, 4, 250-260.
- MARWICK, A. H. D. & STARKS, H. J. H. (1941) Stresses between tyre and road. *Journal of Civil Engineers*, 6, 309-325.
- MELAN, E. (1936) Theorie statisch unbestimmter systeme aus idealplastischen baustoff. *Sitz. Ber. Ak. Wiss. Wien. Ila*, 145, 195.
- MILLER, J. S. & BELLINGER, W. Y. (2003) Distress identification manual for the long-term pavement performance program. IN FOURTH (Ed.) Virginia, Federal Highway Administration.
- MONISMITH, C. L. & BROWN, S. F. (1999) Developments in the Structural Design and Rehabilitation of Asphalt Pavements over Three Quarters of a Century. *Journal of the Association of Asphalt Paving Technologist* 68A, 128-251.
- NUNES, M. C. M. & DAWSON, A. R. (1997) Behavior of some pavement foundation materials under repeated loading. *Transportation Research Record* 1577, 1-9.
- NUNN, M. E., BROWN, A., WESTON, D. & NICHOLLS, J. C. (1997) Design of long-life flexible pavements for heavy traffic. TRL Report 250. Crowthorne: Transport and Road Research Laboratory.

- PAPPIN, J. W. (1979) *Characteristics of a granular material for pavement analysis*. Ph.D Thesis. University of Nottingham, Nottingham, United Kingdom.
- POWELL, W. D., POTTER, J. F., MAYHEW, H. C. & NUNN, M. E. (1984) *The structural design of bituminous roads*. TRRL Report LR 1132. Crowthorne: Transport and Road Research Laboratory.
- RAAD, L. & MINASSIAN, G. (2005) The influence of granular base characteristics in upper bound shakedown of pavement structures. *Int. Jnl. Road Materials and Pavement Design*, 6, No.1, 53-80.
- RAAD, L., WEICHERT, D. & HAIDAR, A. (1989) Shakedown and Fatigue of Pavements with Granular Bases. *Transportation Research Record* 1227, 159-172.
- RAAD, L., WEICHERT, D. & NAJM, W. (1988) Stability of multilayer systems under repeated loads. *Transportation Research Record* 1207, 181-186.
- RADOVSKY, B. S. & MURASHINA, N. V. (1996) Shakedown of subgrade soil under repeated loading. *Transportation Research Record* 1547, 82-88.
- SANGREY, D. A., HENKEL, D. J. & ESRIG, M. I. (1969) The effective stress response of a saturated clay soil to repeated loading. *Canadian Geotechnical Journal*, 6, 269-277.
- SARAF, C., MARSHEK, K., CHEN, H., CONNELL, R. & HUDSON, W. R. (1987) The effect of truck tire contact pressure distribution on the design of flexible pavements. *Proc. 6th Int. Conf. on the Structural Design of Asphalt Pavements*. Michigan.
- SCOTT, C. R. (1980) *An Introduction to Soil Mechanics and Foundations*, England, Applied Science Publishers Ltd.
- SEED, H. B. & CHAN, C. K. (1958) Effect of stress history and frequency of stress application on deformation of clay subgrades under repeated loading. *HRB Proceeding*, 37, 555-575.
- SEED, H. B., MCNEILL, R. L. & DE GUENIN, J. (1958) Increased resistance to deformation of clay caused by repeated loading *Proc. ASCE Journal of the Soil Mechanics and Foundations*, 84, No.SM2

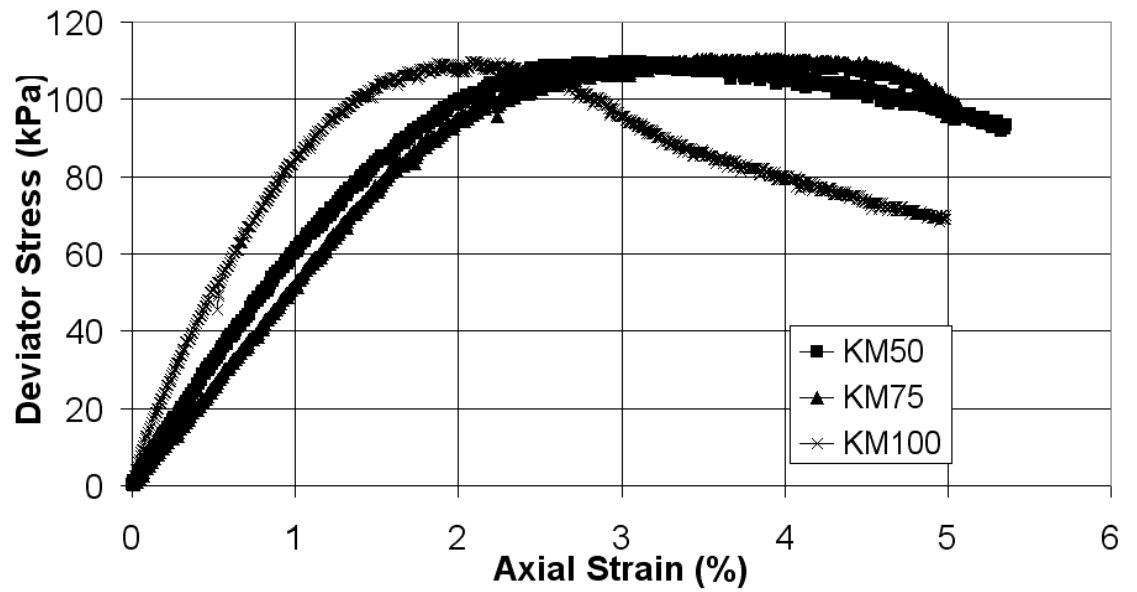
- SHARP, R. W. (1983) *Shakedown analysis and design of pavements*. Ph.D Thesis. University of Sydney, Australia.
- SHARP, R. W. (1985) Pavement design based on shakedown analysis. *Transportation Research Record* 1022, TRB, National Research Record, Washington, D.C., 99-107.
- SHARP, R. W. & BOOKER, J. R. (1984) Shakedown of pavements under moving surface loads. *Journal of Transportation Engineering, ASCE*, 110, No. 1, 1-13.
- THOM, N. H. (1988) *Design of road foundations*. Ph.D Thesis. University of Nottingham, Nottingham, United Kingdom.
- TROLLOPE, D. H., LEE, I. K. & MORRIS, J. (1962) Stresses and deformation in two layers pavement structure under slow repeated loading. *Proceeding 1st Conference Australian Road Research Board*.
- WERKMEISTER, S., DAWSON, A. R. & WELLNER, F. (2001) Permanent deformation behaviour of granular materials and the shakedown concept. *Transportation Research Board 80th Annual Meeting*.
- WERKMEISTER, S., DAWSON, A. R. & WELLNER, F. (2004) Pavement design model for unbound granular materials. *ASCE Journal of Transportation Engineering*, 130 No. 5, 665-674.
- WERKMEISTER, S., DAWSON, A. R. & WELLNER, F. (2005) Permanent deformation behaviour of granular materials *Int. Jnl. Road Materials and Pavement Design* 6, No.1, 31-52.
- WILSON, N. E. & GREENWOOD, J. R. (1974) Pore pressures and strains after repeated loading of saturated clay. *Canadian Geotechnical Journal*, 11, 269-277.
- WONG, S. K., KAPOOR, A. & WILLIAMS, J. A. (1997a) Shakedown limits on coated and engineered surfaces. *Wear* 203-204, 162-170.
- WONG, S. K., KAPOOR, A. & WILLIAMS, J. A. (1997b) Shakedown limits on coated surfaces. *Thin Solid Films* 292, 156-163.

- WOOD, L. E. & GOETZ, W. H. (1956) The strength of bituminous mixtures and their behaviour under repeated load. *Proceedings Highway Research Board*, 35, 405-417.
- WOOD, L. E. & GOETZ, W. H. (1957) Strength of bituminous mixtures and their behaviour under repeated loads, Part II. *Proceedings Highway Research Board* 36, 318-333.
- YAMAMURO, J. A. & LADE, P. V. (1993) Effects of strain rate on instability of granular soils. *Geotechnical Testing Journal, GTJODJ*, Vol. 16, No. 3, 304-313.
- YU, H. S. (2005) Three dimensional analytical solutions for shakedown of cohesive-frictional materials under moving surface loads. *Proceedings of the Royal Society Series A*, 461 (2059), 1951-1964.
- YU, H. S. & HOSSAIN, M. Z. (1997) Finite element models for shakedown analysis of pavements. *Computer Methods and Advances in Geomechanics (Yuan, ed.)*. Balkema, Rotterdam.
- YU, H. S. & HOSSAIN, M. Z. (1998) Lower bound shakedown analysis of layered pavements using discontinuous stress fields. *Computer Methods in Applied Mechanics and Engineering*, 167, 209-222.
- YU, H. S. & SHIAU, S. H. (1999) Finite element method for shakedown analysis of pavements. IN BRADFORD, B., AND FOSTER, EDS. (Ed.) *Mechanics of Structures and Materials* Balkema, Rotterdam.
- YU, H. S. & SHIAU, S. H. (2000) Load and displacement prediction for shakedown analysis of layered pavements. *Transportation Research Record* 1730, 117-124.
- ZHANG, T. & RAAD, L. (2002) An eigen-mode method in kinematic shakedown analysis. *International Journal of Plasticity*, 18, 71-90.

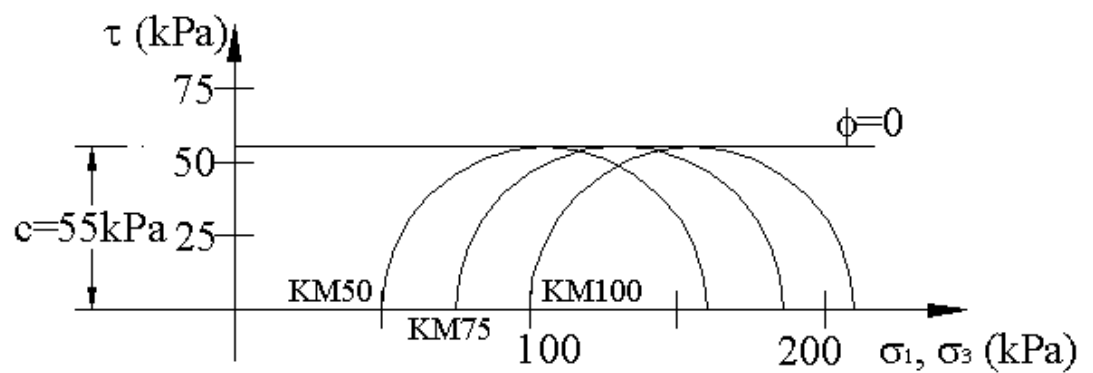


## **Appendix A. Monotonic Load Triaxial Test Results**

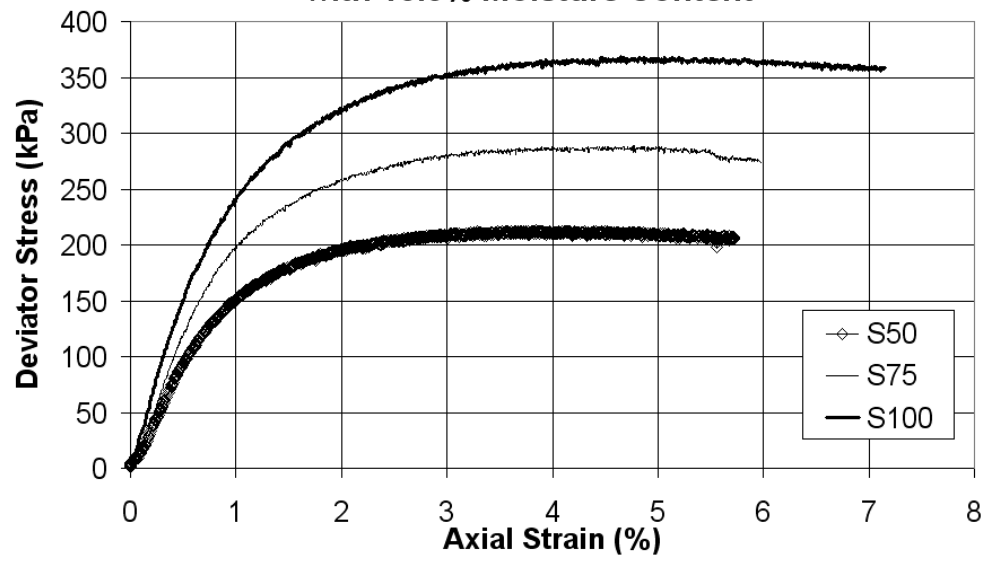
### Monotonic Shear Failure Tests for Keuper Marl (KM) with 15.2% Moisture Content



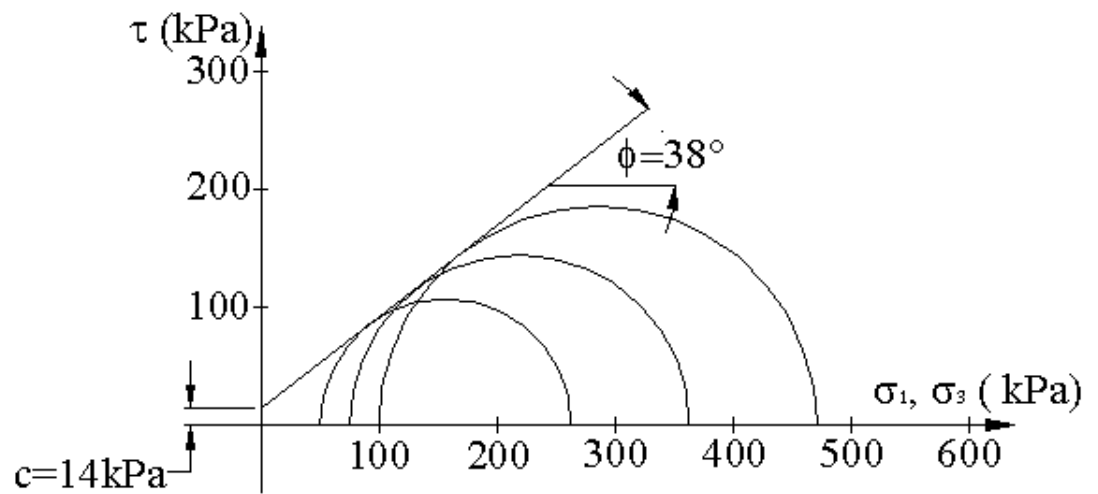
### Mohr Circles for Keuper Marl with 15.2% Moisture Content



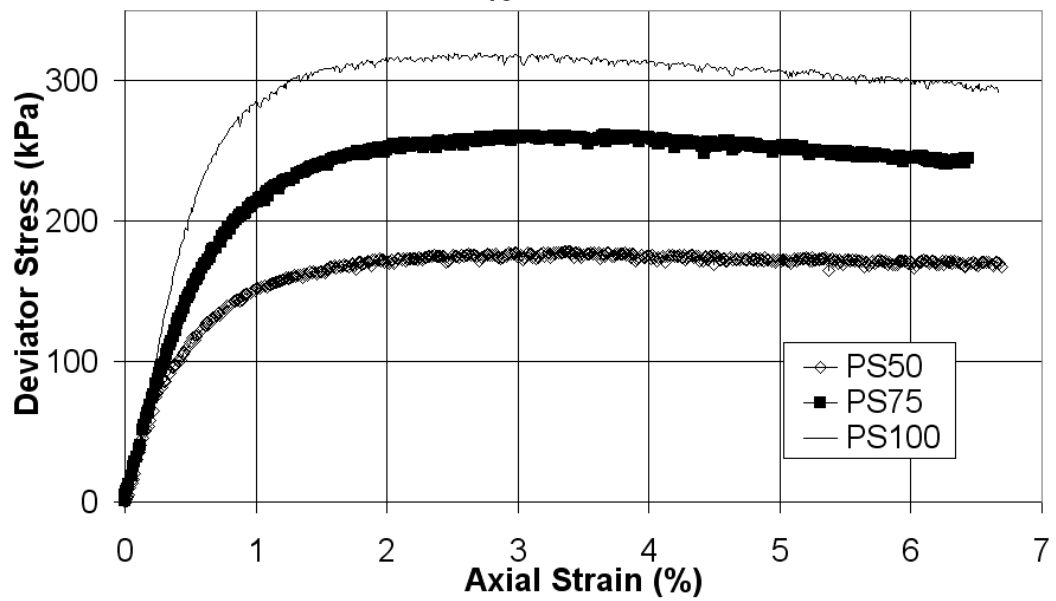
### Monotonic Shear Failure Tests for Silt (S) with 15.5% Moisture Content



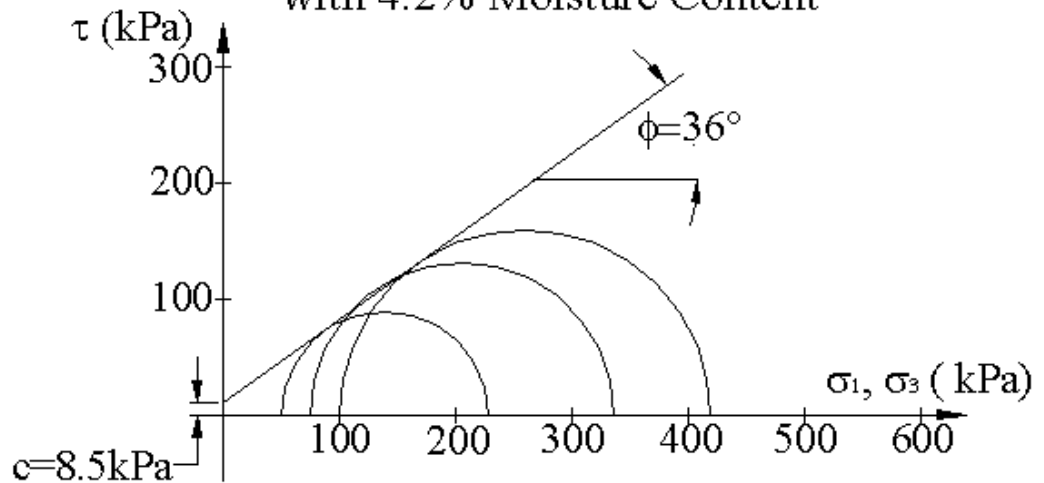
### Mohr Circles for Silt with 15.5% Moisture Content



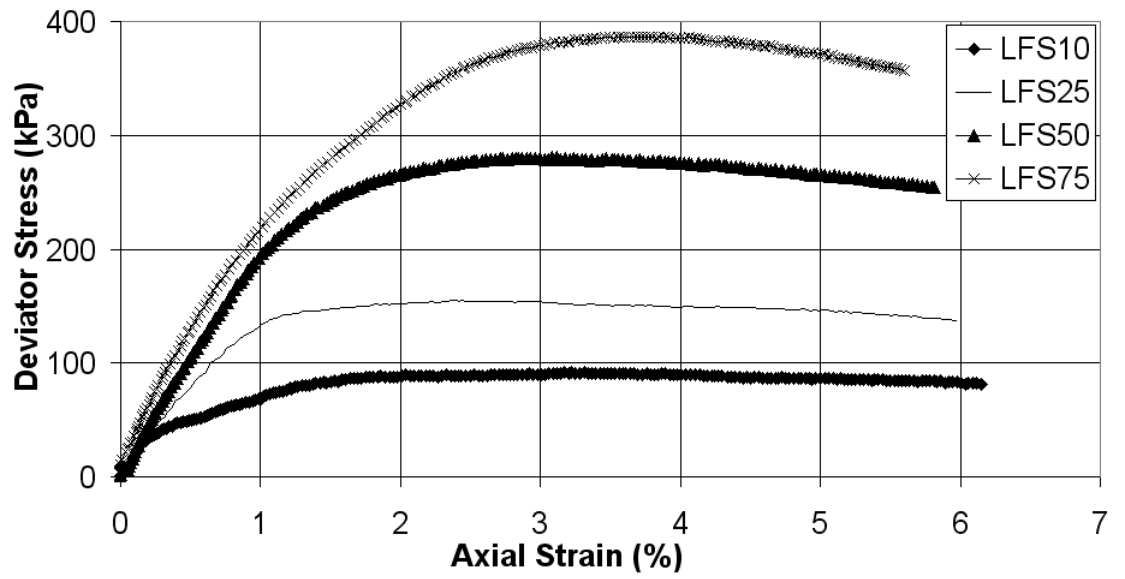
### Monotonic Shear Failure Tests for Portaway Sand (PS) with 4.2% Moisture Content



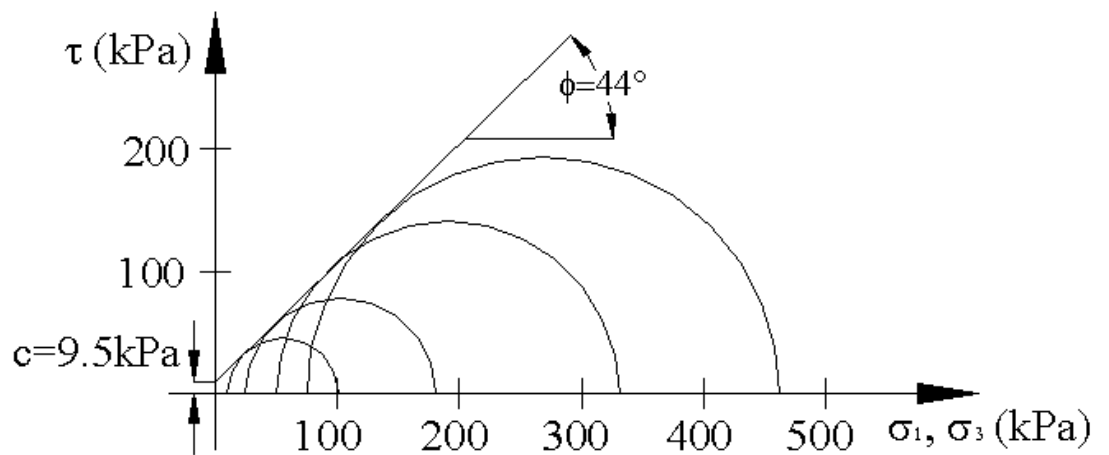
### Mohr Circles for Portaway Sand with 4.2% Moisture Content

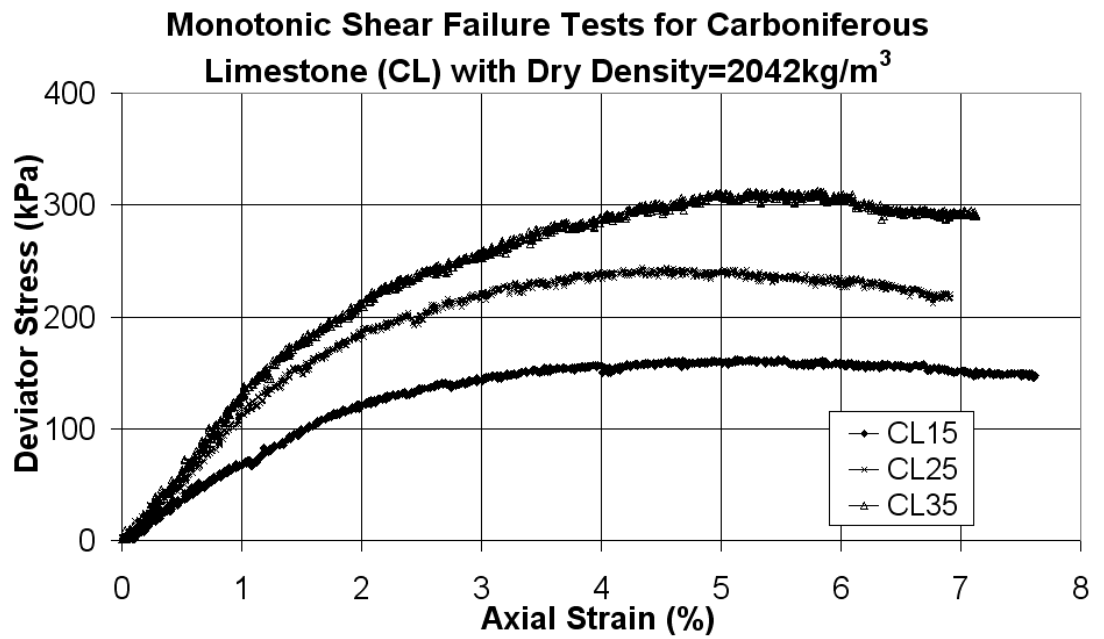


### Monotonic Shear Failure Tests for Langford Fill Sand (LFS) with 9% Moisture Content

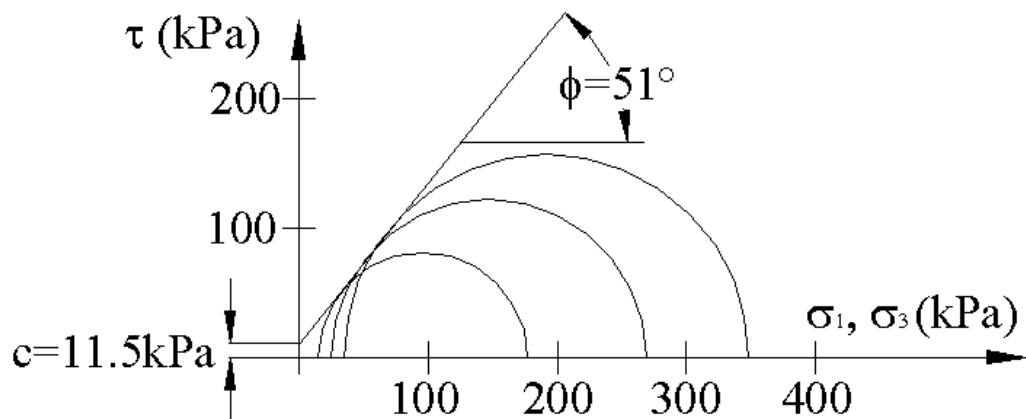


### Mohr Circles for Langford Fill Sand with 9% Moisture Content

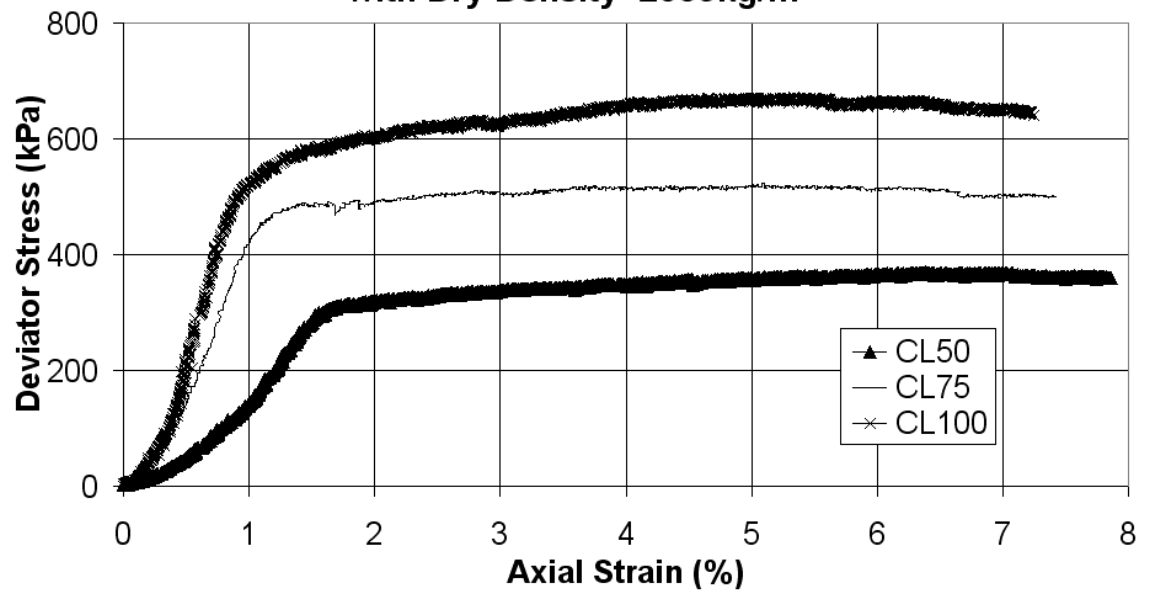




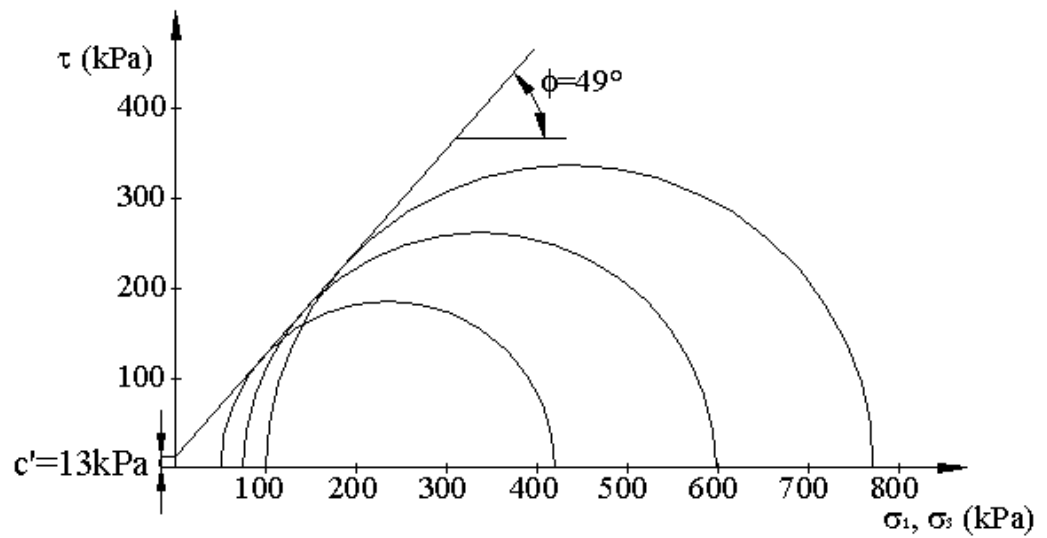
Mohr Circles for Carboniferous Limestone (CL)  
with Dry Density =2042kg/m<sup>3</sup>



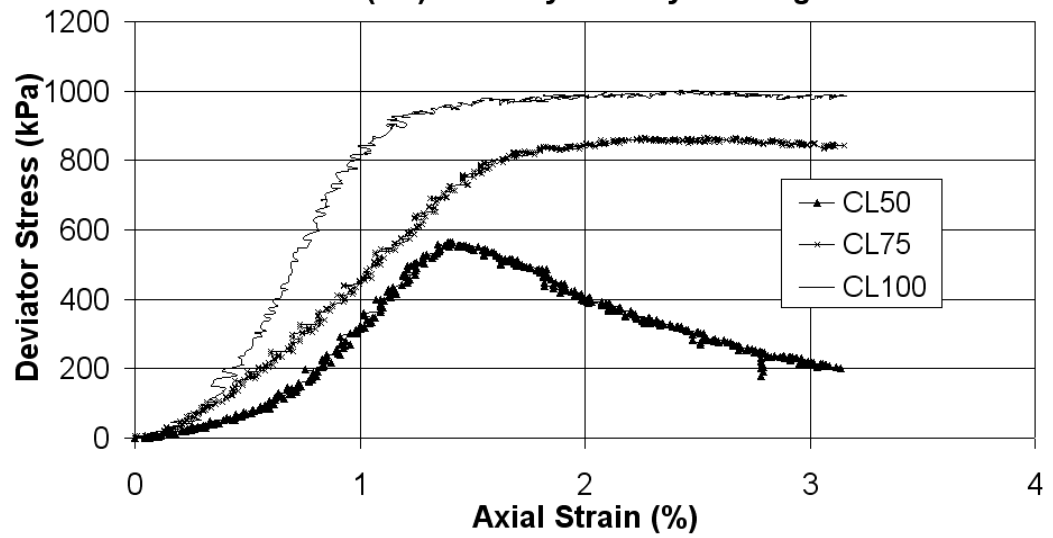
**Monotonic Shear Failure Tests for Granite (G)  
with Dry Density=2059kg/m<sup>3</sup>**



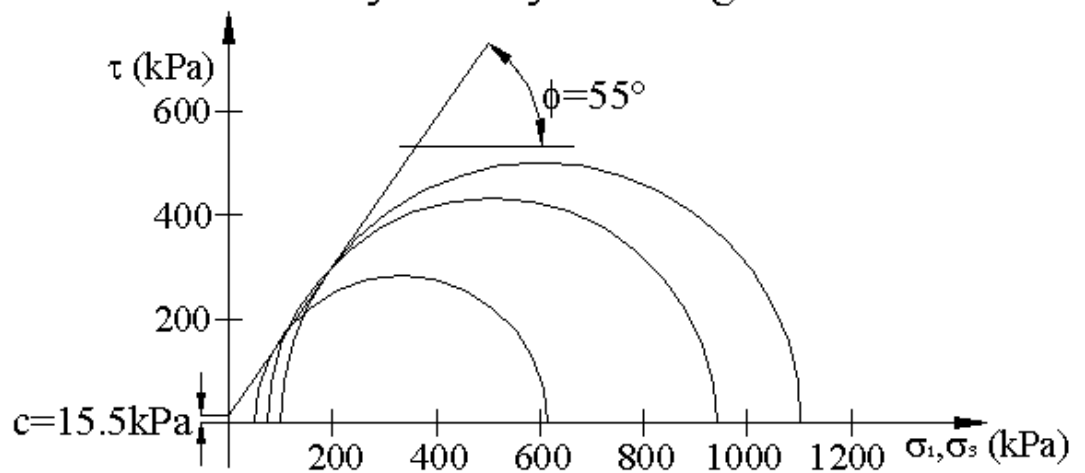
**Mohr Circles for Granite with Dry Density=2059kg/m<sup>3</sup>**



**Monotonic Shear Failure Tests for Carboniferous  
Limestone (CL) with Dry Density=2083kg/m<sup>3</sup>**

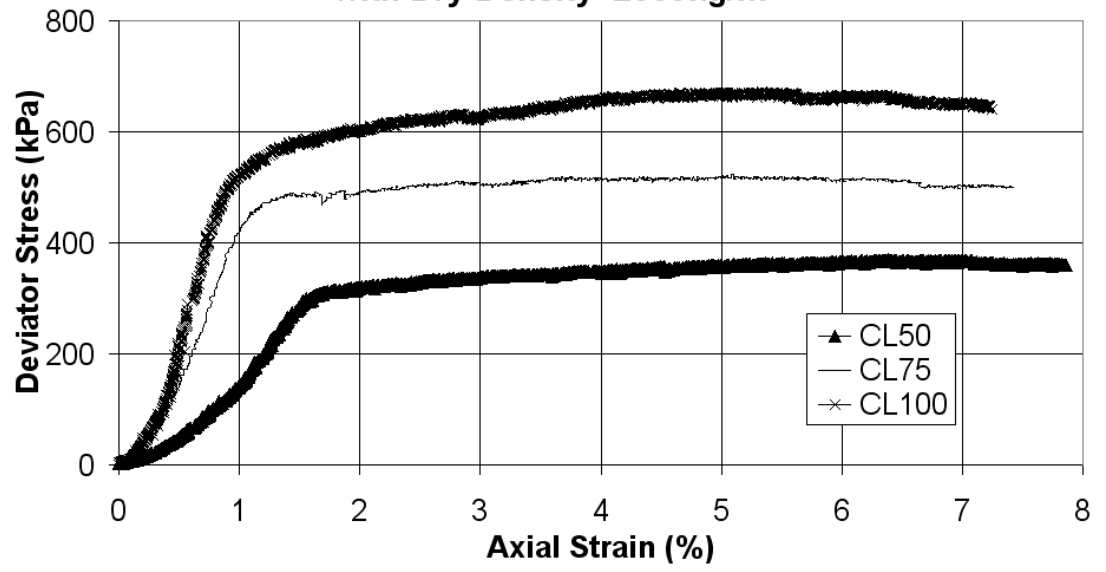


**Mohr Circles for Carboniferous Limestone  
with Dry Density= 2083kg/m<sup>3</sup>**

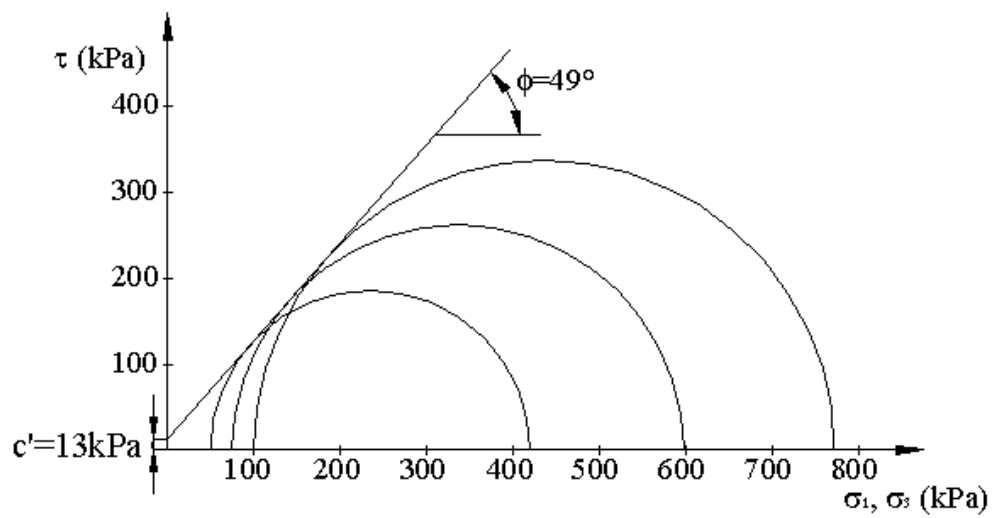




**Monotonic Shear Failure Tests for Granite (G)**  
with Dry Density= $2059\text{kg/m}^3$



Mohr Circles for Granite with Dry Density= $2059\text{kg/m}^3$



## **Appendix B. Wheel Load Calibrations**

### B.1. Wheel Load Calibration at the SW

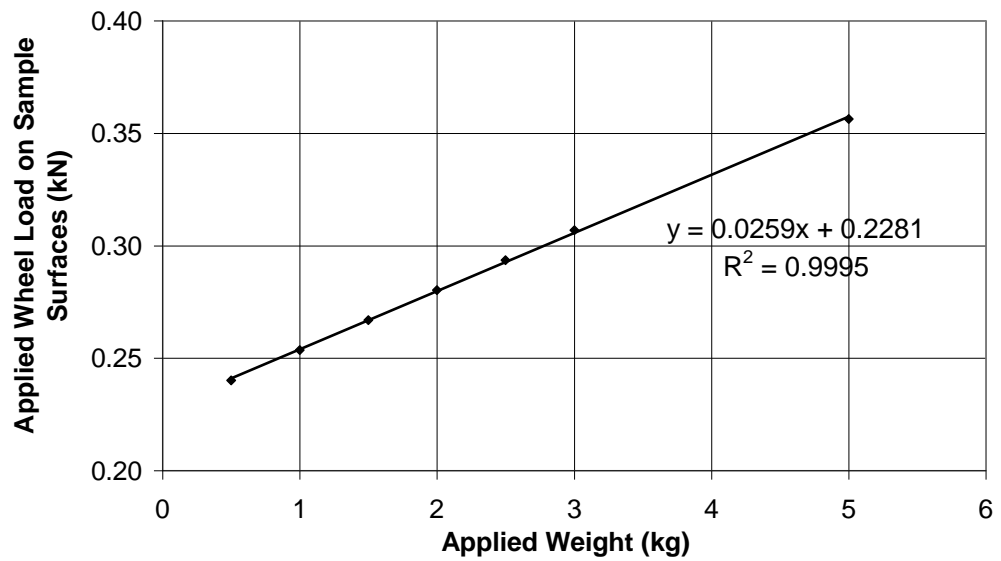


Figure B1. 1 The relations between the applied weight and the wheel load increment

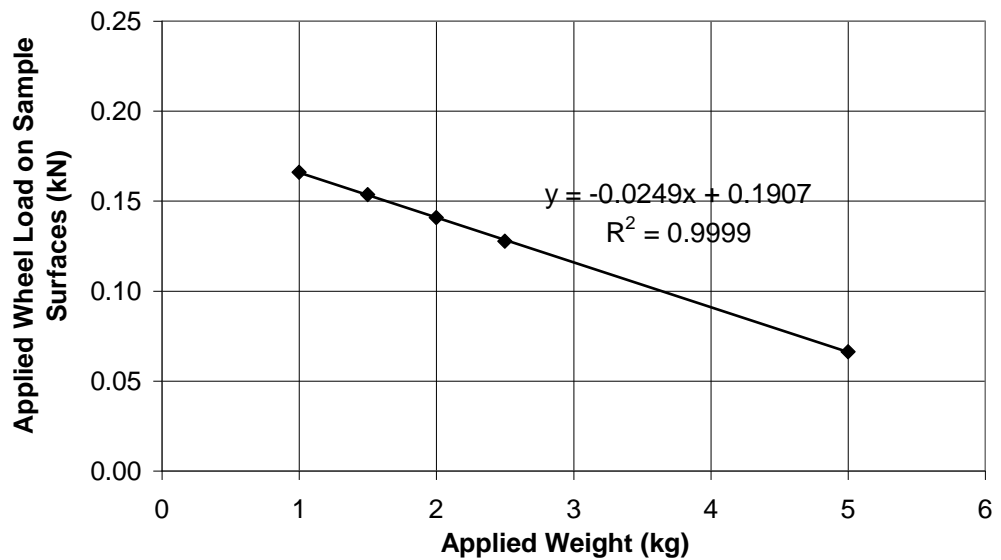


Figure B1. 2 The relations between the applied weight and the wheel load reduction

## B.2 Wheel Load Calibration at the PTF

**Table B2. 1** The relation between the controlled and the applied wheel load in PTF

Controlled Pot	Average Voltage Output (V)	Load (kN)
0.20	2.08	0.98
0.40	2.86	1.35
0.60	3.63	1.71
0.80	4.49	2.12
1.00	5.25	2.47
1.20	6.05	2.85
1.40	6.83	3.22
1.60	7.61	3.59
1.80	8.55	4.03
2.00	9.17	4.32
2.20	9.98	4.70
2.40	10.78	5.08
2.60	11.52	5.43
2.80	12.25	5.77
3.00	12.93	6.09
3.20	13.54	6.38
3.40	14.10	6.64
3.60	14.61	6.88


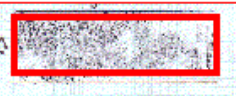







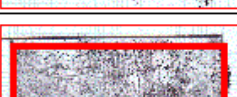

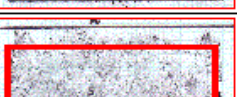





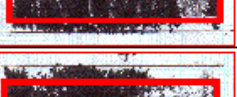
Controlled Pot	Average Voltage Output (V)	Load (kN)
3.70	14.76	6.95
3.80	15.06	7.09
4.00	15.48	7.29
4.20	15.91	7.50
4.40	16.32	7.69
4.60	16.70	7.87
4.80	17.02	8.02
5.00	17.32	8.16
5.20	17.65	8.32
5.40	17.96	8.46
5.60	18.25	8.60
6.00	18.53	8.73
6.50	19.11	9.00
7.00	19.73	9.30
7.50	20.36	9.59
8.00	20.96	9.88
8.50	21.47	10.12

### B.3 Cell Pressure Calibrations at PTF

Pressure Cell No	Applied Pressure (psi)	Applied Pressure (kPa)	Electrical Output (V)	kPa/V
Profile 1				
1	31	213.59	0.63	339
2	31	213.59	0.74	289
3	31	213.59	0.85	251
Profile 2				
4	0	0	0.00	185
	10	68	0.42	
	20	136	0.79	
	30	204	1.08	
	40	272	1.46	
	50	340	1.84	
	60	408	2.20	
	70	476	2.58	
5	0	0	0.00	168
	10	68	0.43	
	20	136	0.82	
	30	204	1.25	
	40	272	1.60	
	50	340	2.00	
	60	408	2.41	
	70	476	2.84	
6	0	0	0.0	372
	10	68	0.4	
	20	136	0.6	
	30	204	0.7	
	40	272	0.8	
	50	340	0.8	
	60	408	1.0	
	70	476	1.1	














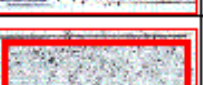

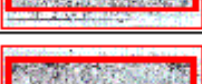











## **Appendix C The Contact Patches of Various Wheel Loads Using the Wheel Tracking Facilities**

**Table C. 1 The wheel contact patches on the Keuper Marl**

Applied Wheel Load (kN)	Contact Patch			Contact Area (mm <sup>2</sup> )
0.116				654
0.141				705
0.166				748
0.178				787
0.214				802
0.254				820

Not to scale





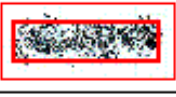










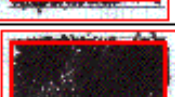














**Table C. 2 The wheel contact patches on the Silt**

Applied Wheel Load (kN)	Contact Patch			Contact Area (mm <sup>2</sup> )
0.079				615
0.091				675
0.116				698
0.141				813
0.166				886
0.214				969
0.254				1052
0.280				1174
0.306				1304

**Not to scale.**



**Table C. 3 The wheel contact patches on the Portaway sand**




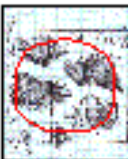










Applied Wheel Load (kN)	Contact Patch			Contact Area (mm <sup>2</sup> )
0.041				609
0.066				657
0.079				688
0.091				730
0.104				794
0.116				810
0.128				966
0.141				994
0.153				1057
0.166				1076

Not to scale

**Table C. 4 Summary of the contact areas using the SW**

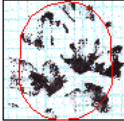

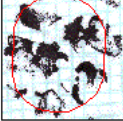
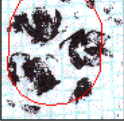
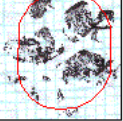
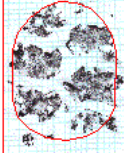
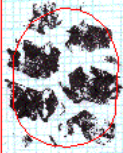
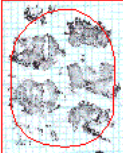
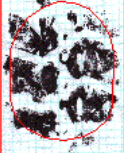
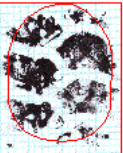
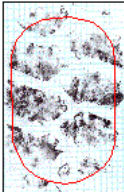
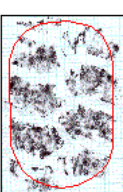
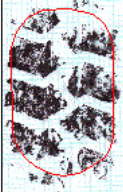


Material Type	Applied Wheel Load (kN)	Contact Area (mm <sup>2</sup> )	Corrected Contact area (mm <sup>2</sup> )	Contact Pressure (kPa)	Corrected contact pressure (kPa)	Difference (%)
Portaway Sand	0.041	609	554	67	74	10
	0.066	657	659	100	100	0
	0.079	688	714	115	111	-4
	0.091	730	764	125	119	-4
	0.104	794	819	131	127	-3
	0.116	810	870	143	133	-7
	0.128	966	920	133	139	5
	0.141	994	975	142	145	2
	0.153	1057	1026	145	149	3
	0.166	1076	1081	154	154	0
Silt	0.091	675	135	653	139	3
	0.116	698	166	723	160	-3
	0.141	813	173	793	178	3
	0.166	886	187	862	193	3
	0.214	969	221	996	215	-3
	0.254	1052	241	1107	229	-5
	0.28	1174	239	1180	237	0
	0.306	1304	235	1252	244	4
Keuper Marl	0.116	654	177	678	171	4
	0.141	705	200	708	199	0
	0.166	748	222	738	225	-1
	0.178	787	226	752	237	-5
	0.214	802	267	795	269	-1
	0.254	820	310	843	301	3

**Table C. 5 The STF wheel contact patches on the Granite**

Applied Wheel Load (kN)	Contact Patch		Contact Area (mm <sup>2</sup> )
1			5494
2			6301
3			9201
4			10782
5			13288
6			15751
7			18136

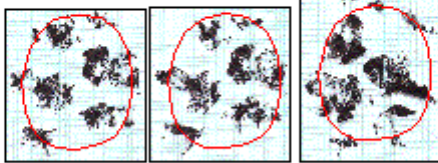
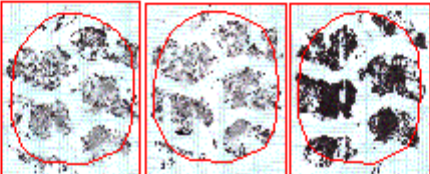
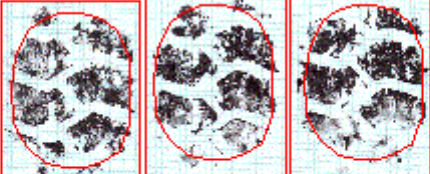
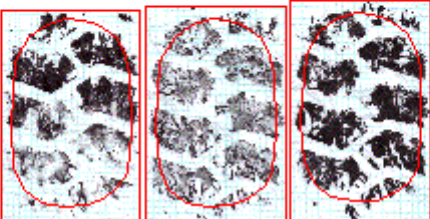
**Not to scale.**

**Table C. 6 The STF wheel contact patches on the crushed Carboniferous Limestone**

Applied Wheel Load (kN)	Contact Patch					Contact Area (mm <sup>2</sup> )
1						6852
2						10720
3						13167

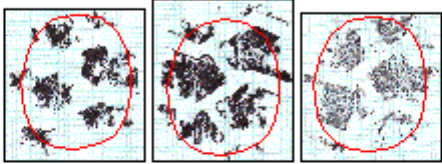

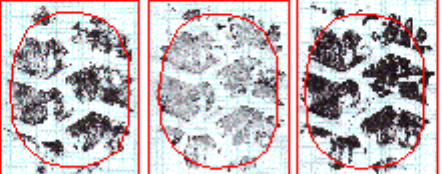

**Not to scale.**

**Table C. 7 The STF wheel contact patches on the crushed Granite placed above the Portaway Sand**

Applied Wheel Load (kN)	Contact Patch	Contact Area (mm <sup>2</sup> )
1	 Three grayscale images showing the contact patch of a wheel on crushed granite at 1 kN load. Each image shows a circular contact area with a red outline, containing dark, irregular shapes representing the contact pattern. The images are arranged horizontally.	6555
2	 Three grayscale images showing the contact patch of a wheel on crushed granite at 2 kN load. Each image shows a circular contact area with a red outline, containing dark, irregular shapes representing the contact pattern. The images are arranged horizontally.	9224
3	 Three grayscale images showing the contact patch of a wheel on crushed granite at 3 kN load. Each image shows a circular contact area with a red outline, containing dark, irregular shapes representing the contact pattern. The images are arranged horizontally.	10450
4	 Three grayscale images showing the contact patch of a wheel on crushed granite at 4 kN load. Each image shows a circular contact area with a red outline, containing dark, irregular shapes representing the contact pattern. The images are arranged horizontally.	13767

**Not to scale.**

**Table C. 8 The STF wheel contact patches on the crushed Granite placed above the Silt**

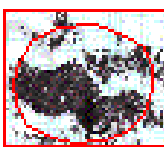
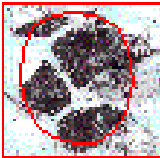
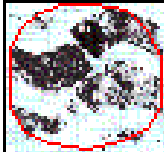

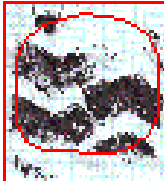
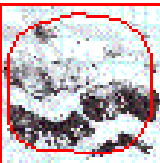
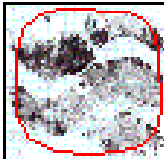
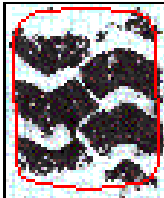
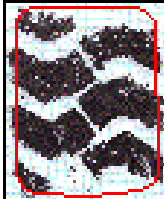

Applied Wheel Load (kN)	Contact Patch	Contact Area (mm <sup>2</sup> )
1		6402
2		9153
3		10313
6		15277

**Not to scale.**

**Table C. 9 Summary of the contact areas using the STF**

<b>Material Type</b>	<b>Applied Force (kN)</b>	<b>Contact Area (mm<sup>2</sup>)</b>	<b>Corrected Contact Area (mm<sup>2</sup>)</b>	<b>Contact Pressure (kPa)</b>	<b>Corrected Contact Pressure (kPa)</b>	<b>Difference (%)</b>
Granite	1	5494	4753	182	210	16
	2	6301	6928	317	289	-9
	3	9201	9104	326	330	1
	4	10782	11279	371	355	-4
	5	13288	13455	376	372	-1
	6	15751	15630	381	384	1
	7	18136	17806	386	393	2
Granite over Portaway Sand	1	6555	6570	153	152	0
	2	9224	8856	217	226	4
	3	10450	11142	287	269	-6
	4	13767	13428	291	298	3
Granite over Silt	1	6402	6876	156	145	-7
	2	9153	8581	219	233	7
	3	10313	10286	291	292	0
	6	15277	15402	393	390	-1
Carboniferous Limestone over Keuper Marl	1	6852	7089	146	141	-3
	2	10720	10246	187	195	5
	3	13167	13404	228	224	-2

**Table C. 10 The PTF wheel contact patches on the crushed Granite placed above the Keuper Marl**

Applied Wheel Load (kN)	Contact Patch		Contact Area (mm <sup>2</sup> )
1.7			10080
3			14280
4			15686
5			16567
7			21851
8			23351
9			23841


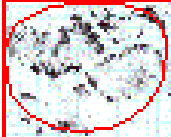
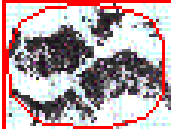

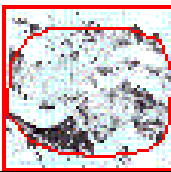

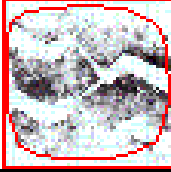
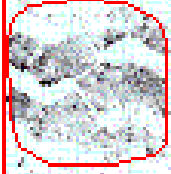
**Not to scale.**



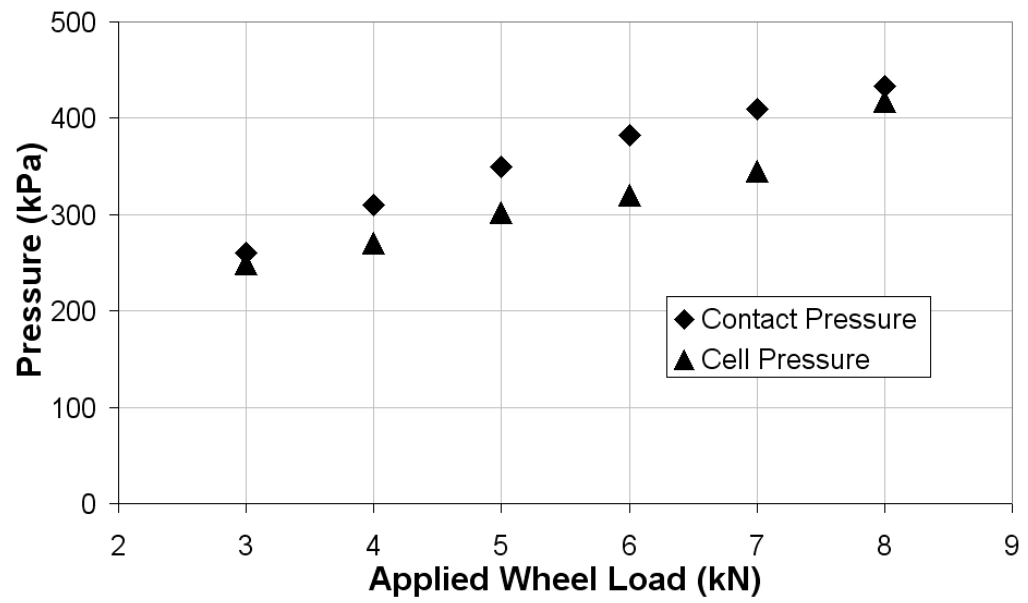
**Table C. 11 Summary of the contact areas using the PTF**

Applied Wheel Load (kN)	Contact Area (mm <sup>2</sup> )	Corrected Contact Area (mm <sup>2</sup> )	Contact Pressure (kPa)	Corrected Contact Pressure (kPa)	Difference (%)	Pressure Cell Reading (volts)	Pressure Cell Reading (kPa)
3	14280	13981	210	215	2	0.415	120
4	15686	15741	255	254	0	0.464	134
5	16567	17502	302	286	5	0.552	159
6	n/a	19263	n/a	311	n/a	0.615	178
7	21851	21023	320	333	4	0.669	193
8	23351	22784	343	351	2	0.742	214
9	23841	24544	378	367	3	0.791	229

**Table C. 12 The PTF wheel contact patches on the crushed Granite placed above the Langford Fill Sand and Keuper Marl**

Applied Wheel Load (kN)	Contact Patch	Contact Area (mm <sup>2</sup> )
1		9264
2		10177
3		11741
4		12407
5		13337
6		15618
7		17265
8		19048

**Not to scale.**



**Figure C. 1 The cell pressures and contact pressures for different PTF wheel loads on the crushed Carboniferous Limestone placed above the Langford Fill Sand and Keuper Marl**

## **Appendix D. Properties of the Wheel Tracking Test Specimens**

**Table D. 1 The soil properties for single layered tests using the SW**

Reference	Material Type	Bulk Density (kg/m <sup>3</sup> )	Moiture Content (%)	Relative Density (%)	Sr (%)	Contact Pressure (kPa)
PS1	Portaway Sand	1889	4.2	90	24	100
		1889	4.0	91	23	111
		1890	4.4	89	25	119
		1880	4.2	88	24	127
		1883	3.9	90	22	154
PS2	Portaway Sand	1889	4.2	90	24	100
		1889	4.2	90	24	111
		1889	4.1	90	23	119
		1885	4.0	90	23	127
		1890	4.2	90	24	154
KM	Keuper Marl	2169	15.2	n/a	95	225
		2167	15.2		94	237
		2162	15.0		93	269
		2164	15.1		93	301
Silt	Silt	1731	15.4	n/a	54	193
		1734	15.2		54	229
		1736	15.0		53	244
		1736	14.9		53	251
		1732	15.3		54	257
		1736	15.2		54	261

Note: 'n/a' means not applicable for the soil. Sr means degree of saturation.

**Table D. 2 The soil properties for single layered tests using the STF**

Reference	Material Type	Thickness (mm)	Bulk Density (kg/m <sup>3</sup> )	Moisture Content (%)	Relative Density (%)	Sr (%)	Contact Pressure (kPa)
Gr	Granite	180	2172	4.0	65	34	289
			2192	3.9	67	35	355
			2200	4.2	68	37	372
			2234	4.0	71	38	384

Note: 'n/a' means not applicable for the soil. Sr means degree of saturation.

**Table D. 3 The soil properties for two layered tests using the STF**

Reference	Material Type	Bulk Density (kg/m <sup>3</sup> )	Moisture Content (%)	Relative Density (%)	Sr (%)	Contact Pressure (kPa)
Gr-Silt	Crushed Granite	2141	4.2	61	33	145
	Silt	1736	15.5	n/a	55	
	Crushed Granite	2142	4.2	62	33	233
	Silt	1736	15.5	n/a	55	
Gr-PS	Crushed Granite	2142	4.2	62	33	292
	Silt	1736	15.5	n/a	55	
	Crushed Granite	2142	4.2	62	33	390
	Silt	1736	15.5	n/a	55	
Gr-PS	Crushed Granite	2140	4.0	62	32	152
	Portaway Sand	1889	4.0	91	23	
	Crushed Granite	2139	4.2	61	33	226
	Portaway Sand	1885	4.1	90	23	
CI-KM1	Crushed Granite	2135	4.0	61	32	269
	Portaway Sand	1880	4.1	89	23	
	Crushed Carboniferous Limestone	2099	2.8	39	23	141
	Keuper Marl	2015	22.0	n/a	94	
CI-KM1	Crushed Carboniferous Limestone	2100	2.9	39	24	195
	Keuper Marl	2012	22.5	n/a	94	
	Crushed Carboniferous Limestone	2099	2.8	39	23	224
	Keuper Marl	2004	23.0	n/a	94	

Note: 'n/a' means not applicable for the soil.

**Table D. 4 The soil properties for two layered test using the PTF  
(Reference: CI-KM2)**

<i>Pavement Layer</i>	<i>Type of Test</i>	
Crushed Carboniferous Limestone	Average Dynamic Cone Penetrometer (mm/blow)	17
	CBR related (%)	11.5
	German Plate Bearing Test (MPa)	34
	Dry Density (kg/m <sup>3</sup> )	2131
	Relative Density (%)	55
	Moisture Content (%)	2.86
Keuper Marl	Average Dynamic Cone Penetrometer (mm/blow)	-
	CBR related (%)	23
	German Plate Bearing Test (MPa)	4
	Dry Density (kg/m <sup>3</sup> )	1789
	Moisture Content (%)	23

Note: ‘-’ means no data available.

**Table D. 5 The soil properties for three layered test using the PTF  
(Reference: CI-LFS-KM)**

<b><i>Pavement Layer</i></b>	<b><i>Type of Test</i></b>	
Crushed Carboniferous Limestone	Average Dynamic Cone Penetrometer (mm/blow)	8
	CBR related (%)	29
	German Plate Bearing Test (MPa)	n/a
	Dry Density (kg/m <sup>3</sup> )	2294
	Relative Density (%)	79
	Moisture Content (%)	0.89
Langford Fill Sand	Average Dynamic Cone Penetrometer (mm/blow)	120
	CBR related (%)	1
	German Plate Bearing Test (MPa)	n/a
	Dry Density (kg/m <sup>3</sup> )	1396
	Relative Density (%)	27
	Moisture Content (%)	7.74
Keuper Marl	Average Dynamic Cone Penetrometer (mm/blow)	-
	CBR related (%)	23
	German Plate Bearing Test (MPa)	4
	Dry Density (kg/m <sup>3</sup> )	1789
	Moisture Content (%)	23

Note: ‘-’ means no data available.

Note:

In-situ tests such as Dynamic Cone Penetrometer and German Dynamic Plate Bearing tests were performed to identify the structural properties.

#### ***Dynamic Cone Penetrometer (DCP)***

The DCP is an in-situ device that used for rapid measurement of the material resistance to penetration in terms of mm/blow while a cone of the device is being driven into the pavement or the subgrade. The DCP that was used to measure the material resistance in the PTF test pit has a 20 mm diameter 60

degree cone of tampered steel which is driven into pavement with an 8 kg sliding hammer dropping over a height of 575 mm, yielding thus a theoretical energy of 45 J or 14.3 J/cm<sup>2</sup>. A reading in these measurements was taken at every blow and plotted in Figure C1.1 including the correlation CBR that developed by Kleyn and Van Herden (see A2465 TRRL Dynamic Cone Penetrometer operating instructions).

### ***German Dynamic Plate (GDP)***

The GDP used for in-situ stiffness measurement has a total mass of 25kg, and a falling mass of 10kg that loads through a rubber buffer the 300mm diameter bearing plate, within which is mounted a velocity transducer. The drop height of the falling mass is set such that peak applied force is 7.07kN (i.e. 100kPa contact stress) when calibrated on a standard (manufacturer's) foundation. Initially the specimen was precompacted by three drops before any measurements were taken to remove any bedding errors. Then it was followed by other three drops to obtain a single value of stiffness which the deflection from the three drops were recorded and displayed on the readout together with the computed average stiffness.



## DCP Test Results of the Two Profiles in the Nottingham PTF

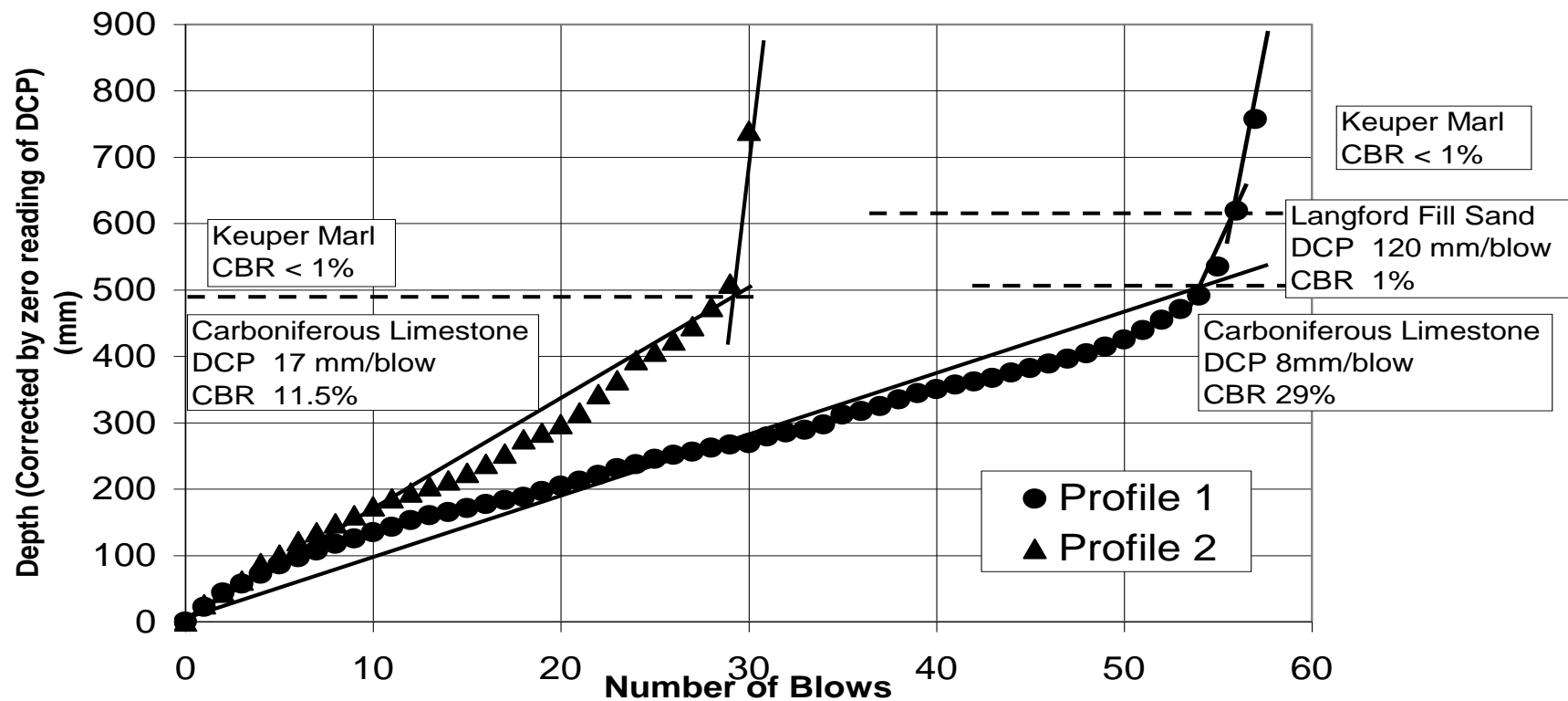


Figure D. 1 DCP Test Results in the PTF

## **Appendix E The vertical permanent deformation data**

Reference	PS1			PS1		
Type of Soil	Portaway Sand			Portaway Sand		
Contact Pressure, kPa	100			111		
Number of Passes	LVDT Reading	Deformation, mm	Deformation Rate, mm/10 <sup>3</sup> pass	LVDT Reading	Deformation, mm	Deformation Rate, mm/10 <sup>3</sup> pass
0	-18.48	0		-14.88	0.00	
10	-18.40	0.08	8.00	-14.71	0.17	17.00
20	-18.22	0.26	18.00	-14.46	0.42	25.00
30	-18.00	0.48	22.00	-14.08	0.80	38.00
40	-17.78	0.70	22.00	-13.86	1.02	22.00
50	-17.74	0.74	4.00	-13.56	1.32	30.00
60	-17.58	0.90	16.00	-13.41	1.47	15.00
70	-17.47	1.01	11.00	-13.18	1.70	23.00
80	-17.30	1.18	17.00	-13.02	1.86	16.00
90	-17.28	1.20	2.00	-12.97	1.91	5.00
100	-17.17	1.31	11.00	-12.91	1.97	6.00
110	-17.14	1.34	3.00	-12.76	2.12	15.00
120	-17.12	1.36	2.00	-12.59	2.29	17.00
130	-17.06	1.42	6.00	-12.56	2.32	3.00
140	-17.02	1.46	4.00	-12.53	2.35	3.00
150	-16.96	1.52	6.00	-12.44	2.44	9.00
160	-16.92	1.56	4.00	-12.36	2.52	8.00
170	-16.91	1.57	1.00	-12.33	2.55	3.00
180	-16.90	1.58	1.00	-12.33	2.55	0.00
190	-16.80	1.68	10.00	-12.25	2.63	8.00
200	-16.80	1.68	0.00	-12.24	2.64	1.00
210	-16.80	1.68	0.00	-12.22	2.66	2.00
220	-16.80	1.68	0.00	-12.18	2.70	4.00
230	-16.77	1.71	3.00	-12.17	2.71	1.00
240	-16.73	1.75	4.00	-12.14	2.74	3.00
250	-16.70	1.78	3.00	-12.03	2.85	11.00
260	-16.68	1.80	2.00	-11.97	2.91	6.00
270	-16.62	1.86	6.00	-11.93	2.95	4.00
280	-16.61	1.87	1.00	-11.9	2.98	3.00
290	-16.59	1.89	2.00	-11.87	3.01	3.00
300	-16.56	1.92	3.00	-11.85	3.03	2.00
310	-16.55	1.93	1.00	-11.82	3.06	3.00
320	-16.54	1.94	1.00	-11.81	3.07	1.00
330	-16.52	1.96	2.00	-11.77	3.11	4.00
340	-16.52	1.96	0.00	-11.77	3.11	0.00
350	-16.50	1.98	2.00	-11.73	3.15	4.00
360	-16.48	2.00	2.00	-11.7	3.18	3.00
370	-16.48	2.00	0.00	-11.7	3.18	0.00
380	-16.48	2.00	0.00	-11.69	3.19	1.00
390	-16.48	2.00	0.00	-11.68	3.20	1.00
400	-16.45	2.03	3.00	-11.65	3.23	3.00
450	-16.39	2.09	1.20	-11.6	3.28	1.00
500	-16.35	2.13	0.80	-11.56	3.32	0.80
550	-16.34	2.14	0.20	-11.5	3.38	1.20
600	-16.33	2.15	0.20	-11.47	3.41	0.60
650	-16.24	2.24	1.80	-11.42	3.46	1.00
700	-16.20	2.28	0.80	-11.36	3.52	1.20
750	-16.14	2.34	1.20	-11.31	3.57	1.00
800	-16.13	2.35	0.20	-11.27	3.61	0.80

Reference	PS1			PS1		
Type of Soil	Portaway Sand			Portaway Sand		
Contact Pressure, kPa	100			111		
Number of Passes	LVDT Reading	Deformation, mm	Deformation Rate, mm/10 <sup>3</sup> pass	LVDT Reading	Deformation, mm	Deformation Rate, mm/10 <sup>3</sup> pass
850	-16.13	2.35	0.00	-11.24	3.64	0.60
900	-16.09	2.39	0.80	-11.23	3.65	0.20
950	-16.06	2.42	0.60	-11.22	3.66	0.20
1000	-16.04	2.44	0.40	-11.2	3.68	0.40
1500	-16.00	2.48	0.08	-11.02	3.86	0.36
2000	-15.82	2.66	0.36	-10.89	3.99	0.26
2500	-15.73	2.75	0.18	-10.78	4.10	0.22
3000	-15.65	2.83	0.16	-10.69	4.19	0.18
3500	-15.58	2.90	0.14	-10.62	4.26	0.14
4000	-15.50	2.98	0.16	-10.58	4.30	0.08
4500	-15.42	3.06	0.16	-10.5	4.38	0.16
5000	-15.35	3.13	0.14	-10.4	4.48	0.20
6000	-15.31	3.17	0.04	-10.29	4.59	0.11
7000	-15.29	3.19	0.02	-10.1	4.78	0.19
8000	-15.10	3.38	0.19	-9.97	4.91	0.13
9000	-15.05	3.43	0.05	-9.86	5.02	0.11
10000	-14.96	3.52	0.09	-9.7	5.18	0.16
11000	-14.93	3.55	0.03	-9.64	5.24	0.06
12000	-14.90	3.58	0.03	-9.62	5.26	0.02
13000	-14.87	3.61	0.03	-9.61	5.27	0.01
14000	-14.84	3.64	0.03	-9.59	5.29	0.02
15000	-14.80	3.68	0.04	-9.57	5.31	0.02
16000	-14.77	3.71	0.03	-9.56	5.32	0.01

Reference	PS1			PS1		
Type of Soil	Portaway Sand			Portaway Sand		
Contact Pressure, kPa	119			127		
Number of Passes	LVDT Reading	Deformation, mm	Deformation Rate, mm/10 <sup>3</sup> pass	LVDT Reading	Deformation, mm	Deformation Rate, mm/10 <sup>3</sup> pass
0	-17.54	0.00		-16.3	0.00	
10	-16.68	0.86	86.00	-14.89	1.41	141.00
20	-15.72	1.82	96.00	-13.7	2.60	119.00
30	-14.91	2.63	81.00	-13.03	3.27	67.00
40	-14.42	3.12	49.00	-12.43	3.87	60.00
50	-14.31	3.23	11.00	-12.2	4.10	23.00
60	-13.97	3.57	34.00	-11.95	4.35	25.00
70	-13.87	3.67	10.00	-11.7	4.60	25.00
80	-13.75	3.79	12.00	-11.65	4.65	5.00
90	-13.59	3.95	16.00	-11.6	4.70	5.00
100	-13.44	4.10	15.00	-11.43	4.87	17.00
110	-13.38	4.16	6.00	-11.25	5.05	18.00
120	-13.19	4.35	19.00	-11.07	5.23	18.00
130	-13.16	4.38	3.00	-11.05	5.25	2.00
140	-13.13	4.41	3.00	-11	5.30	5.00
150	-13.07	4.47	6.00	-10.86	5.44	14.00

Reference	PS1			PS1		
Type of Soil	Portaway Sand			Portaway Sand		
Contact Pressure, kPa	119			127		
Number of Passes	LVDT Reading	Deformation, mm	Deformation Rate, mm/10 <sup>3</sup> pass	LVDT Reading	Deformation, mm	Deformation Rate, mm/10 <sup>3</sup> pass
160	-12.96	4.58	11.00	-10.8	5.50	6.00
170	-12.91	4.63	5.00	-10.78	5.52	2.00
180	-12.86	4.68	5.00	-10.71	5.59	7.00
190	-12.79	4.75	7.00	-10.66	5.64	5.00
200	-12.74	4.80	5.00	-10.59	5.71	7.00
210	-12.71	4.83	3.00	-10.59	5.71	0.00
220	-12.67	4.87	4.00	-10.47	5.83	12.00
230	-12.62	4.92	5.00	-10.43	5.87	4.00
240	-12.6	4.94	2.00	-10.4	5.90	3.00
250	-12.56	4.98	4.00	-10.34	5.96	6.00
260	-12.56	4.98	0.00	-10.29	6.01	5.00
270	-12.53	5.01	3.00	-10.26	6.04	3.00
280	-12.47	5.07	6.00	-10.2	6.10	6.00
290	-12.44	5.10	3.00	-10.11	6.19	9.00
300	-12.42	5.12	2.00	-10.09	6.21	2.00
310	-12.4	5.14	2.00	-10.08	6.22	1.00
320	-12.36	5.18	4.00	-10.04	6.26	4.00
330	-12.34	5.20	2.00	-10	6.30	4.00
340	-12.32	5.22	2.00	-9.99	6.31	1.00
350	-12.3	5.24	2.00	-9.91	6.39	8.00
360	-12.28	5.26	2.00	-9.91	6.39	0.00
370	-12.22	5.32	6.00	-9.87	6.43	4.00
380	-12.18	5.36	4.00	-9.85	6.45	2.00
390	-12.16	5.38	2.00	-9.78	6.52	7.00
400	-12.16	5.38	0.00	-9.78	6.52	0.00
450	-12.14	5.40	0.40	-9.67	6.63	2.20
500	-12.07	5.47	1.40	-9.55	6.75	2.40
550	-11.98	5.56	1.80	-9.53	6.77	0.40
600	-11.92	5.62	1.20	-9.37	6.93	3.20
650	-11.89	5.65	0.60	-9.35	6.95	0.40
700	-11.85	5.69	0.80	-9.26	7.04	1.80
750	-11.81	5.73	0.80	-9.17	7.13	1.80
800	-11.8	5.74	0.20	-9.12	7.18	1.00
850	-11.75	5.79	1.00	-9.01	7.29	2.20
900	-11.68	5.86	1.40	-8.99	7.31	0.40
950	-11.65	5.89	0.60	-8.9	7.40	1.80
1000	-11.63	5.91	0.40	-8.87	7.43	0.60
1500	-11.39	6.15	0.48	-8.47	7.83	0.80
2000	-11.24	6.30	0.30	-7.52	8.78	1.90
2500	-11.11	6.43	0.26	-6.81	9.49	1.42
3000	-11.02	6.52	0.18	-6.31	9.99	1.00
3500	-10.92	6.62	0.20	-5.83	10.47	0.96
4000	-10.87	6.67	0.10	-5.62	10.68	0.42
4500	-10.74	6.80	0.26	-5.35	10.95	0.54
5000	-10.66	6.88	0.16	-5.1	11.20	0.50
6000	-10.59	6.95	0.07	-4.55	11.75	0.55
7000	-10.47	7.07	0.12	-4.24	12.06	0.31
8000	-10.35	7.19	0.12	-3.87	12.43	0.37
9000	-10.23	7.31	0.12	-3.64	12.66	0.23

Reference	PS1			PS1		
Type of Soil	Portaway Sand			Portaway Sand		
Contact Pressure, kPa	119			127		
Number of Passes	LVDT Reading	Deformation, mm	Deformation Rate, mm/10 <sup>3</sup> pass	LVDT Reading	Deformation, mm	Deformation Rate, mm/10 <sup>3</sup> pass
10000	-10.11	7.43	0.12	-3.32	12.98	0.32
11000	-9.98	7.56	0.13	-3.11	13.19	0.21
12000	-9.8	7.74	0.18	-2.88	13.42	0.23
13000	-9.69	7.85	0.11	-2.79	13.51	0.09
14000	-9.58	7.96	0.11	-2.6	13.70	0.19
15000	-9.53	8.01	0.05	-2.45	13.85	0.15
16000	-9.47	8.07	0.06	-2.25	14.05	0.20

Reference	PS1			PS2		
Type of Soil	Portaway Sand			Portaway Sand		
Contact Pressure, kPa	154			100		
Number of Passes	LVDT Reading	Deformation, mm	Deformation Rate, mm/10 <sup>3</sup> pass	LVDT Reading	Deformation, mm	Deformation Rate, mm/10 <sup>3</sup> pass
0	-14.56	0.00		-18.48	0	
10	-10.4	4.16	416.00	-18.47	0.01	1.00
20	-9.69	4.87	71.00	-18.47	0.01	0.00
30	-8.19	6.37	150.00	-18.46	0.02	1.00
40	-7.92	6.64	27.00	-18.46	0.02	0.00
50	-7.54	7.02	38.00	-18.45	0.03	1.00
60	-7.13	7.43	41.00	-18.45	0.03	0.00
70	-6.78	7.78	35.00	-18.37	0.11	8.00
80	-6.4	8.16	38.00	-18.30	0.18	7.00
90	-6.16	8.40	24.00	-18.28	0.20	2.00
100	-6.02	8.54	14.00	-18.27	0.21	1.00
110	-5.82	8.74	20.00	-18.19	0.29	8.00
120	-5.53	9.03	29.00	-18.23	0.25	-4.00
130	-5.52	9.04	1.00	-18.20	0.28	3.00
140	-5.26	9.30	26.00	-18.17	0.31	3.00
150	-5.25	9.31	1.00	-18.11	0.37	6.00
160	-5.15	9.41	10.00	-18.08	0.40	3.00
170	-4.9	9.66	25.00	-18.10	0.38	-2.00
180	-4.69	9.87	21.00	-18.05	0.43	5.00
190	-4.64	9.92	5.00	-18.00	0.48	5.00
200	-4.48	10.08	16.00	-17.96	0.52	4.00
210	-4.37	10.19	11.00	-17.98	0.50	-2.00
220	-4.26	10.30	11.00	-17.95	0.53	3.00
230	-4.25	10.31	1.00	-17.91	0.57	4.00
240	-4.05	10.51	20.00	-17.91	0.57	0.00
250	-4	10.56	5.00	-17.89	0.59	2.00
260	-3.95	10.61	5.00	-17.90	0.58	-1.00
270	-3.88	10.68	7.00	-17.89	0.59	1.00
280	-3.78	10.78	10.00	-17.86	0.62	3.00
290	-3.68	10.88	10.00	-17.84	0.64	2.00

Reference	PS1			PS2		
Type of Soil	Portaway Sand			Portaway Sand		
Contact Pressure, kPa	154			100		
Number of Passes	LVDT Reading	Deformation, mm	Deformation Rate, mm/10 <sup>3</sup> pass	LVDT Reading	Deformation, mm	Deformation Rate, mm/10 <sup>3</sup> pass
300	-3.58	10.98	10.00	-17.83	0.65	1.00
310	-3.41	11.15	17.00	-17.81	0.67	2.00
320	-3.33	11.23	8.00	-17.79	0.69	2.00
330	-3.27	11.29	6.00	-17.76	0.72	3.00
340	-3.11	11.45	16.00	-17.81	0.67	-5.00
350	-3.09	11.47	2.00	-17.74	0.74	7.00
360	-3.08	11.48	1.00	-17.81	0.67	-7.00
370	-2.99	11.57	9.00	-17.79	0.69	2.00
380	-2.89	11.67	10.00	-17.75	0.73	4.00
390	-2.79	11.77	10.00	-17.76	0.72	-1.00
400	-2.74	11.82	5.00	-17.70	0.78	6.00
450	-2.44	12.12	6.00	-17.69	0.79	0.20
500	-2.07	12.49	7.40	-17.67	0.81	0.40
550	-1.79	12.77	5.60	-17.62	0.86	1.00
600	-1.56	13.00	4.60	-17.62	0.86	0.00
650	-1.43	13.13	2.60	-17.60	0.88	0.40
700	-1.2	13.36	4.60	-17.57	0.91	0.60
750	-0.96	13.60	4.80	-17.51	0.97	1.20
800	-0.78	13.78	3.60	-17.54	0.94	-0.60
850	-0.53	14.03	5.00	-17.51	0.97	0.60
900	-0.36	14.20	3.40	-17.49	0.99	0.40
950	-0.33	14.23	0.60	-17.47	1.01	0.40
1000	-0.12	14.44	4.20	-17.42	1.06	1.00
1500	1.03	15.59	2.30	-17.34	1.14	0.16
2000	2.18	16.74	2.30	-17.28	1.20	0.12
2500	3.22	17.78	2.08	-17.25	1.23	0.06
3000	4.26	18.82	2.08	-17.21	1.27	0.08
3500	5.01	19.57	1.50	-17.18	1.30	0.06
4000	5.75	20.31	1.48	-17.15	1.33	0.06
4500	5.85	20.41	0.20	-17.12	1.36	0.06
5000	5.94	20.50	0.18	-17.09	1.39	0.06
6000	6.77	21.33	0.83	-17.04	1.44	0.05
7000	7.6	22.16	0.83	-16.88	1.60	0.16
8000	8.43	22.99	0.83	-16.85	1.63	0.03
9000	9.26	23.82	0.83	-16.81	1.67	0.04
10000	10.92	25.48	1.66	-16.78	1.70	0.03
11000	11.32	25.88	0.40	-16.77	1.71	0.01
12000	11.72	26.28	0.40	-16.76	1.72	0.01
13000	12.34	26.90	0.62	-16.75	1.73	0.01
14000	13.15	27.71	0.81	-16.74	1.74	0.01
15000	13.64	28.20	0.49	-16.73	1.75	0.01
16000	14.30	28.86	0.66	-16.72	1.76	0.01

Reference	PS2			PS2		
Type of Soil	Portaway Sand			Portaway Sand		
Contact Pressure, kPa	111			119		
Number of Passes	LVDT Reading	Deformation, mm	Deformation Rate, mm/10 <sup>3</sup> pass	LVDT Reading	Deformation, mm	Deformation Rate, mm/10 <sup>3</sup> pass
0	-13.46	0.00		-15.52	0.00	
10	-13.12	0.34	34.00	-14.67	0.85	85.00
20	-12.90	0.56	22.00	-14.00	1.52	67.00
30	-12.68	0.78	22.00	-13.56	1.96	44.00
40	-12.57	0.89	11.00	-13.11	2.41	45.00
50	-12.45	1.01	12.00	-12.76	2.76	35.00
60	-12.34	1.12	11.00	-12.60	2.92	16.00
70	-12.22	1.24	12.00	-12.31	3.21	29.00
80	-12.07	1.39	15.00	-12.23	3.29	8.00
90	-12.05	1.41	2.00	-12.13	3.39	10.00
100	-12.00	1.46	5.00	-12.05	3.47	8.00
110	-11.97	1.49	3.00	-11.95	3.57	10.00
120	-11.92	1.54	5.00	-11.90	3.62	5.00
130	-11.84	1.62	8.00	-11.76	3.76	14.00
140	-11.80	1.66	4.00	-11.70	3.82	6.00
150	-11.77	1.69	3.00	-11.62	3.90	8.00
160	-11.75	1.71	2.00	-11.56	3.96	6.00
170	-11.71	1.75	4.00	-11.52	4.00	4.00
180	-11.67	1.79	4.00	-11.49	4.03	3.00
190	-11.60	1.86	7.00	-11.46	4.06	3.00
200	-11.59	1.87	1.00	-11.41	4.11	5.00
210	-11.57	1.89	2.00	-11.38	4.14	3.00
220	-11.54	1.92	3.00	-11.31	4.21	7.00
230	-11.50	1.96	4.00	-11.28	4.24	3.00
240	-11.48	1.98	2.00	-11.25	4.27	3.00
250	-11.46	2.00	2.00	-11.18	4.34	7.00
260	-11.44	2.02	2.00	-11.15	4.37	3.00
270	-11.42	2.04	2.00	-11.10	4.42	5.00
280	-11.40	2.06	2.00	-11.06	4.46	4.00
290	-11.37	2.09	3.00	-11.04	4.48	2.00
300	-11.35	2.11	2.00	-11.02	4.50	2.00
310	-11.32	2.14	3.00	-10.97	4.55	5.00
320	-11.31	2.15	1.00	-10.95	4.57	2.00
330	-11.29	2.17	2.00	-10.93	4.59	2.00
340	-11.27	2.19	2.00	-10.89	4.63	4.00
350	-11.24	2.22	3.00	-10.85	4.67	4.00
360	-11.23	2.23	1.00	-10.81	4.71	4.00
370	-11.22	2.24	1.00	-10.77	4.75	4.00
380	-11.20	2.26	2.00	-10.75	4.77	2.00
390	-11.17	2.29	3.00	-10.74	4.78	1.00
400	-11.15	2.31	2.00	-10.70	4.82	4.00
450	-11.05	2.41	2.00	-10.64	4.88	1.20
500	-10.96	2.50	1.80	-10.55	4.97	1.80
550	-10.93	2.53	0.60	-10.45	5.07	2.00
600	-10.90	2.56	0.60	-10.38	5.14	1.40
650	-10.86	2.60	0.80	-10.34	5.18	0.80
700	-10.80	2.66	1.20	-10.30	5.22	0.80
750	-10.75	2.71	1.00	-10.22	5.30	1.60
800	-10.73	2.73	0.40	-10.18	5.34	0.80
850	-10.70	2.76	0.60	-10.13	5.39	1.00



Reference	PS2			PS2		
Type of Soil	Portaway Sand			Portaway Sand		
Contact Pressure, kPa	111			119		
Number of Passes	LVDT Reading	Deformation, mm	Deformation Rate, mm/10 <sup>3</sup> pass	LVDT Reading	Deformation, mm	Deformation Rate, mm/10 <sup>3</sup> pass
900	-10.60	2.86	2.00	-10.08	5.44	1.00
950	-10.52	2.94	1.60	-10.02	5.50	1.20
1000	-10.40	3.06	2.40	-10.00	5.52	0.40
1500	-10.18	3.28	0.44	-9.71	5.81	0.58
2000	-10.02	3.44	0.32	-9.64	5.88	0.14
2500	-9.87	3.59	0.30	-9.60	5.92	0.08
3000	-9.71	3.75	0.32	-9.55	5.97	0.10
3500	-9.56	3.90	0.30	-9.50	6.02	0.10
4000	-9.40	4.06	0.32	-9.40	6.12	0.20
4500	-9.37	4.09	0.06	-9.35	6.17	0.10
5000	-9.34	4.12	0.06	-9.20	6.32	0.30
6000	-9.30	4.16	0.04	-9.10	6.42	0.10
7000	-9.25	4.21	0.05	-8.97	6.55	0.13
8000	-9.11	4.35	0.14	-8.83	6.69	0.14
9000	-9.09	4.37	0.02	-8.69	6.83	0.14
10000	-9.08	4.38	0.01	-8.56	6.96	0.13
11000	-9.04	4.42	0.04	-8.43	7.09	0.13
12000	-9.01	4.45	0.03	-8.33	7.19	0.10
13000	-8.94	4.52	0.07	-8.25	7.27	0.08
14000	-8.88	4.58	0.06	-8.16	7.36	0.09
15000	-8.82	4.64	0.06	-8.07	7.45	0.09
16000	-8.77	4.69	0.05	-7.98	7.54	0.09
50000	-8.20	5.26	0.02			

Reference	PS2			PS2		
Type of Soil	Portaway Sand			Portaway Sand		
Contact Pressure, kPa	127			154		
Number of Passes	LVDT Reading	Deformation, mm	Deformation Rate, mm/10 <sup>3</sup> passes	LVDT Reading	Deformation, mm	Deformation Rate, mm/10 <sup>3</sup> passes
0	-17.46	0.00		-14.91	0.00	
10	-15.51	1.95	195.00	-8.30	6.61	661.00
20	-13.62	3.84	189.00	-6.07	8.84	223.00
30	-13.15	4.31	47.00	-5.97	8.94	10.00
40	-12.76	4.70	39.00	-5.87	9.04	10.00
50	-12.71	4.75	5.00	-4.72	10.19	115.00
60	-12.50	4.96	21.00	-3.56	11.35	116.00
70	-12.23	5.23	27.00	-2.93	11.98	63.00
80	-12.23	5.23	0.00	-2.30	12.61	63.00
90	-12.00	5.46	23.00	-1.50	13.41	80.00
100	-11.92	5.54	8.00	-0.96	13.95	54.00
110	-11.70	5.76	22.00	-0.66	14.25	30.00
120	-11.51	5.95	19.00	-0.10	14.81	56.00
130	-11.39	6.07	12.00	0.09	15.00	19.00
140	-11.28	6.18	11.00	0.51	15.42	42.00
150	-11.19	6.27	9.00	0.89	15.80	38.00
160	-11.12	6.34	7.00	1.17	16.08	28.00
170	-10.95	6.51	17.00	1.52	16.43	35.00

Reference	PS2			PS2		
Type of Soil	Portaway Sand			Portaway Sand		
Contact Pressure, kPa	127			154		
Number of Passes	LVDT Reading	Deformation, mm	Deformation Rate, mm/10 <sup>3</sup> pass	LVDT Reading	Deformation, mm	Deformation Rate, mm/10 <sup>3</sup> pass
180	-10.82	6.64	13.00	1.65	16.56	13.00
190	-10.75	6.71	7.00	1.96	16.87	31.00
200	-10.70	6.76	5.00	2.35	17.26	39.00
210	-10.65	6.81	5.00	2.42	17.33	7.00
220	-10.62	6.84	3.00	2.74	17.65	32.00
230	-10.55	6.91	7.00	3.01	17.92	27.00
240	-10.47	6.99	8.00	3.13	18.04	12.00
250	-10.44	7.02	3.00	3.38	18.29	25.00
260	-10.36	7.10	8.00	3.49	18.40	11.00
270	-10.32	7.14	4.00	3.70	18.61	21.00
280	-10.27	7.19	5.00	3.78	18.69	8.00
290	-10.21	7.25	6.00	3.96	18.87	18.00
300	-10.17	7.29	4.00	-15.70	19.10	-1966.00
310	-10.14	7.32	3.00	-15.60	19.20	10.00
320	-10.10	7.36	4.00	-15.54	19.26	6.00
330	-10.08	7.38	2.00	-15.28	19.52	26.00
340	-10.00	7.46	8.00	-15.16	19.64	12.00
350	-9.97	7.49	3.00	-15.00	19.80	16.00
360	-9.91	7.55	6.00	-14.97	19.83	3.00
370	-9.87	7.59	4.00	-14.74	20.06	23.00
380	-9.83	7.63	4.00	-14.70	20.10	4.00
390	-9.81	7.65	2.00	-14.65	20.15	5.00
400	-9.70	7.76	11.00	-14.49	20.31	16.00
450	-9.58	7.88	2.40	-14.34	20.46	3.00
500	-9.48	7.98	2.00	-14.01	20.79	6.60
550	-9.32	8.14	3.20	-13.68	21.12	6.60
600	-9.24	8.22	1.60	-13.49	21.31	3.80
650	-9.12	8.34	2.40	-13.26	21.54	4.60
700	-9.05	8.41	1.40	-13.13	21.67	2.60
750	-9.00	8.46	1.00	-12.83	21.97	6.00
800	-8.87	8.59	2.60	-12.73	22.07	2.00
850	-8.81	8.65	1.20	-12.37	22.43	7.20
900	-8.77	8.69	0.80	-12.17	22.63	4.00
950	-8.65	8.81	2.40	-11.91	22.89	5.20
1000	-8.18	9.28	9.40	-11.85	22.95	1.20
1500	-7.81	9.65	0.74	-10.53	24.27	2.64
2000	-7.65	9.81	0.32	-9.68	25.12	1.70
2500	-7.55	9.91	0.20	-9.13	25.67	1.10
3000	-7.45	10.01	0.20	-8.62	26.18	1.02
3500	-7.25	10.21	0.40	-8.04	26.76	1.16
4000	-7.03	10.43	0.44	-7.49	27.31	1.10
4500	-6.91	10.55	0.24	-7.02	27.78	0.94
5000	-6.51	10.95	0.80	-6.18	28.62	1.68
6000	-6.25	11.21	0.26	-5.61	29.19	0.57
7000	-5.98	11.48	0.27	-4.90	29.90	0.71
8000	-5.54	11.92	0.44	-4.16	30.64	0.74
9000	-4.97	12.49	0.57	-3.51	31.29	0.65
10000	-4.92	12.54	0.05	-3.02	31.78	0.49
11000	-4.75	12.71	0.17	-2.41	32.39	0.61
12000	-4.55	12.91	0.20	-1.92	32.88	0.49
13000	-4.37	13.09	0.18	-1.35	33.45	0.57

Reference	PS2			PS2		
Type of Soil	Portaway Sand			Portaway Sand		
Contact Pressure, kPa	127			154		
Number of Passes	LVDT Reading	Deformation, mm	Deformation Rate, mm/10 <sup>3</sup> pass	LVDT Reading	Deformation, mm	Deformation Rate, mm/10 <sup>3</sup> pass
14000	-4.20	13.26	0.17	-0.83	33.97	0.52
15000	-4.02	13.44	0.18	-0.31	34.49	0.52
16000	-2.25	15.21	1.77	0.21	35.01	0.52

Reference	Silt			Silt		
Type of Soil	Silt			Silt		
Contact Pressure, kPa	193			229		
Number of Passes	LVDT Reading	Deformation, mm	Deformation Rate, mm/10 <sup>3</sup> pass	LVDT Reading	Deformation, mm	Deformation Rate, mm/10 <sup>3</sup> pass
0	-17.91	0		-16.24	0.00	
10	-16.85	1.06	106.00	-15.12	1.12	112.00
20	-16.35	1.56	50.00	-14.45	1.79	67.00
30	-16.03	1.88	32.00	-13.98	2.26	47.00
40	-15.73	2.18	30.00	-13.71	2.53	27.00
50	-15.54	2.37	19.00	-13.50	2.74	21.00
60	-15.41	2.50	13.00	-13.26	2.98	24.00
70	-15.29	2.62	12.00	-13.08	3.16	18.00
80	-15.14	2.77	15.00	-12.95	3.29	13.00
90	-15.03	2.88	11.00	-12.75	3.49	20.00
100	-14.89	3.02	14.00	-12.62	3.62	13.00
110	-14.84	3.07	5.00	-12.51	3.73	11.00
120	-14.77	3.14	7.00	-12.39	3.85	12.00
130	-14.66	3.25	11.00	-12.33	3.91	6.00
140	-14.57	3.34	9.00	-12.21	4.03	12.00
150	-14.50	3.41	7.00	-12.13	4.11	8.00
160	-14.48	3.43	2.00	-12.04	4.20	9.00
170	-14.39	3.52	9.00	-11.97	4.27	7.00
180	-14.35	3.56	4.00	-11.89	4.35	8.00
190	-14.30	3.61	5.00	-11.86	4.38	3.00
200	-14.28	3.63	2.00	-11.77	4.47	9.00
210	-14.25	3.66	3.00	-11.69	4.55	8.00
220	-14.19	3.72	6.00	-11.65	4.59	4.00
230	-14.14	3.77	5.00	-11.63	4.61	2.00
240	-14.12	3.79	2.00	-11.53	4.71	10.00
250	-14.08	3.83	4.00	-11.50	4.74	3.00
260	-14.04	3.87	4.00	-11.45	4.79	5.00
270	-14.02	3.89	2.00	-11.40	4.84	5.00
280	-13.98	3.93	4.00	-11.35	4.89	5.00
290	-13.92	3.99	6.00	-11.30	4.94	5.00
300	-13.90	4.01	2.00	-11.29	4.95	1.00
310	-13.89	4.02	1.00	-11.28	4.96	1.00
320	-13.86	4.05	3.00	-11.25	4.99	3.00
330	-13.84	4.07	2.00	-11.20	5.04	5.00
340	-13.83	4.08	1.00	-11.18	5.06	2.00
350	-13.76	4.15	7.00	-11.12	5.12	6.00
360	-13.73	4.18	3.00	-11.09	5.15	3.00

Reference	Silt			Silt		
Type of Soil	Silt			Silt		
Contact Pressure, kPa	193			229		
Number of Passes	LVDT Reading	Deformation, mm	Deformation Rate, mm/10 <sup>3</sup> pass	LVDT Reading	Deformation, mm	Deformation Rate, mm/10 <sup>3</sup> pass
370	-13.71	4.20	2.00	-11.07	5.17	2.00
380	-13.70	4.21	1.00	-11.05	5.19	2.00
390	-13.69	4.22	1.00	-11.02	5.22	3.00
400	-13.66	4.25	3.00	-11.00	5.24	2.00
450	-13.59	4.32	1.40	-10.93	5.31	1.40
500	-13.53	4.38	1.20	-10.87	5.37	1.20
550	-13.46	4.45	1.40	-10.77	5.47	2.00
600	-13.40	4.51	1.20	-10.71	5.53	1.20
650	-13.39	4.52	0.20	-10.70	5.54	0.20
700	-13.31	4.60	1.60	-10.63	5.61	1.40
750	-13.26	4.65	1.00	-10.61	5.63	0.40
800	-13.22	4.69	0.80	-10.59	5.65	0.40
850	-13.19	4.72	0.60	-10.54	5.70	1.00
900	-13.16	4.75	0.60	-10.53	5.71	0.20
950	-13.14	4.77	0.40	-10.52	5.72	0.20
1000	-13.09	4.82	1.00	-10.50	5.74	0.40
1500	-12.92	4.99	0.34	-10.38	5.86	0.24
2000	-12.75	5.16	0.34	-10.27	5.97	0.22
2500	-12.65	5.26	0.20	-10.16	6.08	0.22
3000	-12.56	5.35	0.18	-10.06	6.18	0.20
3500	-12.49	5.42	0.14	-10.03	6.21	0.06
4000	-12.45	5.46	0.08	-9.99	6.25	0.08
4500	-12.38	5.53	0.14	-9.96	6.28	0.06
5000	-12.34	5.57	0.08	-9.89	6.35	0.14
6000	-12.28	5.63	0.06	-9.86	6.38	0.03
7000	-12.22	5.69	0.06	-9.82	6.42	0.04
8000	-12.16	5.75	0.06	-9.78	6.46	0.04
9000	-12.11	5.80	0.05	-9.75	6.49	0.03
10000	-12.05	5.86	0.06	-9.70	6.54	0.05
11000	-12.04	5.87	0.01	-9.67	6.57	0.03
12000	-12.00	5.91	0.04	-9.65	6.59	0.02
13000	-11.97	5.94	0.03	-9.63	6.61	0.02
14000	-11.95	5.96	0.02	-9.62	6.62	0.01
15000	-11.93	5.98	0.02	-9.59	6.65	0.03
16000	-11.90	6.01	0.03	-9.56	6.68	0.03
50000	-11.51	6.40	0.01	-9.13	7.11	0.01

Reference	Silt			Silt		
Type of Soil	Silt			Silt		
Contact Pressure, kPa	244			251		
Number of Passes	LVDT Reading	Deformation, mm	Deformation Rate, mm/10 <sup>3</sup> pass	LVDT Reading	Deformation, mm	Deformation Rate, mm/10 <sup>3</sup> pass
0	-17.08	0.00		-17.68	0.00	
10	-15.12	1.96	196.00	-14.81	2.87	287.00
20	-13.87	3.21	125.00	-13.59	4.09	122.00
30	-13.30	3.78	57.00	-12.72	4.96	87.00
40	-12.74	4.34	56.00	-12.08	5.60	64.00
50	-12.56	4.52	18.00	-11.61	6.07	47.00
60	-12.15	4.93	41.00	-11.19	6.49	42.00
70	-12.02	5.06	13.00	-10.91	6.77	28.00
80	-11.81	5.27	21.00	-10.55	7.13	36.00
90	-11.63	5.45	18.00	-10.37	7.31	18.00
100	-11.47	5.61	16.00	-10.12	7.56	25.00
110	-11.30	5.78	17.00	-9.99	7.69	13.00
120	-11.15	5.93	15.00	-9.84	7.84	15.00
130	-11.06	6.02	9.00	-9.75	7.93	9.00
140	-11.00	6.08	6.00	-9.56	8.12	19.00
150	-10.94	6.14	6.00	-9.44	8.24	12.00
160	-10.88	6.20	6.00	-9.33	8.35	11.00
170	-10.80	6.28	8.00	-9.22	8.46	11.00
180	-10.70	6.38	10.00	-9.10	8.58	12.00
190	-10.58	6.50	12.00	-9.02	8.66	8.00
200	-10.55	6.53	3.00	-8.96	8.72	6.00
210	-10.46	6.62	9.00	-8.87	8.81	9.00
220	-10.46	6.62	0.00	-8.77	8.91	10.00
230	-10.42	6.66	4.00	-8.72	8.96	5.00
240	-10.32	6.76	10.00	-8.67	9.01	5.00
250	-10.28	6.80	4.00	-8.58	9.10	9.00
260	-10.24	6.84	4.00	-8.55	9.13	3.00
270	-10.25	6.83	-1.00	-8.47	9.21	8.00
280	-10.24	6.84	1.00	-8.39	9.29	8.00
290	-10.11	6.97	13.00	-8.38	9.30	1.00
300	-10.09	6.99	2.00	-8.35	9.33	3.00
310	-10.06	7.02	3.00	-8.30	9.38	5.00
320	-10.02	7.06	4.00	-8.23	9.45	7.00
330	-10.00	7.08	2.00	-8.20	9.48	3.00
340	-10.03	7.05	-3.00	-8.17	9.51	3.00
350	-9.93	7.15	10.00	-8.11	9.57	6.00
360	-9.92	7.16	1.00	-8.07	9.61	4.00
370	-9.86	7.22	6.00	-8.06	9.62	1.00
380	-9.82	7.26	4.00	-8.04	9.64	2.00
390	-9.84	7.24	-2.00	-7.99	9.69	5.00
400	-9.83	7.25	1.00	-7.97	9.71	2.00
450	-9.77	7.31	1.20	-7.87	9.81	2.00
500	-9.71	7.37	1.20	-7.79	9.89	1.60
550	-9.60	7.48	2.20	-7.69	9.99	2.00
600	-9.52	7.56	1.60	-7.61	10.07	1.60
650	-9.48	7.60	0.80	-7.53	10.15	1.60
700	-9.46	7.62	0.40	-7.49	10.19	0.80
750	-9.43	7.65	0.60	-7.43	10.25	1.20
800	-9.40	7.68	0.60	-7.40	10.28	0.60
850	-9.38	7.70	0.40	-7.35	10.33	1.00

Reference	Silt			Silt		
Type of Soil	Silt			Silt		
Contact Pressure, kPa	244			251		
Number of Passes	LVDT Reading	Deformation, mm	Deformation Rate, mm/10 <sup>3</sup> pass	LVDT Reading	Deformation, mm	Deformation Rate, mm/10 <sup>3</sup> pass
900	-9.35	7.73	0.60	-7.30	10.38	1.00
950	-9.30	7.78	1.00	-7.25	10.43	1.00
1000	-9.24	7.84	1.20	-7.20	10.48	1.00
1500	-9.00	8.08	0.48	-6.96	10.72	0.48
2000	-8.86	8.22	0.28	-6.82	10.86	0.28
2500	-8.77	8.31	0.18	-6.68	11.00	0.28
3000	-8.74	8.34	0.06	-6.54	11.14	0.28
3500	-8.67	8.41	0.14	-6.49	11.19	0.10
4000	-8.60	8.48	0.14	-6.43	11.25	0.12
4500	-8.54	8.54	0.12	-6.36	11.32	0.14
5000	-8.52	8.56	0.04	-6.32	11.36	0.08
6000	-8.47	8.61	0.05	-6.25	11.43	0.07
7000	-8.42	8.66	0.05	-6.21	11.47	0.04
8000	-8.39	8.69	0.03	-6.17	11.51	0.04
9000	-8.36	8.72	0.03	-6.13	11.55	0.04
10000	-8.29	8.79	0.07	-6.08	11.60	0.05
11000	-8.27	8.81	0.02	-6.04	11.64	0.04
12000	-8.26	8.82	0.01	-6.00	11.68	0.04
13000	-8.24	8.84	0.02	-5.97	11.71	0.03
14000	-8.20	8.88	0.04	-5.94	11.74	0.03
15000	-8.16	8.92	0.04	-5.91	11.77	0.03
16000	-8.13	8.95	0.03	-5.88	11.80	0.03
50000	-7.63	9.45	0.01	-5.36	12.32	0.02

Reference	Silt			Silt		
Type of Soil	Silt			Silt		
Contact Pressure, kPa	257			261		
Number of Passes	LVDT Reading	Deformation, mm	Deformation Rate, mm/10 <sup>3</sup> pass	LVDT Reading	Deformation, mm	Deformation Rate, mm/10 <sup>3</sup> pass
0	-16.65	0.00		-13.36	0.00	
10	-13.00	3.65	365.00	-4.54	8.82	882.00
20	-10.98	5.67	202.00	-1.88	11.48	266.00
30	-10.14	6.51	84.00	-0.67	12.69	121.00
40	-9.22	7.43	92.00	0.33	13.69	100.00
50	-8.58	8.07	64.00	1.06	14.42	73.00
60	-8.00	8.65	58.00	1.57	14.93	51.00
70	-7.54	9.11	46.00	1.98	15.34	41.00
80	-7.15	9.50	39.00	2.55	15.91	57.00
90	-6.82	9.83	33.00	2.93	16.29	38.00
100	-6.55	10.10	27.00	3.45	16.81	52.00
110	-6.26	10.39	29.00	3.86	17.22	41.00
120	-6.07	10.58	19.00	4.04	17.40	18.00
130	-5.90	10.75	17.00	4.36	17.72	32.00
140	-5.59	11.06	31.00	4.63	17.99	27.00
150	-5.40	11.25	19.00	4.99	18.35	36.00

Reference	Silt			Silt		
Type of Soil	Silt			Silt		
Contact Pressure, kPa	257			261		
Number of Passes	LVDT Reading	Deformation, mm	Deformation Rate, mm/10 <sup>3</sup> pass	LVDT Reading	Deformation, mm	Deformation Rate, mm/10 <sup>3</sup> pass
160	-5.21	11.44	19.00	5.17	18.53	18.00
170	-5.01	11.64	20.00	5.50	18.86	33.00
180	-4.81	11.84	20.00	5.66	19.02	16.00
190	-4.74	11.91	7.00	5.86	19.22	20.00
200	-4.51	12.14	23.00	6.21	19.57	35.00
210	-4.30	12.35	21.00	6.25	19.61	4.00
220	-4.12	12.53	18.00	6.44	19.80	19.00
230	-4.05	12.60	7.00	6.67	20.03	23.00
240	-3.86	12.79	19.00	6.92	20.28	25.00
250	-3.76	12.89	10.00	7.12	20.48	20.00
260	-3.75	12.90	1.00	7.31	20.67	19.00
270	-3.52	13.13	23.00	7.43	20.79	12.00
280	-3.46	13.19	6.00	7.69	21.05	26.00
290	-3.34	13.31	12.00	7.84	21.20	15.00
300	-3.25	13.40	9.00	7.88	21.24	4.00
310	-3.12	13.53	13.00	8.09	21.45	21.00
320	-2.96	13.69	16.00	8.24	21.60	15.00
330	-2.90	13.75	6.00	8.32	21.68	8.00
340	-2.86	13.79	4.00	8.55	21.91	23.00
350	-2.74	13.91	12.00	8.60	21.96	5.00
360	-2.67	13.98	7.00	8.74	22.10	14.00
370	-2.61	14.04	6.00	8.88	22.24	14.00
380	-2.50	14.15	11.00	8.97	22.33	9.00
390	-2.44	14.21	6.00	9.18	22.54	21.00
400	-2.34	14.31	10.00	9.23	22.59	5.00
450	-2.10	14.55	4.80	9.35	22.71	2.40
500	-1.93	14.72	3.40	9.80	23.16	9.00
550	-1.71	14.94	4.40	10.20	23.56	8.00
600	-1.54	15.11	3.40	10.42	23.78	4.40
650	-1.41	15.24	2.60	10.67	24.03	5.00
700	-1.23	15.42	3.60	10.92	24.28	5.00
750	-1.11	15.54	2.40	11.16	24.52	4.80
800	-1.04	15.61	1.40	11.37	24.73	4.20
850	-0.96	15.69	1.60	11.65	25.01	5.60
900	-0.87	15.78	1.80	11.72	25.08	1.40
950	-0.60	15.88	2.00	11.80	25.16	1.60
1000	-0.33	16.15	5.40	11.94	25.30	2.80
1500	-0.24	16.41	0.52	13.08	26.44	2.28
2000	0.04	16.69	0.56			
2500	0.16	16.81	0.24			
3000	0.26	16.91	0.20			
3500	0.31	16.96	0.10			
4000	0.42	17.07	0.22			
4500	0.45	17.10	0.06			
5000	0.49	17.14	0.08			
6000	0.56	17.21	0.07			
7000	0.62	17.27	0.06			
8000	0.67	17.32	0.05			
9000	0.71	17.36	0.04			
10000	0.76	17.41	0.05			
11000	0.80	17.45	0.04			

<b>Reference</b>	<b>Silt</b>		
<b>Type of Soil</b>	<b>Silt</b>		
<b>Contact Pressure, kPa</b>	<b>257</b>		
<b>Number of Passes</b>	<b>LVDT Reading</b>	<b>Deformation, mm</b>	<b>Deformation Rate, mm/10<sup>3</sup>pass</b>
12000	0.83	17.48	0.03
13000	0.86	17.51	0.03
14000	0.89	17.54	0.03
15000	0.92	17.57	0.03
16000	0.95	17.60	0.03

<b>Reference</b>	<b>KM</b>			<b>KM</b>		
<b>Type of Soil</b>	<b>Keuper Marl</b>			<b>Keuper Marl</b>		
<b>Contact Pressure, kPa</b>	<b>225</b>			<b>237</b>		
<b>Number of Passes</b>	<b>LVDT Reading</b>	<b>Deformation, mm</b>	<b>Deformation Rate, mm/10<sup>3</sup>pass</b>	<b>LVDT Reading</b>	<b>Deformation, mm</b>	<b>Deformation Rate, mm/10<sup>3</sup>pass</b>
0	-15.76	0		-16.29	0.00	
10	-15.45	0.31	31.00	-15.87	0.42	42.00
20	-15.23	0.53	22.00	-15.59	0.70	28.00
30	-15.07	0.69	16.00	-15.38	0.91	21.00
40	-15.00	0.76	7.00	-15.31	0.98	7.00
50	-14.82	0.94	18.00	-15.28	1.01	3.00
60	-14.81	0.95	1.00	-15.19	1.10	9.00
70	-14.73	1.03	8.00	-15.08	1.21	11.00
80	-14.66	1.10	7.00	-14.99	1.30	9.00
90	-14.63	1.13	3.00	-14.96	1.33	3.00
100	-14.63	1.13	0.00	-14.95	1.34	1.00
110	-14.62	1.14	1.00	-14.94	1.35	1.00
120	-14.58	1.18	4.00	-14.92	1.37	2.00
130	-14.53	1.23	5.00	-14.84	1.45	8.00
140	-14.47	1.29	6.00	-14.83	1.46	1.00
150	-14.45	1.31	2.00	-14.81	1.48	2.00
160	-14.43	1.33	2.00	-14.81	1.48	0.00
170	-14.42	1.34	1.00	-14.79	1.50	2.00
180	-14.41	1.35	1.00	-14.78	1.51	1.00
190	-14.40	1.36	1.00	-14.77	1.52	1.00
200	-14.38	1.38	2.00	-14.73	1.56	4.00
210	-14.36	1.40	2.00	-14.70	1.59	3.00
220	-14.35	1.41	1.00	-14.67	1.62	3.00
230	-14.33	1.43	2.00	-14.59	1.70	8.00
240	-14.32	1.44	1.00	-14.58	1.71	1.00
250	-14.31	1.45	1.00	-14.58	1.71	0.00
260	-14.29	1.47	2.00	-14.57	1.72	1.00
270	-14.28	1.48	1.00	-14.56	1.73	1.00
280	-14.27	1.49	1.00	-14.56	1.73	0.00
290	-14.26	1.50	1.00	-14.55	1.74	1.00
300	-14.26	1.50	0.00	-14.54	1.75	1.00
310	-14.25	1.51	1.00	-14.53	1.76	1.00
320	-14.24	1.52	1.00	-14.52	1.77	1.00
330	-14.23	1.53	1.00	-14.51	1.78	1.00
340	-14.22	1.54	1.00	-14.50	1.79	1.00
350	-14.20	1.56	2.00	-14.50	1.79	0.00



Reference	KM			KM		
Type of Soil	Keuper Marl			Keuper Marl		
Contact Pressure, kPa	225			237		
Number of Passes	LVDT Reading	Deformation, mm	Deformation Rate, mm/10 <sup>3</sup> pass	LVDT Reading	Deformation, mm	Deformation Rate, mm/10 <sup>3</sup> pass
360	-14.19	1.57	1.00	-14.49	1.80	1.00
370	-14.18	1.58	1.00	-14.48	1.81	1.00
380	-14.18	1.58	0.00	-14.44	1.85	4.00
390	-14.17	1.59	1.00	-14.40	1.89	4.00
400	-14.17	1.59	0.00	-14.40	1.89	0.00
450	-14.15	1.61	0.40	-14.37	1.92	0.60
500	-14.13	1.63	0.40	-14.36	1.93	0.20
550	-14.12	1.64	0.20	-14.35	1.94	0.20
600	-14.11	1.65	0.20	-14.34	1.95	0.20
650	-14.11	1.65	0.00	-14.34	1.95	0.00
700	-14.10	1.66	0.20	-14.34	1.95	0.00
750	-14.09	1.67	0.20	-14.34	1.95	0.00
800	-14.09	1.67	0.00	-14.34	1.95	0.00
850	-14.09	1.67	0.00	-14.34	1.95	0.00
900	-14.09	1.67	0.00	-14.34	1.95	0.00
950	-14.08	1.68	0.20	-14.33	1.96	0.20
1000	-14.08	1.68	0.00	-14.33	1.96	0.00
1500	-14.01	1.75	0.14	-14.22	2.07	0.22
2000	-14.00	1.76	0.02	-14.20	2.09	0.04
2500	-13.99	1.77	0.02	-14.15	2.14	0.10
3000	-13.99	1.77	0.00	-14.13	2.16	0.04
3500	-13.98	1.78	0.02	-14.12	2.17	0.02
4000	-13.98	1.78	0.00	-14.12	2.17	0.00
4500	-13.97	1.79	0.02	-14.12	2.17	0.00
5000	-13.97	1.79	0.00	-14.12	2.17	0.00
6000	-13.96	1.80	0.01	-14.12	2.17	0.00
7000	-13.95	1.81	0.01	-14.12	2.17	0.00
8000	-13.93	1.83	0.02	-14.11	2.18	0.01
9000	-13.92	1.84	0.01	-14.11	2.18	0.00
10000	-13.91	1.85	0.01	-14.10	2.19	0.01
11000	-13.90	1.86	0.01	-14.09	2.20	0.01
12000	-13.89	1.87	0.01	-14.03	2.26	0.06
13000	-13.88	1.88	0.01	-14.02	2.27	0.01
14000	-13.87	1.89	0.01	-14.02	2.27	0.00
15000	-13.86	1.90	0.01	-14.01	2.28	0.01
16000	-13.85	1.91	0.01	-14.01	2.28	0.00
40000	-13.50	2.26	0.01	-14.00	2.29	0.00

Reference	KM			KM		
Type of Soil	Keuper Marl			Keuper Marl		
Contact Pressure, kPa	269			301		
Number of Passes	LVDT Reading	Deformation, mm	Deformation Rate, mm/10 <sup>3</sup> pass	LVDT Reading	Deformation, mm	Deformation Rate, mm/10 <sup>3</sup> pass
0	-14.22	0.00		-13.79	0.00	
10	-13.69	0.53	53.00	-10.63	3.16	316.00
20	-13.17	1.05	52.00	-8.83	4.96	180.00
30	-12.74	1.48	43.00	-7.70	6.09	113.00
40	-12.55	1.67	19.00	-6.08	7.71	162.00
50	-12.37	1.85	18.00	-5.31	8.48	77.00
60	-12.04	2.18	33.00	-4.70	9.09	61.00
70	-12.02	2.20	2.00	-4.25	9.54	45.00
80	-11.91	2.31	11.00	-3.73	10.06	52.00
90	-11.78	2.44	13.00	-3.20	10.59	53.00
100	-11.65	2.57	13.00	-2.53	11.26	67.00
110	-11.54	2.68	11.00	-1.97	11.82	56.00
120	-11.53	2.69	1.00	-1.60	12.19	37.00
130	-11.40	2.82	13.00	-0.90	12.89	70.00
140	-11.24	2.98	16.00	-0.58	13.21	32.00
150	-11.19	3.03	5.00	0.25	14.04	83.00
160	-11.10	3.12	9.00	0.51	14.30	26.00
170	-11.01	3.21	9.00	1.05	14.84	54.00
180	-11.00	3.22	1.00	1.90	15.69	85.00
190	-10.97	3.25	3.00	2.50	16.29	60.00
200	-10.80	3.42	17.00	2.77	16.56	27.00
210	-10.72	3.50	8.00	-16.47	17.03	47.00
220	-10.70	3.52	2.00	-15.61	17.89	86.00
230	-10.63	3.59	7.00	-15.37	18.13	24.00
240	-10.58	3.64	5.00	-14.20	19.30	117.00
250	-10.43	3.79	15.00	-13.83	19.67	37.00
260	-10.38	3.84	5.00	-13.06	20.44	77.00
270	-10.35	3.87	3.00	-12.55	20.95	51.00
280	-10.34	3.88	1.00	-12.19	21.31	36.00
290	-10.32	3.90	2.00	-11.42	22.08	77.00
300	-10.30	3.92	2.00	-10.75	22.75	67.00
310	-10.27	3.95	3.00	-10.17	23.33	58.00
320	-10.19	4.03	8.00	-9.48	24.02	69.00
330	-10.10	4.12	9.00	-8.96	24.54	52.00
340	-10.05	4.17	5.00	-8.30	25.20	66.00
350	-10.02	4.20	3.00	-7.77	25.73	53.00
360	-10.00	4.22	2.00	-7.29	26.21	48.00
370	-9.99	4.23	1.00	-6.76	26.74	53.00
380	-9.93	4.29	6.00	-6.01	27.49	75.00
390	-9.89	4.33	4.00	-5.46	28.04	55.00
400	-9.85	4.37	4.00	-4.75	28.75	71.00
450	-9.85	4.37	0.04	-2.18	31.32	51.40
500	-9.85	4.37	-0.03	-0.35	33.15	36.60
550	-9.85	4.37	0.00	0.00	33.50	7.00
600	-9.85	4.37	0.00	2.38	35.88	47.60
650	-9.85	4.37	-0.01	3.55	37.05	23.40
700	-9.85	4.37	0.00			
750	-9.85	4.37	0.00			
800	-9.85	4.37	0.00			

<b>Reference</b>	<b>KM</b>		
<b>Type of Soil</b>	<b>Keuper Marl</b>		
<b>Contact Pressure, kPa</b>	<b>269</b>		
<b>Number of Passes</b>	<b>LVDT Reading</b>	<b>Deformation, mm</b>	<b>Deformation Rate, mm/10<sup>3</sup>pass</b>
900	-8.50	5.72	1.00
950	-8.45	5.77	1.00
1000	-8.38	5.84	1.40
1500	-7.41	6.81	1.94
2000	-6.82	7.40	1.18
2500	-6.82	7.40	0.00
3000	-6.82	7.40	0.00
3500	-6.82	7.40	0.00
4000	-6.82	7.40	0.00
4500	-6.82	7.40	0.00
5000	-6.82	7.40	0.00
6000	-5.84	8.38	0.98
7000	-5.82	8.40	0.02
8000	-5.80	8.42	0.02
9000	-5.75	8.47	0.05
10000	-5.74	8.48	0.01
11000	-5.73	8.49	0.01
12000	-5.65	8.57	0.08
13000	-5.59	8.63	0.06
14000	-5.50	8.72	0.09
15000	-5.45	8.77	0.05
16000	-5.40	8.82	0.05

Reference	Gr			Gr		
Type of Soil	Granite			Granite		
Contact Pressure, kPa	289			355		
Number of Passes	LVDT Reading	Deformation, mm	Deformation Rate, mm/10 <sup>3</sup> pass	LVDT Reading	Deformation, mm	Deformation Rate, mm/10 <sup>3</sup> pass
0	104.0	0.0		105.5	0.00	
100	111.5	7.50	75.00	113.5	8.00	80.00
200	112.5	8.50	10.00	115.0	9.50	15.00
300	113.0	9.00	5.00	116.0	10.50	10.00
400	114.0	10.00	10.00	116.5	11.00	5.00
500	115.0	11.00	10.00	117.0	11.50	5.00
600	115.5	11.50	5.00	117.0	11.50	0.00
700	116.0	12.00	5.00	118.0	12.50	10.00
800	116.5	12.50	5.00	118.5	13.00	5.00
900	116.8	12.75	2.50	119.0	13.50	5.00
1000	117.0	13.00	2.50	119.5	14.00	5.00
1500	117.0	13.00	0.00	120.0	14.50	1.00
2000	117.0	13.00	0.00	121.0	15.50	2.00
2500	117.0	13.00	0.00	121.5	16.00	1.00
3000	117.0	13.00	0.00	122.0	16.50	1.00
3500	117.0	13.00	0.00	122.5	17.00	1.00
4000	117.0	13.00	0.00	123.0	17.50	1.00
4500	117.0	13.00	0.00	123.5	18.00	1.00
5000	117.0	13.00	0.00	123.5	18.00	0.00
6000	117.0	13.00	0.00	124.0	18.50	0.50
7000	117.0	13.00	0.00	124.0	18.50	0.00
8000	117.0	13.00	0.00	124.3	18.75	0.25
9000	117.0	13.00	0.00	124.8	19.25	0.50
10000	117.0	13.00	0.00	125.0	19.50	0.25
15000	117.0	13.00	0.00	126.0	20.50	0.20
50000	117.0	13.00	0.00	126.0	20.50	0.00

Reference	Gr			Gr		
Type of Soil	Granite			Granite		
Contact Pressure, kPa	372			384		
Number of Passes	LVDT Reading	Deformation, mm	Deformation Rate, mm/10 <sup>3</sup> pass	LVDT Reading	Deformation, mm	Deformation Rate, mm/10 <sup>3</sup> pass
0	73.0	0.00		94.0	0.00	
100	81.5	8.50	85.00	104.0	3.16	31.60
200	84.5	11.50	30.00	104.5	4.96	18.00
300	85.5	12.50	10.00	108.0	6.09	11.30
400	86.0	13.00	5.00	108.0	7.71	16.20
500	87.0	14.00	10.00	110.0	8.48	7.70
600	87.5	14.50	5.00	111.0	9.09	6.10
700	88.0	15.00	5.00	112.5	9.54	4.50
800	88.5	15.50	5.00	112.5	10.06	5.20
900	89.5	16.50	10.00	112.5	10.59	5.30
1000	89.5	16.50	0.00	113.0	11.26	6.70
1500	90.8	17.75	2.50	114.3	11.82	1.12
2000	92.0	19.00	2.50	115.5	12.19	0.74
2500	92.0	19.00	0.00	116.0	12.89	1.40
3000	92.5	19.50	1.00	116.5	13.21	0.64
3500	93.0	20.00	1.00	117.0	14.04	1.66
4000	93.3	20.25	0.50	117.0	14.30	0.52
4500	93.5	20.50	0.50	117.0	14.84	1.08
5000	93.8	20.75	0.50	118.0	15.69	1.70
6000	94.3	21.25	0.50	119.0	16.29	0.60
7000	94.8	21.75	0.50	119.5	16.56	0.27
8000	95.5	22.50	0.75	120.0	17.03	0.47
9000	96.0	23.00	0.50	120.0	17.89	0.86
10000	96.0	23.00	0.00	121.0	18.13	0.24

Reference	Gr-PS			Gr-PS		
Contact Pressure, kPa	152			226		
Number of Passes	LVDT Reading	Deformation, mm	Deformation Rate, mm/10 <sup>3</sup> pass	LVDT Reading	Deformation, mm	Deformation Rate, mm/10 <sup>3</sup> pass
0	0.00	0.0		0.00	0.00	
100	4.17	4.17	41.67	9.00	9.00	90.00
200	5.67	5.67	15.00	10.33	10.33	13.33
300	5.67	5.67	0.00	10.83	10.83	5.00
400	6.00	6.00	3.33	11.33	11.33	5.00
500	6.17	6.17	1.67	11.67	11.67	3.33
600	6.50	6.50	3.33	12.75	12.75	10.83
700	6.50	6.50	0.00	13.08	13.08	3.33
800	6.67	6.67	1.67	13.50	13.50	4.17
900	6.92	6.92	2.50	14.17	14.17	6.67
1000	6.92	6.92	0.00	14.50	14.50	3.33
1500	7.17	7.17	0.50	14.50	14.50	0.00
2000	7.17	7.17	0.00	15.00	15.00	1.00
2500	7.17	7.17	0.00	15.33	15.33	0.67
3000	7.17	7.17	0.00	15.67	15.67	0.67
3500	7.17	7.17	0.00	15.75	15.75	0.17
4000	7.33	7.33	0.33	15.83	15.83	0.17
4500	7.33	7.33	0.00	16.00	16.00	0.33
5000	7.33	7.33	0.00	16.17	16.17	0.33
6000	7.33	7.33	0.00	16.17	16.17	0.00
7000	7.33	7.33	0.00	16.17	16.17	0.00
8000	7.33	7.33	0.00	16.50	16.50	0.33
9000	7.33	7.33	0.00	16.50	16.50	0.00
10000	7.33	7.33	0.00	16.67	16.67	0.17
15000	7.33	7.33	0.00	16.67	16.67	0.00
20000	7.33	7.33	0.00	16.67	16.67	0.00
25000	7.33	7.33	0.00	16.83	16.83	0.03
30000	7.33	7.33	0.00	17.67	17.67	0.17
35000	7.33	7.33	0.00	17.67	17.67	0.00
40000	7.33	7.33	0.00	17.67	17.67	0.00

Reference	Gr-PS		
Contact Pressure, kPa	269		
Number of Passes	LVDT Reading	Deformation, mm	Deformation Rate, mm/10 <sup>3</sup> pass
0	0.00	0.00	
100	18.00	18.00	180.00
200	21.42	21.42	34.17
300	23.17	23.17	17.50
400	23.75	23.75	5.83
500	25.67	25.67	19.17
600	26.67	26.67	10.00

Reference	Gr-Silt			Gr-Silt		
Contact Pressure, kPa	145			233		
Number of Passes	LVDT Reading	Deformation, mm	Deformation Rate, mm/10 <sup>3</sup> pass	LVDT Reading	Deformation, mm	Deformation Rate, mm/10 <sup>3</sup> pass
0	110.5	0.0		116.0	0	
100	118.8	8.25	82.50	122.0	11.50	60.00
200	120.5	10.00	17.50	125.0	14.50	30.00
300	120.5	10.00	0.00	128.0	17.50	30.00
400	121.0	10.50	5.00	130.0	19.50	20.00
500	121.0	10.50	0.00	132.0	21.50	20.00
600	121.0	10.50	0.00	132.0	21.50	0.00
700	121.0	10.50	0.00	133.0	22.50	10.00
800	121.0	10.50	0.00	133.5	23.00	5.00
900	121.0	10.50	0.00	134.5	24.00	10.00
1000	121.0	10.50	0.00	134.5	24.00	0.00
1500	121.0	10.50	0.00	135.5	25.00	1.00
2000	121.0	10.50	0.00	136.0	25.50	1.00
2500	121.0	10.50	0.00	136.0	25.50	0.00
3000	121.0	10.50	0.00	136.5	26.00	1.00
3500	121.0	10.50	0.00	136.5	26.00	0.00
4000	121.0	10.50	0.00	136.5	26.00	0.00
4500	121.0	10.50	0.00	136.5	26.00	0.00
5000	121.0	10.50	0.00	137.0	26.50	1.00
6000	121.0	10.50	0.00	137.0	26.50	0.00
7000	121.0	10.50	0.00	137.0	26.50	0.00
8000	121.0	10.50	0.00	137.0	26.50	0.00
9000	121.0	10.50	0.00	137.0	26.50	0.00
10000	121.0	10.50	0.00	137.0	26.50	0.00

Reference	Gr-Silt			Gr-Silt		
Contact Pressure, kPa	292			390		
Number of Passes	LVDT Reading	Deformation, mm	Deformation Rate, mm/10 <sup>3</sup> pass	LVDT Reading	Deformation, mm	Deformation Rate, mm/10 <sup>3</sup> pass
0	110.5	0.00		110.5	0.00	
100	128.5	18.00	180.00	134.0	23.50	235.00
200	132.5	22.00	40.00	138.0	27.50	40.00
300	134.0	23.50	15.00	139.0	28.50	10.00
400	134.5	24.00	5.00	141.5	31.00	25.00
500	135.5	25.00	10.00	141.5	31.00	0.00
600	136.0	25.50	5.00	142.8	32.25	12.50
700	136.3	25.75	2.50	143.0	32.50	2.50
800	137.0	26.50	7.50	143.5	33.00	5.00
900	137.5	27.00	5.00	144.0	33.50	5.00
1000	137.5	27.00	0.00	144.5	34.00	5.00
1500	138.0	27.50	1.00	146.0	35.50	3.00
2000	139.0	28.50	2.00	147.5	37.00	3.00
2500	139.5	29.00	1.00			
3000	139.8	29.25	0.50			
3500	140.0	29.50	0.50			
4000	140.5	30.00	1.00			
4500	141.0	30.50	1.00			
5000	141.5	31.00	1.00			
6000	142.0	31.50	0.50			
7000	142.5	32.00	0.50			
8000	143.0	32.50	0.50			
9000	143.5	33.00	0.50			
10000	144.0	33.50	0.50			



Reference	CI-KM1			CI-KM1		
Contact Pressure, kPa	141			195		
Number of Passes	LVDT Reading	Deformation, mm	Deformation Rate, mm/10 <sup>3</sup> pass	LVDT Reading	Deformation, mm	Deformation Rate, mm/10 <sup>3</sup> pass
0	0.00	0.0		0.0	0.00	
100	6.83	6.83	68.33	16.5	16.50	165.00
200	9.33	9.33	25.00	19.8	19.83	33.33
300	10.00	10.00	6.67	21.2	21.17	13.33
400	11.00	11.00	10.00	22.2	22.17	10.00
500	11.83	11.83	8.33	22.8	22.83	6.67
600	12.17	12.17	3.33	22.8	22.83	0.00
700	12.17	12.17	0.00	23.8	23.83	10.00
800	13.00	13.00	8.33	25.2	25.17	13.33
900	13.00	13.00	0.00	25.8	25.83	6.67
1000	13.00	13.00	0.00	26.5	26.50	6.67
1500	13.17	13.17	0.33	29.5	29.50	6.00
2000	13.33	13.33	0.33	30.2	30.17	1.33
2500	13.50	13.50	0.33	31.0	31.00	1.67
3000	13.50	13.50	0.00	31.7	31.67	1.33
3500	13.50	13.50	0.00	32.5	32.50	1.67
4000	13.50	13.50	0.00	33.5	33.50	2.00
4500	13.50	13.50	0.00	33.5	33.50	0.00
5000	13.50	13.50	0.00	33.5	33.50	0.00
6000	13.50	13.50	0.00	34.7	34.67	1.17
7000	13.50	13.50	0.00	35.8	35.83	1.17
8000	13.50	13.50	0.00	37.0	37.00	1.17
9000	13.50	13.50	0.00	38.2	38.17	1.17
10000	13.50	13.50	0.00	39.0	39.00	0.83
15000	13.50	13.50	0.00	40.0	40.00	0.20
20000	13.50	13.50	0.00	45.5	45.50	1.10
30000	13.50	13.50	0.00	47.2	47.17	0.17
40000	13.50	13.50	0.00	48.8	48.83	0.17

Reference	CI-KM1		
Contact Pressure, kPa	224		
Number of Passes	LVDT Reading	Deformation, mm	Deformation Rate, mm/10 <sup>3</sup> pass
0	0.0	0.00	
100	30.0	30.00	300.00
200	43.5	43.50	135.00
300	50.8	50.83	73.33
400	56.5	56.50	56.67
500	58.7	58.67	21.67

Reference	CI-KM2			CI-KM2		
Contact Pressure, kPa	215			254		
Number of Passes	LVDT Reading	Deformation, mm	Deformation Rate, mm/10 <sup>3</sup> pass	LVDT Reading	Deformation, mm	Deformation Rate, mm/10 <sup>3</sup> pass
0	0.00	0.0		0.0	0.00	
500	6.83	6.83	13.67	21.7	21.67	43.33
1000	7.33	7.33	1.00	26.0	26.00	8.67
2000	8.25	8.25	0.92	30.3	30.33	4.33
3000	8.67	8.67	0.42	32.8	32.83	2.50
4000	8.83	8.83	0.17	35.4	35.42	2.58
5000	9.00	9.00	0.17	37.6	37.58	2.17
10000	9.33	9.33	0.07	42.3	42.33	0.95
20000	9.33	9.33	0.00			
30000	9.33	9.33	0.00			
40000	9.33	9.33	0.00			
50000	9.33	9.33	0.00			
60000	9.33	9.33	0.00			

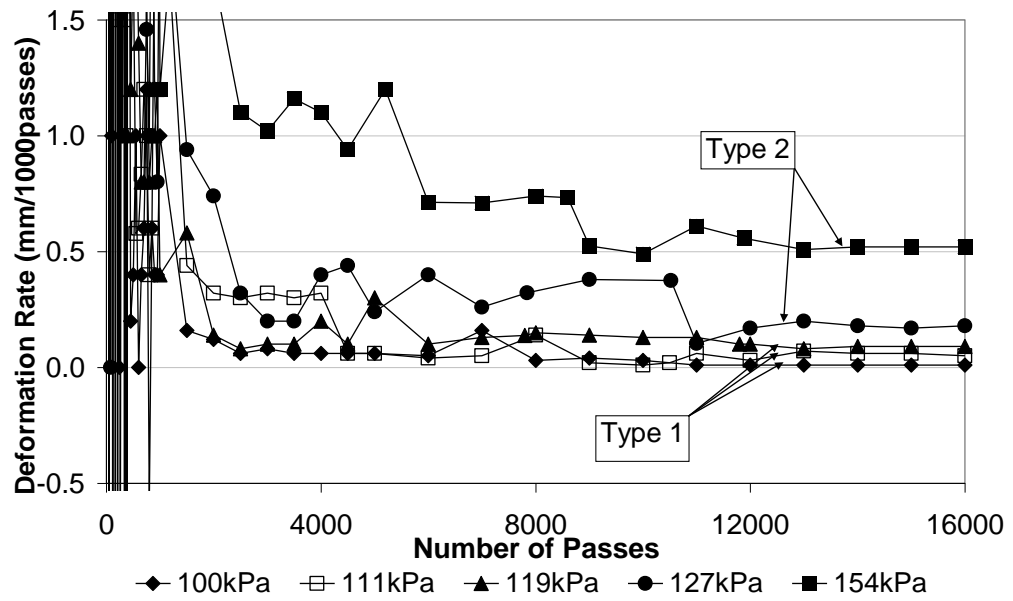
Reference	CI-KM2		
Contact Pressure, kPa	333		
Number of Passes	LVDT Reading	Deformation, mm	Deformation Rate, mm/10 <sup>3</sup> pass
0	0.0	0.00	
500	29.3	29.33	58.67
1000	32.3	32.33	6.00
2000	34.5	34.50	2.17
3000	37.7	37.67	3.17
4000	42.5	42.50	4.83
5000	46.8	46.83	4.33
7000	51.7	51.67	2.42

Reference	CI-LFS-KM			CI-LFS-KM		
Contact Pressure, kPa	310			410		
Number of Passes	LVDT Reading	Deformation, mm	Deformation Rate, mm/10 <sup>3</sup> pass	LVDT Reading	Deformation, mm	Deformation Rate, mm/10 <sup>3</sup> pass
0	0.00	0.0		0.0	0.00	
500	2.75	2.75	5.50	3.2	3.17	6.33
1000	3.13	3.13	0.75	3.3	3.33	0.33
2000	3.50	3.50	0.38	3.7	3.67	0.33
3000	3.63	3.63	0.13	3.8	3.83	0.17
4000	3.63	3.63	0.00	4.0	4.00	0.17
5000	3.63	3.63	0.00	4.2	4.17	0.17
10000	3.63	3.63	0.00	4.2	4.17	0.00
20000	3.63	3.63	0.00	4.8	4.83	0.07
30000	3.63	3.63	0.00	5.5	5.50	0.07
40000	3.63	3.63	0.00	6.2	6.17	0.07
50000	3.63	3.63	0.00	7.2	7.17	0.10

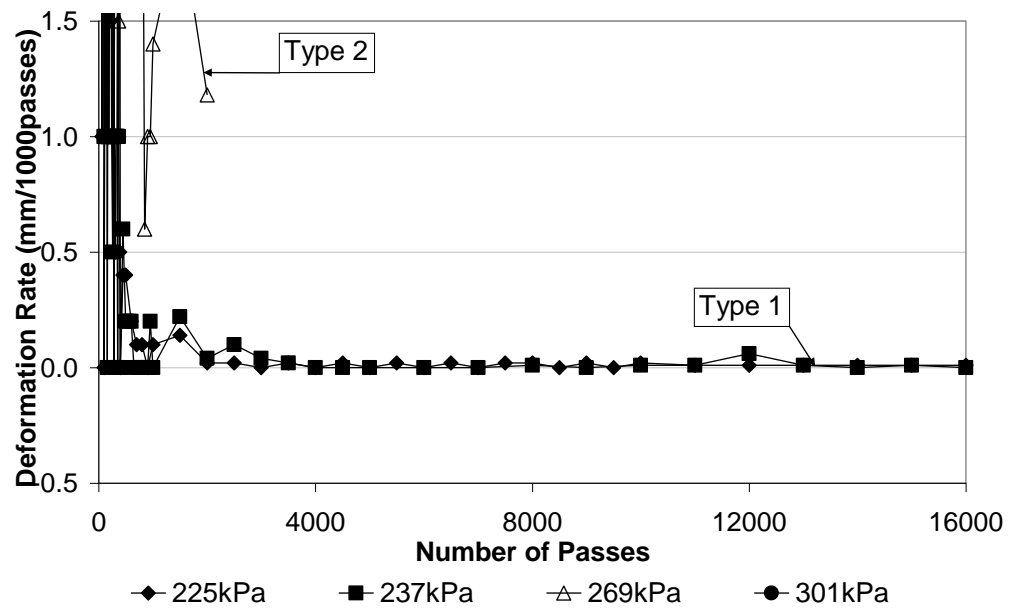
Reference	CI-LFS-KM		
Contact Pressure, kPa	433		
Number of Passes	LVDT Reading	Deformation, mm	Deformation Rate, mm/10 <sup>3</sup> pass
0	0.0	0.00	
500	3.1	3.13	6.25
1000	4.0	4.00	1.75
2000	4.6	4.63	0.63
3000	4.6	4.63	0.00
4000	4.9	4.88	0.25
5000	5.0	5.00	0.13
10000	5.6	5.63	0.13
20000	6.1	6.13	0.05
50000	8.3	8.25	0.07

Reference	CI-LFS-KM		
Contact Pressure, kPa	453		
Number of Passes	LVDT Reading	Deformation, mm	Deformation Rate, mm/10 <sup>3</sup> pass
0	0.00	0.00	
500	4.00	4.00	8.00
1000	5.25	5.25	2.50
2000	6.13	6.13	0.88
3000	6.38	6.38	0.25
4000	6.88	6.88	0.50
5000	7.25	7.25	0.38
10000	8.88	8.88	0.33
20000	10.88	10.88	0.20
30000	11.63	11.63	0.08
40000	12.63	12.63	0.10
50000	13.38	13.38	0.08

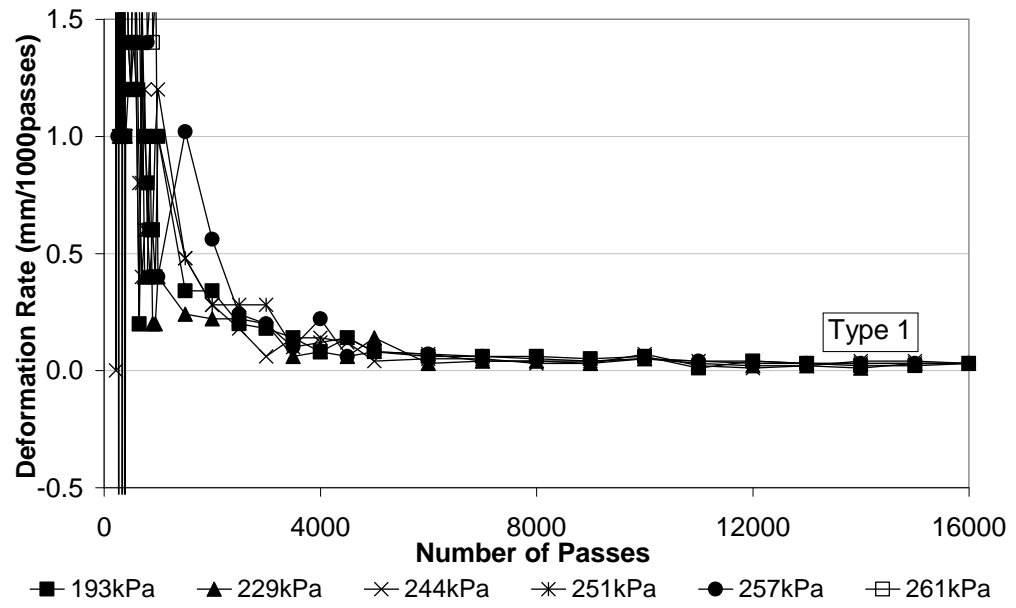
**Appendix F The Charts of the Deformation Rates against the Number of  
Passes of Various Soil Combinations**



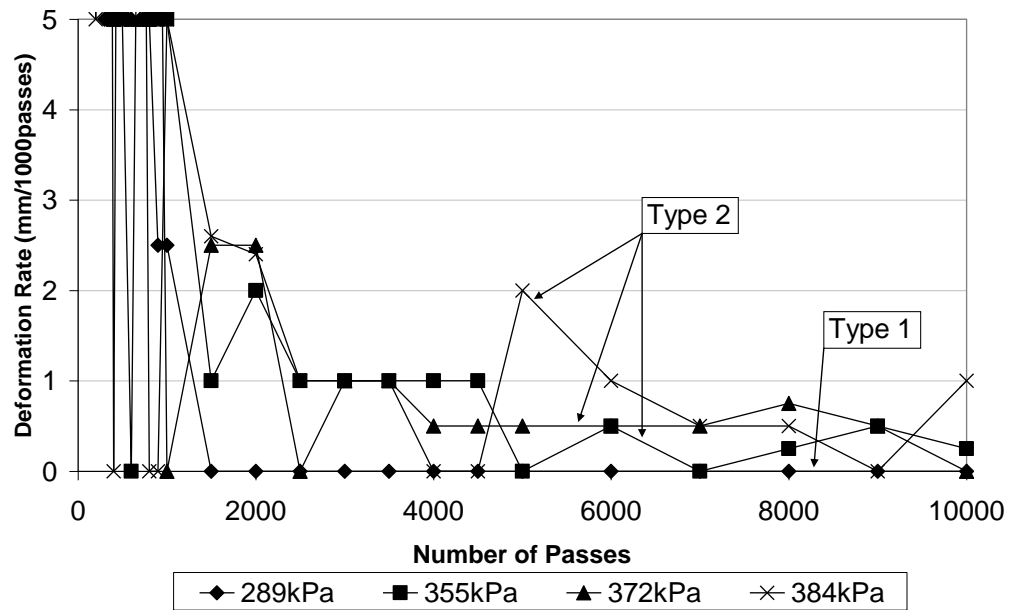
**Figure F. 1 Variation of the deformation rate of PS2 with number of passes for various wheel pressures**



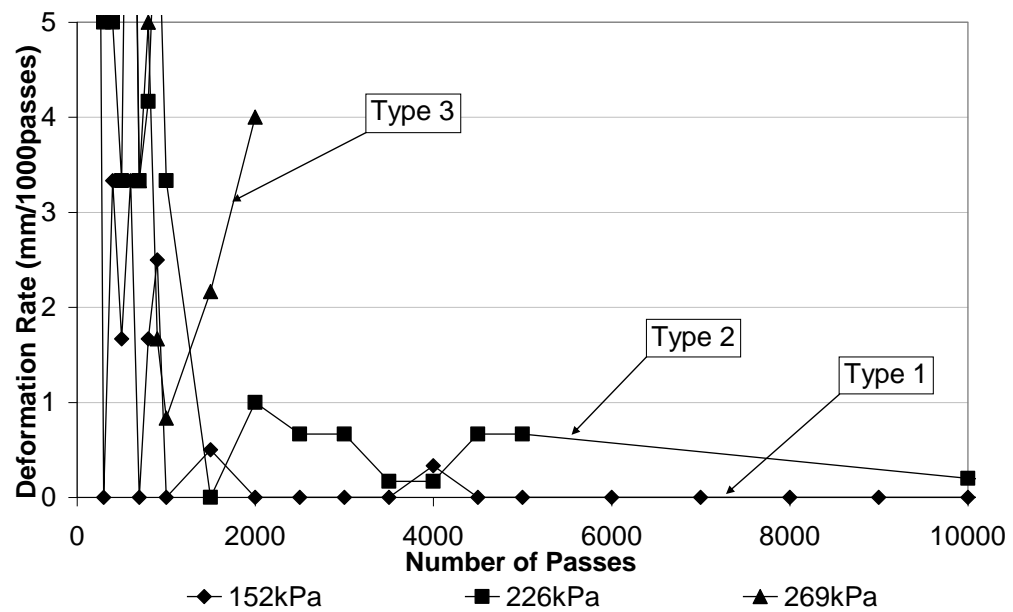
**Figure F. 2 Variation of the deformation rate of KM with number of passes for various wheel pressures**



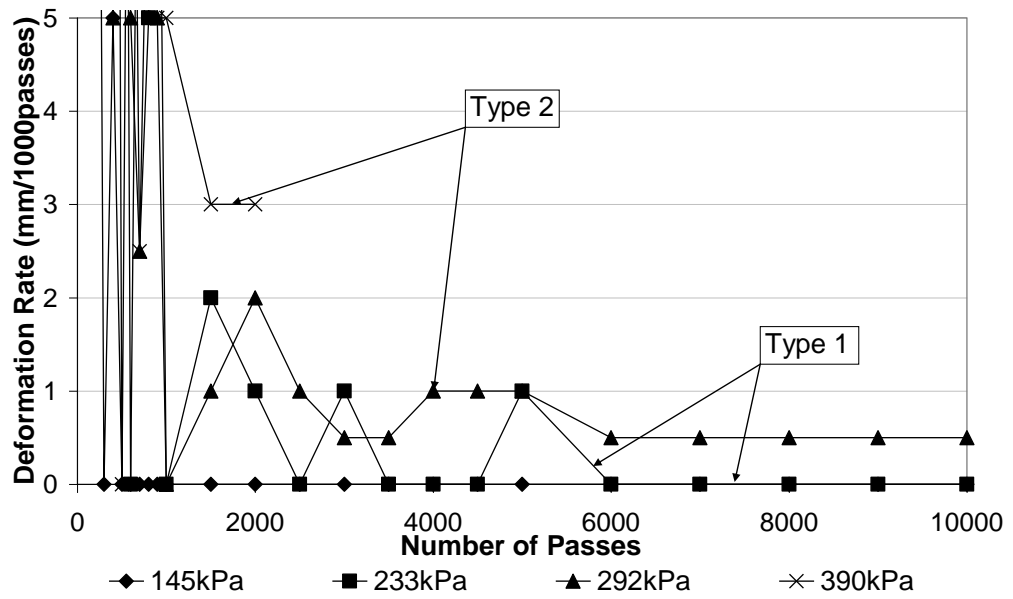
**Figure F. 3 Variation of the deformation rate of Silt with number of passes for various wheel pressures**



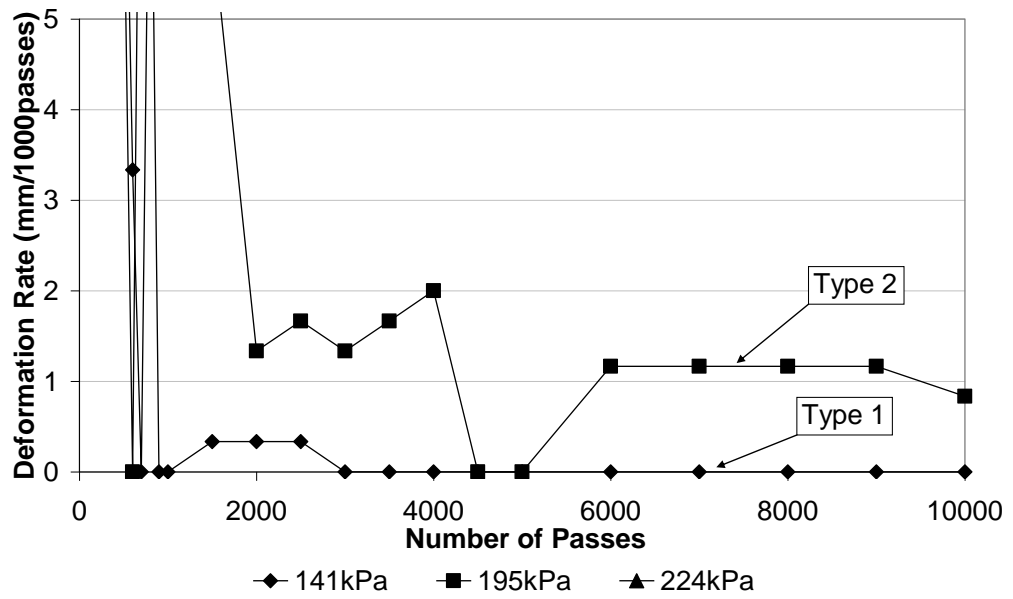
**Figure F. 4 Variation of the deformation rate of Gr with number of passes for various wheel pressures**



**Figure F. 5 Variation of the deformation rate of Gr-PS with number of passes for various wheel pressures**

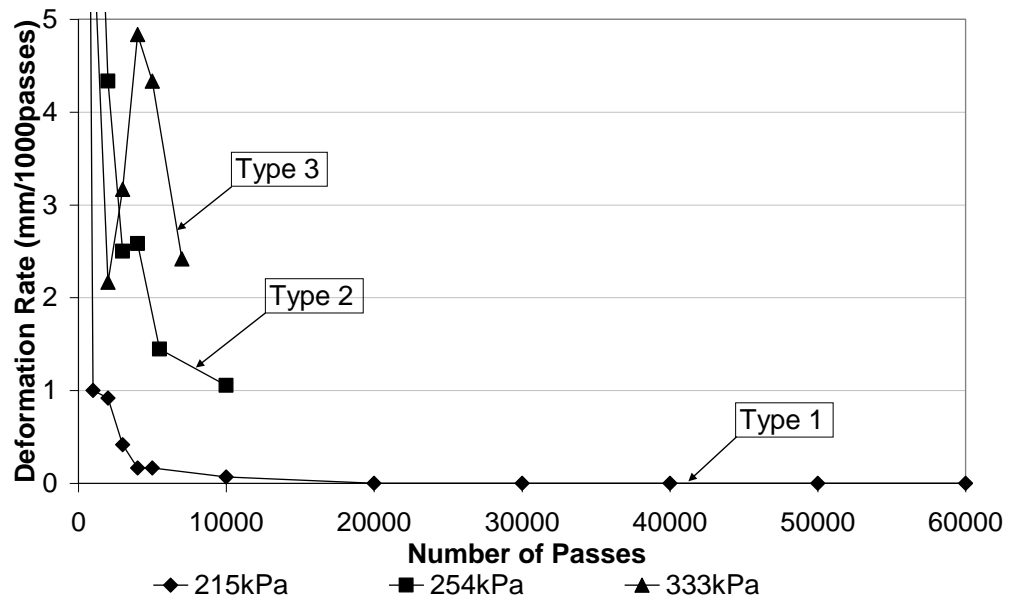


**Figure F. 6 Variation of the deformation rate of Gr-Silt with number of passes for various wheel pressures**

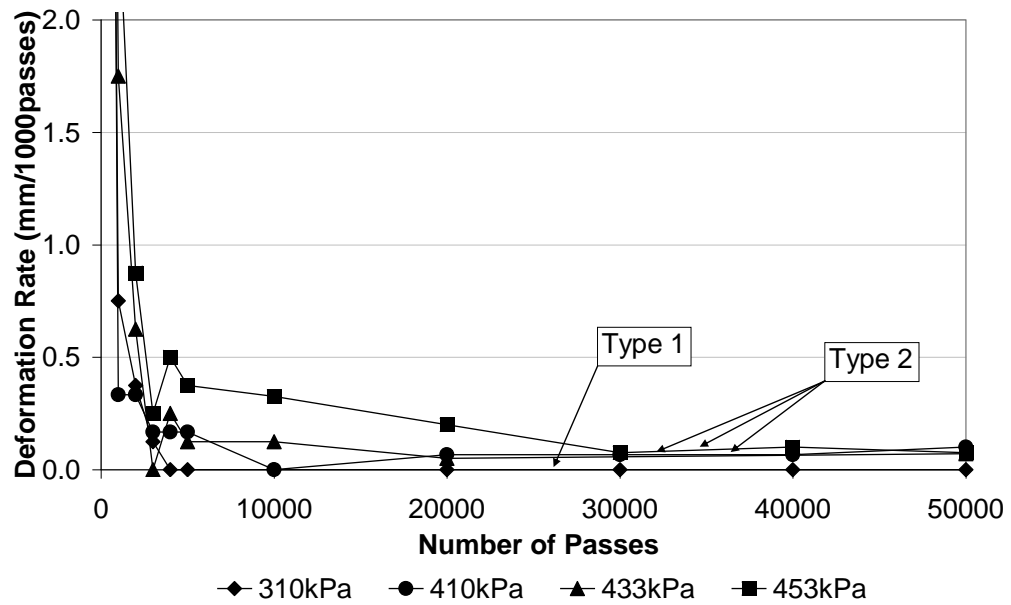


**Figure F. 7 Variation of the deformation rate CI-KM1 with number of passes for various wheel pressures**





**Figure F. 8 Variation of the deformation rate of CI-KM2 with number of passes for various wheel pressures**



**Figure F. 9 Variation of the deformation rate of CI-LFS-KM with number of passes for various wheel pressures**